Tampere University

María Aransáez Ortega

Numerical simulation of the impact response of natural fibre composites

Structural mechanics
Master's Thesis
Tampere, May of 2019

Abstract

Numerical simulation of the impact response of natural fibre composites.
Tampere University (Tampere University of Technology)
Master's Thesis
Master's Degree Programme in Industrial Engineering
May 2019

Tutor: Professor Reijo Kouhia
Supervisor: PhD Karthik Ramakrishnan

The aim of this thesis is study essential stages that develop a FEM, finite element method, via Abaqus to reproduce one experimental test requires. The laboratory research that inspired this thesis was carry out by the Tampere University of Technology material department.

The laboratory experiment was an impact, of a spherical projectile, against a composite plate. The essential and crucial characteristic of that empirical project was the material, which is a natural fiber composite (NFC). This becomes a key factor in the numerical design, because the software does not contain an in-build material conceived to reproduce NFC behaviour. The need to develop a analytical model and afterwards generated a VUMAT is explored.

The thesis has two main parts, the fist one focus in delving and setting the best method to replicate the impact over a traditional composite material plate with the tools Abaqus 2017 provides. After this task, the method will be used in the simulation of a impact over a natural fiber composite plate. With the obtained results the need of a user-material generated by a user-subroutine in Abaqus will be assess. In the case this is required the correct choice will be a VUMAT subroutine, it is used to define the mechanical constitutive behaviour of a material, for elements type C3D8R.

Keywords: Natural fiber composites, impact simulation, FEM, Abaqus, FRP.

Preface

This Master's Thesis was done in the department of Civil Engineering with the research groups of Structural Mechanics, in the Faculty of Built Environment at Tampere University.
I would like to say thank you to my tutors. I am grateful to my thesis's tutor Professor Reijo Kouhia for allowing me to work in this research group, for advising me and his guidance, during the thesis development. I also really appreciate my supervisor PhD Karthik Ramakrishnan support, who has been guiding me during the process, by teaching me and providing me helpful literature and knowledge. Also thank you to all those people, as Jarno Jokinen and the Modelling meeting colleagues, who not hesitated to help me when I have troubles with the simulations. Also, I will like to thank my family and friends, who supported me with love, friendship and understanding, during the 8 months I have work in the thesis.

Thank you for taking the time to read my work.

María Aransáez Ortega.

Tampere, 30 May, 2019.

List of abbreviations and symbols

3D: Three dimensional

ACCs: All-cellulose composites

BVID: Barely Visible Impact Damage

ALLAE: E_{art}: Artificial strain energy associated with constraints used to remove singular modes (such as hourglass control) and with constraints used to make the drill rotation follow the in-plane rotation of the shell elements.[76]

ALLIE: U_{st}: Strain (internal) energy

ALLKE: E_k: Kinetic energy

CC: license Creative Commons license

CDM: Continuum damage mechanics

CODAM: Composite damage model

CZM: Cohesive zone methods

DTL: Damage Threshold Loads

ECDM: Enhanced continuum damage mechanics

DAMAGEFC: Fiber compression damage

DAMAGEFT: Fiber tensile damage

DAMAGEMC: Matrix compression damage

DAMAGEMT: Matrix tensile damage

DAMAGESHR: Shear damage

DOF: Degree of freedom.

FE: Finite Element

FEM: Finite Element Method

FRP: Fiber-reinforced polymers

HVI: High-Velocity Impact

LVI: Low-Velocity Impact

NFC: Natural fiber composite

PFC: Plant fiber composite

PDA: Progressive damage analysis

PE: Polyethylene

PLA: Polylactide

PP: Polypropylene

R3D4: A 4-node 3D bilinear rigid quadrilateral.

R3D3: A 3-node 3D bilinear rigid triangular.

RVE: Reference volume element

S4R: A 4-node doubly curved thin or thick shell, reduced integration, hourglass control, finite membrane strains.

S3R: A 3-node doubly curved thin or thick shell, reduced integration, hourglass control, finite membrane strains.

SC8R: A 8-node quadrilateral in-plane general-purpose continuum shell, reduced integration with hourglass control, finite membrane strains.

SCM: Smeared crack model

TUNI: Tampere Universities

TUT: Tampere University of Technology

URL: Uniform Resource Locator

vs.: Versus

WWFE: World wide Failure Exercise

a**:** acceleration

F**:** force

m**:** mass

ρ: density

E_1: Longitudinal modulus

E_2, E_3: Transverse modulus

ν_{12}: Major Poisson's ratio

ν_{13}, ν_{23}: Poisson's ratio

G_{12}: In-plane shear modulus

G_{13}, G_{12}: Shear modulus

X_T: Longitudinal tensile strength

X_C: Longitudinal compressive strength

Y_T: Transverse tensile strength

Y_C: Transverse compressive strength

S_{12}: Longitudinal shear strength

S_{23}: Transverse shear strength

C_i: Stiffness matrix component

I_i: Invariant

The abbreviations and symbols used in the thesis are collected into a list in alphabetical order, excepts the physical properties' names that are in order of importance.

Contents

List of Figures

List of Tables

Chapter 1

Introduction

Fiber reinforced composites have been during the last decades the top engineering products. Their magnificent rate between the stiffness and the strength against their weight made them so desirable to be the solution to almost all kind of structural problems. But they represent one big problem for the environment. When their operative life ends, their are by definition non-recyclables, causing with their boom a huge amount of waste product that the industry can not manage. In order to face this environmental issue the researches have been during last years exploring and developing new composites material based on natural fiber. These materials are thought to perform as common composites, but with the extra characteristic of been recyclable or at least degradable.

1.1 Motivation

As traditional composites, the performance of this new material have been tested in laboratories, but this has a high cost. So, if there is the willing to make them penetrated in the industry, the use of appropriate numerical analysis, based in trustworthy constitutive models, that reproduce the behaviour of these material against different phenomena are required and have a crucial role in this aim.

Impacts are one of the most tricky phenomena that any structure can face. The structures that the industry manufacture are exposed to them, by the fall or hit of random object, animals blow during the working life of the product or by the droop of tools during maintenance. Another reason to create a good numerical analysis is that the damage generated by the impact sometimes is non-visible, if only occurs inside the lamina, making them non easy to detect until the collapse of the piece, but it is really dangerous in application as aerospace ones, where people life is at stake. Furthermore, as Harpreet Singh and Puneet Mahajan say in the article [77]: *'These kind of impacts lead to damage of composite which may be, at microscopic level, fiber breakage, matrix cracking or delamination.'*

For the reasons aforementioned, this thesis is going to be focus in the footsteps

that reproduce a impact over a natural fiber composite material with FEM, finite element method, need.

1.2 Objectives

The aim of this thesis is to go over the different stages that a impact simulation over a non in-build (in Abaqus) material demands. For that goal several steps had to be followed:

1. Generate an impact in Abaqus/Explicit, establishing the optimal criterion of the different modules that Abaqus has, such as Property, Step or Interaction.
2. Use the develop method to simulate an impact over a natural fiber composite plate, with the Abaqus in-build material.
3. Demonstrate the need of develop a constitutive model for the Flax/PP behaviour facing a low velocity impact (LVI), and its corresponding VUMAT code.

1.3 Memory's description

This thesis has been arranged by the following scheme:

1. Introduction and aim pinpoint.
2. Precedents in the literature about composites material, impacts simulation and natural fiber composite material, emphasizing Flax research.
3. Preliminary simulation: with Abaqus' tools reproduce a LVI over a Kevlar plate. The goal of this is to screen the options' range that program's modules have.
4. Simulation in Abaqus using the develop method of a low velocity impact over a NFC plate.

Chapter 2

Literature Review

Composite materials are defined as the combination of at least two materials, usually a polymer matrix reinforced with a fiber, commonly carbon or glass. The impressive properties achieved with these mixture cannot be achieved by the constituent materials on their own [70]. Fiber reinforced polymer (FRP) composites are extensively used in industries such as automotive, aerospace and civil engineering. Additionally, others areas like furniture industry or sport goods, for example bikes, rackets, golf sticks, even F1 cars are adopting composite materials [56]. These materials have gained widespread use due to their low specific mass and good stiffness. Moreover, they have a high energy absorption capability and are used in impact-resistant structures.

A new class of composite materials that use natural fibers are reinforcements has received increasing attention in the scientific community. It is expected that replacing the synthetic fiber materials such as glass with plant fibers will result in environmental friendly biodegradable materials. Natural Fiber Composites (NFC) scores much better in all the environmental impact indicators (except land use) than glass fibers [56]. In addition, traditional polymers and fibers with petrochemical origin have large *carbon footprint* [62]. The society's demand for sustainable, environmentally friendly products and various regulations and price increases of fossil-fuel based products have led to a rapid expansion of biomaterials. The exploitation of bio-based raw materials are also important considering its recycling possibilities.

2.1 Natural fiber composites materials

Natural fibers have been used by mankind for over 40000 years[14]. Wool, flax or hemp were one of the first fibers used in the human history. But, in the case of structural composites, these materials are relatively new. They were introduced by the research community with the target to solve different problems such as non-recyclability and non-reusability of traditional reinforced composite materials. Cellulose is the major component of all the plant-based fibers. Flax, ramie and

hemp fibers are amongst the cellulose based fibers with highest specific Young's moduli and strengths [55]. Bourmaud et al. [14] remarks that one of the stronger reasons for using plant fiber is: *'Plant structures have outstanding mechanical performances, which are the result of a long evolutionary process of optimization'* by nature. However, according to Shah [73], plant fibers composites represent only around the 1,9% of the 2,4 million tonne in the European Union of Fiber Reinforced Polymers market. A comparison of plant fibers and glass fibers at economical, technical and ecological properties are shown in Table 2.1.

Table 2.1: Comparison of natural fibers and E-glass fibers[73].

	Propreties	**Plant fibers**	**E-glass fiber**
Economical	Annual global production (tonnes)	$31 \cdot 10^6$	$4 \cdot 10^6$
	Distribution for FRPs in EU (tonnes)	Moderate ($40 \cdot 10^3$)	Moderate ($600 \cdot 10^3$)
	Cost of raw fiber (£/kg)	Low (∼0,5-1,5)	Low (1,3)
Technical	Density (g cm-1)	Low (∼1,35-1,55)	High (2,66)
	Tensile stiffness (GPa)	Moderate (∼30-80)	Moderate (73)
	Tensile strength (GPa)	Low (∼0,4-1,5)	Moderate (2-3,5)
	Tensile failure strain (%)	Low (∼1,4-3,2)	Low (2,5)
	Specific tensile stiffness (GPa / g cm-1)	Moderate (∼20-60)	Low (27)
	Specific tensile strength (GPa / g cm-1)	Moderate (∼0,3-1,1)	Moderate (0,7-1,3)
	Abrasive to machines	No	Yes
Ecological	Energy consumption (MJ / kg of fiber)	Low (4-15)	Moderate (30-50)
	Renewable source	Yes	No
	Recyclable	Yes	Partly
	Biodegradable	Yes	No
	Toxic (upon inhalation)	No	Yes

The design of biocomposites involve the same steps as in the traditional ones. For example fiber and matrix selection, fiber dispersion, fiber orientation, porosity, interfacial strength or composite manufacturing process. Fiber selection is complex as the performance of the composite is highly influenced by the type of fiber, harvest time, extraction method, aspect ratio, treatment, etc. [55]. It is important to understand when comparing property data from different sources, that some variables that are not reported can have a huge influence in natural fibers. This means that same fiber can have different values for same properties. The choice of one type of fiber or another is a matter, mainly, on geographical situation of the manufacturing country and the availability of that kind of plant in the area. As an example, Flax is used more in Europe while Asia is more likely to use hemp or jute. It is curious that Asia is the major producer of all the fibers with three exceptions, Sisal whose major producer is South America, Flax whose major producer is Europe and Hemp that Europe and Asia share the amount of production, (data of 2013 [14]). Pickering et al. [55] specifies that varieties of fiber whose compositions are richer in the quantity of cellulose are the ones that has better performance. In addition, the composition with highly aligned cellulose microfibrils have better properties. Those characteristics usually are seen in bast fibers, such as hemp, flax among others. A classification of natural fibers based on the type of plant is shown in Figure 2.1 and the countries where they are principally grown is shown in Table 2.2.

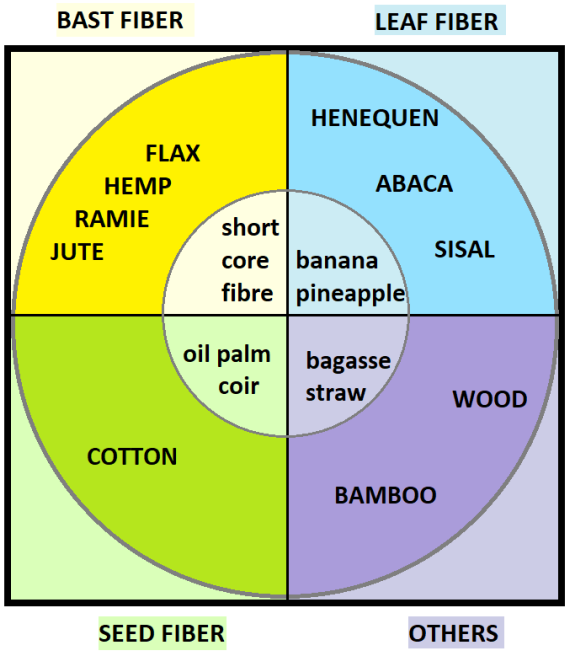

Figure 2.1: Classification of natural fibers[14].

Table 2.2: Different fibers and production countries (2012).[83]

fibers	**Country of origin**
Sisal	Brazil, East Africa, Haiti, Venezuela, Antiqua, Kenya, Tanzania, India
Flax	Poland, Belgium, France, Spain
Hemp	Poland, China, Hungary, France, Romania
Sun Hemp	Nigeria, Guyana, Siera Leone, India
Ramie	Honduras, Mauritius Islands, China
Jute	India, Egypt, Guyana, Jamaica, Ghana, Malawi, Sudan, Tanzania, Brazil
Kenaf	Iraq, Tanzania, Jamaica, South Africa, Cuba, Togo, USA, Thailand
Roselle	Borneo, Guyana, Malaysia, Sri Lanka, Togo, Indonesia, Tanzania
Abaca	Ecuador, Philippines, Colombia
Coir	India, Sri Lanka, Philippines, Malaysia, Brazil
Curaua/Kurowa	Brazil, Colombia, Venezuela, Guyana
Fique	Colombia
Piaçava	Brazil

In terms of mechanical performance, some plant fibers are known to be as tough as conventional glass fibers. For instance, the flax fiber modulus is comparable to that of glass but flax has a lower density. The excellent mechanical properties of such natural fibers, combined with the added functionalities such as acoustic and thermal insulation, vibration damping, and being renewable bring some unique advantages that make them a very attractive material for composites. A brief summary of the advantages and disadvantages of natural fiber composites is given in Table 2.3. However, in order to take advantage of all its benefits and achieve

the envisioned improvements, a good understanding of the behaviour of these composite materials is required.

Table 2.3: Advantages and disadvantages of Natural fiber Composites.[55].

Advantages	**Disadvantages**
• Low density and high specific strength and stiffness.	• Lower durability than for synthetic fiber composites, but can be improved considerably with treatment.
• Fibers are a renewable resource, for which production requires little energy, involves CO_2 absorption, whilst returning oxygen to the environment.	• High moisture absorption, which results in swelling.
• Fibers can be produced at lower cost than synthetic fiber.	• Lower strength, in particular impact strength compared to synthetic fiber composites.
• Low hazard manufacturing processes.	• Greater variability of properties.
• Low emission of toxic fumes when subjected to heat and during incineration at end of life.	• Lower processing temperatures limiting matrix options.
• Less abrasive damage to processing equipment compared with that for synthetic fiber composites.	

2.1.1 Flax fiber composites materials.

Flax has truly accompanied the human history and the birth of the agriculture in the Neolithic period in Mesopotamia around 10000 years BC and throughout the Fertile Crescent[14]. Flax provides one of the best performance of all the natural fibers. As an example the specific modulus of flax fiber, *i.e.* the ratio of the modulus and density, is higher than E-glass fiber [58], see Table 2.4.

Table 2.4: Flax vs. E-glass.[58].

Property	**Flax**	**E-Glass**
E/ρ $[GPa/m^3kg^{-1}]$	38	28

Figure 2.2 shows Flax fiber under the microscopic view. The microstructure of the flax fibers show a stack of different layers of walls consisting of a primary wall and a secondary wall divided into layers S1, S2 and S3. Flax fiber bundles are called *technical fibers* and are made of several elementary fibers joined together by a pectin cement [14].

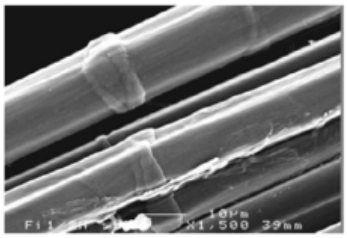

(a) Micrographs of longitudinal flax fibers.

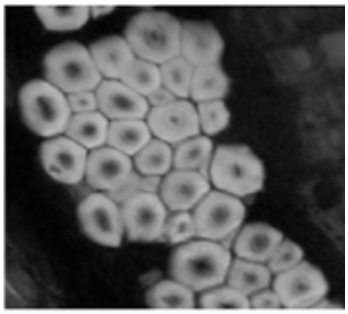

(b) SEM images of flax fibers cross sections.

(c) Schematic representation of the structure of a panel of flax fiber.

Figure 2.2: Flax fiber under the microscope[14].

The scientific community know this plant as *Linum Usitatissimum Linaceae* and the biggest producer of Flax worldwide is France, more specifically the Normandy region, as the Table 2.5 gathers. In 2004 according to [51] based in FAO (Food and Agriculture Organization of the United Nations), Europe represented the 20% of area planted in the world of Flax. Two years later, [50], Europe represented again the 20% of the word surface of Flax's plantation, but it signified 53% of the world production. In 2014, [14] Europe represents two thirds of the world production, this means an increase of 13% of the market production.

Table 2.5: Distribution of the production of Flax in Europe (2004, 2006 and 2014)[51], [50], [14].

Country	**Flax (2004)**[1]	**Flax (2006)**[1]	**Flax (2014)**
France	65%	72%	104 kt
Belgium	15%	15%	10,5 kt
Netherlands	3,6%	4%	2,5 kt
Poland	7%	2,6%	1,5 kt
Czech Republic	4,4%	2,5%	
Baltic States		2,4%	0,8 kt
UK			1,1 kt
Belarus			15 kt
Ukraine			6 kt
Italy			3 kt

Shah et al. [73] attempted to answer the question *Can Flax replace E-glass in structural composites?* with a case study on wind turbine blades with glass and flax fiber composites. It was reported that a flax blade of identical geometry and dimensions was 10% lighter than the E-glass blade. The novel flax fiber blade

[1]The percentages are over the European area planted.

satisfied the test required for the certification standards. The structural integrity passed the *'normal operation loading, without superficial failure'* as well as the *worst case* loading, without functional and catastrophic failure. It is remarkable that the flax and glass fiber blade has a different load-deflection curve and also their failure mode is not identical. Unfortunately the flax blade can not compete with the E-glass one in stiffness, possibly this is a consequence of a poor interface between the fiber and the matrix. But, the flax blade is much more flexible than E-glass one . Also it suffers more relaxation load. Even though it was found that flax is suitable to replace E-glass, the Flax blade in the study cost three times higher than the E-glass one, even though less fibers of flax were used than E-glass fibers. The paramount reason behind this increase in price is that E-glass has a mature market. It is clear that natural fibers are an emerging material but more work is needed before they can be widely used for structural applications.

2.2 Impact behaviour of composites

It is well recognised that fibre reinforced composites are sensitive to damage caused by impact. Composite laminates are less resilient to impact compared to metals which are more ductile and can absorb a large amount of the kinetic energy from impact through bending and plastic deformation. However, composites are brittle and absorb impact energy through different damage mechanisms. Impacts have been divided in the literature in three main families depending on the speed of the impactor; they can be either a Low-Velocity Impact (LVI), High-Velocity Impact (HVI) and ballistic impact[13]. Even very low impact energies could result in non-visible damage, with a significant decrease of the residual properties. For example impact of airplane structures during their service life can be caused by bird strike, hail or tool-drop [13]. Tool-drops are also recurrent in other kind of structures where maintenance or manufacturing operation are carried out. Impact damage on composite laminates can include matrix cracking, delamination, fibre breakage and debonding and the analysis of impact resistance of composites is complicated by these complex damage modes. Impact analysis of composite structures have been a topic of investigation since several years. In fact, there is a whole book **Impact on composite structures** written by Abrate [3], just exploring the wide spectrum of analytical methods to study impact.

Impact knowledge is too important for industry application but unfortunately, they are really difficult to quantify and to understand the dynamic mechanics behind the event. In the last few decades, published literature on impact behaviour and dynamic material characterisation of composites materials, especially traditional GFRP and CFRP composites is well established [49]. These studies are typically coupon tests conducted in the laboratories and supported by numerical modelling using Finite Element Methods (FEM). This methodology has become fundamental in the study of composites, in order to reduce cost of studies and waste of materials. Commonly used machines to perform impact tests are Charpy or Izod but these tests are not useful in composites material studies as these techniques usually

assume a pre-existing notch. For this reason, a majority of composite material impact studies consists of drop-weight impact, where a known mass is fired or released from a certain height over the plate. Another possibility is a gas gun impact at high speed, resulting in a ballistic test. The drop-weight test are closer to the real phenomena that structures suffers in their operative lives. Numerical models are used to predict the behaviour of the specimen under the desired conditions and these models are validated by comparing them with experimental results and data obtained from laboratory tests. It is a constant in papers, as the article [70] says that the: *impact testing of materials is performed to determine the amount of energy that can be absorbed during a suddenly applied force.*

For the purpose of this project, LVI is the important one, furthermore as the article [13] claims it has an particular importance for structure lifetime, because they generate Barely Visible Impact Damage (BVID). A damage produce just inside the material, consisting mainly of delamination. This damage type is really dangerous, because in order to be detected is essentially that a visible damage has to occur simultaneously in that are of the structure. As Rafael Bogenfeld and collaborators remark in the article [13]: *'In addition to the damage itself, the damage visibility determines whether a damage will be discovered and repaired, or not.'*

2.2.1 Impact of natural fiber composites

In the literature of the last decade, there are several articles on the impact resistance of natural fibre reinforced composites [29, 59]. Hoang and Touchard [29] found from their investigation of the low velocity impact behaviour of non-woven flax/polypropylene composites that there was a linear evolution of absorbed energy with impact energy and that fibre areal weight, treatment and matrix recycling have insignificant effect on the energy absorption response of the composite laminate. Puech et al. [59] analysed the impact behaviour of short hemp fibres reinforced PP biocomposites through impact tests and high speed imaging and showed that PP-hemp biocomposites exhibit higher absorbed energies (up to 40%) than PP-glass composites due to higher strain at break. There have also been some experimental impact studies on woven hemp fibres [71], jute fibres [23], and unidirectional and cross-ply flax fabric composites [63, 81, 43]. The pendulum impact setup used for the tests by Sy et al. [81] and the damage profiles from high-resolution photographs of the front and back faces of the unidirectional laminates are shown in Figure 2.3.

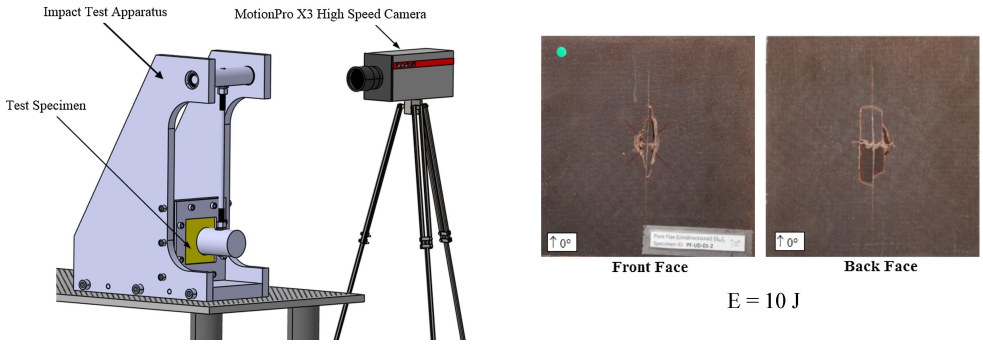

Figure 2.3: Schematic of the pendulum impact test setup used for low velocity impact testing and impacted samples[81].

Puech et al. implemented a high speed imaging acquisition system on the drop-weight impact machine so as to correlate the occurrence of events on the force-displacement curves and appearance and propagation of macro-cracks in the Hemp-PP biocomposite impacted at 12 J as shown in Figure 2.4. The sequence of events showing the beginning of crazing, formation of radial cracks and penetration failure as seen from the high speed camera images of the lower surface are shown to correlate to different stages of the contact force history.

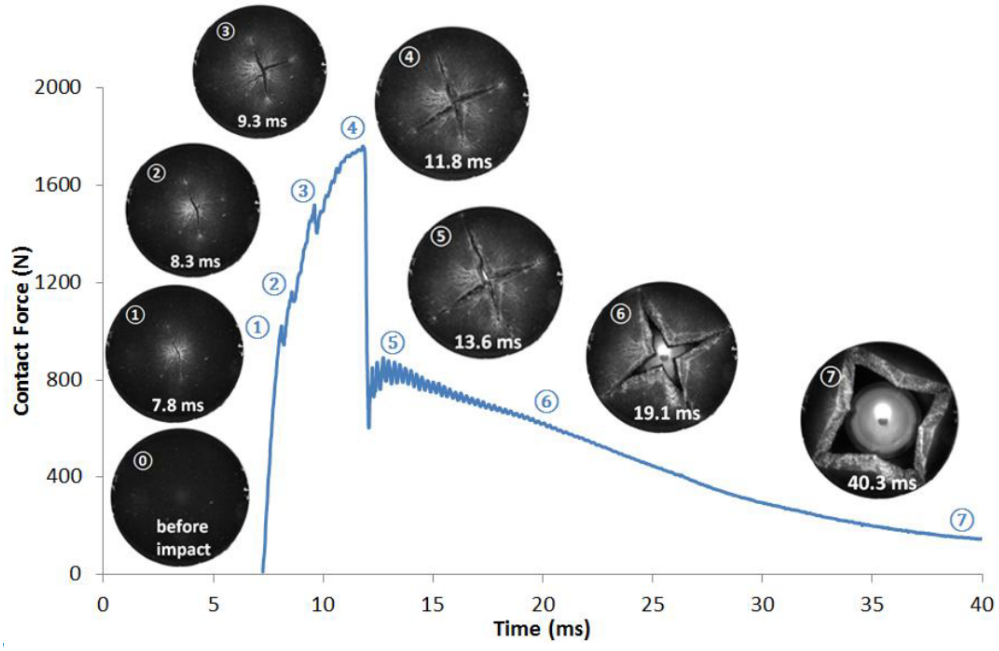

Figure 2.4: Progression of impact events and associated time history of contact force[59].

Liang et al. [43] conducted low velocity impact experiments on thin quasi-isotropic flax/epoxy plates and found that damage in the composite laminate consisted of matrix cracks, delamination and intralaminar transverse cracks. At low energies below perforation threshold (less than 10 J), it was found that the in-plane laminate stiffness did not affect the impact response of flax/epoxy laminates as the energy

dissipation for unidirectional and cross-ply composites was the same despite their difference in stiffness.

2.3 Numerical modelling of composites

The current practice required for the development and certification of new composite structures follows a building block approach starting from simple (generic) coupons, for basic material characterisation, and moving to more complex structural details [25]. One approach for reducing development time and cost of composite structures is to increase the use of modelling and simulation at all levels of the product development cycle. Extensive experimentation is prohibitively expensive and numerical models provide a more efficient solution to understanding the mechanical performance of the composites. The aerospace and automotive industries have been at the forefront of integrating modelling and simulation tools into their product development. However, in order to obtain accurate results that correspond to the reality, massive computational and modelling time and effort is required [13]. There is a strong need for replacing some of experimental testing with simulation, but the inadequacy of existing simulation tools to reliably predict the structural response of composites under damage-inducing loads is an ongoing challenge [25].

Bogenfeld et al. [13] remarked that LVI cases have been developed by many analytically and numerical models. The crucial steps in a model creation are the prediction of the contact force history and the full response of the structure [2]. The article [2] is a comparison study of the different models that exits for analysing the impacts dynamics. Its target is to select which method fulfills better each impact case. It advocates for using energy-balance model to estimate the maximum contact force and duration of the contact. The infinite plate model is recommended for assessing the effects of plate deflection and the response, how the waves travel from the impact point to the edge of the plate. The book **Terminal ballistics** [67] shows numerical models for ballistic impact and what is behind those models. The codes for compute numerical simulation of HVI are known as *hydrocodes*. The main advantages of those codes are the ability of give information that are beyond laboratory test and analysis. They are effective for solving conservation equations of mass, momentum and energy. The relevant data related with the material properties belong to the equation of state, which related the density, the pressure and temperature which characterize the state and its constitutive relations, for strength and failure characteristics. Some of the most famous constitutive model were proposed by Wilkins in 1964, Johnson and Cook in 1983, the rate-independent model of Steinberg in 1987 and the Zerilli and Armstrong in 1987. In order to solve the equations hydrocodes transform the continuum nature of them into discrete events.

Impact simulation in finite element softwares has a series of complicated numerical issues. The principal ones are material, geometry and boundary nonlinearities [45]. They are closely related with the damage constitutive model, damage evolution

law, the failure criteria and the time-stepping algorithm. While the main objectives of those models are the prediction of delamination, fiber failure and inter-fiber damage[13], they forecast the damage type and the shape, depending in the model strategy and the detail taken. For example, crack length of the fiber is nearly predicted by all numerical models that assess damage. However, permanent indentation needs additional implementations to be reproduced [13]. Literature in this topic covers a huge range of approaches to the problem, from a single degree of freedom to a finite element models on micro-scale, as the figure 2.5 shows. Bogenfeld et al. [13] presented a good guide when analysing impact on the structural level, they *'introduce the methods available in the literature and explain the corresponding modelling techniques and fundamental equations briefly.'*

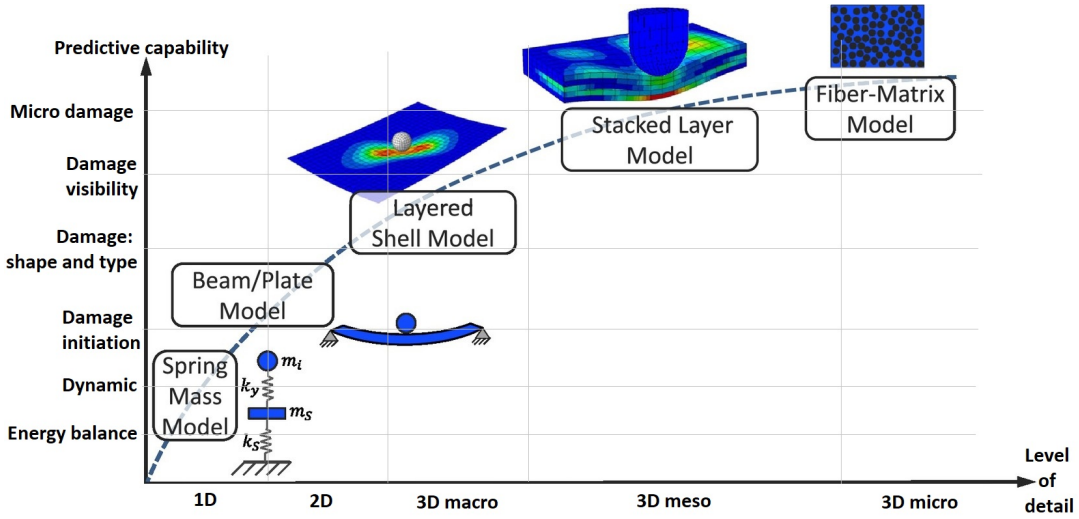

Figure 2.5: Development of impact analysis methods[13].

The impact analysis method development and abstraction is divided and summarized in the Bogenfeld's article as following[13]:

Multi-body system with spring connection: They capture the elastic impact response, taking into account the plate deformation of the structure and the local surface indentation. They normally allow an estimation of impact duration, maximum contact force and impactor displacement.

Plate models: This models include more natural frequencies of the impact system. The technique capture the undamaged dynamic behaviour with higher accuracy than spring-mass approximations, extended with the inclusion of specific non-linearities of the materials.

Damage Threshold Loads (DTL): They are the combination of spring-mass and plate model with empirical or analytical predictions of DTL.

FEM variations: depending in the laminate's abstraction, it can be differentiated *macro-*, *meso-* or *micro-scale*.

Macro-model: Layered-shell approaches are included in this group, they allows to evaluate of failure conditions on the ply-level and the corresponding stiffness degradation, some upgraded ones included, nowadays, a stacking of sub-laminates. Recommended for quick estimations.

Meso-model: There is a huge variety, such as interface model or ply model. The element type and the meshing approach are essential characteristics in which recent models differ. As them can work with any homogenized failure condition, the choice of them is also an important parameter. Typical approaches capture intra-ply damage through continuum damage mechanics. Currently some others approaches have appeared. It is important to say that the computation effort is high and numerical difficulties have been reported. Recommended for better damage results.

Micro-model: Micromechanical models predict the fracture of inter-fiber. Those models need to be coupled with a reference volume element (RVE) in a multiscale approach.

It is also important to remark that the development of numerical methods is highly linked to the development of the computational capacity. So the methods have become more accurate and capture more detail with the increase of capacity in computing. Even though the prediction capability is satisfactory, the computation effort liked to this capacity is already very high for small specimens [13]. In simulations of impacts, there are reports of computation time from 19 h on 32 CPUs up to 48 h on 40 CPUs, when a very fine mesh is applied. In order to reduce those times usually the refined mesh is only applied in the impact area.

Table 2.6: Collection of six modelling approaches which have been benchmarked.[13].

	Spring mass	**Ortho. plate**	**Layered-Shell**	**Stacked-Shell**	**Stacked-Solid**	**Splitting**
Abstraction scale	Global impact system	Macro	Macro	Macro-meso	Meso	Meso
Ply elements	Homogenized in a spring	Analytic plate	S4R	S4R	C3D8R	C3D8R + COH3D8
Interface	–	–	Integration point	COH3D8	Cohesive surfaces	COH3D8
Analysis environment	Scilab	Scilab	Abaqus standard	Abaqus explicit	Abaqus explicit	Abaqus explicit
Delamination	Threshold force	Threshold force	Quad strain	Quad strain	Quad strain	Quad strain
Fiber failure	–	–	Max strain	Max strain	Max strain	Max strain
Inter-fiber Failure	–	–	Hashin	Hashin	Quad strain	Quad strain (cohesive elements)
Damage Evolution	–	Secant stiffness limit	Bilinear	Bilinear	Bilinear	Bilinear
Closest literature Models	Abrate 1991	Dobyns 1981 Olsson 1992	Baaran 2003 Karger 2008	Chen et al. 2017	Liu 2016	Hongkarnjanakul 2013

S4R: linear shell elements with reduce integration.
C3D8R: linear solid elements with reduce integration.
COH3D8: cohesive elements.

The article aforementioned [13] concluded that impact simulations is still a challenge nowadays. Some, methods do not use physically correct damage behaviour, and they recommended to use a macro-scale model with layered-shell element, for quick estimations. But for more accurate damage simulation, it is

recommended to use a meso-scale approach which can capture the impact and its damage in a physical plausible way . Moreover as Serge Abrate [2] says impacts do not have a generalized behaviour. Some of them deform the plate just in the area of impacts while others produce deformation in the whole structure. In addition some plates absorb most of the energy, but in some cases the energy is restituted to the projectile. The main reason for models is that they allow a better comprehension about the way the material absorbs the energy and the failure modes they have. The complexity of the failure and the dynamic behaviour depends if the material is ductile or brittle, being the first one easier. Damage zone of a brittle material can spread out of the impact area, and the factor between the tensile and compressive strength could be around 10. The study in FEM software about the behaviour of the material under this physical phenomena takes another level of importance while verifying quality and good performance of the structures, because in multiple occasion the damage caused by an impact only occurs inside the piece, so it can not see by the human eye, and in structures application for the aerospace industry this can have really dangerous consequences.

Developing numerical methods that are able to predict the behaviour of the different composites material against impact situations is a key thing. Many researchers have used commercial Finite Element packages such as LS-Dyna[1] and Abaqus to model the impact response of sandwich panels [87, 68, 78, 82, 25, 16]. The combination of improved constitutive modelling of constituents and decreased computational costs make it possible to utilise continuum modelling of composites to simulate the macroscopic impact response. The simplest models consider only the elasticity of the composite and more complicated material laws take into account a large number of phenomena such as damage and viscoplasticity. Most of the composite material models in FE codes are phenomenological models that describe the global constitutive behaviour as it is difficult to model every type of damage and its subsequent softening effects in a complicated 3D microstructure with micro-mechanics models. The plasticity models, for instance, describe the non-linear deformation through a stress strain relation measured at the macroscopic level. Also, in literature more simple models can be find whose target is a quick computation. For example, stress and displacement in 2D unidirectional FRP, like the one presented for Beyerline and Landis in [12]. Their model is based in the virtual work and FEM. It is said to be *'an important prerequisite for simulations and modelling of random fracture patterns, as would naturally develop in a real composite'* under tension or compression load. In particular to compute displacements and axial stresses in fiber and matrix.

2.3.1 Damage modelling

The behaviour of composite structures including the effects of damage is very complex and is dependent on a range of parameters including the geometry, material, lay-up, loading conditions, load history and failure modes. A complete constitutive model of composite material that can predict the mechanical

[1] Commercial explicit finite element software.

performance and the development of damage leading to failure is still an ongoing research endeavour. Damage, generally, can be divided in two big categories inter-laminar failure, such as delamination and intra-laminar failure, fiber or matrix breakage, fiber-matrix de-cohesion [64]. Normally, a well designed lamina has its fiber failure mode, both compression and tensile load, controlled by its proper ultimate load. Matrix cracks are the initiation of lamina degradation. This triggers other damage events, such as delamination or debonding in the link fiber matrix[9]. Also, cracks allows the penetration of liquid and contaminant gases that degrade the fibers and their interface with the matrix. This leads in the necessity of recreate matrix cracking in the numerical models to obtain accurate results. An accurate prediction of damage evolution lies in the appropriate choice of the material length scale. Nowadays the damage is normally study in micro-scale, meso-scale or macro-scale also know as structural-scale. Composite are usually quasi-brittle materials, in those cases, damage is a non-local event whose evolution depends in the interplay material-structure[27]. This characteristic represents a problem with the various scales of resolution, because as Forghani et al. say in their paper[27]: *'some averaging schemes becomes questionable as the characteristic material length, which is linked to the constitutive model at the macro-scale, cannot be built up from lower scales in a hierarchical manner'.*

Fracture mechanics and damage assessment is such an important issue, that there have been three *World wide Failure Exercise* (WWFE) congresses by the time. In the WWFE-II (part b) twelve leading failure criteria, to predict the response of FRP when they are subjected to stress, were compare[34]. With the results a ranking bases in quantitative and qualitative parameters has been done in order to identify weaknesses and strengths of the models, being a handy resource to future selections of the appropriate model that suit best the study case. The WWFE-III's aim was to verify and benchmark the available failure models which are able to handle cracks and damage development in multi-directional FRP[35]. One of the undesired conclusions is that failure models present some difficulties to predict the inelastic behaviour of composites laminate[27].

Another phenomena that some popular method neglect is the gradual redistribution of stresses in the lamina, when the damage has been initiated. Parameters as the degradation factor that some methods use are undesirable, because they change with the ply sequence and the material. Moreover, when damage happens the stresses are redistributed into the undamaged area of the specimen. The effective stress in undamaged areas becomes higher than nominal stress. For the failures modes compression and tension have different effects, and this has to be taken into account while creating a numerical model. Also, plastic deformation occurs in undamaged areas and internal forces are supported by effective or undamaged areas [17]. So, a good constitutive model for a Fiber-reinforced materials (FRP) should include the mechanical behaviour before damage initiation, the damage initiation itself and propagation and also the postfailure behaviour[18].

A summary about the impact analysis methods and the classification to three main applied prediction methods was provided [13].

1. **Delamination threshold forces:** It is key to analyses the damage develops by the impact through analytical models. The lamina characteristics and the out of plane loading are the base of the formulas of the method. This methods was developed by Olsson, but also by Jackson and Poe. By the nature of this methods, the projected area of delamination is required to be equal to the delamination area in each interface.

2. **Cohesive zone methods (CZM):** It is indispensable in meso-scale methods, because it is the interface methods between the plies. It is used to capture the delamination damage, furthermore no initial crack is needed in this assessment. CZM can be described as a fracture-mechanical methods that represents the initiation, as well as the propagation of a crack in a chosen interface. This methods was initiated by Dugdale and Barenblatt.

3. **Continuum damage mechanics (CDM)**: It is the one use for many impact assessment methods in order to capture the intra-ply failure mode. It was proposed by Kacharov in 1958. At a later stage in the 80's decade, Chaboche and Lemaitre used CDM to solve some fatigue problems. CDM is based in the homogenization of a crack, where an effective stress is the resultant of the nominal stress multiplies by a factor of **(1-d)**. Being this factor, **(1-d)**, the ratio of remaining load and **d** the degradation status.

Ply discount method is the simplest model to simulate structural behaviour of lamina composites. But also, the least accurate model to assess matrix damage[8]. This method reproduce the damage response of each ply independently of the neighbouring ones. It is common to use cohesive interfaces in order to connect the different plies[27]. This method usually overestimates the stiffness changes which leads to large errors in energy dissipation prediction. But, its asymptotic values of modulus reduction are enough accurate. Barbero's paper [9] says that the more widespread analysis methods for composite material, in lamina way, are based on strength criteria. These methods are dependent of experimental values for strength. Their problem is that those parameters are thickness and ply sequence dependent. A better option are models based in material properties, for example the Energy criteria one. Other two good methods are Continuum Damage Mechanics (CDM) and analytical solution of stress-strain in a volume cell. Continuum damage mechanics (CDM) is able to model the initiation and development of the damage, and also the stiffness degradation. Its application is in lamina scale and reflects the failure modes [17]. As always they have their pros and cons. One of the problems with CDM is their mesh dependency, when they are locally formulated. There are some approaches to mitigate the dependency, usually relying on local theories or rescaling of damage mechanical constitutive laws [75].

The prediction of damage initiation and accumulation for lamina common polymers matrix composite has a high interest among others. PDA (progressive damage analysis) in Abaqus requires a linear elastic material for when there is no damage, in conjunction with the Hashin damage initiation criteria. The user provides to Abaqus six strength values, and four extra values of critical energy

release rate. Material models with a strain softening behaviour can produce mesh dependent solution. Abaqus reduce this dependency with the characteristic length. In this way the model goes form stress-strain to a stress-displacement constitutive model. This method determines two *in situ* strength, F_{2t} and F_6, in addition to the critical energy release rate, G^c_{mt}. When the crack occurs in the 90° ply, also when the ply is a 70°, the prediction of PDA is good. But PDA predictions are not good enough when the shear load is significant. Perhaps this is a consequence of the dependency of the shear damage variable. The method is accurate for cracking in mode I, but deficient in mix modes cases with shear. In the article [27], they improve their previous *Composite damage model*, CODAM, developed to predict non-linear in-plane response of composite by the use of continuum damage mechanics, the results is the *CODAM2*. The CODAM was mainly based in smeared crack while CODAM2 introduces a non-local regularization scheme that reduce the mesh dependency and orientation sensitivity issues. CODAM was implemented as a user material model in LS-Dyna and after that incorporate as in-build material of the program. A simplier version is available for Abaqus. CODAM2 reflects the decrease of stiffness as a consequence of matrix cracking and fiber breakage *'and, in so doing attributes distinct strain-softening curves to the fiber- and matrix-dominated stress components in each layer.'* Simon et al. [75] presented a CDM for layered composites and showed that their model is able to address interlaminar damage progression and delamination. Its formulation is based in a thermodynamical manner, relying in a thermodynamic force and a damage surface,

$$\boldsymbol{Y}_i(\sigma, d) = \rho \frac{\partial \chi(\sigma, d)}{\partial d_i} \quad \text{and} \quad f(\boldsymbol{Y}(d), \delta) = \hat{f}(\boldsymbol{Y}(d)) - \gamma(\delta). \tag{2.1}$$

The model is mesh independent thanks to a regularization scheme whose origin is the energy dissipated during cracks opening. They implemented their model in a UMAT subroutine and concluded that it *'can be applied for predicting intralaminar damage propagation as well as delamination between layers of laminated composite structure'.*

2.3.2 Challenges in modelling approaches for Natural fiber composites

As modelling of impact of composites is an emerging field, there are just a few papers in the literature on the simulation of natural fibre composites compared to number of papers and research on traditional composite materials. Even though natural fibers are the heart of current scientific concern, its mechanical properties are poorly known, despite the aforementioned efforts[58]. Natural fiber composites, in particular plants (NFC) one, have non-linear stress strain curves. The article [73] claims that this is consequence of the lower elastic strain limit those material presents, with a value of around 0,15%. This means that the plastic deformation starts actually early in the curve due to micro-damage. Such a behavior has been

linked to the presence of kink bands in the fibers, causing local stress concentrations facilitating debonding. Besides, continuous reduction of composite stiffness with growing strain, as opposed to a nearly constant stiffness of flax fibers at high strains, has been related to progressive damage of the matrix, fibers/yarns, and their interface [36]. However, Batra et al. [10] says that is common in the assessment of damage on FRP composites to neglected the inelastic behaviour. But, in the case of LVI this phenomena can be ignore because the damage and failure initiated firstly by bending stresses. According to Chen and Morozov [18] the material models that neglected the plastic effect on the failure of composite, usually underestimate the ability of energy absorption of the structure itself. This thesis is also reflected in [16]. In the article [41] they for example make this assumption. They relied in the elastic-brittle behaviour of FRP where damage initiation typically occurs without significant plastic deformation and plasticity can be neglected. Moreover, it is demonstrated that post-failure progressive degradation of stiffness, improve the predictions of the constitutive models in impact simulation and the contact force history. Therefore, a typical linear elastic assumption for the mechanical behaviour of flax fiber composites is not entirely justified and alternative constitutive laws are required to have accurate models. Mechanical behaviour of materials is typically defined as a constitutive stress-strain relation, where the stress is a function of the strain, strain rate, strain history, temperature and material properties.

There are a few articles about natural fiber composite materials focused in constitutive models of the material behaviour and simulations in steady state situations. A detailed study was conducted by Zhong et al. about Flax/PP composite, resulting in the article [88]. They perform laboratory tests and also two finite element analysis, a multi-scale and a micro-scale, both in Abaqus using a user-subroutine. In the micro-scale model Flax is considered transversely isotropic and PP isotropic linear elastic, Maximum stress failure criteria is used to describe damage initiation for the fibers, however for the matrix the criteria is a modified Von Mises. The macro-scale analysis is a progressive damage one. In this case the damage initiation and the material degradation is simulated with a USDFLD[2] user subroutine. The micro-scale FE model predicts brittle failure, which in experimental test showed similarly. Also the stiffness is well predicted. Unfortunately, the strength values have discrepancies, they assume this happens because of the linear behaviour choose. In combination both model are a good way to predict the tensile strength, peak flexure load, damage modes of Flax/PP under three-point bending loading conditions.

One of the most ambitious models is the one proposed by Ebina et al. in the paper [24]. They propose a model which is a join of three different ones, cohesive zone model (CZM), enhanced CDM (ECDM) and smeared crack model (SCM). Each of them calculate one different damage aspects of the lamina. SCM recreates fiber damage under tensile and compression stress, ECDM models in-plane cracks while CZM generates delaminations. They implemented they model with a user-

[2]It allows you to define field variables at a material point as functions of time or of any of the available material point quantities listed in the Output Variable[76]

subroutine, VUMAT[3], in Abaqus/Explicit. They used continuum shell elements, which means that out of plane components are non-existent. The total model is able to predict in a good way: the maximum impact load, the time point at the maximum impact load and the trend of delamination scope. But unfortunately, it underestimates the damage diameter of the damage area, they believed that this is due to *'the lack of definition of the interaction between matrix cracks and delamination'*[24].

Barbero et al. [9] proposed a constitutive model to *'predict stiffness reduction due to transverse matrix cracking is derived for laminae with arbitrary orientation, subject to in-plane stress, embedded in laminates with symmetric but otherwise arbitrary laminate stacking sequence'*. Their method has two well differentiated parts; the calculation of damage variables, transverse and shear stiffness reduction as function of cracking density, and the damage activation function. They concluded that the stiffness prediction of this model is accurate as well as the redistribution of the stress after analyses with the model several ply orientations and compare them with experimental test. One of the previous academics, years later, published [8].

Batra et al. [10] presents a model of elastoplastic deformation. They chose Matzenmiller as damage evolution criteria. And the derived effects are calculated using Aboudi's method, but with a correction they used *'the continuity of shear tractions across cell boundaries relaxed'*. They assumed elastoplastic deformation of matrix and elastic deformation of fiber. In this model delamination is also considered using a Cohesive zone model available in Abaqus. This model replicates in an accurate way the failure mechanisms and the history of total axial forces. It is really interesting that: *'Fibers below the impactor fail in compression, and the matrix in the bottom-most plies fails in tension.'*

Singh and Mahajan [77] presented an elasto-plastic damage model for FRP. It simulates progressive damage and damage induced for inelastic deformation as consequence of LVI. They assumed that damage is initiated and developed with permanent deformation. As damage initiates with the generation of micro-cracks, the stress is assigned to the undamaged area of the material, where damage surface and plastic surface grow. The CDM theory is based in the expression

$$\sigma = [1 - \frac{A_d}{A_o}]\sigma_e \quad \text{and} \quad \sigma_e = \frac{P}{(A_o - A_d)}, \tag{2.2}$$

where σ is the nominal stress, σ_e is the effective stress, A_o is the undamaged area, A_d is the damage area and P is the nominal force.

The model neglects the plastic deformation in fiber direction, due to the main dependency that the lamina has in the fiber for this direction. In the FEM, a VUMAT subroutine of Abaqus, Hashin's criteria initiates the intra-

[3]It is used to define the mechanical constitutive behaviour of a material, for elements C3D8R. The shear strain components in user-subroutine VUMAT are stored as tensor components and not as engineering components; this is different from user subroutine UMAT in Abaqus/Standard, which uses engineering components[76].

laminar damage, while inter-laminar damage is generated with cohesive surface formulation. The model results are loyal to reality as well as delamination.

In 2012 Chen et al. [17] published a elastoplastic model for the progressive failure analysis of composites materials. Their constitutive model is able to predict the damage initiation and also the postfailure response of composites which show plasticity behaviour. For simplicity they used an isotropic hardening law expressed in terms of plastic strain. The model was built-in Abaqus/Standar FE program by the use of the user-subroutine UMAT. In the Figure 2.6 the flow chart of the UMAT subroutine is presented. This model shows accurate predictions of failures load for carbon fiber reinforced plastic.

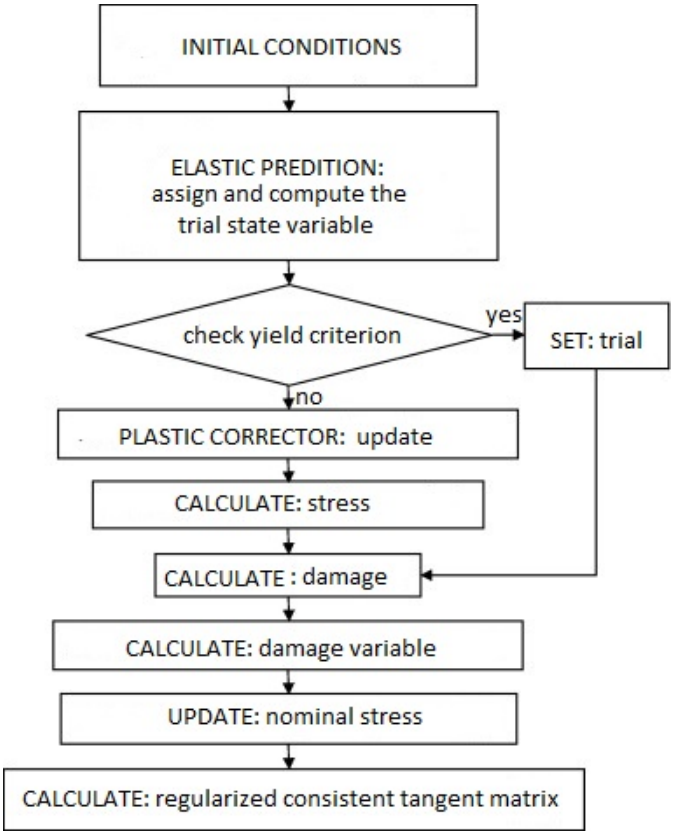

Figure 2.6: Example of a flow chart of a UMAT sub-routine[17].

Some years later they wrote the paper [18]. It is elasto-viscoplastic model thought to be implemented for structures subjected to multiple strain rates. It is based in strain rate-dependent yield criterion and for plastic loading-unloading it is used the Kuhn-Tucker condition. Same as in their other model, they implemented this in a UMAT sub-routine. Though the elastoplastic and elasto-viscoplastic models developed were for traditional composite materials, they can be adapted for use in natural fiber composites.

Similar to non-linearity, the strain-rate dependency of composites material is not always considered in doing impact simulations [18]. FRP are time dependent in most of the cases, due to their polymeric matrix. Their behaviour is viscoelastic,

they are dependent of the microstructure. Rami M. Haj-Ali and Anastasia H. Muliana [28] present a condensed and complete review of viscoelastic models and studies performed about composite materials during recent history. The first one was conducted by Lou and Schapery in 1957, which laid the foundations for later research based on it. Although, the article is focus on the creation of an integrate micromechanical and structural model for non-linear viscoelastic assessment for lamina composite materials. They concluded that the non linear viscoelastic response of fiber reinforced polymers (FRP) material can be calibrated thanks to the overall creep response of the lamina's off-axis response. They were able to implement their model into a Finite element one in an Abaqus' user-subroutine, UMAT[4]. Micromechanical viscoelastic models have a clear advantage over homogenized anisotropic viscoelastic models. This is because the time-dependent behaviour of polymers matrix has unique attributions. The equation

$$\epsilon^t \equiv \epsilon(t) = g_0^{\sigma^t} D_0 \sigma^t + g_1^{\sigma^t} \int_0^t [\Delta D^{\Psi^t - \Psi^\tau} \frac{d(g_2^{\sigma^t} \sigma^t)}{d\tau} d\tau]$$
$$\text{and} \quad \Psi^t \equiv \Psi(t) = \int_0^t [\frac{d\xi}{a_\sigma^{\sigma^\xi} a_T^T a_e} d\tau]. \tag{2.3}$$

(Where: D_0 is instantaneous uniaxial elastic compliance, ΔD is the uniaxial transient compliance, g_0, g_1, g_2 *and* a_σ are nonlinear viscoelastic parameter, a_σ, a_T *and* a_e are the stress, temperature, and aging time-scaling factors and Ψ is the reduced time.)

is the expression of the single integral constitutive model, a non linear viscoelastic model, created by Schapery in 1969[28]. This models was later generalized improving it with the material aging. And also, they are strong conditioned by the previous thermomechanical state, load state and environmental conditions. The dependency on environmental effects is higher in amorphous polymers, because temperature and moisture enhances the non-linearity of deterioration and deformation phenomena. On the other hand, unidirectional FRP are rarely affected in the axial stiffness and strength by time-dependency, thanks to the elastic behaviour of the fibers. Liang et al. [43] also noted that there was not a significant rate dependence at low velocities and that the behaviour of flax/epoxy composites could be predicted by their quasi-static response. Material becomes stiff during aging according to Struik, in Haj-Ali paper [28]. The equation that represent the transient creep strain proposed by him is

$$d\lambda = a_{t_e}(t)dt, \quad a_{t_e}(t) = (\frac{t_e}{e_e + t})^\mu, \quad \text{and} \quad \mu = -\frac{dlog(a_{t_\epsilon})}{dlog(t_\epsilon)}. \tag{2.4}$$

(Where: t_e is he aging time at the start of the test and μ is the logarithmic shift rate.)

[4]It can be used to define the mechanical constitutive behaviour of a material.[76]

Polâine et al. [58] developed a phenomenological model in order to find the elastic, viscoelastic and viscoplastic components parts for the mechanical behaviour of the fibers. Their model is based on eight independent variables and their are substantiated in experimental data. The main outcomes obtained are that the viscoelastic effects at room temperature (20°C) are negligible, while the non-linear effects are consequence of the viscoplasticity of the material. These effects are duplicated by two hardening phenomena combination, one linear describing the translation of elastic domain and the second one non-linear which describes the a coupling between translation and contraction of elastic domain. Their model is developed from

$$\epsilon = \epsilon^e + \epsilon^{in} = \epsilon^e + \epsilon^{ve} + \epsilon^{vp}, \tag{2.5}$$

where ϵ^e is the instantaneous reversible strain, ϵ^{ve} is the time-dependent reversible strain (viscoelastic contributor) and finally ϵ^{vp} is the time-dependent irreversible strain (viscoplastic contributor). As the article concludes the numerical model simulates correctly the behaviour of Flax/epoxy for progressive loading, creep test and relaxation test. They confirm that the first region of tensile curves is quasi-elastic against the second region which is viscoelastoplastic. For simplification purpose they not include inter-face fiber matrix mechanism.

Another article that proposes a constitutive rheological model for flax's behaviour is [69]. Viscoplastic and viscoelastic effects are shown in NFC during different experimental test. Their model target is to predict the viscoplastic behaviour of NFC form with PLA matrix and flax, jute or cotton fiber. The model is describe in three different branches in parallel (Figure 2.7), where each of them represent a different behaviour of the material. The first branch is a Yeon model, it represents the non-linear effects based in rubber behaviour using the strain energy density function. The second one is a Maxwell model which introduces the viscous behaviour by a spring and a damper in series. And finally the third one includes the plasticity by a friction model, similar to the Maxwell one, it is a spring and a frictional element in series. Yeoh and friction branch are told to be strain rate independent. The model was calibrated by three different tests, two relaxation test and a quasi-static one. It can be consider validated, although its predictions are not perfect, even so flax and jute composites are better predicted than cotton.

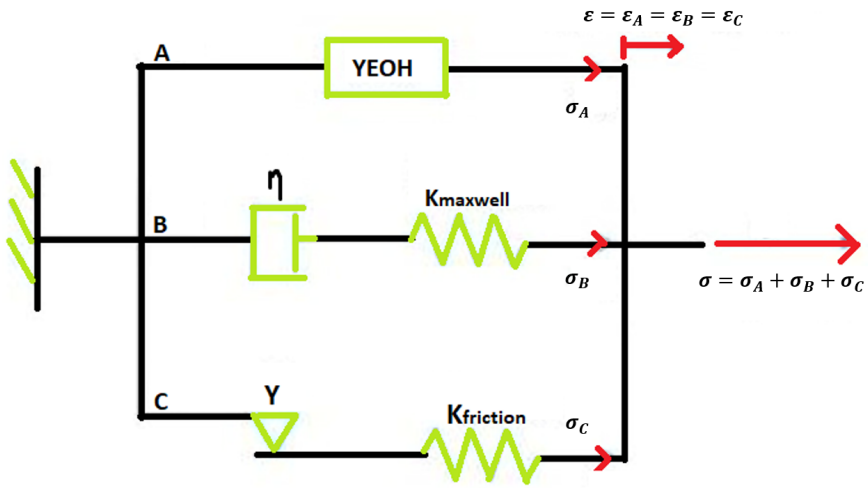

Figure 2.7: Rheological model scheme. (**A:** non-linear, **B:** viscous effects and **C:** plasticity) [69].

Draw from the aforementioned article [69], another article was publish. The article [33] uses their constitutive model to study the performance of Flax/PP submitted to a LVI. Its conclusions are that the numerical model overestimated damage area for low impact energy while underestimated it for impact energy close to penetration one. But contact force, absorbed energy and failure modes are well predicted for it. One of the paper more close to the aim of this thesis is the article wrote by M.Abida et al. [1]. They develop a 3D elastic-viscoplastic model, it includes the orthotropic elasticity and the anisotropic viscoplastic behaviour of Flax/Epoxy. The hardening uses in the model is isotropic with Hill criterion and it is optimized with the Johnson-Cook exponential law. The model is implemented in an UMAT subroutine, via Abaqus/Standard. The conclusion they reached is that the impact velocity has a high influence in the response of the plate. They obtained some undulations in the simulation curves, which they determined that are a consequence of the rigidity of the plate.

2.4 Summary

In this chapter, a detailed introduction to a new class of composites with fiber reinforcements derived from plants was provided. In particular, it was shown that flax fiber reinforced composites have been identified as a potential replacement of glass fibers in structural composites. This is mainly, due to the excellent specific properties of the flax fiber composites. However, impact damage is a strong limitation of FRP composites due to their complex damage modes include matrix cracking, delamination, fibre breakage and debonding. The study of impact resistance of composites is typically done experimentally, but numerical modelling provides an efficient alternative to expensive testing. Many researchers have developed numerical methods that are able to predict the impact response of the

different composites using commercial Finite Element packages such as LS-Dyna and Abaqus. Despite the many years of research, accurate numerical simulation of impacts are still a challenge. One of the particular challenges with modelling natural fiber composites is that the mechanical behaviour is non-linear for even small strains and that typical models do not consider phenomena like plasticity and viscoplasticity. New constitutive laws that can capture the physical phenomena occurring in the composites during high strain rate loading, including different modes of damage, need to be developed and validated. This topic is important to increase the widespread adoption of these new environment-friendly materials. In the following chapter, a numerical methodology based on Finite Element Methods is used to study the impact of traditional composite materials to be a reference case.

Chapter 3

Simulation of low velocity impact of Kevlar composite

It is evident from the literature review presented in the previous chapter that the numerical simulation of impact of composites is not a trivial task. As the article [13] by Raffael Bogenfeld mentions *'achieving satisfactory results requires massive computation and modeling efforts'*. The target of this chapter is to identify all the parameters required to perform a low velocity impact simulation of a fiber reinforced composite. A composite with Kevlar fiber reinforcements in an epoxy matrix is chosen for the study based on the experimental study and numerical analysis of similar composites published as: **The influence of acrylate triblock copolymer embedded in matrix on composite structures' responses to low-velocity impacts** and **Finite element modelling of the low velocity impact response of composite plates with block copolymer nano-reinforcements**by Denneulin et al. [22] and Ramakrishnan et al. [60] respectively. The geometry and the material parameters were selected from these articles. This allows to check the veracity of the different material parameters and to validate the numerical methodology.

3.1 Model description

The Finite Element software Abaqus was chosen for the numerical simulation. Abaqus Software is a product of: *Dassault Systemes SIMULIA Corporation* and is a general purpose finite element code capable of simulating a wide variety of problems. The FE modelling of large deformation dynamic problems such as the impact case require the use of Explicit domain of the Abaqus software. This is necessary because time variable cannot be neglected in order to simulate properly the impactor's inertia influence in a LVI. The explicit time integration also has fewer problems with convergence compared to an implicit integration.

The experimental case was done with a plate form by 3 layers of woven Kevlar 129 fabric, with $[0/90]_3$ layup, (Saatilar Style 802; taffeta 190 g/m^2; thickness: 260 μm) in a thermoset epoxy precursor DGEBA matrix. This fabrics were

selected to be able to balanced ply properties and improved interlaminar features in comparison with a unidirectional layup [22]. Kevlar[1] is a polyamide synthetic fiber, its main advantage are its strength and its manufacturing which is easy. Epoxy is a thermostable polymer, it possesses high mechanical and thermal strength and good mechanical features.

The low velocity impact testing of the Kevlar composites were accomplished using a drop tower. A schematic setup of the drop tower is shown in Figure 3.1. A hemispherical steel impactor was dropped with two initial velocities of 3,13 and 4,43 m/s, respectively. The impact tests has an initial energy of approximately 8 and 16 J, respectively.

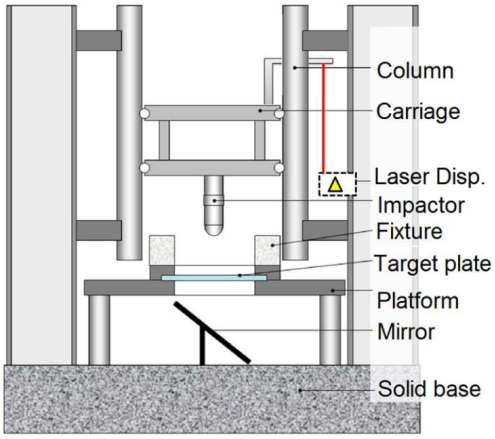

Figure 3.1: Drop tower setup of the experimental test[60].

The problem consists in a impactor with *hemispherical* shape over a square composite plate embedded between two fixtures, as the figure 3.5 shows. The setting components dimensions and properties bounded are the following ones:

- Striker/impactor (bullet shape):
  - Diameter equal to 16 mm.
  - Length equal to 16 mm.
  - Mass of 1,77 kg.
- Fixtures:
  - Length 125 by 125 mm.
  - Thickness of 5 mm.
  - Diameter of the inner circle 70 mm.
  - Mass of 20 kg.
- Plate:

[1]It was synthesized for Stephanie Kwolek in 1965, for the first time.

- Length 100 by 100 mm.
- Thickness 0,8 mm.
- Material is Kevlar/epoxy, its properties are presented in the table 3.4

The figure 3.2 shows the force value obtained by the article [60] during the laboratory test, this force is going to be the reference of this chapter. From the force vs. time curve shown for kevlar impact, four phases can be identified: (i) Elastic bending of the plate, where the force increases progressively until the force reaches 1 kN, (ii) first decrease in the rigidity of the sample due to damage initiation in the composite structure. These damages are mainly matrix cracking and are responsible for a small change in slope, (iii) the force decreases significantly because of the damage propagated in the structure, evident in fiber breakage in the localised region of impact, and finally (iv) a last phase corresponding to the residual strength of the plate and the dry friction during penetration.

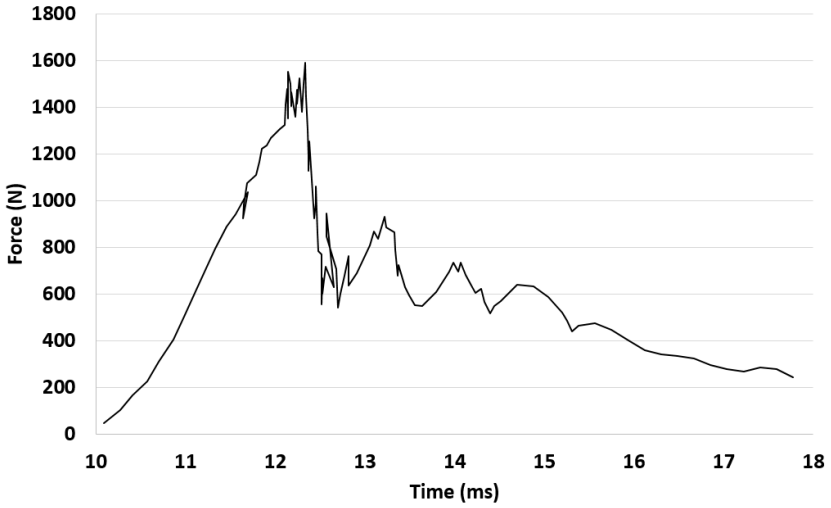

Figure 3.2: Contact force of the experimental test[60].

3.1.1 Geometric modelling

The generation of the model geometry and defining of material properties involves different steps. First of the **Abaqus' Modules** is the **Part module**, in which three different geometries corresponding to the fixtures, the striker and the composite target are are modelled with appropriate dimensions. The fixtures and impactor are modelled as discrete rigid parts. That means that material properties are not needed. Only, the mass that must be given in the part's center of mass. Meanwhile, the plate is defined as a deformable shell for the variants 3.2.1.2, 3.2.2.1 and 3.2.4.1, and the rest are modelled as a deformable solid. This choice resonates in the **Property module** and in the constitutive equation behind the results, the target is to assess how much the results are deteriorated by neglecting the out of plane conditions.

Shell elements are use when the third direction dimension is significantly smaller in comparison with the in plane dimension. The plate of this chapter meets this condition, its dimensions are 100x100 mm against 0,8 mm of thickness. This discretization of a body use *Conventional shell* elements. The geometry is a reference surface and its thickness value is introduced through the **Property module**.

In opposition to shell parts there are solid parts. In this case the entire 3D body is discretized by the use of *Continuum Shell* elements. The part thickness is defined in the element nodal geometry. The elements only count with displacement degrees of freedom (DOF), while *Conventional shell* ones have in addition rotational DOF (Figure 3.3). *Continuum shell* elements seems like 3D *Continuum solids*, but kinematic and constitutive behaviour are closer to *Conventional shells*. *Continuum shell* elements are based in first-order layer-wise composite theory, they reproduce the effects of transverse shear deformation and the possible thickness changes suffered by the specimen.

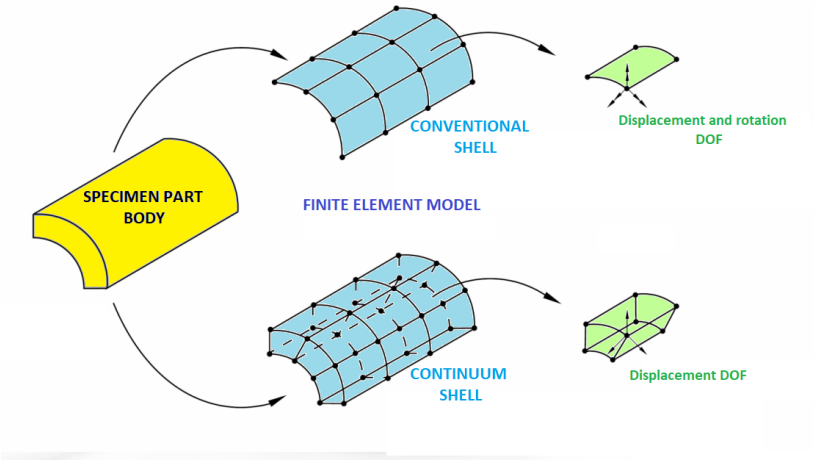

Figure 3.3: Conventional vs continuum shell element[76].

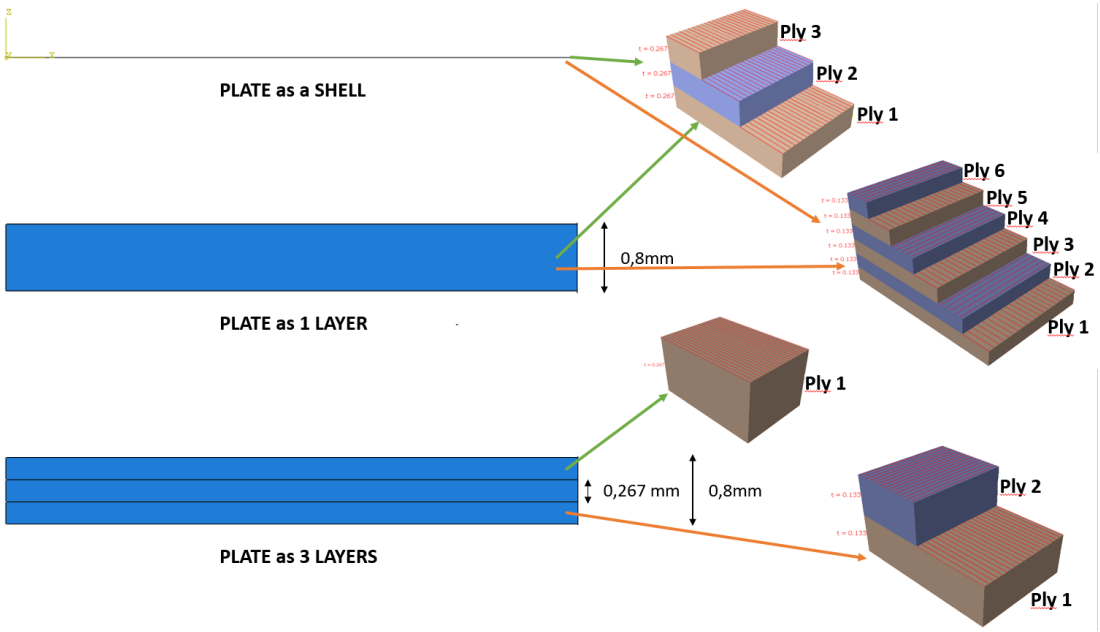

Figure 3.4: Shell, 1 layer and 3 layers plate vs ply. (Clarification about the difference in this thesis between layer and ply)

The final assembly for the simulation is shown in the Figure 3.5. In it the two fixtures (top and bottom), the impactor and the plate are shown.

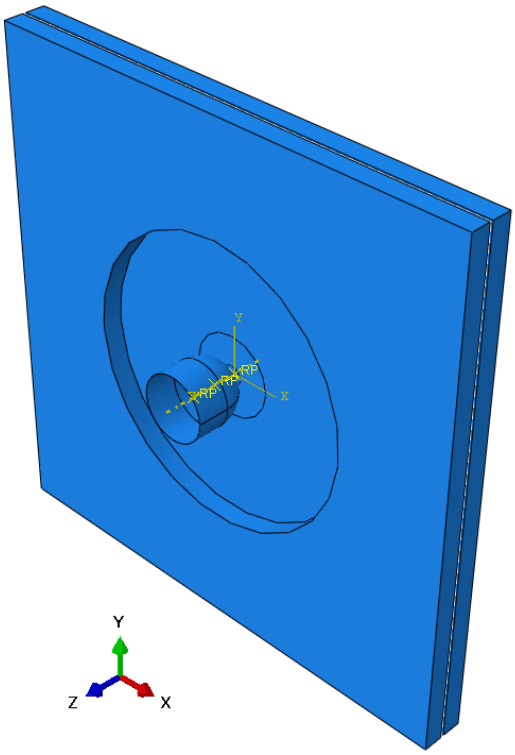

Figure 3.5: Assembly of finite element model of Kevlar/Epoxy.

This chapter is divided in three main sections looking at different element

formulations:

Plate property as *isotropic material*: 3.2.1. This section has two variants, one modelling the plate as a shell and a second modelling it as a solid.

Composite layup $[0]_3$: 3.2.2. This section has three variants, one modelling the plate as a conventional shell and two modelled as continuum shell, with the different that one is a single layer with 3 plies and the other are 3 layers with 1 ply each. (Figure 3.4)

Composite layup $[0/90]_3$: 3.2.4. This section has the same variants than the 3.2.2 excluding the layup. The continuum shell variants are a single layer with 6 plies and the other are 3 layers with 2 ply each. (Figure **??**)

3.1.2 Contact and boundary condition

The boundary conditions of the model and the velocity of the impactor are defined in **Load module**. The speed was set in *Predefined field manager*, as a linear speed of 3,13 m/s applied in the gravity center of the striker. The boundary conditions were imposed in the tool with the same name, they are applied in centre of gravity of the parts. The fixtures are encastred and the striker is only allowed to move in the z-direction.

Finally, contact interaction are defined. This problem required the definition of two different type's of contact, one between the plate and the fixture, a second one between the striker and the plate. Moreover, for some of the problem's variant, a third contact is required between the layers of the plate. These contacts are define in the **Interaction module**. Also, it is necessary to assign *Rigid body* constrain to the fixtures and the impactor, respectively, in order to define correctly them.

Table 3.1: Contact parameter: Layer to layer

Tangential behaviour	Frictionless
Normal behaviour	
Pressure overclosures	Hard-contact
Constraint reinforcement method	Default
Cohesive behaviour	
Any slave nodes experiencing contact	Default method
Damage	
Initiation	
Criterion	Max. nominal stress
Normal	33 MPa
Shear 1	54 MPa
Shear 2	54 MPa
Evolution	
Type	Energy
Softening	Linear
Mix mode behaviour	Power law, Energy
BK exponent	1,45
Fracture energy	
Normal	330 mJ
Shear 1	800 mJ
Shear 2	800 mJ
Stabilitation	
Viscosity coeff.	$1 \cdot 10^{-9}$

Table 3.2: Contact parameter: fixture and plate

Tangential behaviour (Penalty)	
Friction coeff.	0,6
Fraction of characteristic surface dimension	0,005
Normal behaviour	
Pressure overclosures	Hard-contact
Constraint reinforcement method	Default

Table 3.3: Contact parameter: Impactor and plate

Tangential behaviour (Penalty)	
Friction coeff.	0,3
Fraction of characteristic surface dimension	0,005
Normal behaviour	
Pressure overclosures	Hard-contact
Constraint reinforcement method	Default

3.1.3 Mesh definition

Mesh module perhaps is the one that has more impact in the simulation results. Different parameters must be selected in order to obtain accurate results, and to avoid the program abortion. To create a mesh the element size, the element distribution and the shape of the elements must be selected. In addition, others hidden parameters must be checked. In the tool *Assign element type*, there are three main parameters that have to be picked, the *Hourglass control*, the *Element deletion* and finally the *Max degradation*(D_{max}).

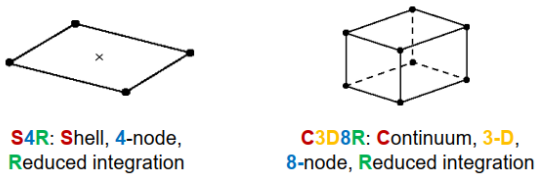

Figure 3.6: S4R vs C3D8R elements[76].

The plate's partition has also been studied. Several ways to divide the plate were proved, with the aim of avoiding *Extremely distorted element* problem. Finally, two circles (with radius 10 mm and 2,5 mm each) in the center of the plate (Figure 3.7a) were chosen as partitions. The mesh definition was *Hex, Sweep, Advancing front* and its aspects is shown in the figure 3.7b. The Abaqus' documentation[76] says that *The software creates swept meshes by internally generating the mesh on an edge or face and then sweeping that mesh along a sweep path.* The *Stack orientation* must be checked, all the element of the same face must have the same orientation. Finally, the *hourglass parameters* were selected. Of the three options given by Abaqus, the appropriate option for our problem was *Enhanced* hourglass mode.

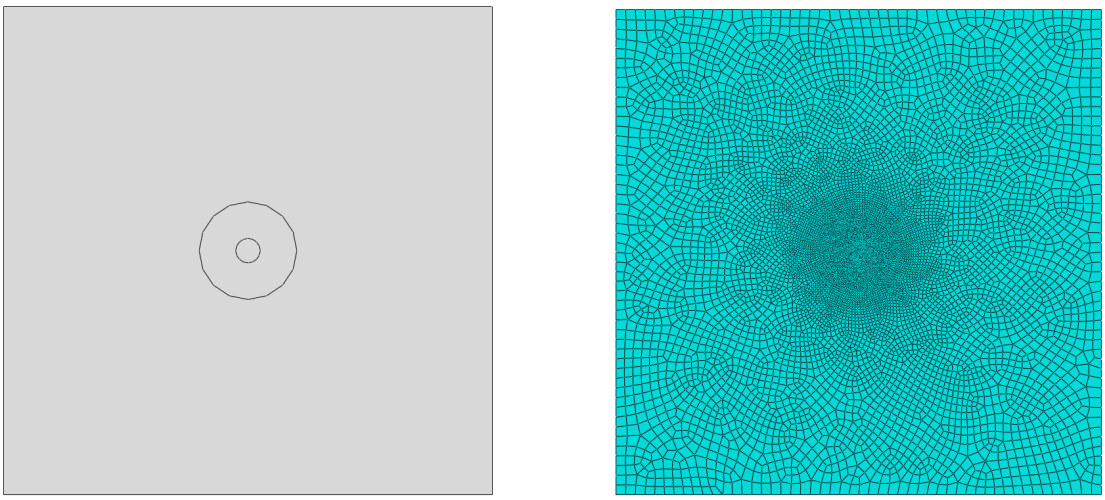

(a) Partitions in the plate. (b) Plate meshing .

Figure 3.7: Mesh.

3.1.4 Material model

The Kevlar composite was modelled using elastic lamina properties for a $[0/90]_3$ laminate in longitudinal and transverse directions and strength values in tension and compression. The table 3.4 shows the properties of the Kevlar FRP obtained from the literature that were used in the model.

Table 3.4: Material properties of Kevlar/epoxy composite [60]

Mechanical Properties	Kevlar/epoxy
Density, ρ (kg/m^3)	$1,22 \cdot 10^3$
Longitudinal modulus, E_1 (GPa)	34,5
Transverse modulus, E_2 (GPa)	34,5
Major Poisson's ratio, ν_{12}	0,07
In-plane shear modulus, G_{12} (GPa)	2,96
Shear modulus, G_{13} (GPa)	4
Shear modulus, G_{23} (GPa)	4
Longitudinal tensile strength, X_T (MPa)	480
Longitudinal compressive strength, X_C (MPa)	266
Transverse tensile strength, Y_T (MPa)	480
Transverse compressive strength, Y_C (MPa)	266
Longitudinal shear strength, S_{12} (MPa)	40
Transverse shear strength, S_{23} (MPa)	40
Longitudinal tensile fracture energy (mJ)	80
Longitudinal compressive fracture energy (mJ)	80
Transverse tensile fracture energy (mJ)	0,2
Transverse compressive fracture energy (mJ)	1
Viscosity coef. in Long. tensile Dir.	$1 \cdot 10^{-12}$
Viscosity coef. in Long. compressive Dir.	$1 \cdot 10^{-12}$
Viscosity coef. in Trans. tensile Dir.	$1 \cdot 10^{-12}$
Viscosity coef. in Trans. compressive Dir.	$1 \cdot 10^{-12}$

The last stage related with the material definition is carried out in the output variables in the Field History variables of **Step Module**. In it the failure criteria are selected. In this thesis two types of damage parameters are input:

Damage initiation for fiber-reinforced composites: DMICRT, HSNFTCRT, HSNFCCRT, HSNMTCRT and HSNMCCRT.

Damage evolution and element removal for fiber-reinforced composites[2]: DAMAGEFT, DAMAGEFC, DAMAGEMT, DAMAGEMC and DAMAGESHR.

The first group of output variables *Damage initiation* according to Abaqus' documentation *'refers to the onset of degradation point'*[76]. They are based on

[2]DAMAGEFT (fiber tension), DAMAGEFC (fiber compression), DAMAGEMT (matrix tension), DAMAGEMC (matrix compression) and DAMAGESHR (shear).

Hashins' theory (1980: setting α as 0) which has four initiation mechanisms[3]:

Fiber tension (HSNFTCRT): if $\sigma_{11} \geq 0$

$$F_f^t = \left(\frac{\sigma_{11}}{X^T}\right)^2 + \alpha \left(\frac{\tau_{12}}{S^L}\right)^2 \tag{3.1}$$

Fiber compression (HSNFCCRT): if $\sigma_{11} < 0$

$$F_f^c = \left(\frac{\sigma_{11}}{X^C}\right)^2 \tag{3.2}$$

Matrix tension (HSNMTCRT): if $\sigma_{22} \geq 0$

$$F_m^t = \left(\frac{\sigma_{22}}{X^T}\right)^2 + \left(\frac{\tau_{12}}{S^L}\right)^2 \tag{3.3}$$

Matrix compression (HSNMCCRT): if $\sigma_{22} < 0$

$$F_m^c = \left(\frac{\sigma_{22}}{2S^T}\right)^2 + \left[\left(\frac{Y^C}{2S^T}\right)^2 - 1\right]\frac{\sigma_{22}}{X^C} + \left(\frac{\tau_{12}}{S^L}\right)^2 \tag{3.4}$$

The second group of output variables *Damage evolution and element removal* according to Abaqus' documentation *'assumes that damage is characterized by progressive degradation of material stiffness, leading to material failure'*[76]. The damage variable follows a curve form by two slopes, as the Figure 3.8 shows, it is based in Davila and Camanho energy dissipated law, presented in their work of cohesive elements.

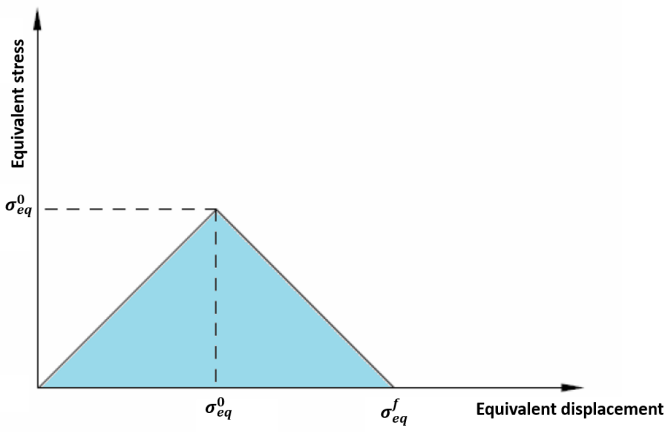

Figure 3.8: Equivalent stress versus equivalent displacement[76].

[3] X^T is the longitudinal tensile strength; X^C is the longitudinal compressive strength; Y^T is the transverse tensile strength; Y^C is the transverse compressive strength; S^L is the longitudinal shear strength; S^T is the transverse shear strength; α is the coefficient that determines the contribution of the shear stress to the fiber tensile initiation criterion; and σ_{11}, σ_{22} and σ_{12} are components of the effective stress tensor.

The way of obtain the damage variables for each particular mode is

$$d = \frac{\delta_{eq}^{f}(\delta_{eq} - \delta_{eq}^{0})}{\delta_{eq}(\delta_{eq}^{f} - \delta_{eq}^{0})}, \tag{3.5}$$

where δ_{eq}^{0} is the initial equivalent displacement at which the initiation criterion for that mode was met and δ_{eq}^{f} is the displacement at which the material is completely damaged in this failure mode. The damage is iniciated when $\delta_{eq} \geq \delta_{eq}^{0}$.[76]

Typical results of the simulation of an impact on a Kevlar composite plate for an initial velocity of 3,13 m/s is shown in Figure 3.9. It can be seen that the force time history shows that the contact force increases up to a peak force of 2000 N and then the force decreases back to zero denoting unloading of the plate. It can be seen that the total contact duration is approximately 10 milliseconds. The contour plot of the displacement at maximum displacement (i.e. when the impactor reaches the lowest position before rebounding) shows a local displacement at the point of impact of 9.6 mm but there is also global deformation of the plate till the edge of the clamp.

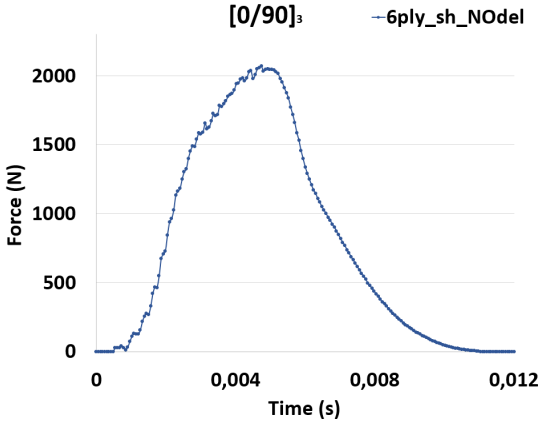

(a) Force vs. time.

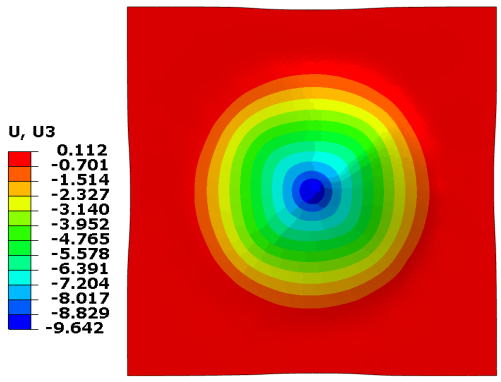

(b) Maximum displacement (mm).

Figure 3.9: For a simulation without element deletion, $[0/90]_3$.

It should be noted that in this case, the parameter *Element deletion* in the mesh control parameters of the plate is set to NO and there is no erosion of elements that have failed. A similar model with *Element deletion*, in which elements that get truly deformed during the simulation disappear, to avoid problems or fake solution. The parameter *Max degradation* is used to reaches a solution avoiding computational problems of the software[76]. This parameters was determined with these simulations. It is set in a value 0,9. In this way, the element is removed when all the failures modes reach the value D_{max} selected. The Figure 3.10 show the curves force-time and the maximum displacements suffer by a conventional shell plate with element deletion. As it can be seen there are major differences that make the *No deletion* case worst predicts the response of the plate. Although both curve until the peak force have a similar slope, the peak force of the *No deletion* curve value is higher than the *deletion* case, in addition the pattern of the

curves after the maximum values is completely difference. The *No deletion* curve has a smooth decrease while the *deletion* curve has a sudden decrease followed by a decrease which has a damping behaviour. It can be seen also that the maximum displacement obtained by the *No deletion* case is smaller and it is lost the knowledge about the damage hole shape.

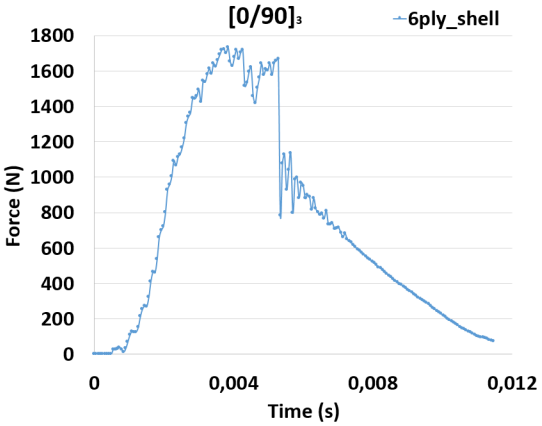

(a) Force vs. time.

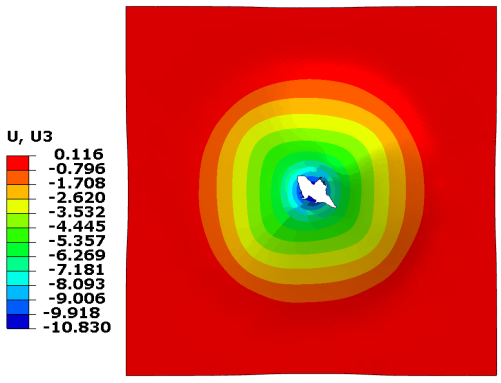

(b) Maximum displacement (mm).

Figure 3.10: For a simulation with element deletion, $[0/90]_3$.

3.2 Results and discussion

The results of Abaqus simulation for the LVI in the 8 variants are presented in this section. The main parameters of interest are the contact force (peak value), the displacement and three energies. The strain energy (U_{st}, ALLIE), the kinetic energy (E_k: ALLKE) and the artificial energy (E_{art}: ALLAE[4]). E_{art} smaller values mean that more accurate results will be obtained[5].

The progression of the impact is shown in the Figure 3.11. The images represent the z-displacement of the bottom ply of the plate during the simulation of a low velocity impact at different times. It can be seen in (a) that there is no contact between the impactor and the target as the displacement values are close to 0. At time = 0,96 ms, there is contact in the centre of the plate and we can begin to see the deformation. In the third figure representing the point of the peak force, there is cracking in the plate, in the next figure the failure crack is clearly accentuated at the point of maximum displacement. Finally, the images at the end of contact and at the end of the simulation are given showing the unloaded target.

[4]Artificial strain energy associated with constraints used to remove singular modes (such as hourglass control).[76]

[5]In the 8 variants this energy remains with a small value.

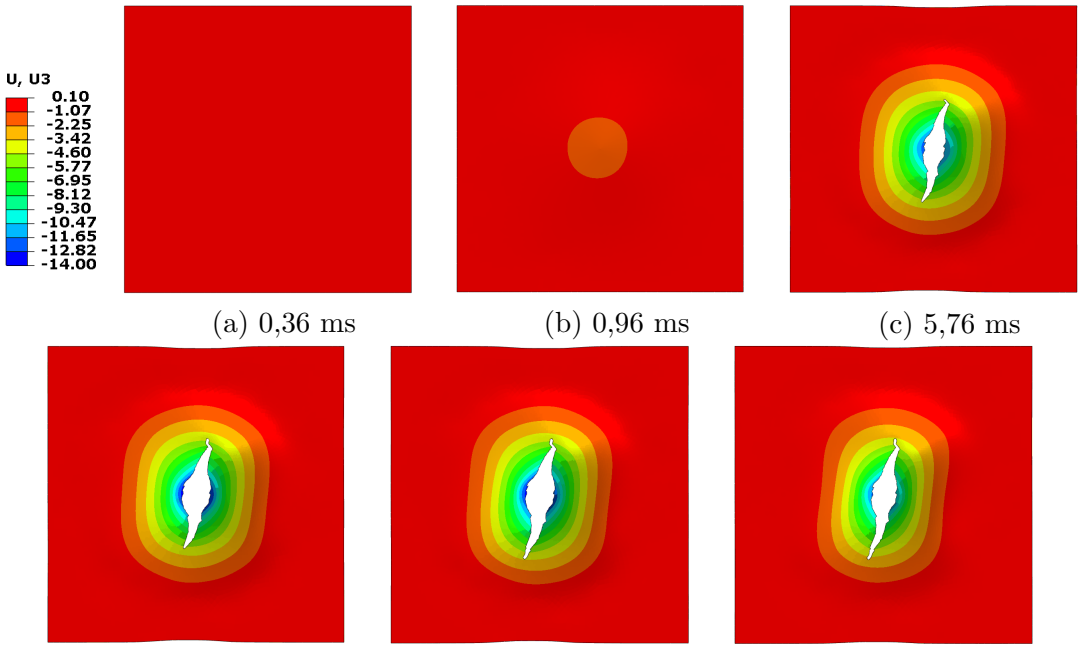

(a) 0,36 ms (b) 0,96 ms (c) 5,76 ms

(d) 7,92 ms (e) 9 ms (f) 12 ms

Figure 3.11: Progression during the simulation for the isotropic shell (Displacement [mm]).

Figure 3.12 show the paramount parameters of interest in the chapter study. The charts represents the response in contact force, displacement and energy internal (U_{st}) and kinetic (E_k) for the plate with $[0/90]_3$ layup. It can be seen that the force increases almost linearly until it reaches the peak. The drop in force corresponds to the initiation of failure. The displacement of the impactor curve shows the loading and then unloading of the plate. The initial kinetic energy of the impactor is close to 8.7 J and this energy is converted to internal energy of the plate during the impact.

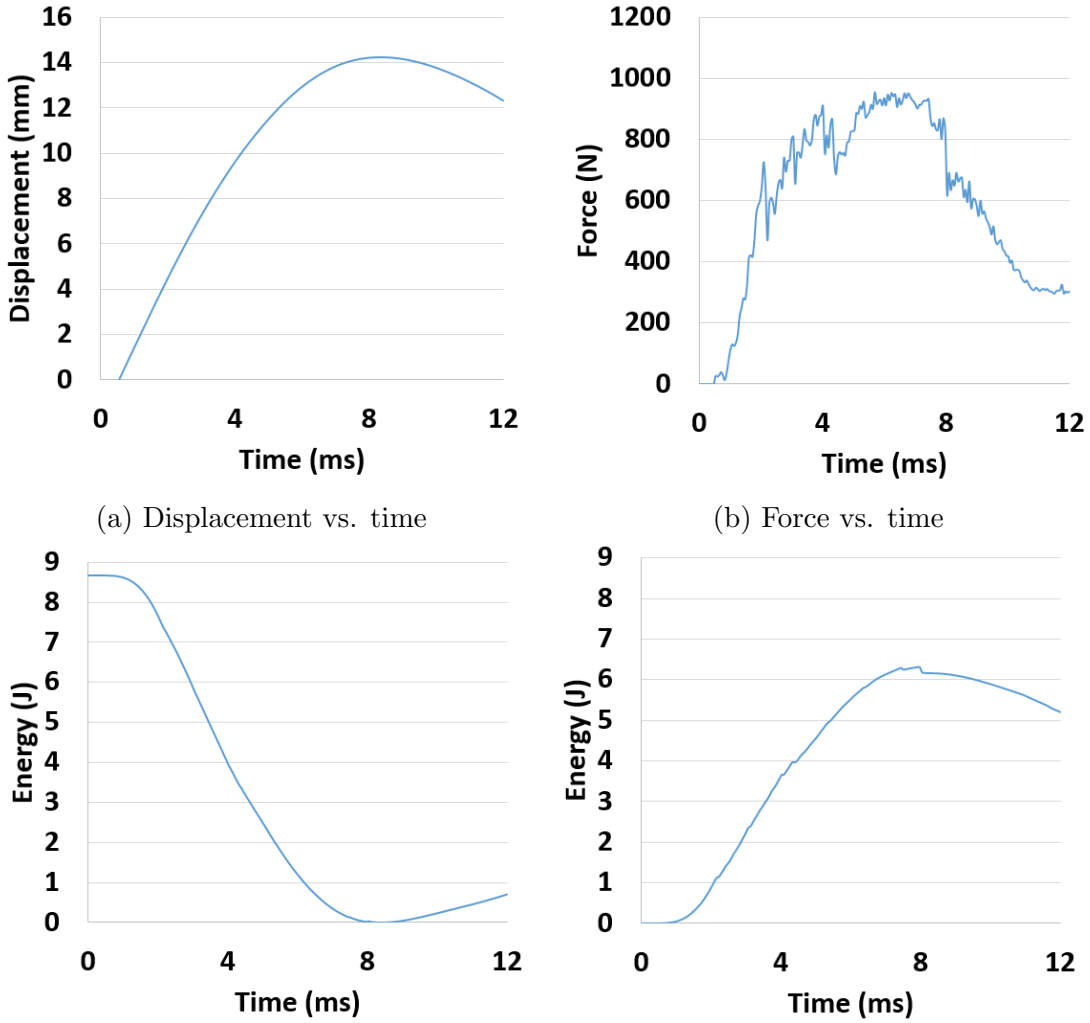

(a) Displacement vs. time

(b) Force vs. time

(c) E_k vs. time

(d) U_{st} vs. time

Figure 3.12: Displacement, contact force and energy versus time plot.

3.2.1 Plate as an isotropic material

The firstly the plate was modelled as simple as possible, a shell with thickness properties as a section. This possibility exits, because the Young's modulus in longitudinal and transverse directions are the same, as it can be seen in the table 3.4. The next variant is a bit more complicated, the plate is a solid part, but maintaining the material as a section. Also a brief comment about the distribution of the damage criteria selected, is presented per variant. (The figures of the distributions can be seen in the appendix B)

3.2.1.1 Plate modelled as a shell

The peak force (Figure B.1b) has a value of 955 N. The lower value of E_k is coincident with the highest value of U_{st} (Figure B.1a), this is the moment when

the striker bounce back. This point is also represented in the figure B.1b, when the contact force stars to decrease.

In the group of figures of the damage initiation and evolution criteria (Figures B.2, B.3, B.4, B.5) as it was expected the damage initiates in the areas surrounding the impact point and in perpendicular (in-plane) of the fiber 0°direction. The fiber compression mode has a 2wings shape, on either side of the hole, while matrix compression, fiber and matrix tension present a chromosome shape distribution. Shape and values for damage initiation are the same in both points of simulation (Figures B.2, B.3). In damage evolution there are three main distribution shapes. For the shear, fiber and matrix tension modes the shape is similar of a chromosome, but this areas have different size and values, the only modes that has area with value 1 is Shear. Matrix compression mode has the damage distributed in the area of the fixture edges and in the edge of the hole. Finally, fiber compression mode has only damage distributed in the perpendicular to the fiber direction, it is remarkable that along with the shear mode that the damage distribution grows between the maximum displacement and the final point of the simulation.

The Figure 3.13 shows the plate deformation in the point of maximum displacement and at the end of the computation. The deformation shape and the displacement value are pretty much the same on both, the maximum displacement is 13,748 mm and the end displacement is 12,106 mm which is not a big different. This could mean that the plate has not a bouncing behaviour, being 12,106 mm a permanent deformation or that the program would have needed more *step time* being 12,106 mm not the permanent displacement.

(a) Maximum

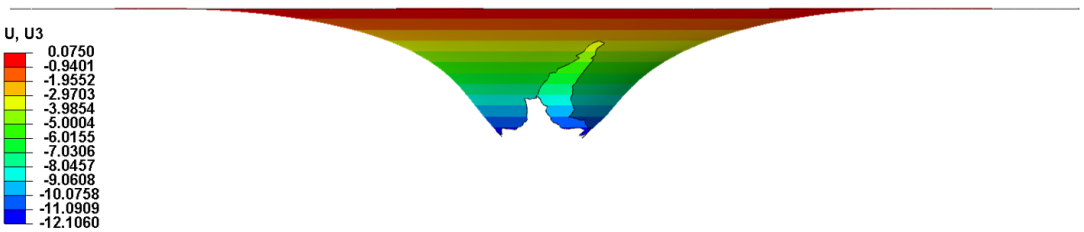

(b) At the end.

Figure 3.13: Displacement (mm) for the plate modelled as a shell with section properties.

3.2.1.2 Plate modelled as a solid

First it is notice, in comparison with the variant 3.2.1.2 is the difference in the value of the peak force. In this case has a value of 1367,454 N. Another difference is that contact force reaches the 0 value. Which corresponds with the approach of E_k and U_{st}. The bouncing behaviour of the plate is reproduced (Figure 3.14), in contrast to the previous variant (3.2.1.2).

In the group of figures of the damage initiation and evolution criteria (Figures B.7, B.8, B.9, B.10) the damage initiates again in the areas around the impact point, but in this variant against the variant , the distribution in the perpendicular fiber direction does not touch the plate edges. This time the distribution of the damage initiation modes invades more area in the fiber direction that the shell variant. Another paramount difference between the two variants is in the size of the damage evolution modes distribution. In this case the areas are substantial smaller, the matrix compression modes is the most different one. However, as well as the shell case only fiber compression and shear mode suffers and increment in area and value between the maximum displacement and end point of the simulation.

The figure 3.14 are the displacements and the deformations that the plate suffers in the simulation. The maximum displacement is 11,1426 mm, while the final displacement is 3,9511 mm. The plate recovers more half of the maximum displacement (around 7 mm). In this variant the deformation is consider permanent, because the contact force is 0 at the end of the simulation.

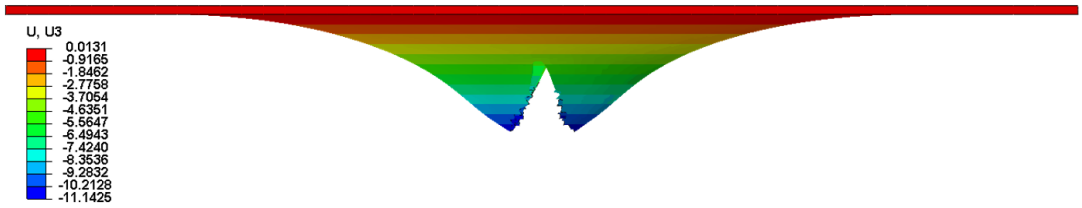

(a) Maximum.

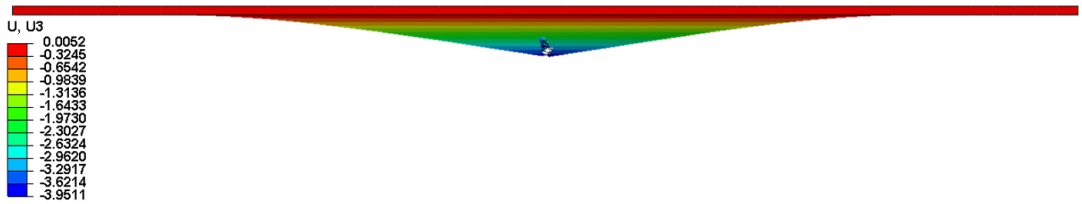

(b) At the end.

Figure 3.14: Displacement (mm) for the plate modelled as a solid with section properties.

3.2.1.3 Comparison of shell and solid isotropic models

The graphs in the Figure 3.15 shows the force against the displacement for the two variants. The two curves of the chart have the expected shape reproducing in

a good way the behaviour of the real material subjected to a LVI. But, the solid variant is much more stiffer than the shell model. As they reflect in the shell curve the peak force is considerable smaller than the solid one, making the maximum displacement bigger than the solid one, these cause that the shell curve is displace to the right and lower than the solid model.

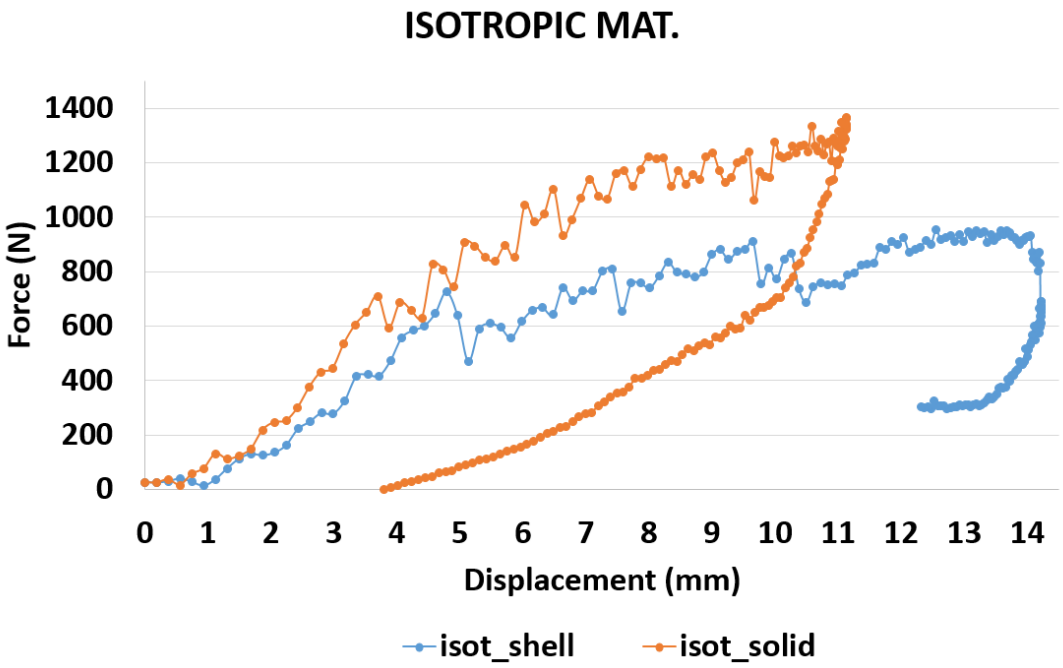

Figure 3.15: Force versus the displacement for isotropic material (shell and solid).

3.2.2 Plate layout $[0]_3$

After modeling the material as isotropic in the previous section, the model was updated by modelling the plate with composite material definition. Firstly it was modelled as a conventional shell part and after, it was improved by modelling it as continuum shell. The continuum shell plate has two variants, one has 1 layer with 3 plies and the other has 3 layers with 1 ply each. This second variant was the target to allow the delamination study. In addition to the different behaviour that each layers can have.

3.2.2.1 Plate modelled as conventional shell 1 layer with 3ply

The figure B.11 shows the energies and the contact force. The curves follow similar shape than the isotropic material case. This variant has in common with the isotropic shell (3.2.1.2) that the contact force does not reaches 0 value in the simulation. The peak force is between the isotropic cases with a value of 1109,11 N. As a consequence that the force does not reaches 0 value, E_k and U_{st} do not get closer enough.

In the group of figures of the damage initiation and evolution criteria (Figures B.12, B.13, B.14, B.15) the damage initiates again in the same areas of the plate, their shape for this variant is extremely close to the ones of the isotropic shell (3.2.1.2). And the same occurs with the distribution shape of the damage evolution modes. However this time, the *chromosome's legs* of the shear and matrix tension modes are wider, while the wings of the fiber compression mode are narrower. Again, only fiber compression and shear mode increase in size and value between the masimum displacement and end point.

In the figure 3.16 can be seen the plate deformation in the two main points of the simulation. The maximum displacement is 13,3 mm and the final displacement is 10,24 mm. As in the case of a isotropic shell (3.2.1.2) the plate's bouncing behaviour is not reproduced. Perhaps if the contact forced would reach the 0 value the bouncing behaviour would have been copied. So, again it can not be said that 10,24 mm is the definitive displacement.

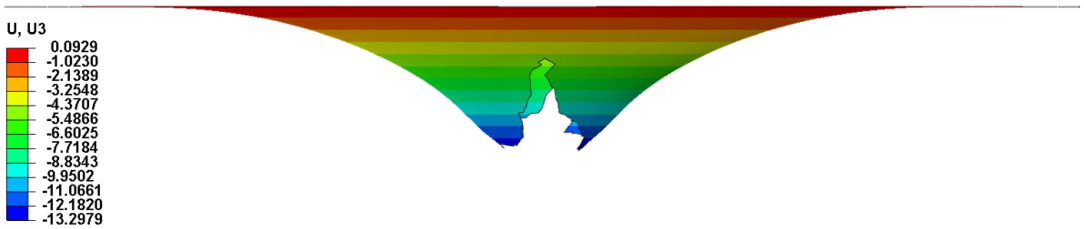

(a) Maximum.

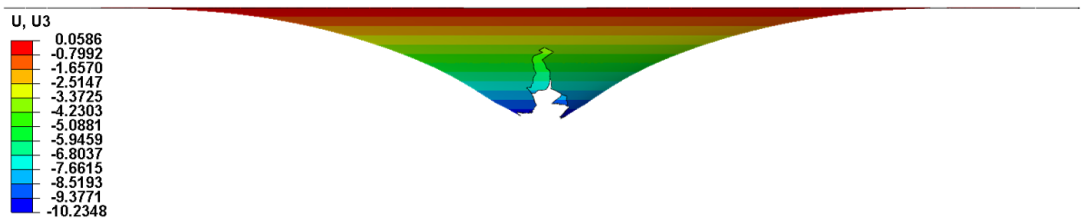

(b) At the end.

Figure 3.16: Displacement (mm) for the plate modelled as conventional shell (1 layer with 3ply).

3.2.2.2 Plate as continuum shell 1 layer with 3 plies.

In the figures B.16 are collect the contact force and the energies versus the time. The first noticeable change is that the force (Figure B.16b) this times reaches the value of 0. The E_k and U_{st} curves approach to each other while the force decreases, becoming from a certain point a constant. The peak force that the variant present is a bit lower than the isotropic solid variant, here it has a value of 1318,66 N around 40 N less than the variant 3.2.1.2. Comparing this value with the variant 3.2.2 the difference is bigger around 200 N higher.

In the group of figures of the damage initiation and evolution criteria (Figures B.17, B.18, B.19, B.20) the damage initiates in similar shape and size than the isotropic solid variant (3.2.1.2) with the difference that in this case the bottom

chromosome's legs reach the edge of the plate. Same situation suffers the damage evolution distribution modes, only the shear and matrix tensile modes have a slightly different shape. Equal to all the variant that until this part of the chapter have been carried out only the damage evolution distribution growth in shear and fiber compression modes.

In the figures 3.17 represent the displacement of the plate. The maximum displacement corresponds to a value of 11,1305 mm, while at the end the value is reduced to 4,99 mm. Similarly to the variant of isotropic solid variant (3.2.1.2) the bouncing behaviour is clear, with a difference of around 6 mm of recovery, which is a bit more than the half of the maximum displacement. The final displacement can be considered as permanent deformation because the contact force reaches 0 value.

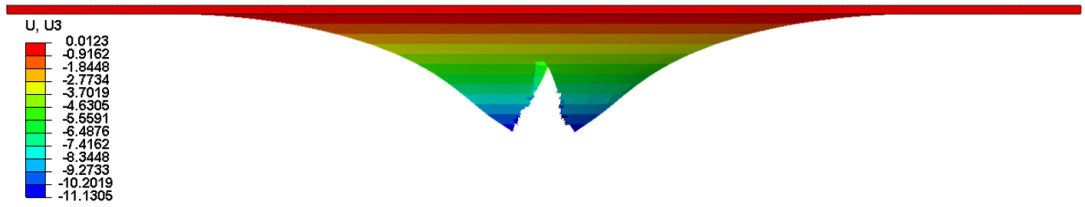

(a) Maximum

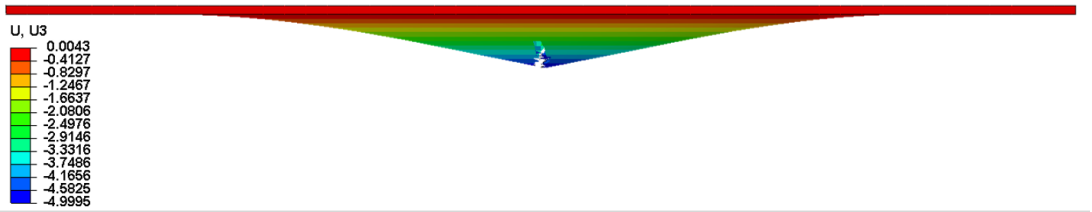

(b) At the end.

Figure 3.17: Displacement (mm) for the plate modelled as a continuum shell (1 layer with 3ply).

3.2.2.3 Plate as continuum shell 3 layers with 1 ply each.

The figure B.21 shows the energies and the contact force of the simulation. This time the forces reaches at the end the 0 value, but the curves of E_k and U_{st} does not get constant as other simulations have done. Also some characteristic are a constant in the 5 variants, until the moment presented, the point where E_k and U_{st} cross is around the value time of 0,004 close to the peak force value. This value is 1320,72 N which is a match to the value of the case3.2.2.2.

In the group of figures of the damage initiation and evolution criteria (Figures B.22, B.23, B.24, B.26) of this variant some interesting features are shown. This case makes clear that in the shell variant as well as the case with one layer representing the whole plate, the simulation only displays the behaviour of the damage criteria belonging to the bottom ply of the layup. It is evident that the damage initiation distribution for this case bottom layers mirror the ones of the variant 3.2.2.2 with

minor differences. The top *chromosome's legs* are touching the plate's edges and in matrix compression mode the X shape that exists around the hole is more obvious and bigger in size and value. In all the variants, until this moment, and in this variant bottom layer the fiber and matrix tension modes does not present damage initiation where the fixtures' edge are in contact with the plate. On the contrary, in fiber compression mode this area (circumferential shape) presents damage initiation. In the top layer this area is not affected in fiber and matrix compression, the ones affected in the bottom layer. The top layer presents damage initiation in X shape (in $\pm$ 45°fiber direction) for the fiber tension and matrix compression, being bigger in shape the area of the fiber tension mode. In matrix tension mode the damage initiation distribution shape is similar to the bottom one. Damage evolution also is displayed, in all the previous cases the behaviour of the bottom layer. The shape of the bottom layer distribution for all the modes of this variant are coincident with the ones of the variant 3.2.2.2. But like in damage initiation, the size of the distributions are bigger and top *chromosome's legs* of the modes that present this shape are touching the edge of the plate. As always the only modes that present evolution in shape and size are the shear and fiber compression, in both layers. Shear and matrix tension present similar distribution shape for their bottom and top layer, while the other modes not. Fiber and matrix compression modes distribution in top layer is essentially non-existent.

The below pictures, figure 3.18, show the plate deformation at two point of the simulation. The displacement values are 11,33 mm and 5,66 mm, respectively for the maximum displacement and the end displacement. The end displacemment can be consider permanent because the contact force is 0 at the end. As in the previous variant 3.2.2.2, the software reproduce the bouncing behaviour of the plate, in addition the displacement values are close enough between the variant.

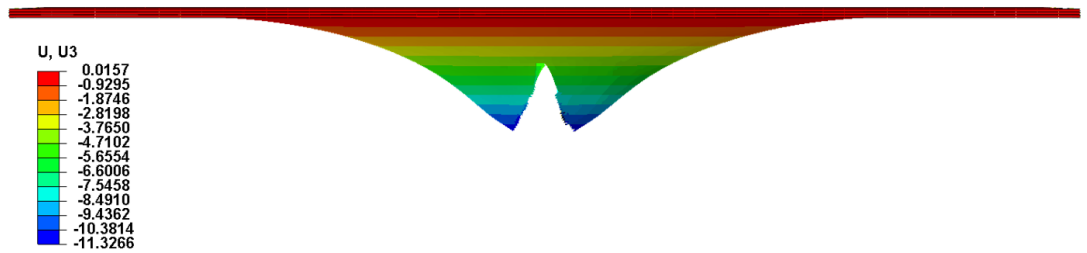

(a) Maximum.

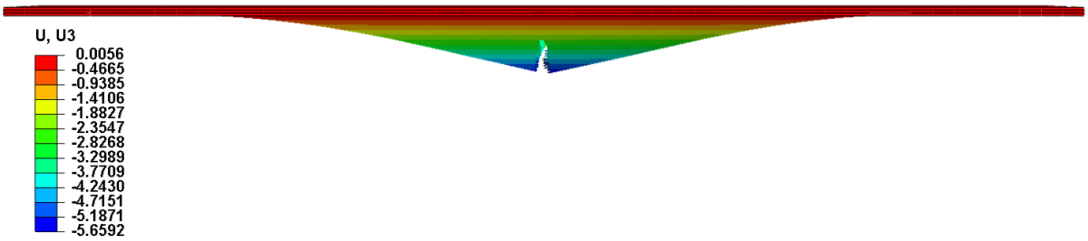

(b) At the end.

Figure 3.18: Displacement (mm) for the plate modelled as continuum shell (1 layer with 3ply).

3.2.2.4 Three variants comparison

The chart in the figure 3.19 represent the three variants curves of the model of $[0]_3$ for force versus displacement. As it can be appreciated the 2 curves of the solid plates are precise between them. The shell curve, as in the previous section 3.2.1, has it *vertex* again displace to the right and down comparing to the solid curves ones. But in contrast with the curves of the isotropic material model the peak force is closer between the three curves, although the maximum displacement is again little bit far from the solid curves.

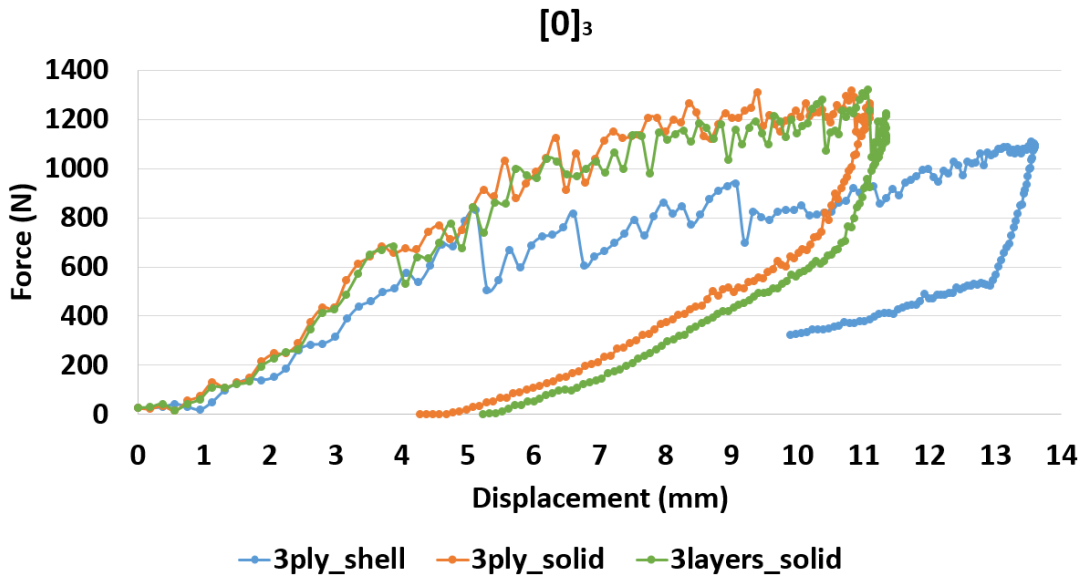

Figure 3.19: Force versus the displacement for $[0]_3$ layup (shell, 3plys and 3 layers).

3.2.3 Isotropic versus $[0]_3$

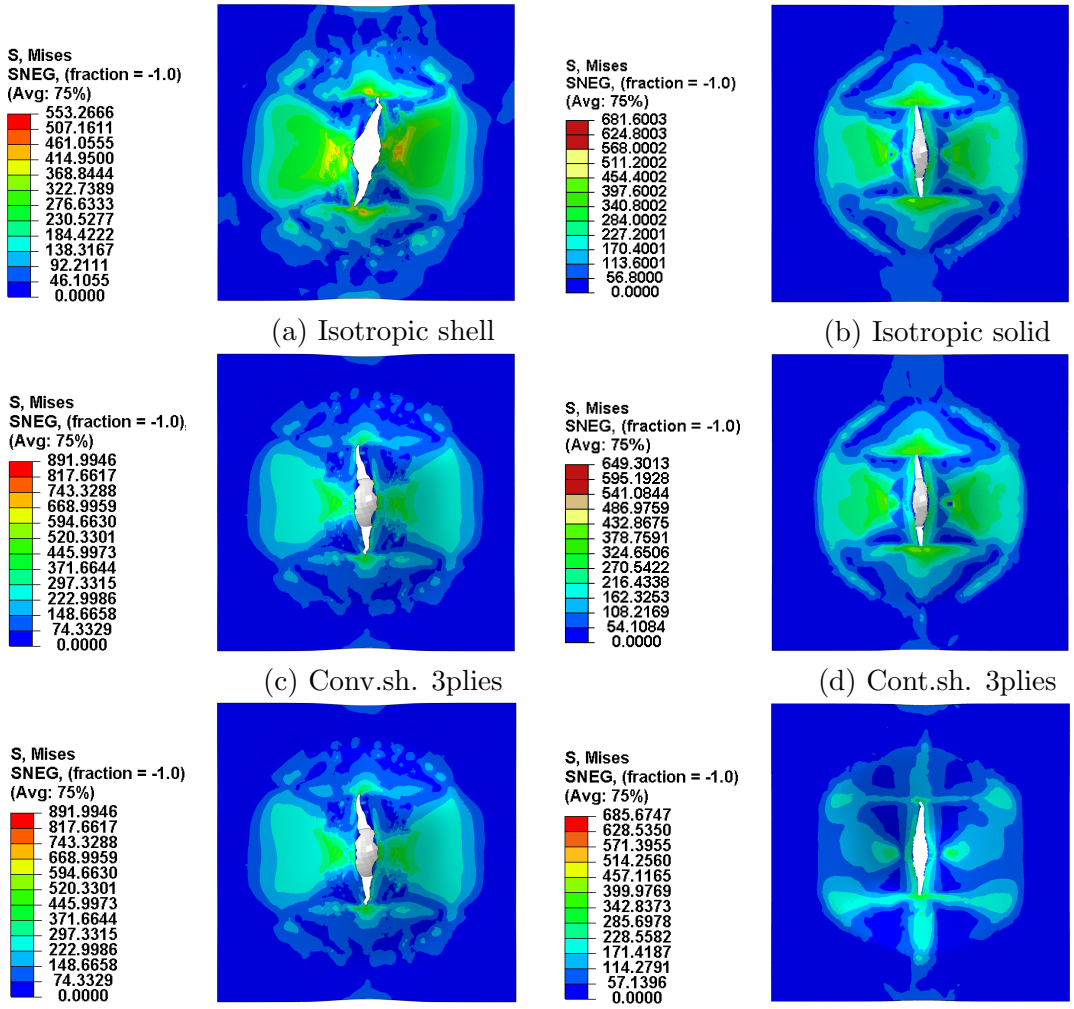

(a) Isotropic shell (b) Isotropic solid

(c) Conv.sh. 3plies (d) Cont.sh. 3plies

(e) Cont.s. 3layers, b.l. (f) Cont.s. 3layers, t.l.

Figure 3.20: Von Mises stress distribution comparison between the different variants of $[0]_3$ layup at the point of maximum displacement.

A comparison of the Von Mises stress distribution at the time of maximum displacement for the different modelling approaches of $[0]_3$ layup is shown in Figure 3.20. As the figures show all of them present similar shape of failure in the composite, but there are some minor differences that makes more accurate some of the variant than the others. The isotropic shell case has the hole shifted to the left while the rest of them are to the right. The isotropic solid and the continuum shell had pretty much the same Von Misses stress distribution, although in the isotropic ones the maximum value of stress is a bit bigger (681,6 vs. 649,3 MPa). The conventional shell mirror the bottom distribution of stress and the values of the 3 layer continuum shell, but in it the opportunity to observe the distribution of the top layers is lost. In the 3 layers variant it is shown clear that the top layer develops less stress than bottom one (200 MPa of difference), also the distribution of the stress is different, however in both of them the distribution is

perpendicular to the 0°fiber orientation. This shape of the failure is not similar to the observed phenomenon in the experiment and it is clear that the layup of $[0]_3$ is not suitable for the woven composite. Even though the material parameters given to the model are for woven composite with 0 and 90 degree fibers and the thickness is maintained the same for all the simulations, it is necessary to explicitly define a layup of alternating 0 and 90 degree plies. Even though, the shell variants present a important advantage, its simulation time, while the 3 layer variant took about 3 days to be completed the shell cases only took a bit more than 15 minutes.

3.2.4 Plate layout $[0/90]_3$

Finally a 6 ply laminate was launched. In this case, as in the previous ones, firstly a shell part plate was modelled and afterwards a solid part plate was done. In this problem, the plate with continuum shell properties was done again two times. One corresponding to 1 layer with 6 plys and the second was a 3 layers with 2 plys each. As in the case of the $[0]_3$ plate this variants were done in order to study the delamination behaviour and its influence, and to be able to observe the difference damage initiation and evolution response of the top an bottom layer.

The damage progression combined with the displacement of the plate during the simulation is shown in the Figure 3.21, the images represent the bottom ply of the layup $[0/90]_3$ in different points of the simulation.

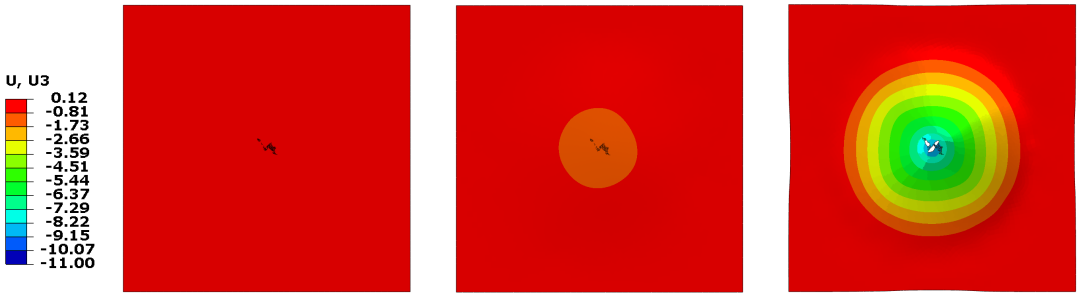

(a) 0,12 ms (b) 0,84 ms (c) 3,84 ms

(d) 5,4 ms (e) 9 ms (f) 12 ms

Figure 3.21: Progression during the simulation for the bottom ply $[0/90]_3$ (Displacement [mm]).

3.2.4.1 Plate as conventional shell, 1 layer with 6 plies.

The first change of this variant with respect the others is in the energies and contact force curves (Figure B.28), the E_k and U_{st} cross before the 0,004 point time, although they follow the same path than always. The contact force curve has a similar behaviour than the *expected one* (Figure 3.2), it present four differentiated parts. The first one from the origin to time 0,004 the curve grows with a constant slope, until it reaches its maximum, follow by the vibration of the curve around this value until the point of time 0,005, more or less. The next two parts are the decrease of the value, the fist is a sudden vertical decrement at 0,005 follow by a constant negative slope approximating to 0. The sudden decrease in the force is coincident with the minimum and maximum of E_k and U_{st} respectively.

In the group of figures of the damage initiation and evolution criteria (Figures B.29, B.30, B.31, B.32) of this case can be seen different distribution shapes for the damage initiation and evolution as it was expected, because now the plate has fiber in 0°and 90°orientation. The damage initiation distribution are bigger in the fiber tension and matrix modes. The fiber tension and the matrix compression presents the same distribution shape but flip (In Fiber tension is oriented in fiber 0°direction, while for matrix tension is in fiber 90°orientation). Both of them are X shape around the impact point with the ends of the *X's legs* after the undamaged area where fixture edge contact the plate. In the two compression modes the distribution has two main areas, one around the impact point[6] and a second one in the fixtures edge area[7]. It have to be taken into account that the display distribution corresponds to the bottom ply of the layup, in this case a 90°orientation ply[8]. In damage evolution, breaking the trend, any mode evolves between the two points of study. Fiber and matrix tension modes presents X shape for distribution (In matrix mode is oriented in fiber 0°direction, while for fiber mode is in fiber 90°orientation). Fiber and matrix compression show affected areas in the surrounding of the impact point, but matrix one in the fixture edge area presents also damage evolution. Finally shear mode distribution has two chromosome shape in 90°and 0°fiber orientation.

Figure 3.22 shows the displacement suffers by the plate during and at the end of the simulation. The values are 10,83 mm for the maximum displacement while for the end displacement is around 7 mm smaller, being 3,4162 mm.As the contact for does not reaches 0 this final displacement can be vary, but the change will be similar because the force is nearly 0 at the end.

[6]In Fiber mode is oriented in fiber 0°direction, while for Matrix mode is in fiber 90°orientation.

[7]In Fiber mode is oriented in fiber 0°direction, while for Matrix mode is in fiber 90°orientation, too.

[8]From what the cases of $[0]_3$ have previously demonstrated.

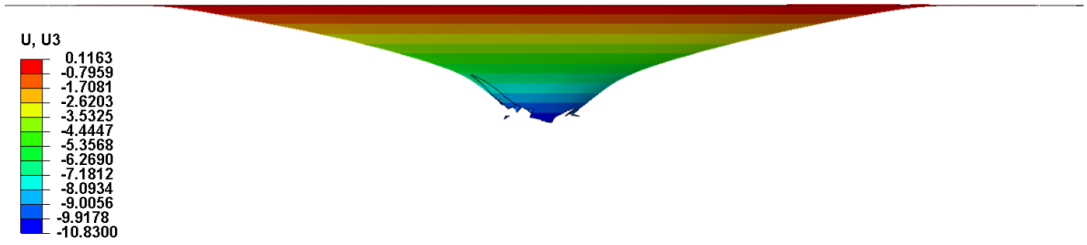

(a) Maximum

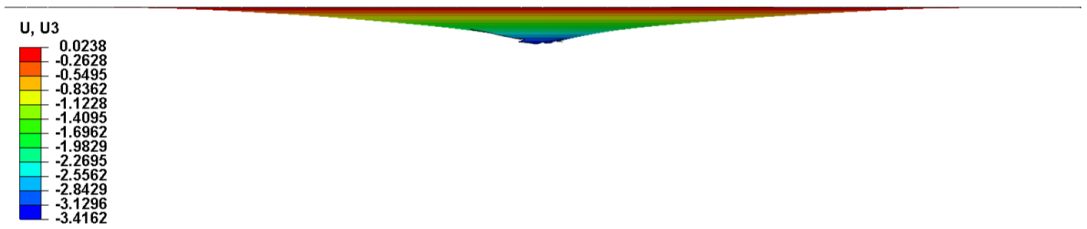

(b) At the end.

Figure 3.22: Displacement (mm) for the plate modelled as conventional shell (1 layer with 6ply).

3.2.4.2 Plate as continuum shell 1 layer with 6 plies.

The energies curves (Figure B.33) follow the same pattern that in the rest of the chapter. Some minor changes are that the cross between the E_k and U_{st} curves are clearly before 0,004 time and in both of them, but more pronounced in the U_{st}, there is a peak that it is coincident with the contact force curve peak. This time the force curve reaches the 0 value (unlikely the invariant 3.2.4.1) and the energies become constants. The force curve has two maximums, until the second one (relative maximum) its shape is actually close to the article one (3.2).

In the group of figures of the damage initiation and evolution criteria (Figures B.34, B.35, B.36, B.37) their distribution shapes have the same patterns than the ones belonging to the variant 3.2.4.1, with the difference that all of them are more slender. This is more clear in fiber and matrix compression modes in initiation, while in tension modes the X shape is a bit diffused, but the X *legs* are more elongated than in the conventional shell variant. The most important thing is that this is the first variant in which a evolution for a initiation modes appears. Both of compression modes suffer a expansion in shape between maximum displacement and end point. In the damage evolution modes again the only ones that increases in size are fiber compression and shear. Although the damage distribution for matrix and shear modes lose the extensions that make them touch the plate's edges. And in fiber tension mode the symmetry[9] is lost too. Another different with the previous variant, it that the areas where there are distribution of damage evolution the value is closer to 1.

In the below figure 3.23 represents the displacement and the deformation shape of the plate. The different between the two displacements is the around 4 mm, being

[9] in 90°direction

8,3265 mm in the pint of maximum displacement and 4,782 mm at the end of the simulation. This displacement and its consequent deformation can be consider permanent because the contact force reaches 0, and the energies get constant.

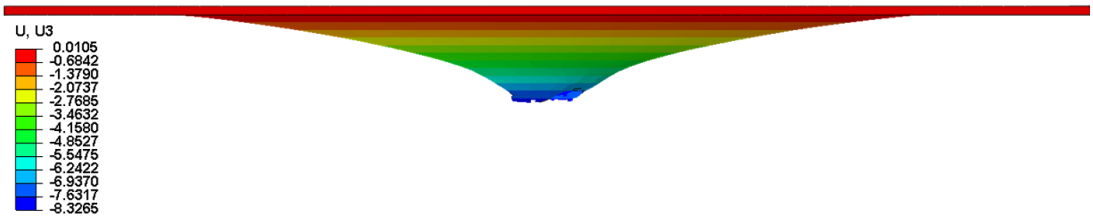

(a) Maximum.

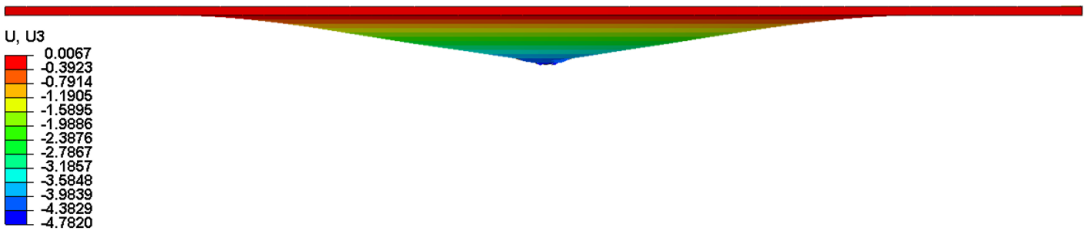

(b) At the end.

Figure 3.23: Displacement (mm) for the plate modelled as continuum shell (1 layer with 6ply).

3.2.4.3 Plate as continuum shell 3 layer with 2 plies each.

The energies curves (Figure B.38) maintain the behaviour of all the previous cases, but this time E_k and U_{st} curves are smooth and them do not present any sudden peak, as the variant 3.2.4.2. Again they cross before 0,004 time point, but this time the maximum and the minimum of U_{st} and E_k, respectively, are coincident in time. Ones the contact force curve is 0, E_k curve gets constant, but not U_{st} which shows a really slow slope. However this time they are extremely close compare to the other variants. About the force curve is like a *Normal distribution* shape center at 0,004 time value.

In the group of figures of the damage initiation and evolution criteria (Figures B.39, B.40, B.41, B.43) there is a major and important different, this time any hole is created. This derives in losing distribution of initiation and evolution damage in the point of impact for the compression modes, in both layers in evolution and just in the bottom layers for initiation. Despite this, the shape of the distributions of the bottom plate are mirrored form the variant 3.2.4.2. As in the 1 layer variant in damage initiation can be appreciated an increment of size for the compression modes. In evolution damage distribution fiber compression, matrix tension and shear are the modes whose distributions size evolves from the point of maximum displacement to the end point.

In the following figure 3.24 shows the plate deformation at the end of the computation and also in the point of maximum displacement. The values of the

displacement are 8,2858 mm for the maximum point and 4,2085 mm for the end point. The difference between them is as in the previous variant of around 4 mm.

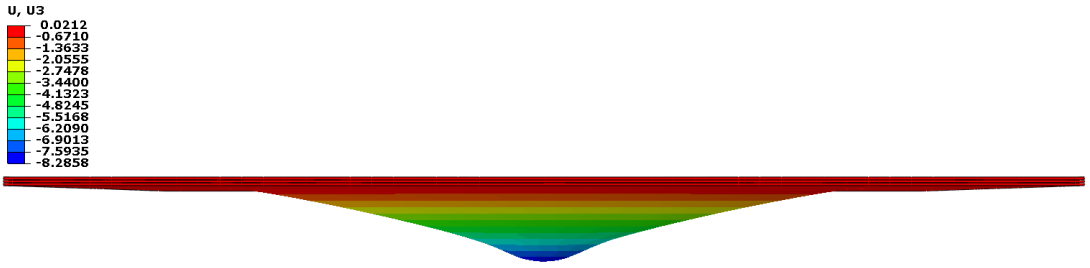

(a) Maximum.

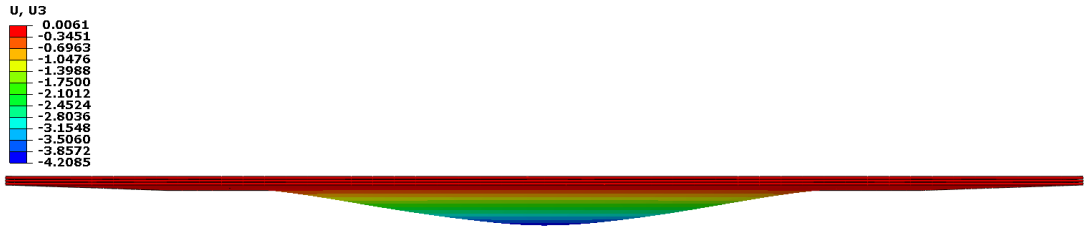

(b) At the end.

Figure 3.24: Displacement (mm) for the plate modelled as continuum shell (3 layers with 2 plies).

3.2.4.4 Three variants comparison

The figure 3.25 is the chart with the three curves of $[0/90]_3$ invariants. It can be seen that the best curve this time is the 3 layer one. The peak force of the the solid curves are again precise between them and also the maximum displacement that the plate suffers. Unlikely, a strange behaviour of the 1 layer curve can be appreciated after the peak force occurs, this can be a consequence of the software computation. Again, as in two previous cases, isotropic material and $[0]_3$ layup, the shell variant underestimated the peak force and overestimate the maximum displacement. This causes that the *vertex* of the curve is displaced to the right and down respected to the 2 solid curves.

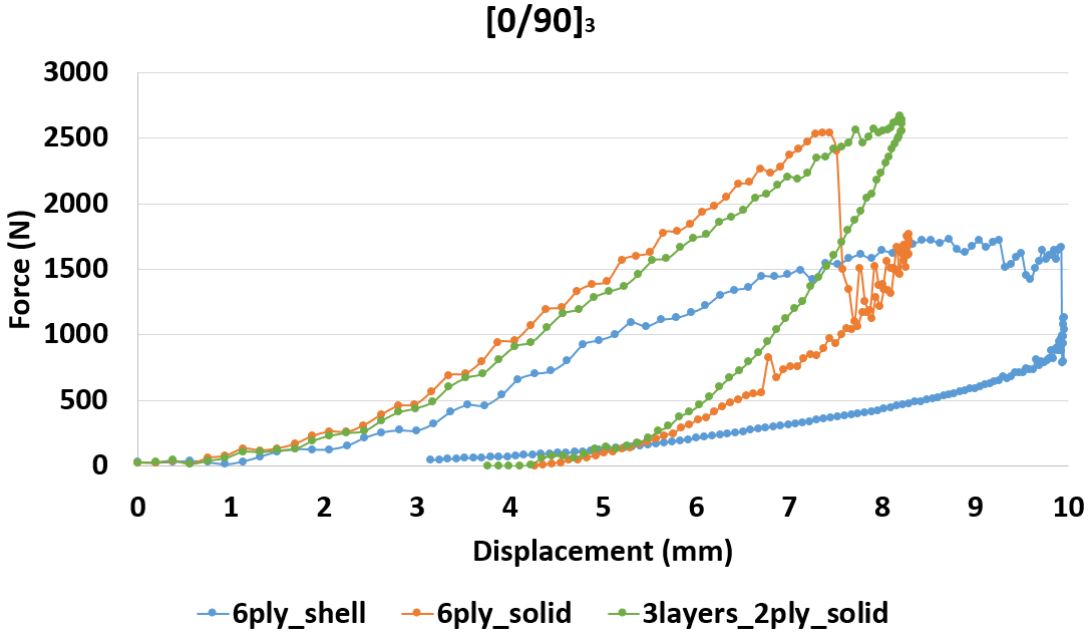

Figure 3.25: Force versus the displacement for the section cases (shell, 6plys).

The below figures show the Von Mises distribution for the three variant simulated with the $[0/90]_3$ layup. The first noticeable thing is that conventional shell and continuum shell with 1 layer have a maximum value of stress around the double than the case of 3 layers continuum shell (1246,8 MPa, 1339,3 MPa versus 541,5 MPa). However the distribution covers more area in the case of 3 layers.

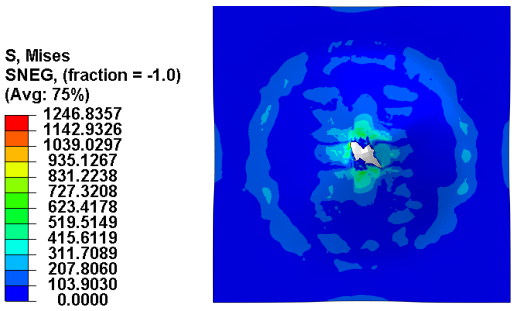

(a) Conventional shell

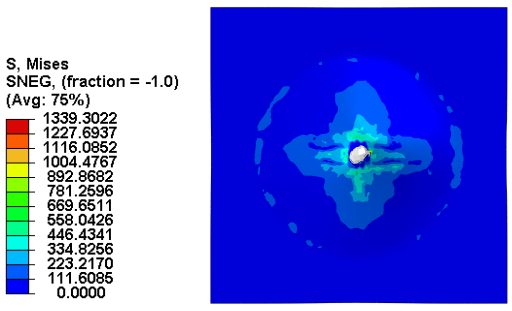

(b) Continuum shell

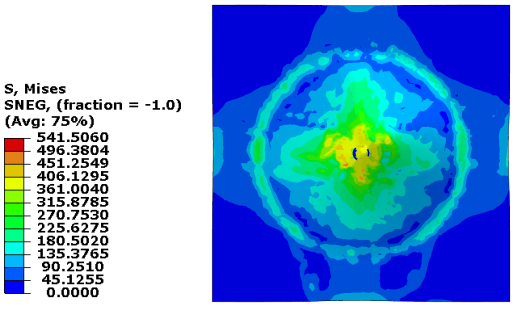

(c) Cont.s. 3layers/2plies, bottom layer

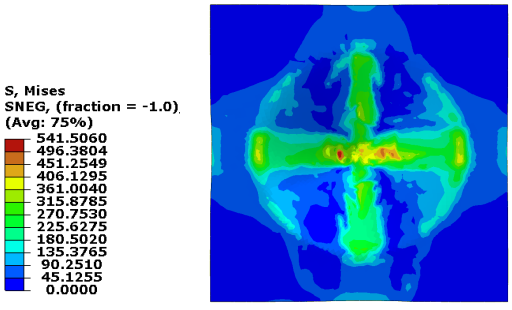

(d) Cont.s. 3layers/2plies, top layer

Figure 3.26: Von Mises stress distribution comparison between the different variants of $[0/90]_3$ layup at the point of maximum displacement.

3.2.5 Summary of different element types

The table 3.5 collects the peak force value, the maximum displacement value and number of mesh elements for the 8 variant cases of the model presented in this chapter. The Figure 3.27 compare their maximum displacement (mm) and the peak force (kN). As the table shows the the damage shape is consistent in the isotropic material and $[0]_3$ layup plate. The damage shape is a essentially vertical line, symmetrically distributed, up and down[10], from the point of impact.

However, non all the cases with a layup of $[0/90]_3$ have the same damage shape. The case of conventional shell and the continuum shell with 1 layer have a almond damage shape, while the 3 layers one has no damage. This could be a consequence of the need of increase the size of the elements around the impact point because, the software was not able to run the case.

The impactor and the fixture during all the cases are R3D4 type of element and the number of them are 229 elements for the impactor and the fixture counts with 1681 of R3D4 and 2 of the type R3D3. The approximated element size for the impactor is of 2 mm and for the fixers of 4 mm. The maximum element size for all the plates is 2 mm.

Table 3.5: Element type, size and number, peak force and damage shape.

Case	Element type	Number of elements	Peak force (N)	Plate's minimum element size (mm)	Shape damage
Isotropic Shell	S4R S3R	17258 542	955,215	0,25	linear slightly diagonal
Isotropic Solid	SC8R	9135	1367,454	0,25	linear vertical
Conv.S. 3ply	S4R S3R	17258 542	1109,11	0,25	linear vertical
Cont.S. 1layer 3plies	SC8R	9135	1318,661	0,25	linear vertical
Cont.S. 3layers 1ply	SC8R	18270[13]	1320,727	0,25	linear vertical
Conv.S. 6ply	S4R S3R	17258 542	1731,967	0,25	non-linear[12]
Cont.S. 1layer 6plies	SC8R	8100	2539,468	0,5	Elliptical close to circular
Cont.S. 3layers 2plies	SC8R	16166[13]	2671,329	0,5	non-damage

[10] In the perpendicular (in-plane) to the 0°fiber direction.
[12] Larger in the left diagonal of the plate and wider in the right diagonal of the plate.
[13] Per layers, so the whole plate has 3 times this value

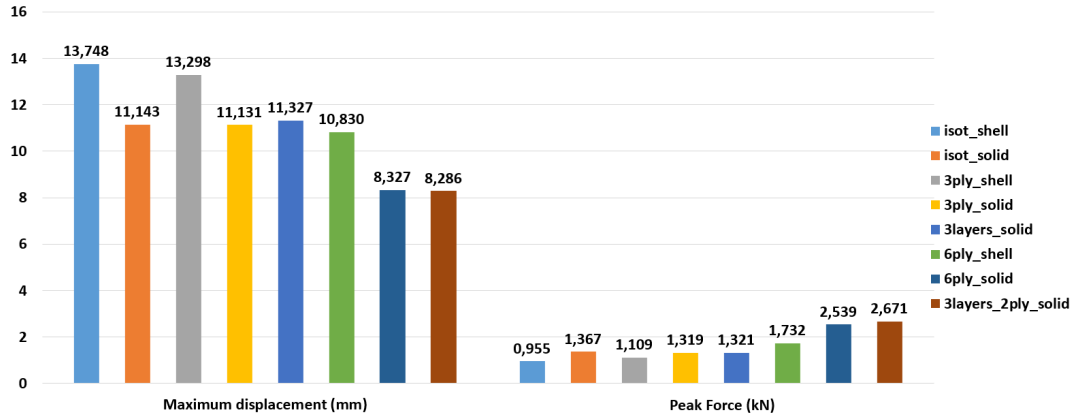

Figure 3.27: Peak Force and maximum displacement of the model variations.

The shell variants of the model with $[0]_3$ layup have copied the bouncing characteristic of the plate worst than the solid ones. Moreover, the solid models peak force is always high than the shell ones. But on the contrary, the maximum displacement of the solid plates is smaller than the shell ones. Meaning that the shell models underestimate the peak force and overestimate the maximum displacement. The peak force value of the model's variants with the layup of $[0/90]_3$ (Table 3.5 and in the Figure 3.27) are close enough to the values presented in the article [60] (Figure 3.2).

It is important to remark that during the simulations of all the cases of this chapter, there was sometimes problems with *extremely element distortion*, this causes the difference in the number of elements in the plate.

Model with plate defines as a solid are more accurate than the shell models. Making the increment in computational time per case being worthy. Additionally, the improvement of the model, doing each ply as a layer and joining them as an assembly, also improve the output results and the quantity of the possible study parameters, such as delamination that doing all the plies in the same layer is not possible.

3.3 Validation of the Kevlar models

With the target to verify the method of modelling the simulation, the article aforementioned [60] was used. For the thesis simulation the impactor is situated 0,5 mm above the plate, as the article recommended in order to reduce simulation time. The result of their simulation are obtained with the software LS-Dyna which treated FRP composite materials linear elastic orthotropic before failure[11].

[11]The constitutive model is based on the theory of continuum damage mechanics (CDM) approach developed by Matzenmiller, Lubliner and Taylor, and called MLT model LS-Dyna Manual (2012)

The curves in the figure 3.28 are confronted the results of the article and the results of this thesis. This proves that the results of the variant of 3 layers are worst than expected, because its mesh is coarse, its curves mirrors the mesh 1 curve of the article chart. On the other hand the continuum shell 1 layer variant reproduces faithfully the experiential curve until its relative maximum. The slope of the linear part of all the curves (the stiffness behaviour of the composite plate) are similar for the experiment and simulations.

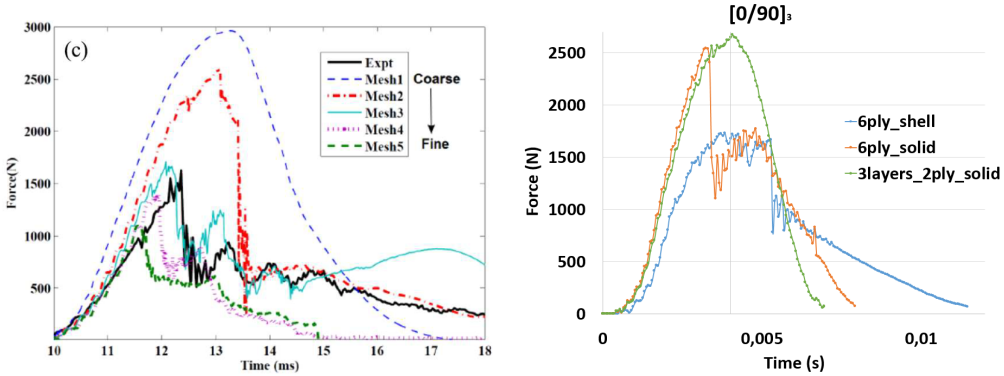

(a) Article simulations [60].

(b) Abaqus simulations.

Figure 3.28: Forces versus the time for the different simulations.

The below curves (Figure 3.29) represent the contact force again the displacement suffered by the plate. It is clear that Abaqus software reproduce better the shape of the curve than LS-Dyna, it is able to simulate the bouncing behaviour of the plate. The most accurate simulation variant is the 1 layer continuum shell, though the force is overestimated, the experimental one was 1880 N and the both of continuum shell variant has a value around 2600 N. The conventional shell on the contrary underestimated the value, but it much closer, 1731,97 N.

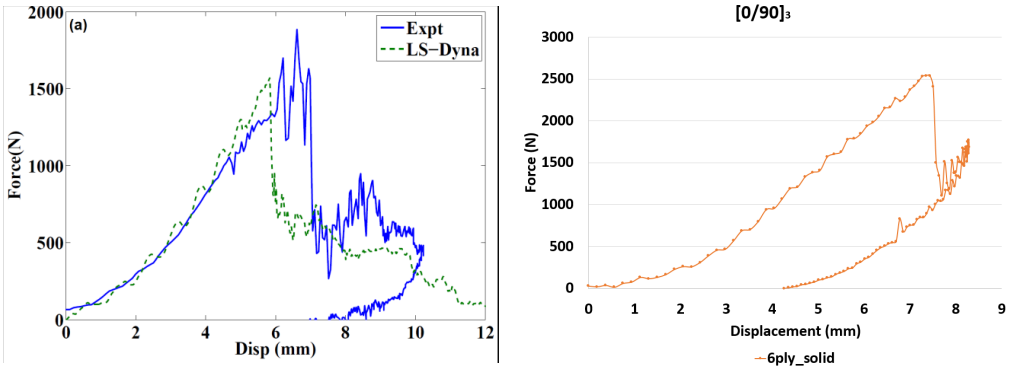

(a) Article's data [60].

(b) Abaqus simulations.

Figure 3.29: Forces versus the displacement comparison.

As can be seen in the figure 3.26b the variant of $[0/90]_3$ layup with 1 layer reproduce with high fidelity the damage hole shape. Sadly the case of 3 layers has not damage

hole, this probably a consequence of the required increment in size for the element around the impact point in order to be able to obtain results of the simulation. The permanent displacement that the experimental specimen suffered was 5,1 mm [60] again the best case is the 1 layer continuum shell with a displacement at the end of the computation of 4,78 mm. This values is better than the one they obtain with LS-Dyna, of 3,9 mm, with is closer to the ones obtained in this thesis for the conventional shell (3,41 mm) and the 3 layer continuum shell (4,21 mm) variants. As the article says if there is no penetration on the plate the displacement is underestimated, the 3 layer continuum shell meets this statement.

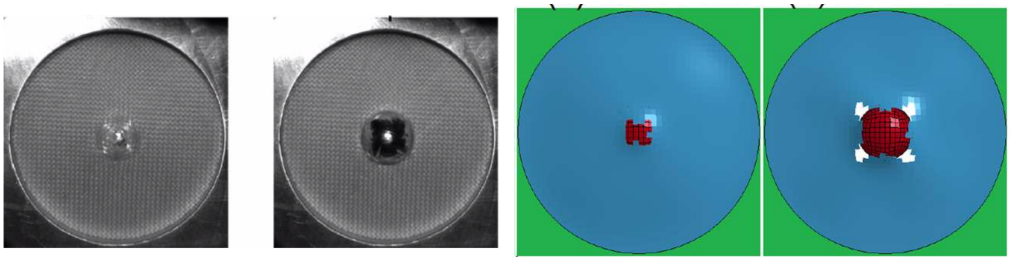

(a) Damage on the experimental test. (b) Damage in LS-Dyna simulation.

Figure 3.30: Images show by the article [60].

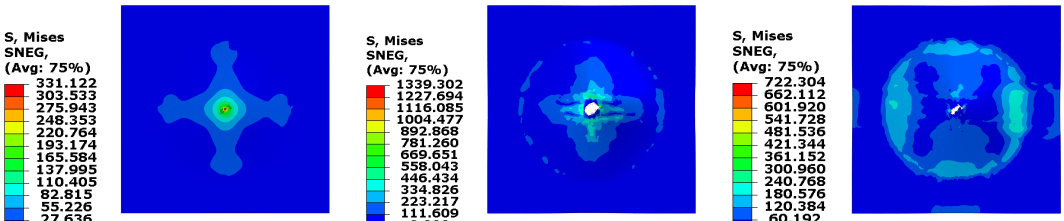

(a) 0,72 ms (b) 3,48 ms (c) 12 ms

Figure 3.31: Damage during the simulation for the bottom ply $[0/90]_3$ (Von Mises [MPa]).

3.4 Conclusion

The target of this chapter was to develop a methodology that simulates in a precise way the response of a traditional composite in lower velocity impact situation. The commercial finite element code Abaqus Explicit was chosen for the simulation. A composite laminate with Kevlar fiber reinforced epoxy was chosen as the material for the modelling as there was experimental data available in the published literature. Different aspects of the development of the numerical model, including the creation of geometry, defining boundary conditions, meshing and material model were described. A composite material law including Hashin criteria for damage initiation and evolution was used for the simulation of the composite laminate. One of the key contributions of this chapter was the comparison of different element types and modelling strategies. The composite laminate was modelled as an isotropic shell, isotropic solid, as well as different composite layups

for conventional and continuum shell elements. The results obtained in terms of the time histories of contact force and impactor displacement as well as stress contours showing the failure modes were compared for the different models. This chapter shows that the plate as a continuum shell modelling each layup's ply as a single layer is the best option. This form allows to study the response of each ply and to assess where the damage initiation and evolution occurs. But, as a disclaimer this advantages are lost if the mesh of the layer requires to be coarse. This situation takes place when the software is not able to simulate the problem with a high number of elements in the mesh.

To sum up it can be confirmed that the methodology developed in this chapter for the simulation of LVI over a composite plate is correct. The next stage of the thesis is to try this methodology with the NFC, Flax/PP. This is done in the chapter 4. The chapter can have two different results, one would be that the in-built material of Abaqus would be able to reproduce the behaviour of the plate, implying that a user-subroutine is not required or all the contrary it can show the actually need of a user material to simulate NFC under impact.

Chapter 4

Simulation of low velocity impact of Flax/PP composite

Natural fiber composites (NFC) are new material in the structural design area. There is limited research on the dynamic behaviour of NFC, making it difficult to understand their response in this circumstances. Even so, the few publications and laboratory tests made show that NFC present non-linear stress-strain behaviour. However, the FE model developed in the previous chapter for the simulation of Kevlar composites used a material model based on the assumption of linear elastic behaviour up to damage initiation. This presents a potential challenge to the simulation of Natural fiber composites. The aim of this chapter is assess the capacity of Abaqus in-built material model (conceived to be used in FRP linear-elastic up to failure) to reproduce the impact response of natural fiber composites. In this chapter, the simulation of a LVI of a square plate of Flax/PP composite by a *hemispherical* impactor is presented. The material is chosen for the study based in the experimental test publish as: **Low Velocity Impact Damage assessment in Natural fibre Biocomposites**[61].

4.1 Model description

Flax is a flowering plant of the *Linaceae* family whose stem is used to manufacture woven fabric in the textile industry and more recently in the structural components. Polypropylene (PP) is a thermoplastic polymer of the *polyolefin* group its main advantage its is strength against chemical solvents. The article's experimental test is performed for plates manufactured from commingled Flax/PP fabrics with surface density of $400 g/m_2$. The composite plates were composed from twistless natural flax fiber and (PP) fiber woven in a balanced 2x2, with a *Twill* architecture [61]. The plate's layup consisted of 10 plies of Flax/PP fabric, the final thickness of the plate was 3,1 mm ± 0,05mm.

In the article they performed five cases, where the drop height varied from 0,1 m to 0,5 m achieving a range of kinetic energies between 3 J and 15 J, a image of the

drop tower used is shown in the Figure 4.1. The simulation in this chapter are the corresponding to 3 and 12 J, which are obtained imposing 1,4 m/s and 2,8 m/s respectively. The figure 4.1 shows the drop tower used in the experimental test. As the article says: *'Low velocity impact testing is typically accomplished using a drop tower with velocities below 10m/s'*. The velocities of this chapter are in this range.

Figure 4.1: Drop tower setup of the experimental test[61].

The problem consists in a impactor *hemispherical* shape over a square natural composite plate clamped between two fixtures, as the figure 4.4 shows. The setting components dimensions and properties bounded are the following ones:

- Impactor (hemispherical shape):
  - Diameter equal to 20 mm.
  - Mass of 3,1 kg.
- Fixtures:
  - Length 100 by 100 mm.
  - Thickness of 10 mm.
  - Diameter of the inner circle 40 mm.
- Plate:
  - Length 100 by 100 mm.
  - Thickness 3,1 mm.

– Material is Flax/PP, its properties are presented in the table 4.1.

The figure 4.2 shows a typical stress-strain curve obtained in the experimental tensile test of the Flax-PP composite[61]. The initial modulus of the composite with the woven layup is about 9 GPa and the maximum stress and failure strain are 80 MPa and 2.4% respectively. It can be seen that compared to a typical composite made from glass, carbon or Kevlar fiber, the behaviour of the stress-strain curve is not linear. This can be due to the realignment of the crimp in the fibers or the sliding between the elementary fibers. Despite the non-linear curve, it can be seen that the failure is quite brittle as seen from the sharp drop of the stress after the peak.

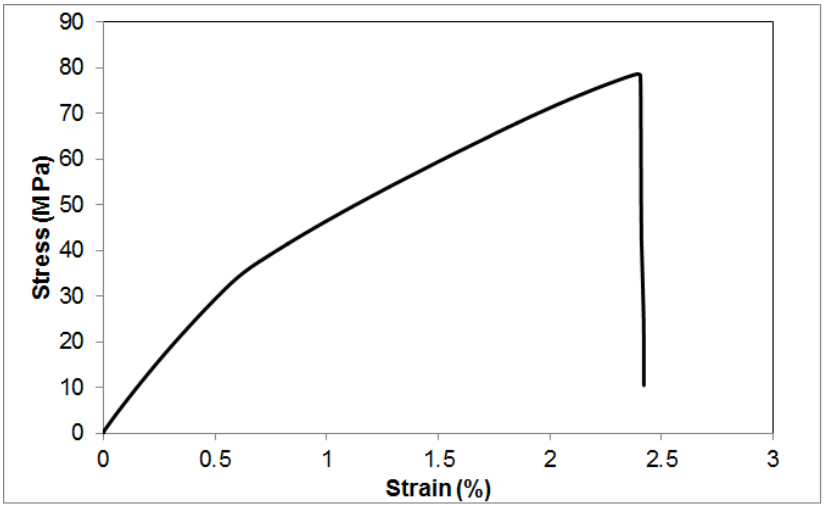

Figure 4.2: Typical stress-strain curve from the experimental tensile test of Flax PP composite[61].

The figure 4.3 shows a typical force curve value obtained in the experimental test of the article [61]. This curve is going to be the reference of this chapter. From the force vs. time curve for the LVI of the flax plate with 3 J as initial energy , three phases can be identified: (i) Elastic bending of the plate, where the force increases linearly until it reaches 1 kN, (ii) a change in the slope of the curve, representing the non-linear material behaviour. This phase is maintained until the peak force is achieved. (iii) The curve starts to represent the fracture or/and unloading of the NFC plate, with a constant slope decrease.

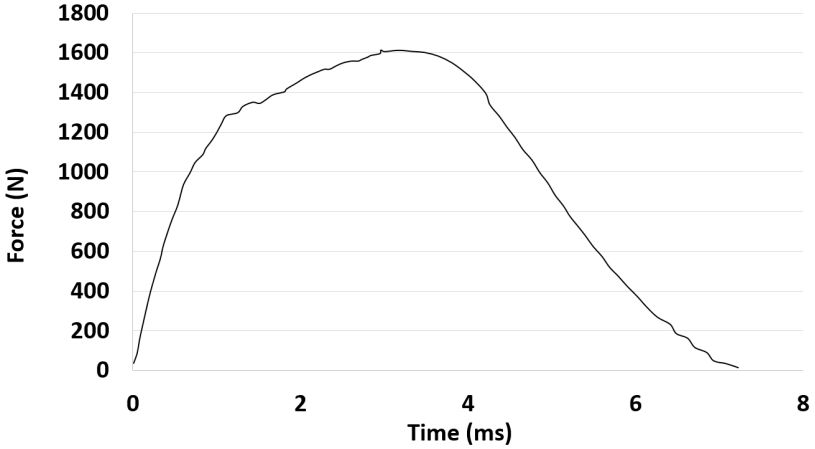

Figure 4.3: Contact force of the experimental test of 3 J[61].

4.1.1 Geometric modelling

In this chapter, the FE software Abaqus is used in the Explicit domain similar to the simulation of Kevlar. The generation of the geometry involves three **Abaqus' Modules** must be set. The first one is the **Part module**, in it two different configurations are done. The fixers and the impactor are modelled as discrete rigid parts. That means that material properties are not needed. Only, the mass must be given in the part's center of mass. Meanwhile, the plate is defined as a deformable solid. The previous chapter 3 has compared the different element types and ways of modelling a composite layup and proved that a *continuum shell* formulation is the best option. This choice resonates in the **Property module** being all the cases modelled as *continuum shell*.

The final assembly for the simulation is shown in the Figure 4.4. In it the two fixtures (top and bottom), the impactor and the plate are shown.

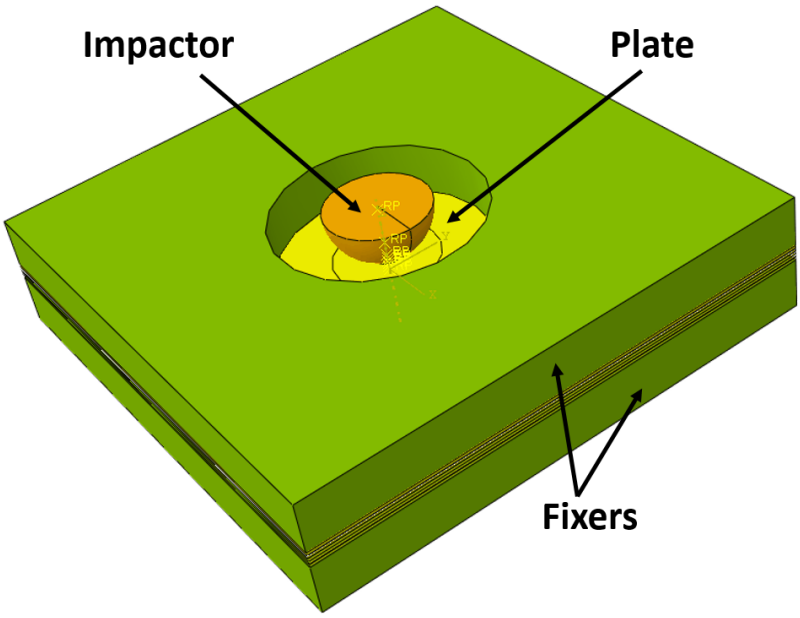

Figure 4.4: Assembly of finite element model of Flax/PP.

This chapter is divided in two main section, each of them contains two simulations with different impactor velocity (1,4 and 2,8 m/s):

Continuum shell 1 layer with 10 plies: 4.2.1.

Continuum shell 5 layer with 2 plies each: 4.2.2.

4.1.2 Contact and boundary condition

The boundary conditions of the model and the velocity of the impactor are defined in the module **Load**, again. The speed was set as a linear speed of 1,4 m/s and 2,8 m/s applied in the impactor's center of mass. The boundary conditions are applied in centre of mass of the fixers and the impactor. The fixers are encastred and the impactor is only allowed to move in the z-direction.

Finally, contact interaction are defined. This problem required the definition of all the contact features that were set in the previous chapter (3). This means that *Layer to layer*, *Fixer and plate* and *Impactor and plate*, are used again (Tables: 3.1, 3.2 and 3.3).

4.1.3 Mesh definition

As in the previous chapter 3 the mesh parameters and distribution is the key part of the model definition. For this chapter the plate's mesh definition are chosen

in accordance with the results obtained in the previous chapter. The plate is partitioned with two center circles (with radius 10 mm and 2,5 mm each) like the figure 3.7a shows, and the mesh definition is *Hex, Sweep, Advancing front* as it can be seen in the figure 3.7b. The final mesh of the assembly is shown in the figure 4.5.

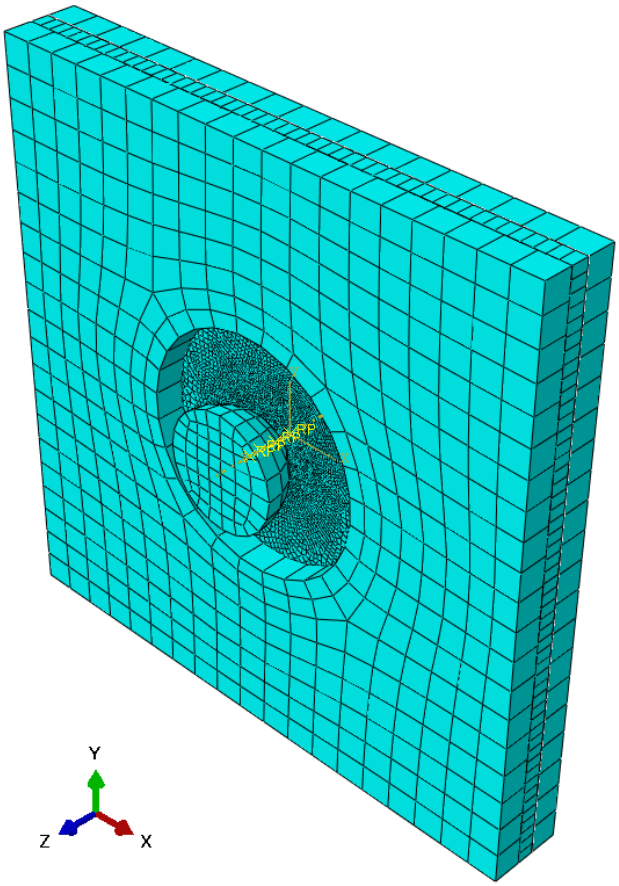

Figure 4.5: Mesh of the assembly.

4.1.4 Material model

Composite materials are classified by their reinforcement and the matrix. In this chapter the selected material is a Continuous[1] fiber reinforced material, Flax (adding the definition of Natural material) and a polymeric matrix, PP (Polypropylene).

In this chapter, in contrast to the previous one (Chapter 3), the layup of the laminate plate remains constant like $[0/90]_5$ for the 4 variants of the problem. The table 4.1 shows the properties of the NFC, Flax/PP obtained from different sources of the literature.

[1]Notwithstanding that Flax fibers are closer to be a short fiber by its origin than a long one, but for the purpose of this thesis flax fibers are going to be consider as if they cover the whole length of the plate in its orientation.

Table 4.1: Mechanical and physical properties of Flax/PP.

Mechanical Properties	Flax/PP
Density ρ (kg/m^3)	$1,25 \cdot 10^3$
Longitudinal modulus E_1 (GPa)	22,98
Transverse modulus E_2 (GPa)	3,03
Transverse modulus E_3 (GPa)	3,03
Major Poisson's ratio ν_{12}	0,38
Poisson's ratio ν_{13}	0,38
Poisson's ratio ν_{23}	0,7
In-plane shear modulus G_{12} (GPa)	1,04
Shear modulus G_{13} (GPa)	1,04
Shear modulus G_{23} (GPa)	1,06
Longitudinal tensile strength X_T (MPa)	334,85
Longitudinal compressive strength X_C (MPa)	246,34
Transverse tensile strength Y_T (MPa)	31,6
Transverse compressive strength Y_C (MPa)	72,1
Longitudinal shear strength S_{12} (MPa)	18,48
Transverse shear strength S_{23} (MPa)	18,33
Longitudinal tensile fracture energy (mJ)	80 mJ
Longitudinal compressive fracture energy (mJ)	80
Transverse tensile fracture energy (mJ)	0,2
Transverse compressive fracture energy (mJ)	1
Viscosity coef. in Long. tensile Dir.	$1 \cdot 10^{-12}$
Viscosity coef. in Long. compressive Dir.	$1 \cdot 10^{-12}$
Viscosity coef. in Trans. tensile Dir.	$1 \cdot 10^{-12}$
Viscosity coef. in Trans. compressive Dir.	$1 \cdot 10^{-12}$

Like in Kevlar/Epoxy chapter to study the response of the plate's material in the **Step Module** the failure and damage criteria are impose. They are maintained[2]: **Damage initiation for fiber-reinforced composites** (DMICRT, HSNFTCRT, HSNFCCRT, HSNMTCRT and HSNMCCRT) and **Damage evolution and element removal for fiber-reinforced composites** (DAMAGEFT, DAMAGEFC, DAMAGEMT, DAMAGEMC and DAMAGESHR).

[2]More information about their definition see Chapter 3

4.2 Results and discussion

The results of Abaqus simulation for the LVI in the 4 variants are presented in this section. The main parameters of interest are the contact force (peak value), the displacement and three energies. The strain energy (U_{st}, ALLIE), the kinetic energy (E_k: ALLKE) and the artificial energy (E_{art}: ALLAE). E_{art} smaller values mean that more accurate results will be obtained[3].

The damage progression combined with the displacement of the plate during the simulation is shown in the Figure 3.21, the images represent the bottom ply of the layup $[0/90]_5$ in different points of the simulation[4].

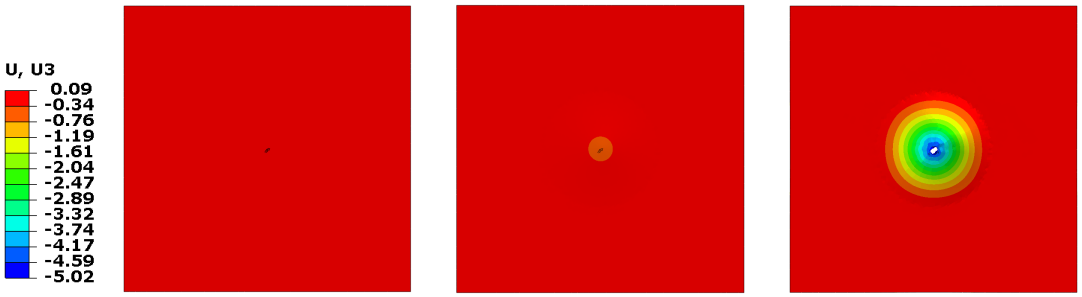

(a) 0,4 ms (b) 1,44 ms (c) 1,76 ms

(d) 3,12 ms (e) 6,08 ms (f) 8 ms

Figure 4.6: Progression during the simulation for the bottom ply $[0/90]_5$, 2,8 m/s (Displacement [mm]).

Figure 4.7 show the paramount parameters of interest in the chapter study. The charts represents the response in contact force, displacement and energy internal (U_{st}) and kinetic (E_k) for the plate with $[0/90]_5$ layup.

[3] In the 4 variants this energy remains with a lower value.

[4] In order to show the damage suffer by some of the layer, the figures show the plate without the layer 1^{st} and 2^{nd}

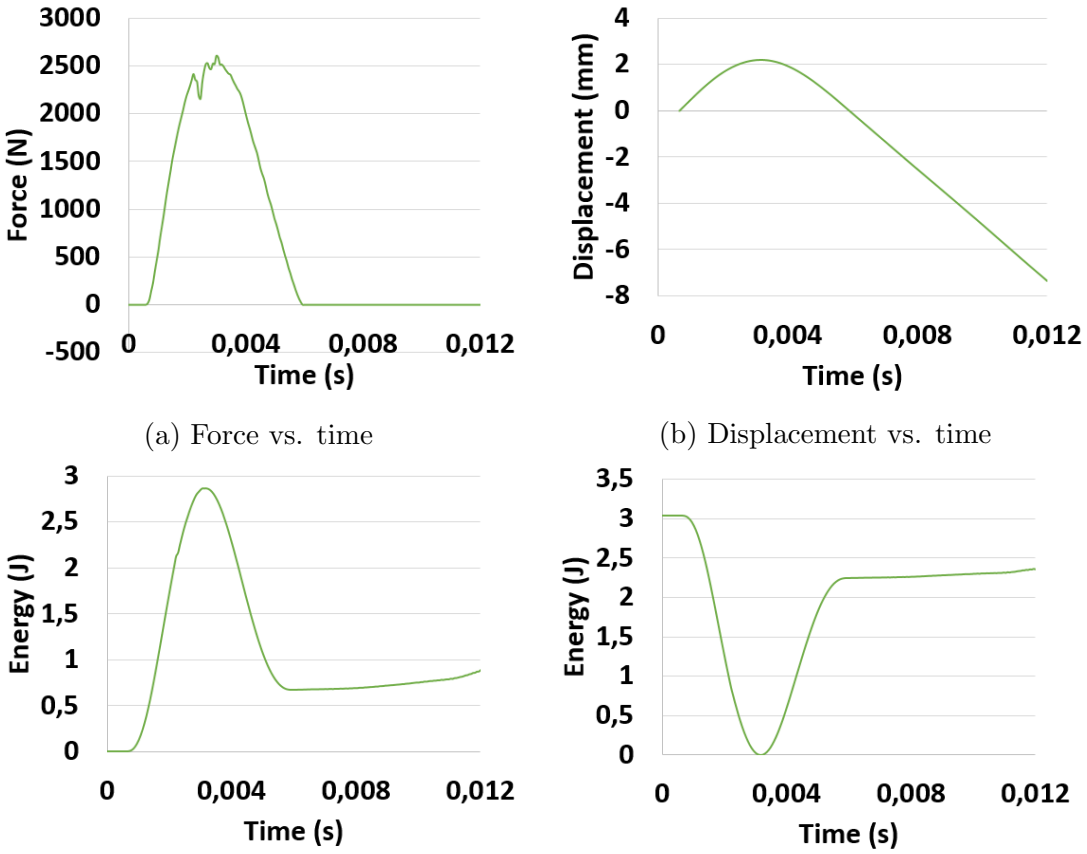

(a) Force vs. time

(b) Displacement vs. time

(c) U_{st} vs. time

(d) E_k vs. time

Figure 4.7: Contact force, displacement and energy versus time plot.

4.2.1 Plate as continuum shell 1 layer with 10 plies.

This section presents the results of the plate model as a single layer, continuum shell containing 10 plies. The Figure 4.8 gathers the plate model and the 10 plies which are contained in the only layer this model is form by, in this way the desire layup is generated.

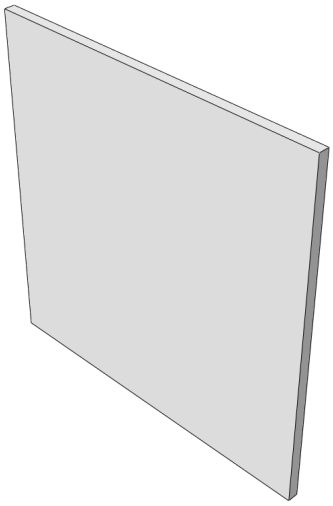

(a) Plate 1 layer.

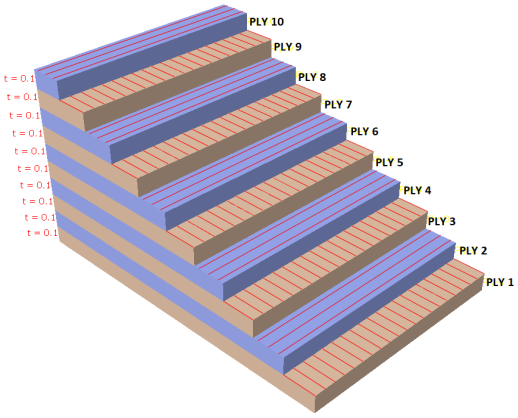

(b) Layup of the layer.

Figure 4.8: Model of the plate.

4.2.1.1 Speed 1400 mm/s

The energies curves (Figure C.1) show how the kinetic energy, E_k, at the beginning of the simulation is 3 J at it was desired. The E_k and U_{st} curves has two cross point at a value of 1,5 J. U_{st} has a maximum value a bit below of 3 J, while the minimum value of the E_k is actually 0. After more or less the 6 ms both energies get constant, E_k a bit below 2,5 J and U_{st} slightly above of 0,5 J. The force curve shares which them the point time where the peak value is place. This curve has a *normal distribution* shape with the maximum value close to 2,5 kN. Also, the three curves share the point where they get constant.

In the group of figures of the damage initiation and evolution criteria (Figures C.2, C.3, C.4, C.5) their distribution shapes do not evolve between the point of maximum displacement and the end of the simulation. The distribution shape of the damage initiation changes between modes. For fiber compression the presented shape is a *Battle axe's blade*, symmetric respect the 90°fiber direction, and the impact point area is not affected. While the fiber tension mode has distribution in the area of the impact point, with a *bone* shape, prolongs in again in the 90°fiber direction. Similarly the matrix tension mode affects the impact point area, but it shape is 0°fiber direction oriented and the shape is more similar to a *butterfly*. Finally, the matrix compression mode presents a symmetric distribution respect the 90°fiber direction with low values and thin area. The shear mode and matrix tension of damage evolution present the same shape of *butterfly* although the matrix mode values are closer to 1. Fiber tension has the *bone* shape distribution located in the area of impact. Compression modes has no meaningful distribution

In the following pictures, figure 4.9 the maximum displacement and the one at the end of the simulation are gather. The maximum displacement has a value of 2,32 mm, while the end value is 0,12 mm. This means that the plate is able to

recover almost its original shape, in addition this deformation can be considerer permanent, because the force reaches the 0 value.

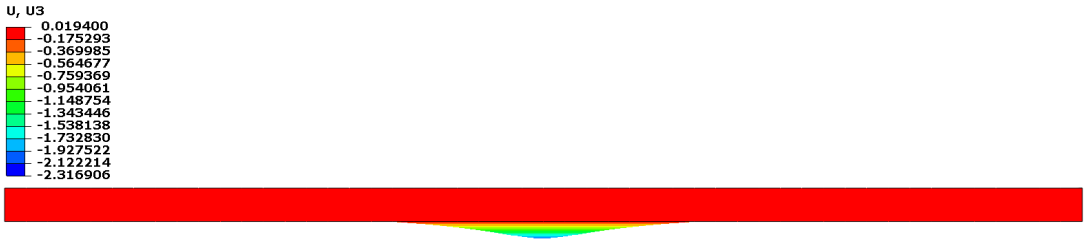

(a) Maximum.

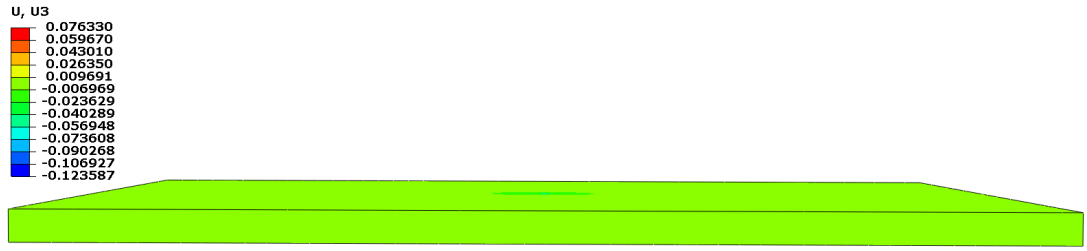

(b) At the end.

Figure 4.9: Displacement (mm) for the plate 1 layer with 10 plies (1,4 m/s).

4.2.1.2 Speed 2800 mm/s

The energies curves (Figure C.6) shows the same tendency that the one corresponding to the 3 J case, before presented. The main difference are in the values as it was expected. The initial value for E_k is 12 J ad the maximum value for U_{st} is a bit below it. The force curve until its peak (above 4,5 kN) follows the same pattern that the previous case, 4.2.1.1, but after this point the decrease part has a more curve shape, the 3 J is straighter. Like in the previous case the three curves get constant at the same time.

In the group of figures of the damage initiation and evolution criteria (Figures C.7, C.8, C.9, C.10) their distribution shapes do not change form the point of maximum displacement and the end of the simulation. The distributions of the damage initiation are similar to the 3 J case, unless the matrix compression mode. This modes presents the *Battle axe's blade* shape but symmetric respect the 0°fiber direction. The other three modes with respect the 3 J case have a increase in size and value. something similar happens to the damage evolution distribution. The tension modes are similar in shape to the 3 J, but with an increase in size and value. The fiber mode presents *Battle axe's blade* shape but symmetric respect the 90°fiber direction, while the matrix compression modes has distribution only in the fixer edge area. Finally the shear mode present distribution in the area where the plate is not in contact with the fixers, specially around the impact point.

In the following Figures, 4.10, show the displacement in two different points of the simulation. The maximum displacement is 5,19 mm and the displacement at the

end is 0,12 mm. It can be see that the plate recovered almost its original shape, the small deformation that it suffer is a permanent one.

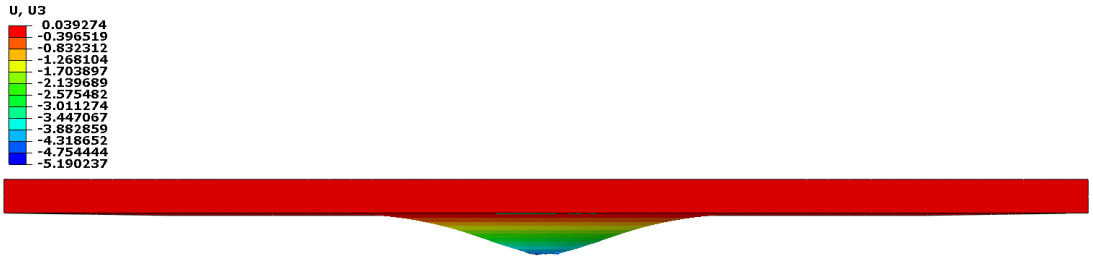

(a) Maximum.

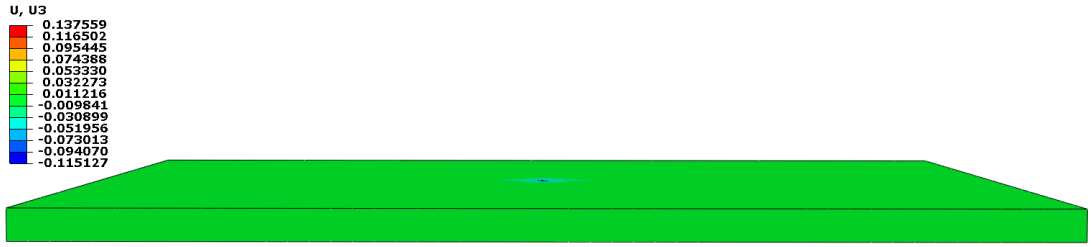

(b) At the end.

Figure 4.10: Displacement (mm) for the plate 1 layer with 10plies (2,8 m/s).

4.2.2 Plate modelled as a solid, continuum shell 5 layers with 2 plies each.

This section presents the results of the plate model as a multiple layer continuum shell containing. The Figure 4.11 shows the plate model by 5 layers and the 2 plies which are contained in each of this layers, in order to generate the willing layup.

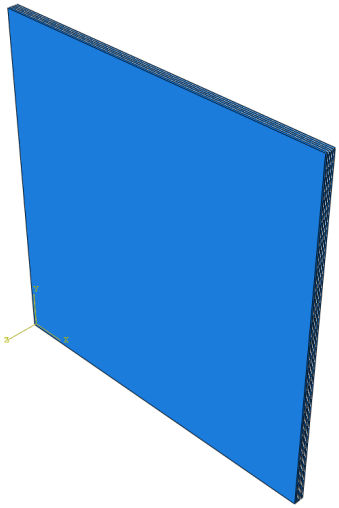

(a) Plate 5 layer.

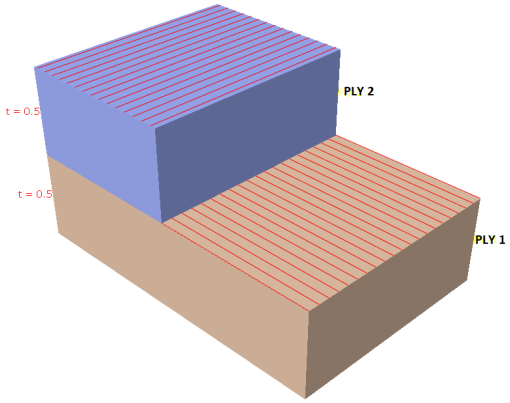

(b) Layup of the layer.

Figure 4.11: Model of the plate.

4.2.2.1 Speed 1400 mm/s

The energies curves and the force curve (Figure C.11) for this variant are quite similar to the variant 4.2.1.1. There are some difference, for example E_k and U_{st} at the end of the simulation start to grow, the slope presented by U_{st} is more annunciated than E_k. In the force curve the firs peak that the curve of 1 layer presents here does not exits. In addition the second peak is clearly more pronounced in this case.

In the group of figures of the damage initiation and evolution criteria (Figures C.12, C.13, C.14, C.16) most of their distribution shapes of the bottom layers are mirrored form the case of 1 layer (section 4.2.1.1). The main difference between the two variants is the evolution that presents some modes distributions, in damage initiation and evolution, that in 1 layer case do not occur. In damage initiation the matrix compression mode distribution, in this case, also present distribution in the fixer edge area. If the free area of the plate (the one which is not in contact with the fixers) is consider, the top layers distributions are located in the area that bottom layers distributions let free (If they area superimposed the circle free area of the plate is obtained). Top layers shape distribution are for fiber compression a *finite* shape symmetric in 0°fiber direction, tension modes have *Battle axe's blade* shape, but in perpendicular orientation, fiber symmetry is around the 90°fiber orientation and matrix in 0°. Finally, matrix compression shape is χ. All the modes suffer a growth in the size form the point of maximum displacement to the end of the simulation. In damage evolution modes only top layers present noticeable change in the distribution between the two pint of study. Fiber modes present distribution around the point of impact in top layer for compression mode, with a *infinite* shape and in bottom layer for the tension mode with a *bone* shape. Matrix modes and shear mode distributions in top layer are really small, but where they are the value is really close to 1. They are located around the impact point and at the end of the simulation it is spread. Bottom layer distribution of matrix tension and shear modes are mirrored the 1 layer case.

The end and the maximum displacement is gather in the Figure 4.12. This values are 0,014 mm and 2,23 mm, respectively. The end value again represents the permanent displacement that the plate would have.

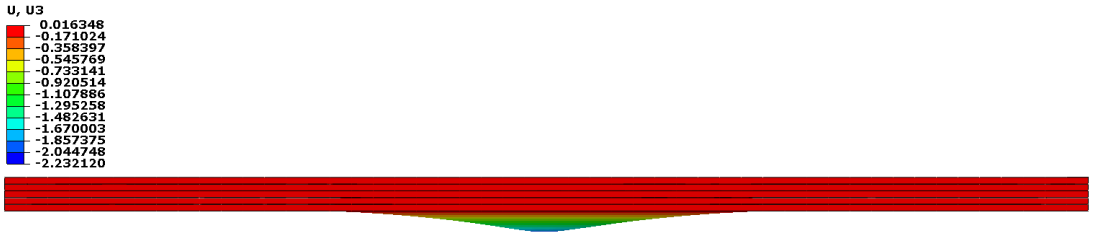

(a) Maximum.

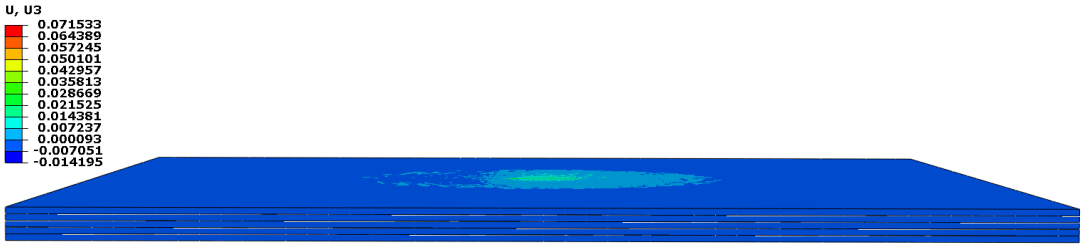

(b) At the end.

Figure 4.12: Displacement (mm) for the plate 5 layers with 2 plies each (1,4 m/s).

4.2.2.2 Speed 2800 mm/s

As in the 3 previous simulations their forces reach 0 value much before 12 ms, it was considered appropriated to simulate with a time of 8 ms instead of 12 ms in order to reduce the computational time, this change does not damage the quality of the results. The energies curves and the force curve (Figure C.18) present the same behaviour of the 3 cases until now studied. Furthermore, the 3 curves are consistent in shape and pattern with the one of the 1 layer with initial energy of 12 J (4.2.1.2).

In the group of figures of the damage initiation and evolution criteria (Figures C.19, C.20, C.21, C.23) distributions shows that the damage initiation suffer some grow in size, but the damage evolution modes remains pretty much the same in the maximum displacement and at the end point of simulation. Damage initiation distributions of the bottom layers mirror the case of 1 layer (4.2.1.2), while the top layers are similar to the ones of the case 4.2.2.1, but the values contained are significantly bigger, most of the area's value is close to 1. In damage evolution the bottom layers distribution are a copy form the 1 layer case, too. But, in fiber modes the values are smaller. This modes in the top layer present also small values in their distributions. Matrix tension and shear mode distributions presents high part of their are with values close to 1. Matrix compression mode has a *flower* distribution in ± 45°fiber direction.

In the following figures, 4.13, are the maximum displacement and at the en d of the simulation for this variant. The maximum value is 5,01 mm while the end one is 0,11 mm, causing a permanent deformation. As in the other cases the plate shows a good recovery of form.

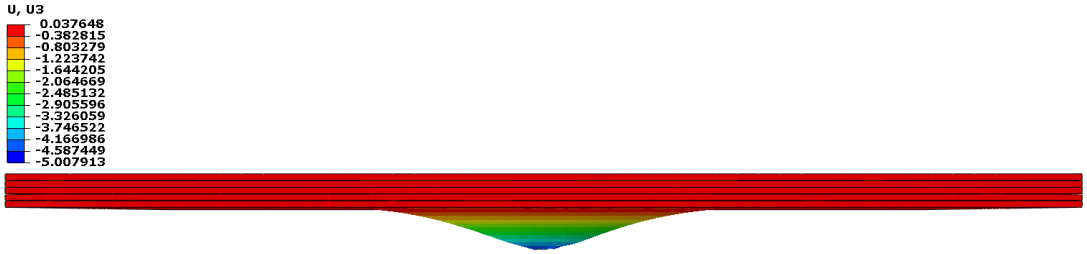

(a) Maximum.

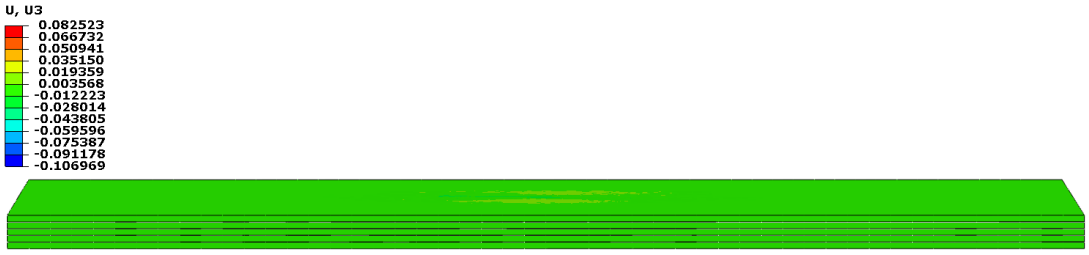

(b) At the end.

Figure 4.13: Displacement (mm) for the plate 5 layers with 2 plies each (2,8/s).

The figures 4.14 collect the damage shape of the model variant, in the second group of images, the two tops layers are taken out in order to be able to see clearly the damage generated by the impact in the three bottom layers. The damage shape that can be seen in the first group of images, corresponding to the maximum displacement, has an *almond* shape.

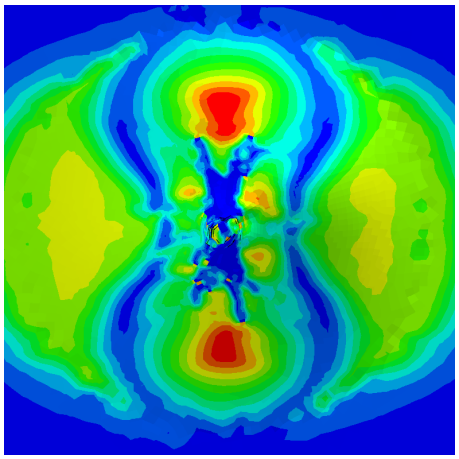

(a) Maximum, all the layers.

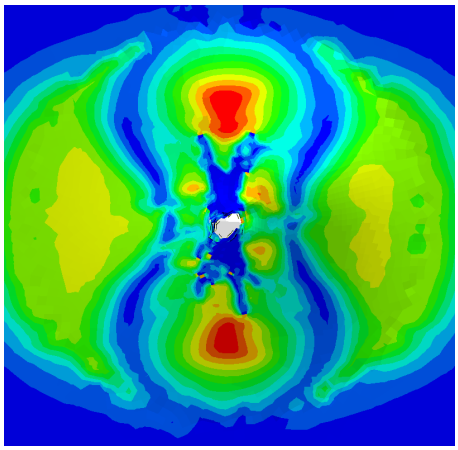

(b) Maximum, without 1 and 2 layers.

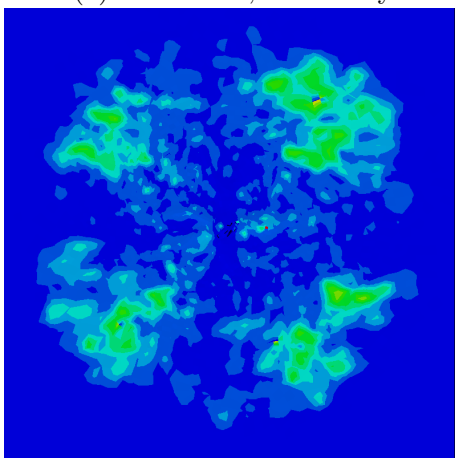

(c) At the end, all the layers.

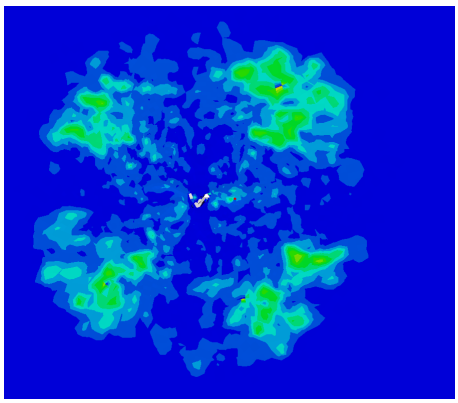

(d) At the end, without 1 and 2 layers.

Figure 4.14: Damage shape for the plate as 5 layer with 2ply each.

4.2.2.3 Four variants comparison

The figure 4.15 shows the four variants' curves of the Flax/PP with a layup $[0/90]_5$. It can be seen that the curves are consistent in shape, and between the curves simulating the same velocity they are also consistent in numerical values[5].

[5]More detailed assessment in the section 4.2.3.

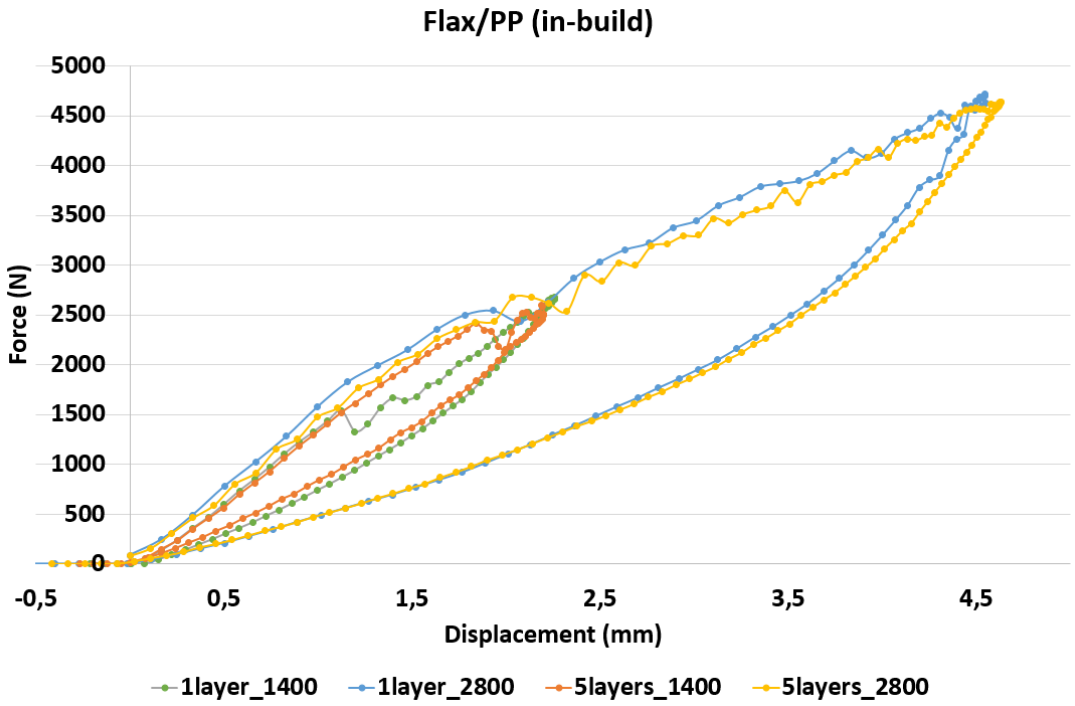

Figure 4.15: Force versus the displacement.

The below figures, 4.16, show the Von Mises stress distribution in the point of maximum displacement and at the end of the simulation, for the variants whose velocity is 1,4 m/s. The distribution shape of both simulations at the maximum displacement is consistent. Also, the maximum value of stress is similar in this point of the simulation, being 334,37 MPa versus 332,95 MPa. Nevertheless, at the end of the simulation the shape of the distribution and the maximum value of the stress is different between the two cases, the 1 layer gives a value of 88,33 MPa while in the 5 layers variants the value is 326,18 MPa. In the most simple variant the distribution of stress is only located in the surroundings of the impact point, for the case 5 layers is more scattered.

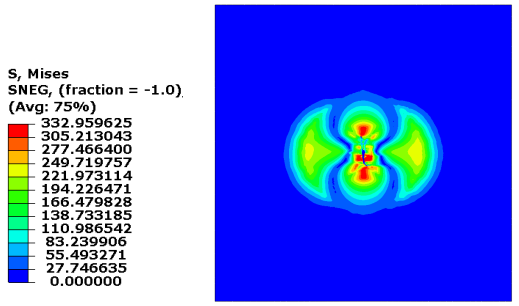

(a) 10plies, max. disp.

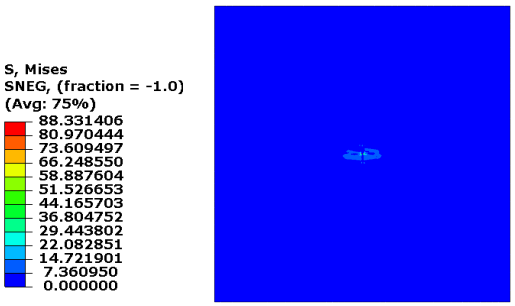

(b) 10plies, at the end.

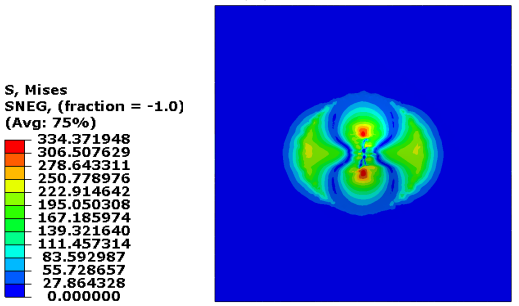

(c) 5layers/2plies, max. disp., b.l.

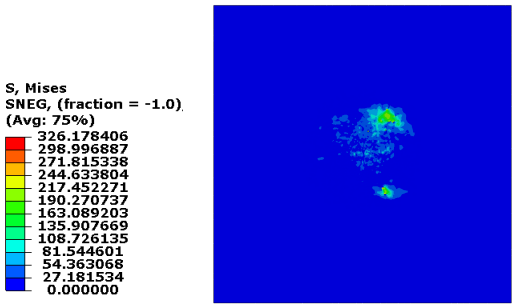

(d) 5layers/2plies , at the end, b.l.

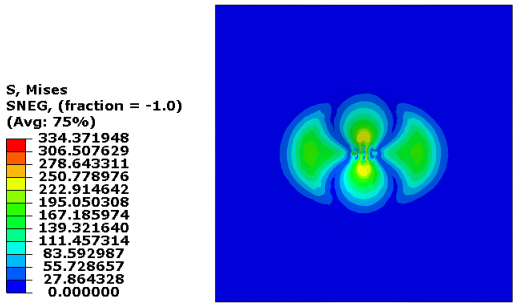

(e) 5layers/2plie , max. disp., t.l.

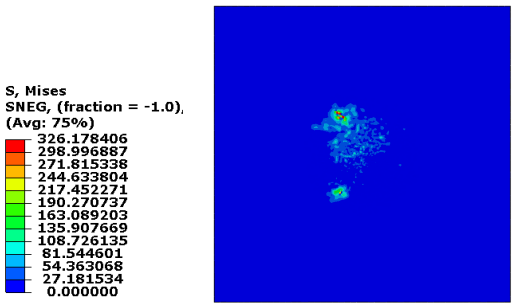

(f) 5layers/2plies , at the end, t.l.

Figure 4.16: Von Mises stress distribution comparison between 3 J variants.

The following figures, 4.17, presents the resulting distribution of Von Mises stress in the simulations whose impactor's velocity is 2,8 m/s. Like the case of 3 J the distribution shape in the maximum displacement point is consistent between the two simulation. But in this case the value is even more close (312,23 MPa against 361,44 MPa). In contrast the distribution at the end of the simulations takes more area in the 5 layer variant, but the maximum value is closer than in the simulations of 3 J (198,59 MPa versus 328,65 MPa). Moreover, the top and bottom ply distributions mirror each other.

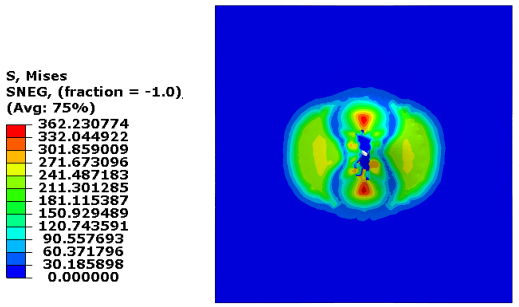

(a) 10plies, max. disp.

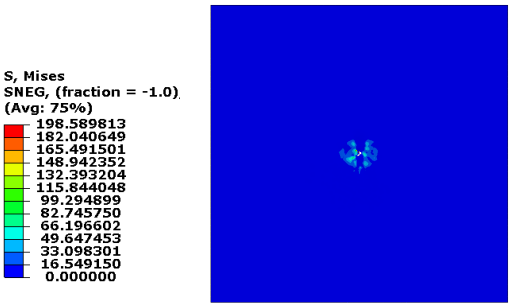

(b) 10plies, at the end.

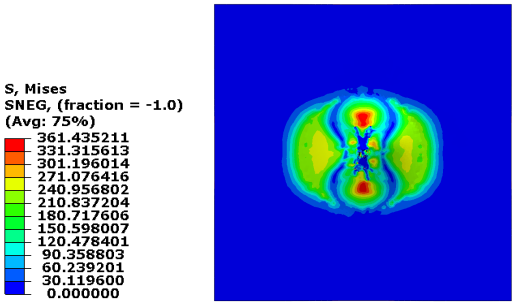

(c) 5layers/2plies, max. disp., b.l.

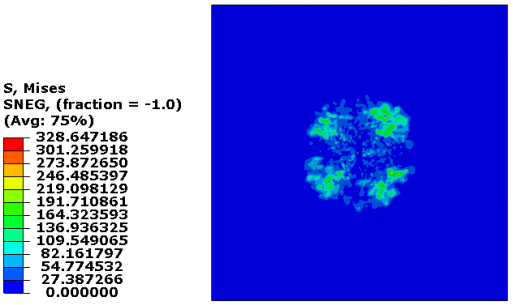

(d) 5layers/2plies , at the end, b.l.

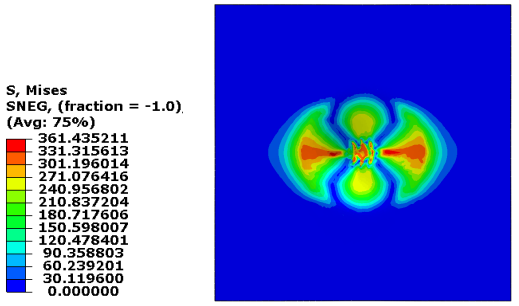

(e) 5layers/2plies, max. disp., t.l.

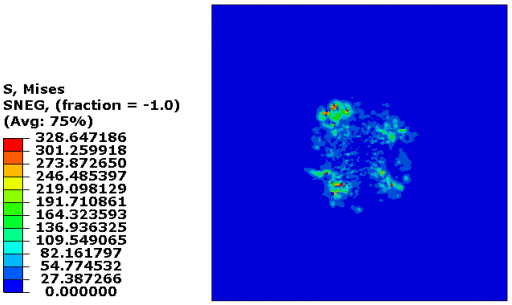

(f) 5layers/2plies , at the end, t.l.

Figure 4.17: Von Mises stress distribution comparison between 12 J variants.

4.2.3 Comparison with experiment

The Figures 4.18 and 4.19 show the force displacement curves obtained in the experimental test and the simulation variants. The curves of the cases with 3 J as initial energy (Figure 4.18) show a similar shape, both presents a *sharp vertex* where the displacement changes of direction. However, the gap between the upper part of the curve and lower ones is bigger in the experimental test than in the simulation ones. The curves of the 12 J (Figure 4.19) as initial energy are completely different. The simulation curves maintain the shape of the 3 J curves, while the experimental test show a more *square* shape. The gap between the two curves branches (loading and unloading) is actually wide in the experimental case. In addition, in this same curve can be clearly differentiate three parts (2 increasing slopes and 1 decreasing slope), while in the simulation curves there are simply 2 parts.

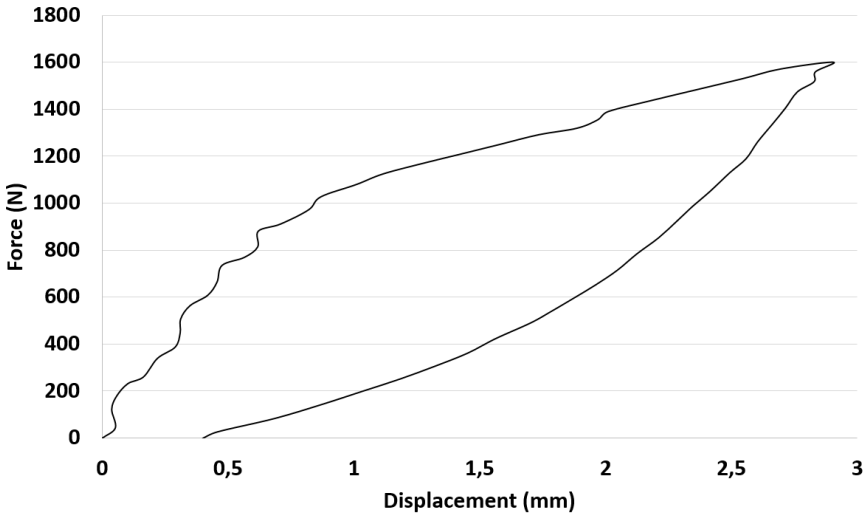

(a) Article simulations [61].

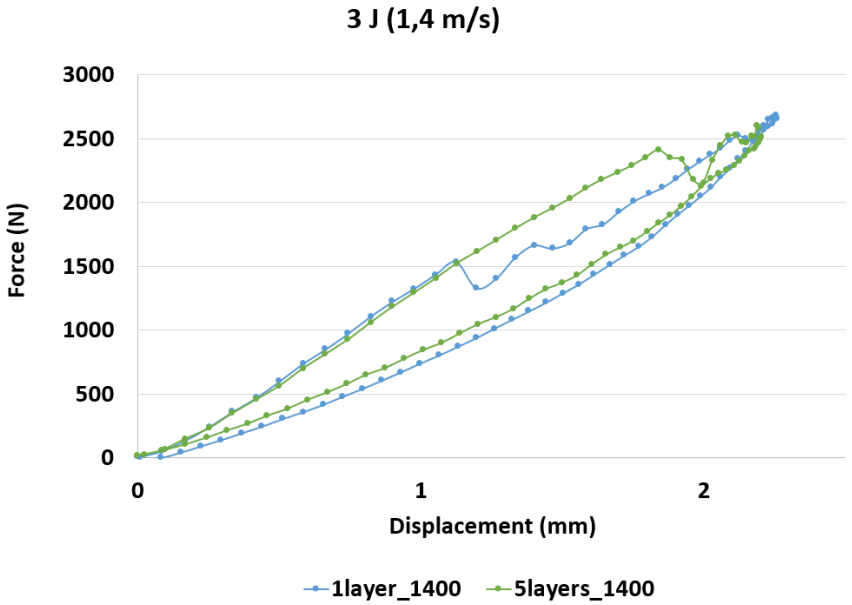

(b) Abaqus simulations.

Figure 4.18: Forces versus displacement for 3 J simulations.

If the curves (Figure 4.18) are assessed in detail, other important difference are shown. The experimental curve has a peak force of 1600 N, with a maximum displacement of 3 mm and a permanent displacement of 0,5 mm, approximately. This means that the plate present a recovery of 83,34%. The simulation curves present a peak force of 2600 N, a 38% of overestimation. The maximum displacement is 2,232 mm (25% smaller than the expected one) and the end one is 0,014 mm (97,2% smaller than the experimental one), the plate's recovery is of 99,4%, being 15,5% larger than the real one.

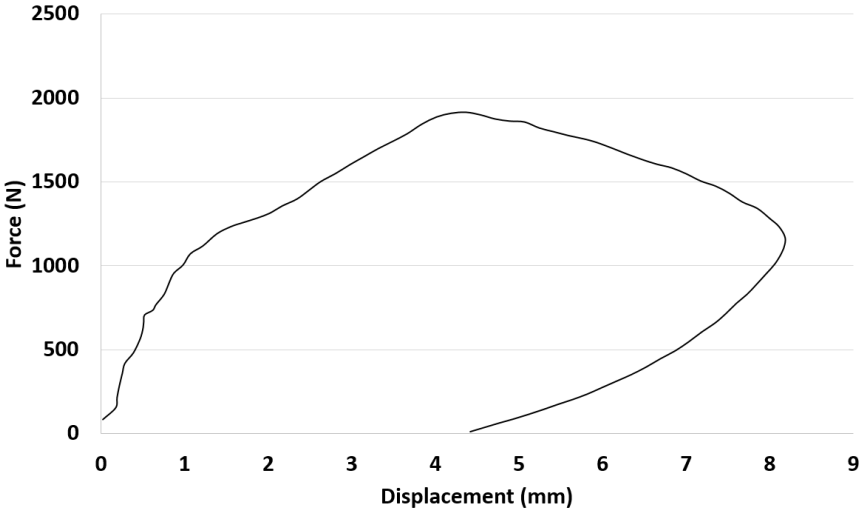

(a) Article simulations [61].

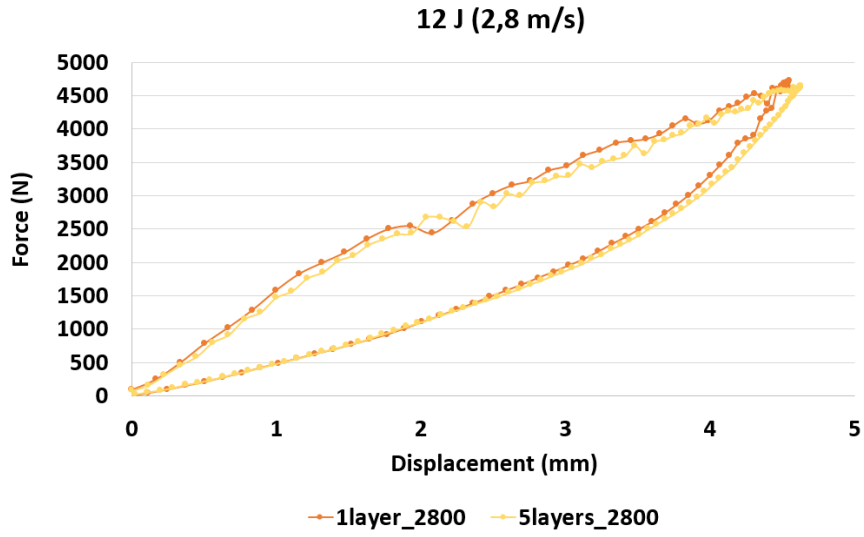

(b) Abaqus simulations.

Figure 4.19: Forces versus displacement for 12 J simulations.

If the above curves (Figure 4.19) are studied into detail, like in the 3 J cases other difference pop up. The experimental curve has a peak force of 1800 N, with a maximum displacement of 8 mm and a permanent displacement of 4 mm, approximately. Meaning that the plate present a recovery of 50%. The simulation curves present a peak force of 4700 N, overestimating this value a 61%. The maximum displacement is 5 mm (37,5% smaller than the expected one) and the end one is 0,11 mm (97,25% smaller than the experimental one), the plate's recovery is of 97,8%, being 47,8% bigger than the real one.

The table 4.2 collects the peak force, the maximum displacement and the mesh information for the 4 variant cases of the model presented in this chapter. The Figure 4.20 show the peak force and the maximum displacement, too. As the table shows the low velocity cases have similar results, but in the higher speed that it

is not the case, the damage shape has a huge difference, because in the model of 1 layer there is not damage while in the 5 layers case there is. This can be consequence of the plate definition, because as it is gathered the damaged only appears in the bottom layers of the laminated, which is impossible to reproduce in a model of 1 layer.

The type and number of elements that the mesh of the impactor and the fixer, respectively. During all the cases the elements of theimpactor are R3D4 type, with 150 elements, while the fixer counts with 1160 elements of R3D4 type. The approximated element size for the impactor is of 3 mm and for the fixers of 4,5 mm. The maximum element size for all the plates is 2 mm.

Table 4.2: Element type, size and number, peak force and damage shape.

Case	Speed (mm/s)	Element type	Number of elements	Peak force (N)	Plate's minimum element size (mm)	Shape damage
10ply 1layer	1400	SC8R	9135	2678,24	0,25	non-damage
10ply 1layer	2800	SC8R	9794	4720,04	0,5	Elliptical close to circular
10ply 5layer	1400	SC8R	9135[1]	2600,9	0,25	non-damage
10ply 5layer	2800	SC8R	8548[1]	4640,63	0,35	Elliptical close to circular[2]

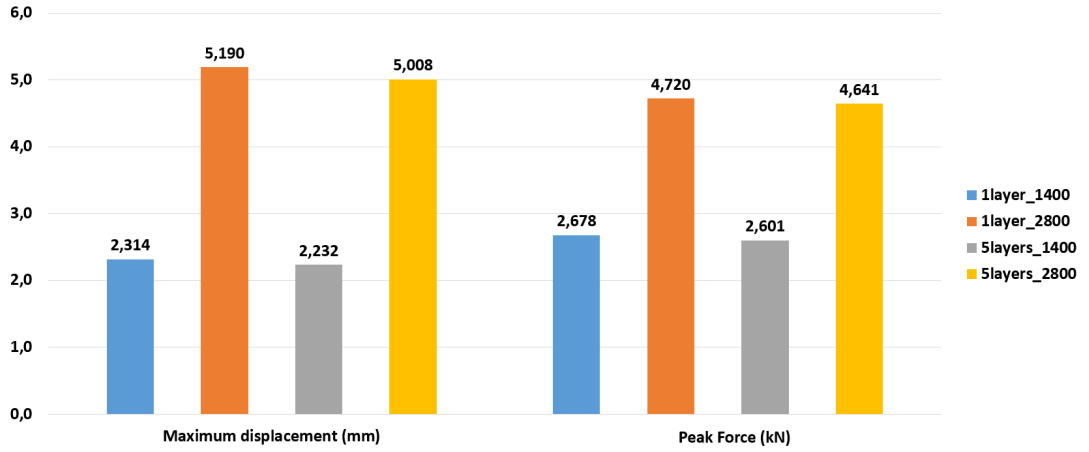

Figure 4.20: Peak Force of and maximum displacement the model variations.

It is still maintain the recommendation of model each ply of the layup as a single layer. If not some important information is lost, as the variant of 2,8 m/s shows. In this cases the 1 layer variant show hole damage for the whole layup, but the improved case of 5 layers clearly show that this damage is only in the 3 bottom layers, this fundamental feature is completely lost in the simple case.

With the aim to ascertain if the Abaqus simulation with in-built composites material model is capable of reproducing the behaviour of a plate made of Flax/PP

[1]Per layers, so the whole plate has 5 times this value
[2]Just damage the 3^{rd}, 4^{th} and 5^{th} layers of the plate, the 1^{st} and 2^{nd} non damage.

in a LVI, the results presented in this chapter are compared with the experimental data of [61].

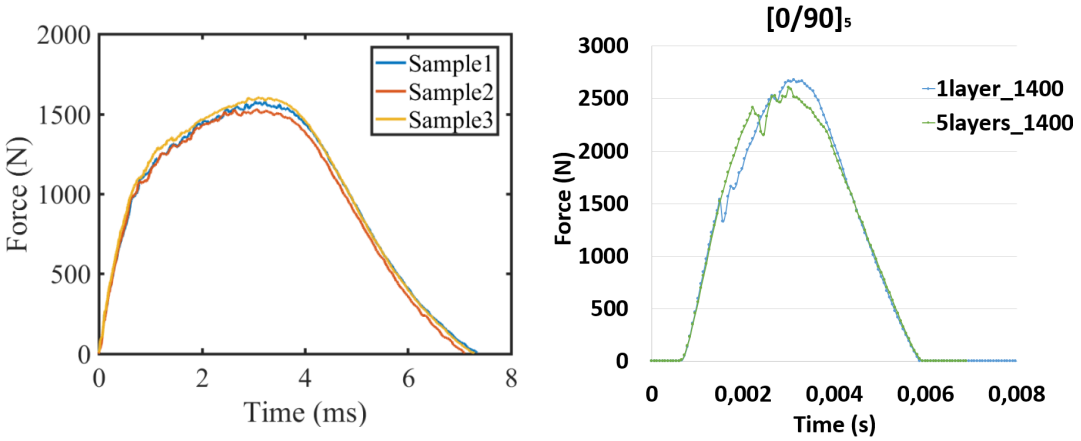

(a) Experimental results [61].

(b) Abaqus simulations.

Figure 4.21: Forces versus the time comparison (3 J).

It can be observed in the above figures (Figure 4.21) that the force curve's pattern are slightly different between the article ones and the curves of this chapter simulation. As they said in their curve has a *bell* shaped, while the curves of the simulations are more close to a *normal distribution* shape. Their curves starts with the linear increase with a high slope in force until it reaches 1 kN, in the simulation curves this increment is maintained until the peak force (approximately 2,5 kN). After their curve presents the non-linear material behaviour up to more or less 1,55 kN, which corresponds with the peak force, this part is not clear in the simulation curves, it could be say that the 1 layer case has a bit of change in its slope but the 5 layer variant does not show any change. Finally their curves present the material's unloading or fracture, this slope in the simulation curves is steeper, reaching the 0 value before the experimental test.

In an impact the kinetic energy that the impactor has is transferred to the plate, this energy is shown in the displacement and deformation of the plate itself but also part of it its dissipated in damage form. This dissipated energy is the main cause of the decreases in energy when the plate bounced back. This energy difference is due to the damage and the plastic deformation (permanent displacement that the plate has at the end of the experiment of simulation). The below figures (Figure 4.22) shows the internal energy of the plate. It can be seen that the gap between the final value of the energy and the initial one is much bigger in the experimental case than the one of the simulation, around 2 J against 0,5 J which is a significant difference. The peak energy value of the simulation is close to the experimental one approximately 3 J, but the slope of the experimental curve to reach this peak is more smooth than the simulation one.

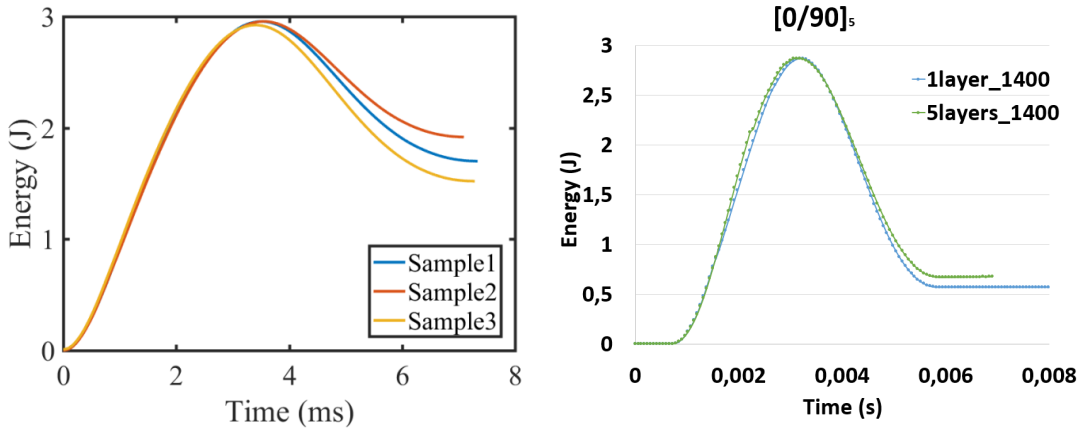

(a) Experimental results [61].

(b) Abaqus simulations, U_{st}.

Figure 4.22: Energy versus the time comparison.

Last but not least, the Figure 4.23 shows the damage that the plate under the experimental case of 12 J suffers. In the same way, the Figure 4.24 shows the response of the simulation[6]. Here, the main difference between the experimental and the simulation results see. The Flax/PP plate in the experimental case has a damage hole with a *cross* shape, that it is prolonged in perpendicular directions. However the simulation displays again the *almond* shape shown before in the chapter of Kevlar/Epoxy.

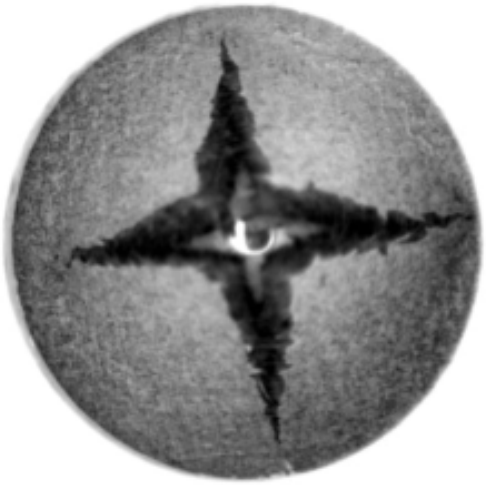

Figure 4.23: Damage of the plate shows by the article [61].

[6]In order to show the damage suffer by some of the layer, the figures show the plate without the layer 1^{st} and 2^{nd}

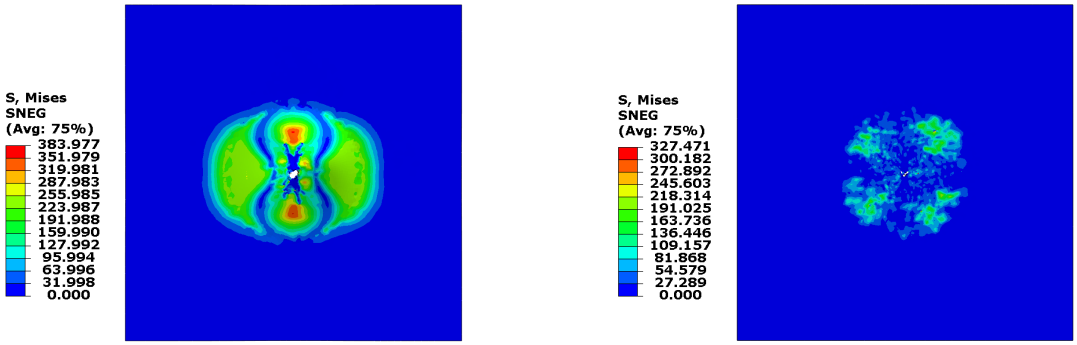

(a) 3,12 ms (b) 8 ms

Figure 4.24: Damage during the simulation for the bottom ply $[0/90]_5$ (12 J)(Von Mises [MPa]).

4.3 Conclusion

The target of this chapter was to check if the methodology developed in the previous chapter 3 was able to simulates in a precise way the response of a natural fiber composite in lower velocity impact situation. This chapter shows that the in-build material Abaqus provides is not able to do it. The difference in the damage shape and in the energy with the experimental case is important.

This chapter show the need of develop a constitutive model for the Flax/PP composite that can be transformed in a VUMAT user-subroutine. In this way the correct behaviour of the plate can be simulate, obtaining accurate values for the force, energies and damage shape.

Chapter 5

Conclusions

A new class of composite material, known as Natural Fiber Composites, has appeared in the structure industry scenario linked to a society more aware of environmental sustainability. This new group of materials are also subjected to be tested in laboratory, in order to prove their validity in the task. But, those experiments have a high cost in resources. They consume high levels of money and material. So, as in the traditional composite material case the development of constitutive models, linked to numericals simulations and their corresponding codes which are used in commercial finite element softwares are imperative, Ls-Dyna or Abaqus are two good examples of FE packages. NFC based in Flax fibers are the most promising ones in substituting glass fiber composites. Mainly, due to their excellent specific properties.

Damage assess by numerical simulation has been a research field for many years, but it is still challenging to reach the optimum results. There are many methods implemented for traditional FRP. Focusing in the damage generated by a Low Velocity Impact the number is a bit lower, but for NFC they are almost nonexistent. Perhaps, due to particular challenges like the mechanical behaviour, which is non-linear for even small strains and that typical models do not consider phenomena like plasticity and viscoplasticity. New constitutive laws that can capture the physical phenomena that are involve in an impact, such as different damage modes, are required to be developed and validate.

This thesis target was to build up a workflow method to simulate through Abaqus a low velocity impact over a plate composes by Flax/PP. The workflow was developed over a traditional FRP material, and ones it is achieved it is tested in the desired material. Simulate an impact in Abaqus was complex. This complexity result in different unwilling software responses during the whole development of the thesis method. The paramount one was *extremely distortion element* . This error that the software gives when running a case was a major concern and a huge amount of time of the thesis was inverted in avoid and solve this error. The issue thing is that the solution to this error message is not universal, and the optimum solution for the thesis simulation was found in the chapter 3. For this chapter a Kevlar/epoxy composite lamina was chosen as plate material as there

was experimental data available in the literature. It presents the different aspects of the workflow such as geometry modelling, contact and boundary conditions selection or mesh and material definition. Also, in it different approach to geometry and material modelling has been explored, the plate was defined as isotropic shell, isotropic solid, as well as different composite layups for conventional and continuum shell elements, with the results the best approach is picked. The best option is to model the plate as a continuum shell with each of its layup's ply as a single layer. In this way the response and the behaviour of each ply can be study. The workflow was validated correlating the result with the article [60] data.

The chapter 4 shows the results obtained with the thesis method in the case of a Flax/PP plate. The aim was to prove if the method developed using the in-build material that Abaqus provides for fiber composites, is suitable for simulate an LVI over a NFC. The chapter shows a clear need of developing a user-material via a VUMAT subroutine. The method is not able to predict in a precise way the response of the Flax/PP, the different between the simulation values and the experimental data of the article [61] are actually uneven. This leads to create a required VUMAT. This VUMAT must be based in a constitutive model which reproduces the response of the NFC flax under the force of a low velocity impact, introducing the present non-linear stress-strain nature of the NFC.

5.1 Future jobs

VUMAT subroutine is used to define the mechanical constitutive behaviour of a material, known as a user-material. It has the capacity of *'use and update solution-dependent state variables*, *use any field variables that are passed in'*, as well as *'be used in an adiabatic analysis, provided you define both the inelastic heat fraction and the specific heat for the appropriate material definitions and you store the temperatures and integrate them as user-defined state variables.'*[76] All this allows the user to extend the capability of the in-build material of Abaqus, to elements with other stress states that are not a plane stress formulation. VUMAT sub-routines are usually long codes that required to be simulate in simple cases firstly, in order to be able to assess their bugs or weaknesses. And after this 1 element cases are fully working the whole problem is simulated.

Developing the damage-elastic law that represent the physical behaviour of the Flax/PP is a extremely challenging and arduous task. During the evolution of this thesis there were at least two clear attempts of model, but any of them fulfill the required expectations. The main future job that this thesis leaves is to improve the constitutive model in order to make it useful. And afterwards, to implement it in a user-subroutine code. One this is achieve the VUMAT should be tested in more than one impact simulation through Abaqus, changing properties of the material and also geometrical properties. If this shows any weakness of the code it should be improve again. At the end constitutive models and they numerical simulations are iterative problems that must be correct and improve constantly taking in advance the new development of computational of scientific tools.

The begging of the constitutive model was based in the theory of invariant of tensor functions, developed from the specific strain energy function W, which depends itself of the two symmetric tensor, the strain tensor ϵ and the damage tensor $\boldsymbol{D}$, being W(ϵ, $\boldsymbol{D}$). In addition, two dual quantities were used, the thermodynamic force dual to the strain and the damage rate, expressed as

$$\boldsymbol{\sigma} = \frac{\partial W}{\partial \boldsymbol{\varepsilon}}, \quad \text{and} \quad \boldsymbol{Y} = -\frac{\partial W}{\partial \boldsymbol{D}}. \tag{5.1}$$

The damage was presented as an damage evolution function expressed as

$$\dot{\boldsymbol{D}} = \frac{g(\boldsymbol{D})}{t_{\mathrm{d}}} \left\langle \frac{f(\boldsymbol{Y})}{Y_{\mathrm{ref}}} \right\rangle^{r} \frac{\partial f}{\partial \boldsymbol{Y}}, \tag{5.2}$$

where $\boldsymbol{Y}$ is the thermodynamic force, Y_{ref} is an arbitrary reference value of the thermodynamic force, f is the damage surface and $g(\boldsymbol{D})$ is a function of invariants.

Chapter A

Before the preliminary simulation

This chapter collects three pre-cases that were done before starting with the preliminar simulation itself. This was done in order to understand the dynamism and the module of the program interphase. Three different impacts were generated, two of them have a bullet shape impactor and another has a pendulum impactor. The two first have metallic plates, and the third one has a composite material plate.

The figure A.1 shows an cylindrical bullet impacting in a metallic plate. For this case the impose condition was a linear speed in the gravity center of the striker, and the edge of the plate was encastre. The figure A.1b shows the obtained results of the simulation. However, the interest in this case was more about the understanding of the program's modules than the final results.

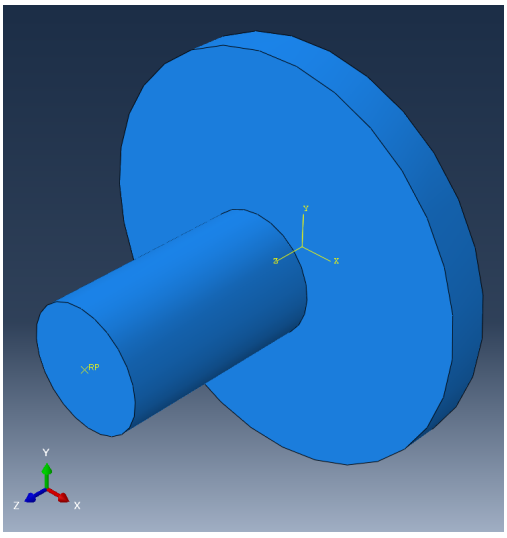

(a) Assembly.

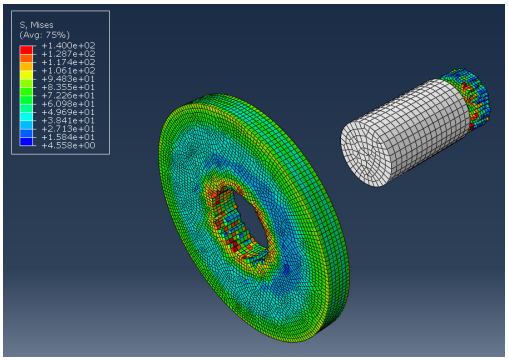

(b) S, Von Misses solutions, visualization module.

Figure A.1: Impact with a cylindrical impactor over a circular plate.

Hereunder, the figure A.2 shows the second case that was done to improve the

skills related with the software. This time a pendulum impact was generated. In contrasts to the first impact, where the speed was a rotational one imposes in a far point of the gravitational center, the point was where a rope, in a real case, would have be attached to the ceiling. Another change is the shape of the plate and the strike, as the figure reflects, the impactor is a sphere and the plate is an square, and again its edge are encastre.

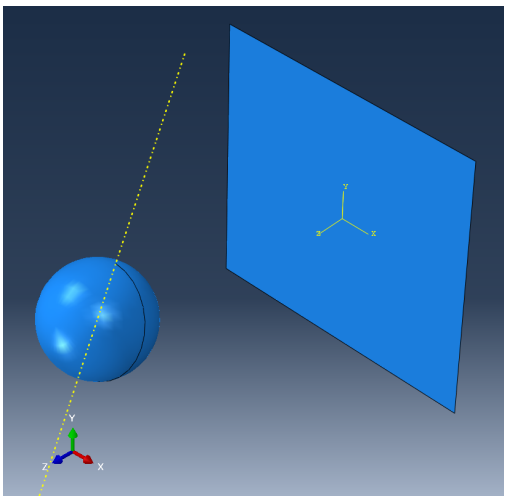

(a) Assembly.

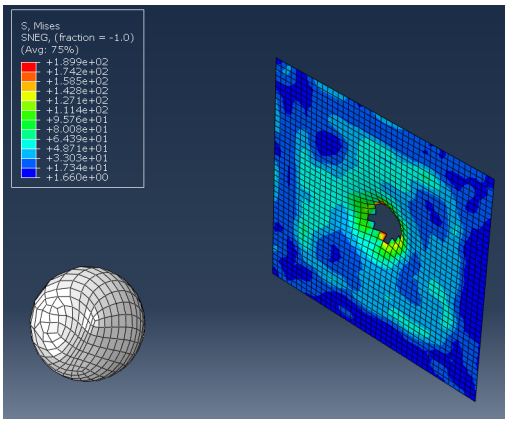

(b) S, Von Misses solutions, visualization module.

Figure A.2: Pendulum impact with a sphere impactor over a square plate.

The final case in this learning process was a bullet shape striker. Here the main change is the material of the plate, in this case a composite material is implemented. The plate was formed with a four ply composite. Another remarkable change is that this case is a quarter of the problem, in order to study the time implication of the number of elements.

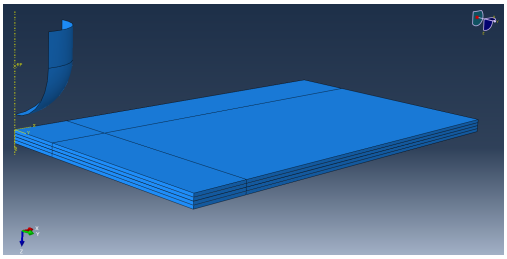

(a) Assembly.

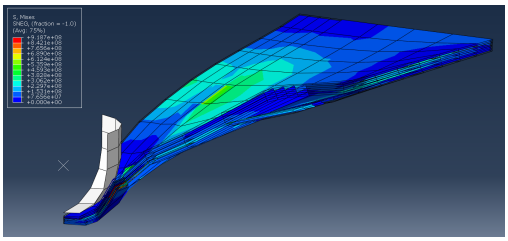

(b) S, Von Misses solutions, visualization module.

Figure A.3: Impact with a sharp impactor over a square plate.

These three previous cases where taken from YouTube [4, 5, 38], but several problems appears. When a composite material is used, the way in which the two first videos are created, can not be followed. Abaqus has not implemented in the library for composite any module for plastic behaviour, it is required to generated a sub-routine. This is the first time that the requirement of implement a user material popped up. When a impact is carry out in the Explicit domain

of Abaqus using a composite material plate, the case becomes extremely sensitive to the mesh. Not only to the size of element, as normally any FEM is normally affected, but also to the definition of the element that form the mesh.

Finally, the case that is studied in the chapter 3 is in a way a mixture of the three pre-cases. It has a spherical impactor and a square composite material plate. Thanks to this first approach it is bolstered the need to do an assessment of mesh sensitivity and definition, in order to know the correct parameters to avoid the abortion of the program and be able to obtain results that are as closer as the reality.

Chapter B

Kevlar/Epoxy output figures

B.1 Plate as a isotropic material

B.1.1 Plate modelled as a shell

The Figure B.1 represent the energies and the contact force, respectively, versus the time.

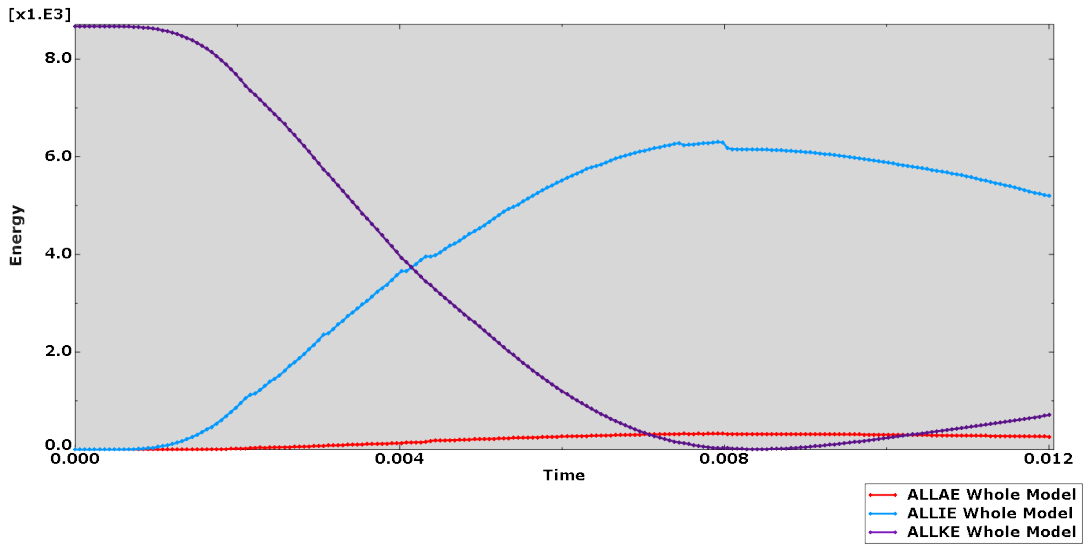

(a) Energies vs. time.

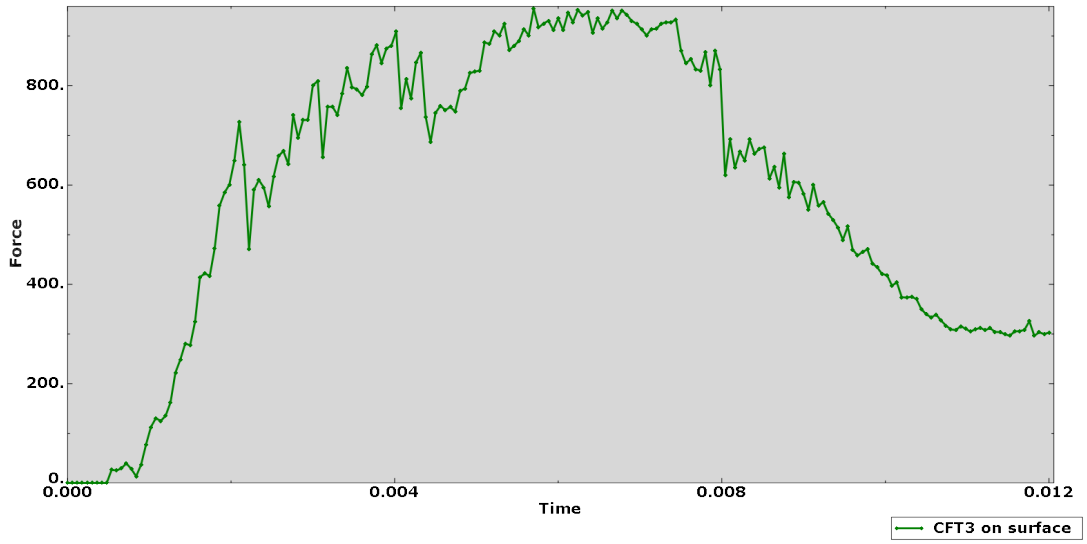

(b) Force vs. time.

Figure B.1: Plate modelled as a isotropic shell.

The figures B.2, B.3, B.4 and B.5 show the distribution (by colour maps) of the different failure criteria, that in the *Step module* are selected and the stress of Von Misses distribution over the plate.

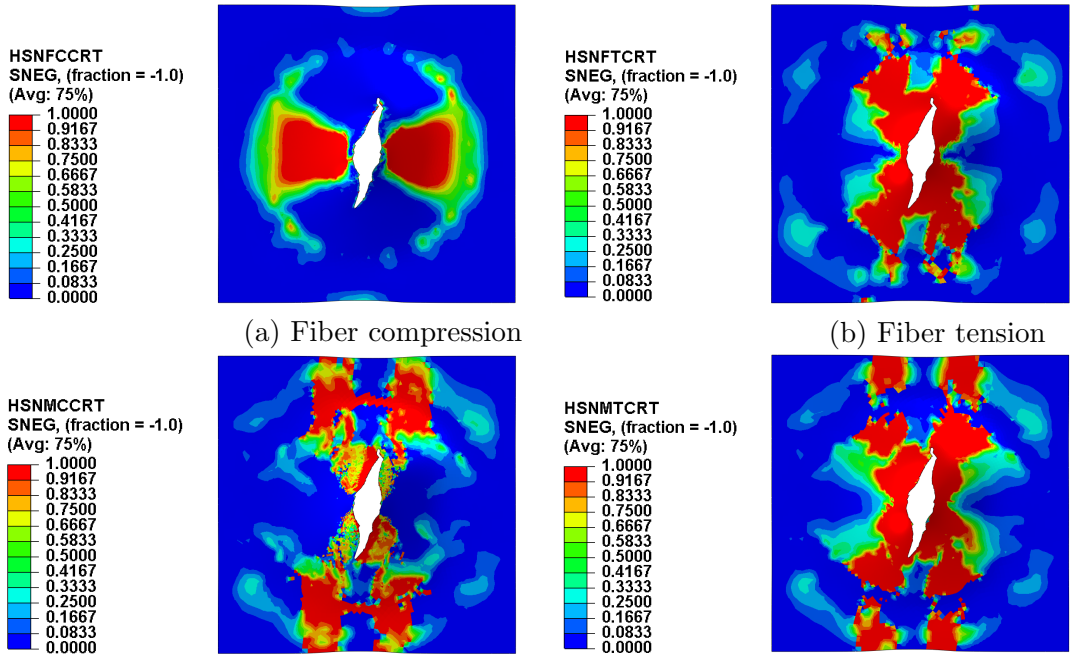

(a) Fiber compression (b) Fiber tension

(c) Matrix compression (d) Matrix tension

Figure B.2: Damage initiation (Hashin failure criteria) at the maximum deformation.

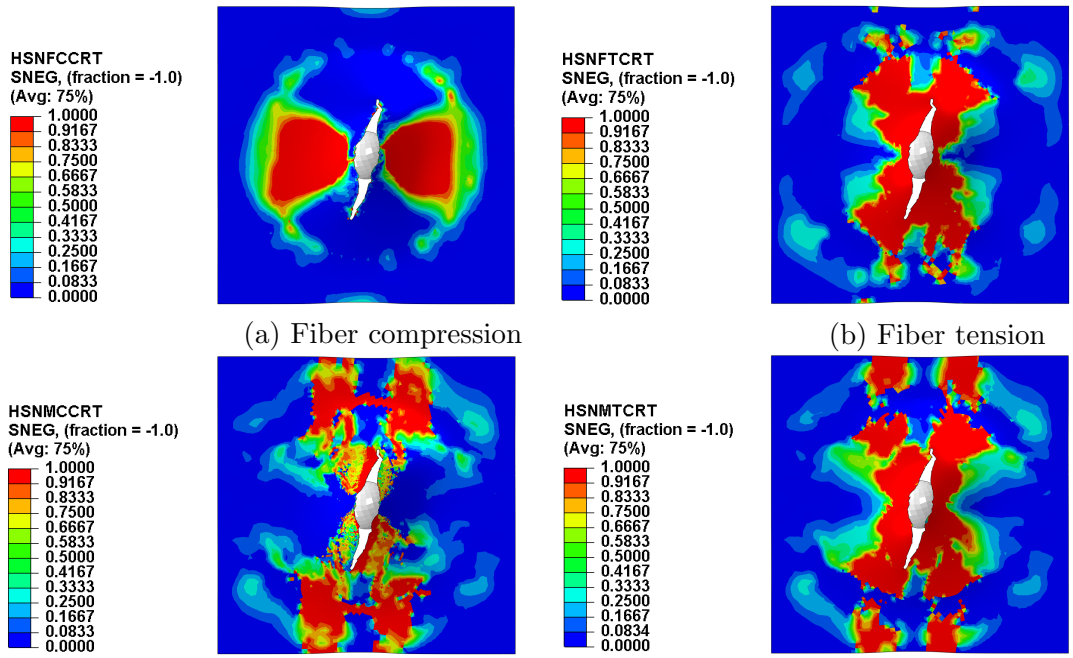

(a) Fiber compression (b) Fiber tension

(c) Matrix compression (d) Matrix tension

Figure B.3: Damage initiation (Hashin failure criteria) at the end deformation.

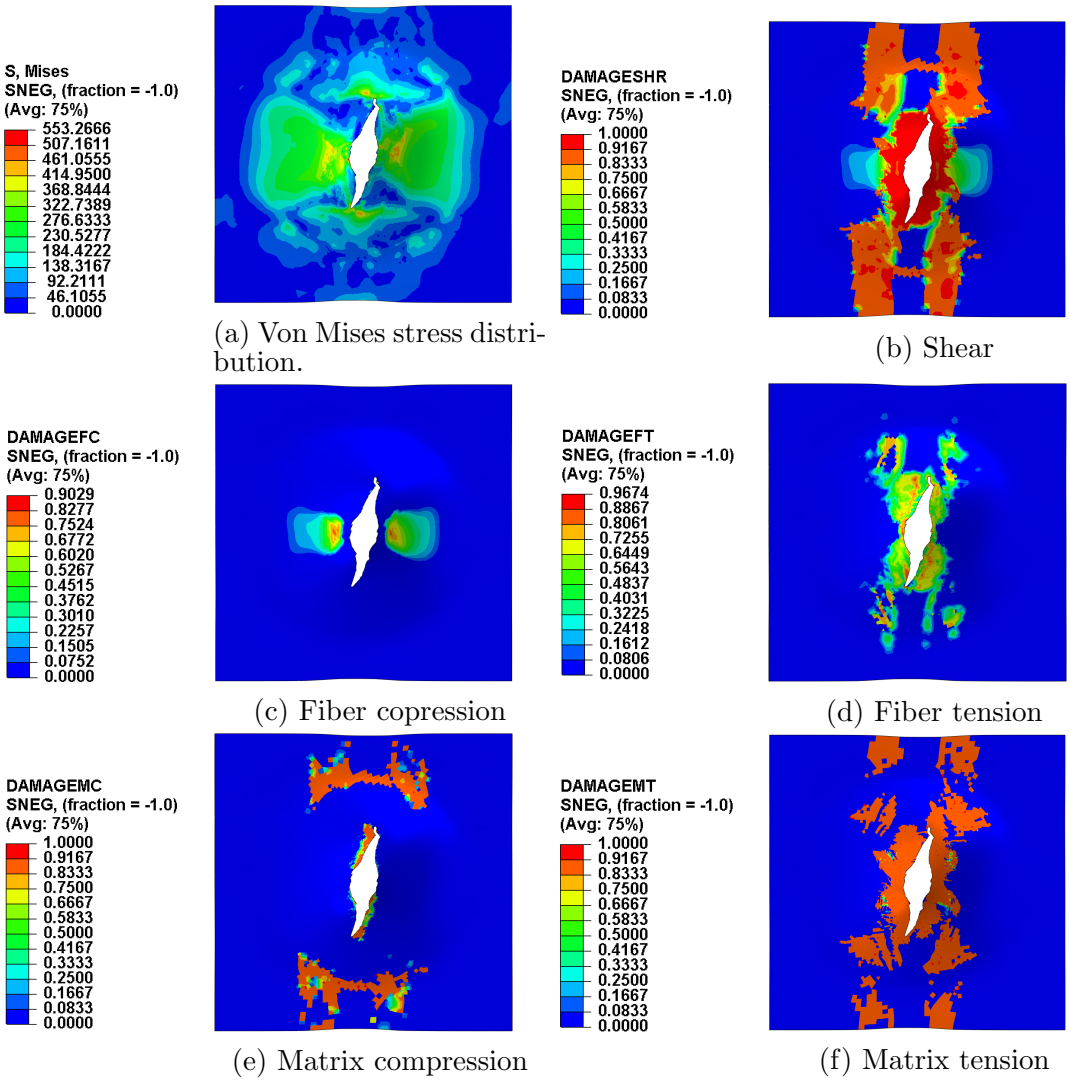

(a) Von Mises stress distribution.

(b) Shear

(c) Fiber copression

(d) Fiber tension

(e) Matrix compression

(f) Matrix tension

Figure B.4: Damage evolution and stress distribution at the maximum deformation..

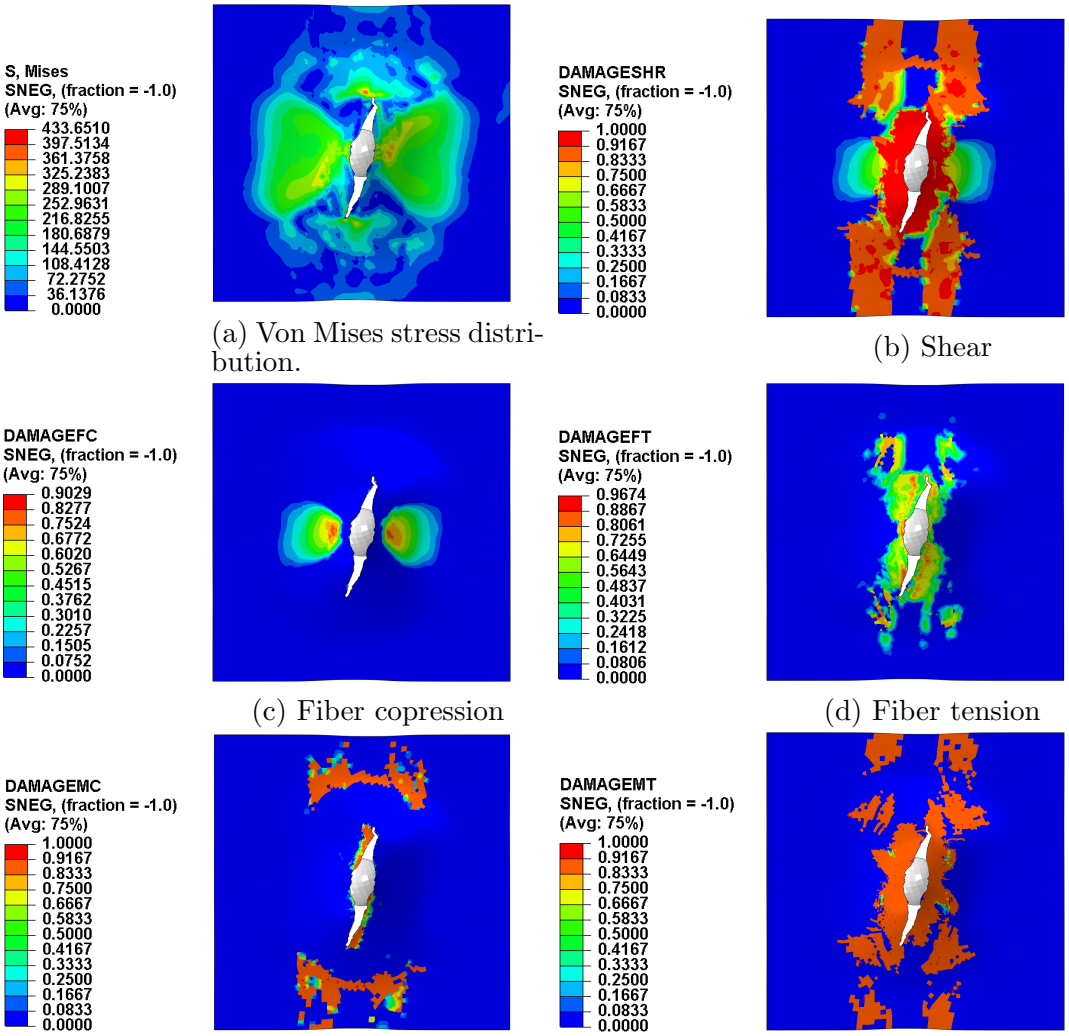

(a) Von Mises stress distribution.

(b) Shear

(c) Fiber copression

(d) Fiber tension

(e) Matrix compression

(f) Matrix tension

Figure B.5: Damage evolution and stress distribution at the end deformation..

B.1.2 Plate modelled as a solid

The two charts in the figure B.6 show the energy and the force, respectively, versus the time.

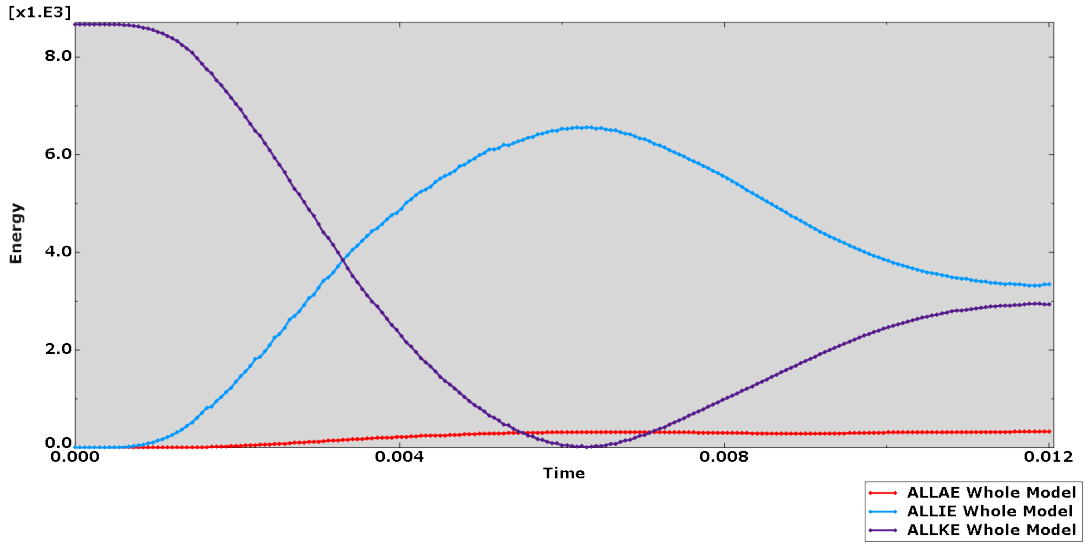

(a) Energies vs. time.

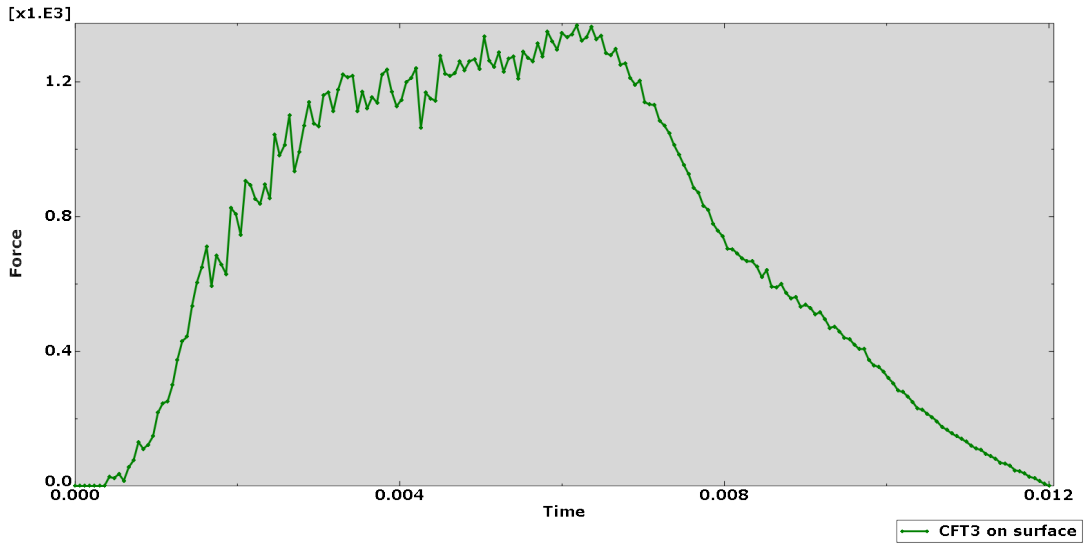

(b) Force vs. time.

Figure B.6: Plate modelled as a isotropic solid.

The figures B.7, B.9, B.8 and B.10 show the the distribution (by colour maps) of the different failure criteria, that in the *Step module* are selected and the stress of Von Misses distribution over the plate.

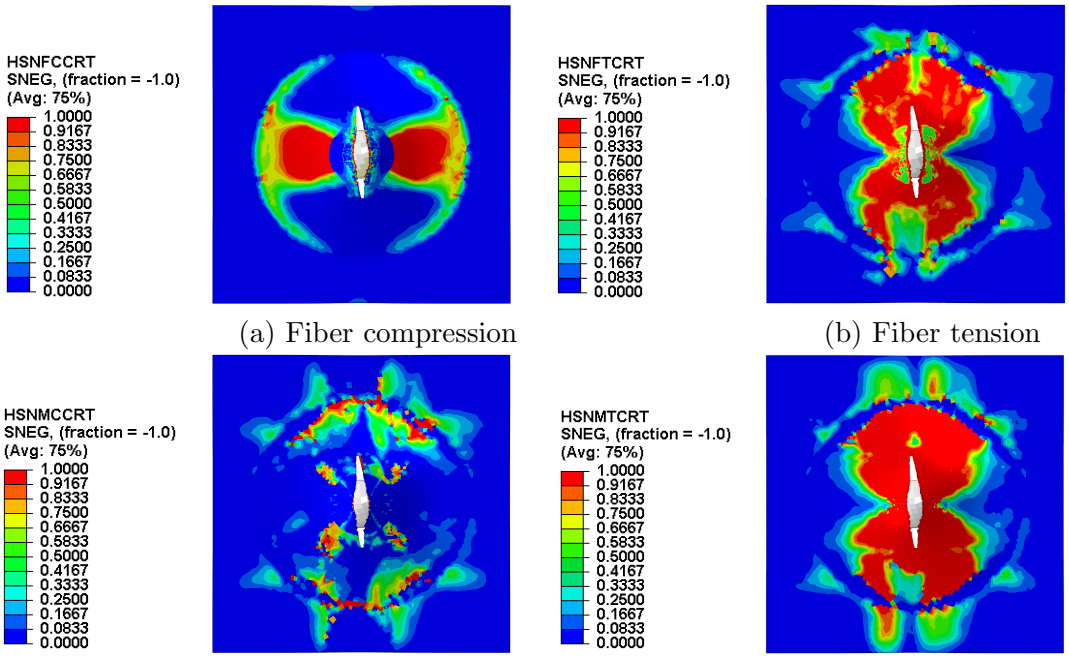

(a) Fiber compression (b) Fiber tension

(c) Matrix compression (d) Matrix tension

Figure B.7: Damage initiation (Hashin failure criteria) at the maximum deformation.

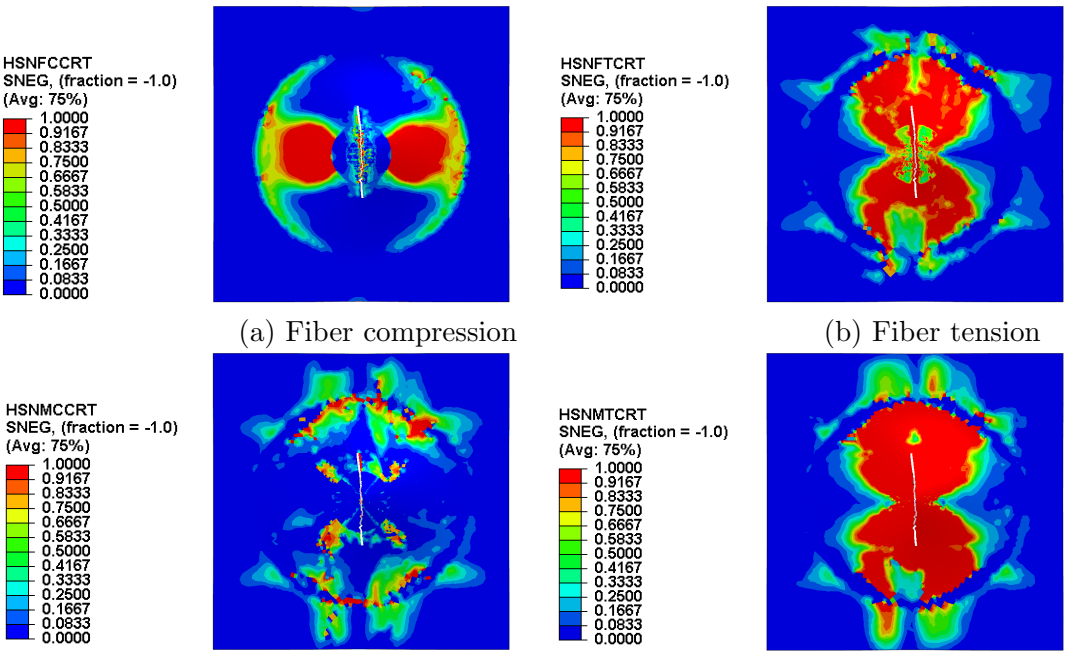

(a) Fiber compression (b) Fiber tension

(c) Matrix compression (d) Matrix tension

Figure B.8: Damage initiation (Hashin failure criteria) at the end deformation.

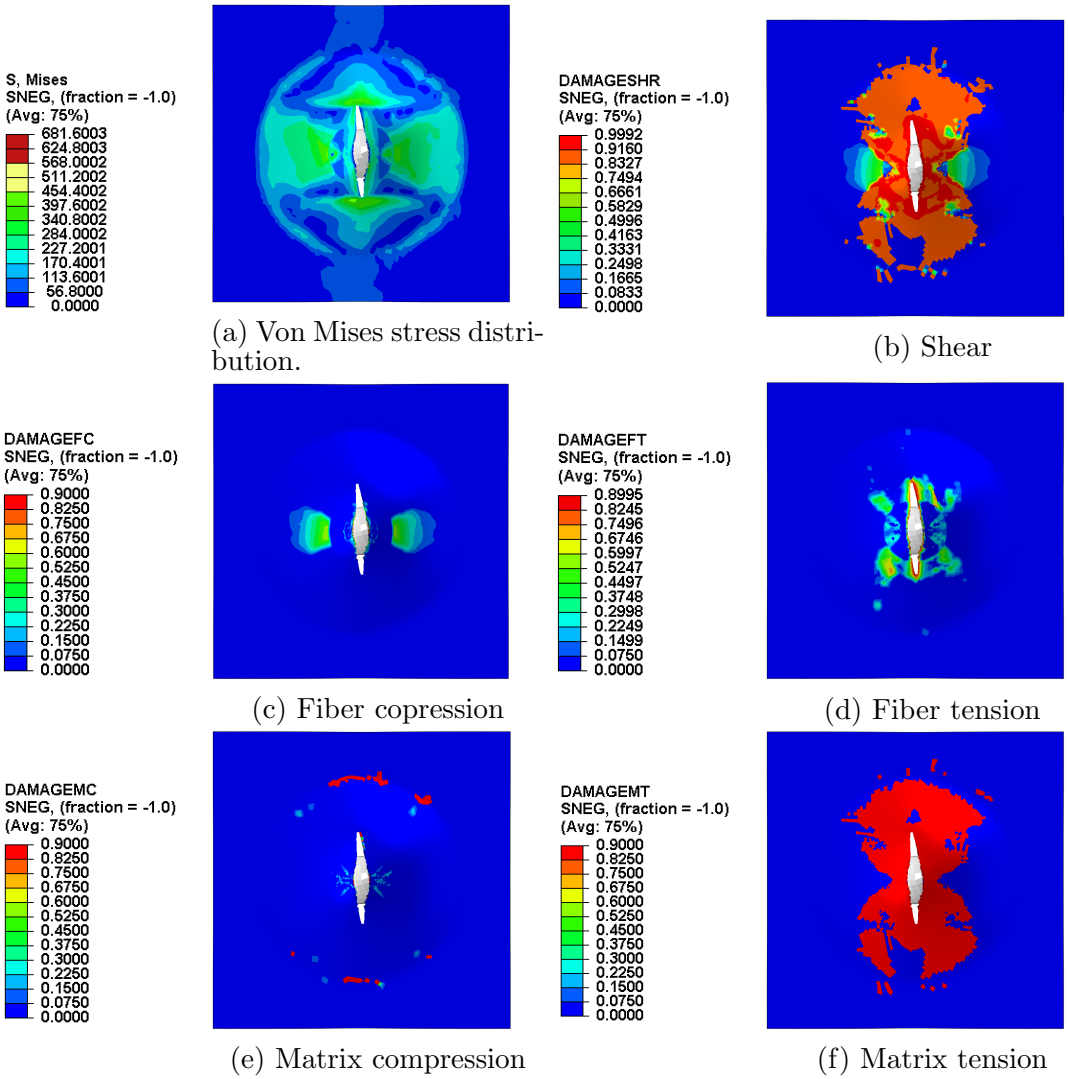

(a) Von Mises stress distribution.

(b) Shear

(c) Fiber copression

(d) Fiber tension

(e) Matrix compression

(f) Matrix tension

Figure B.9: Damage evolution and stress distribution at the maximum deformation.

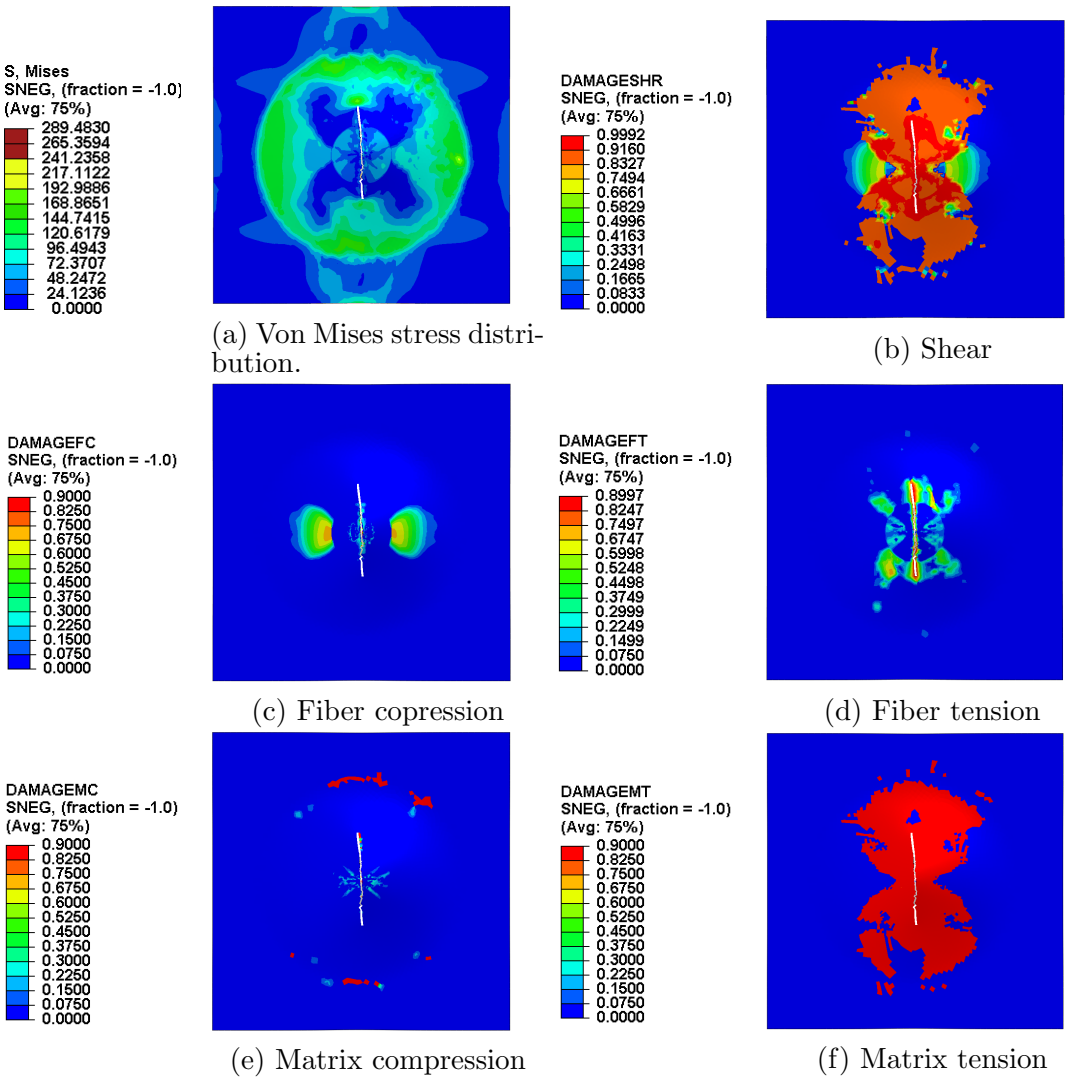

(a) Von Mises stress distribution.

(b) Shear

(c) Fiber copression

(d) Fiber tension

(e) Matrix compression

(f) Matrix tension

Figure B.10: Damage evolution and stress distribution at the end deformation..

B.2 Plate layout $[0]_3$

B.2.1 Conventional shell

The two charts that are gathered in the figure B.11 shows the energy and the force, respectively, versus the time.

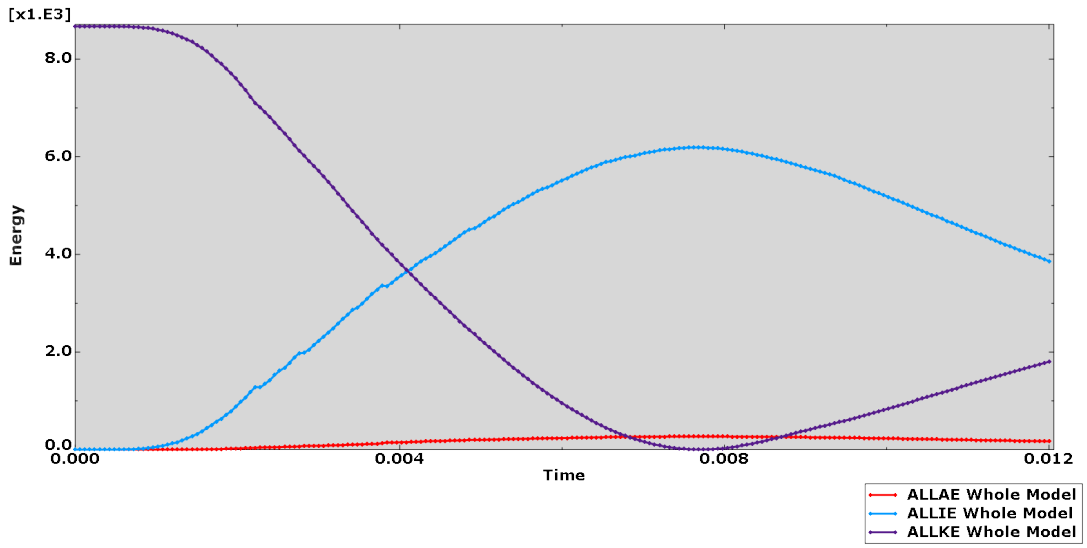

(a) Energies vs. time.

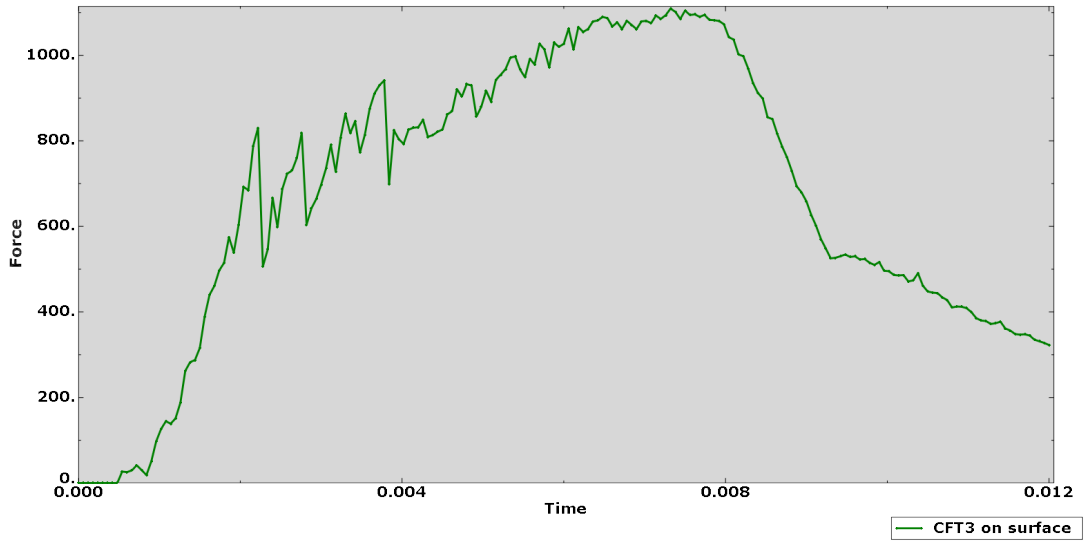

(b) Force vs. time.

Figure B.11: Plate modelled as a shell with conventional properties (1 layer with 3ply).

The figures B.12, B.14, and B.13 and B.15 show the the distribution (by colour maps) of the different failure criteria, that in the *Step module* are selected and the stress of Von Misses distribution over the plate.

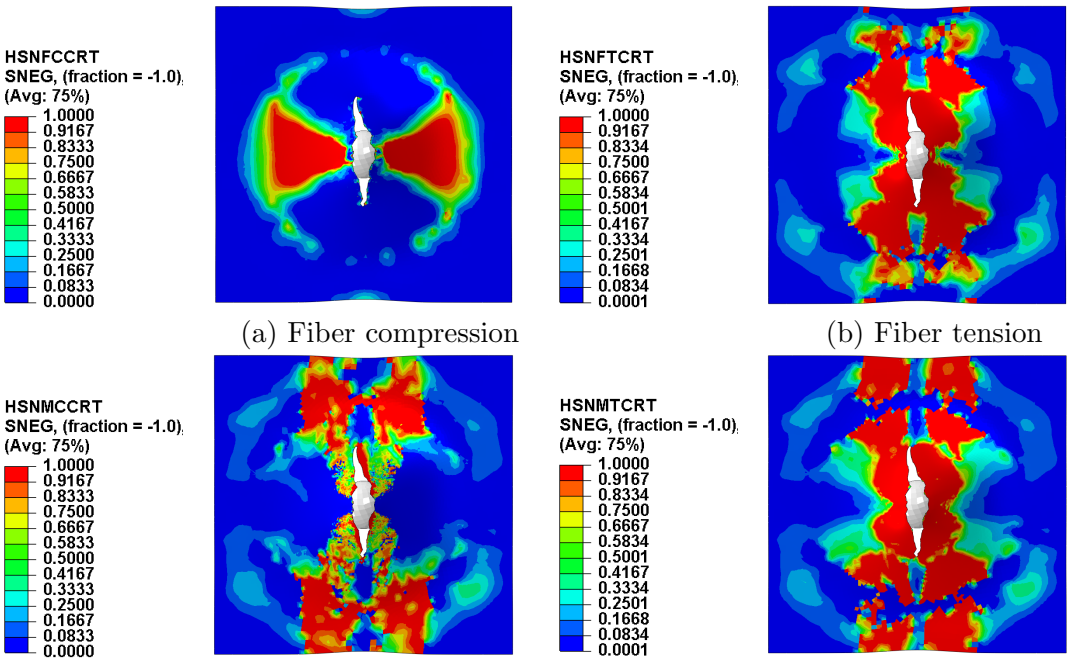

(a) Fiber compression (b) Fiber tension

(c) Matrix compression (d) Matrix tension

Figure B.12: Damage initiation (Hashin failure criteria) at the maximum deformation.

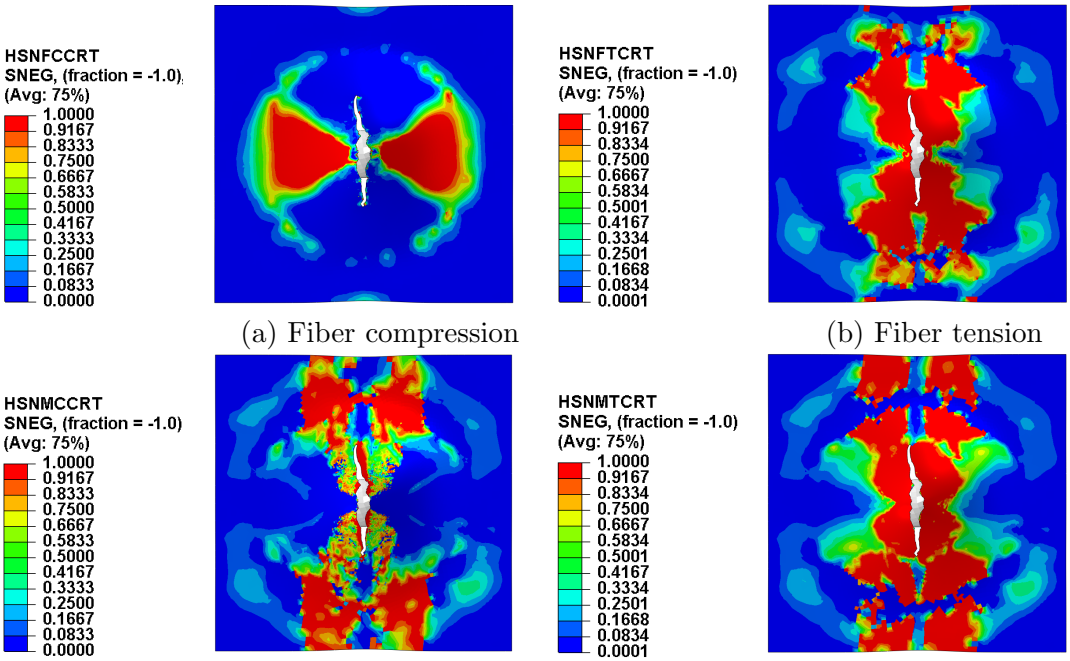

(a) Fiber compression (b) Fiber tension

(c) matrix compression (d) Matrix tension

Figure B.13: Damage initiation (Hashin failure criteria) at the end deformation.

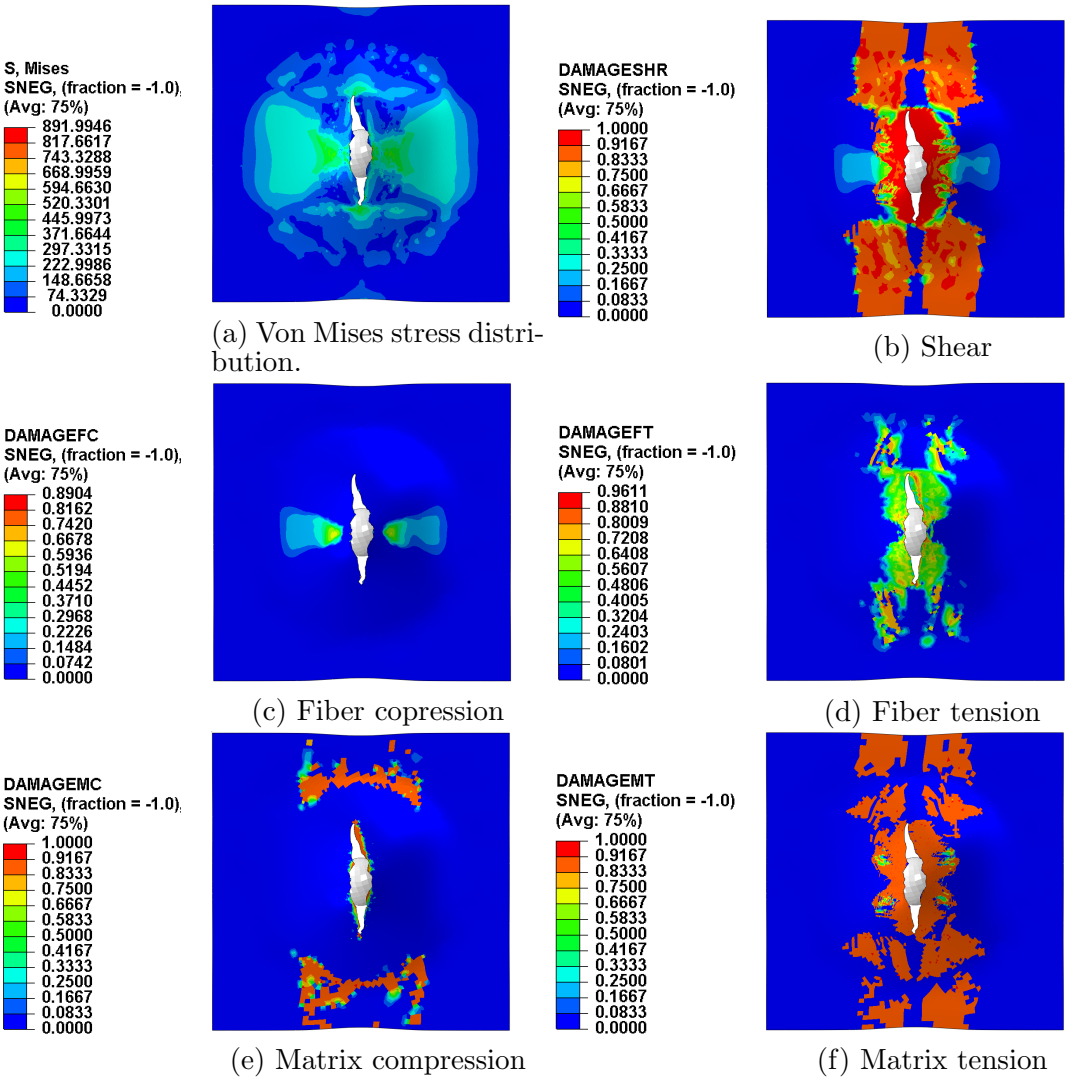

(a) Von Mises stress distribution.

(b) Shear

(c) Fiber copression

(d) Fiber tension

(e) Matrix compression

(f) Matrix tension

Figure B.14: Damage evolution and stress distribution at the maximum deformation.

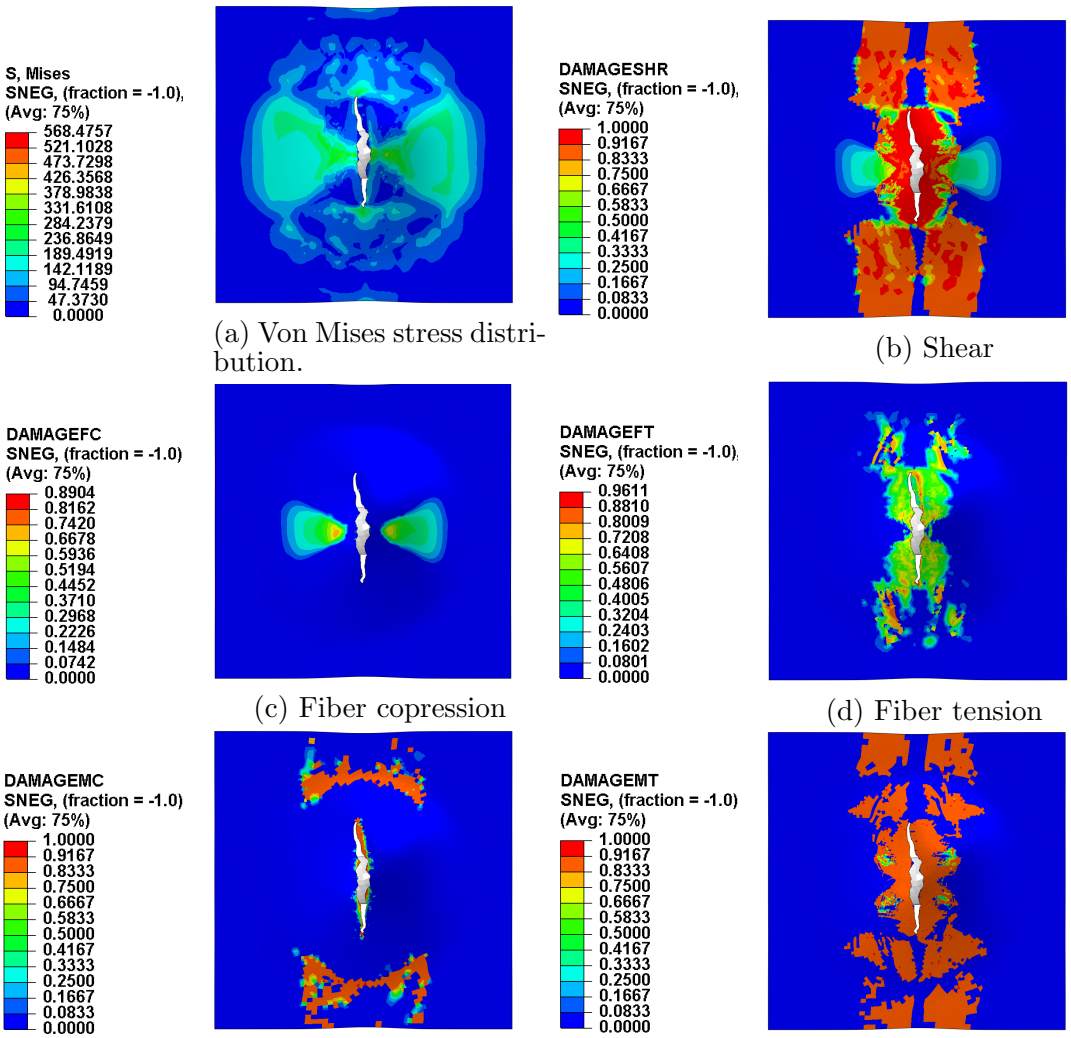

(a) Von Mises stress distribution.

(b) Shear

(c) Fiber copression

(d) Fiber tension

(e) Matrix compression

(f) Matrix tension

Figure B.15: Damage evolution and stress distribution at the end deformation..

B.2.2 Continuum shell, 1 layer with 3 plies

The two charts that are gathered in the figure B.16 shows the energy and the force, respectively, versus the time.

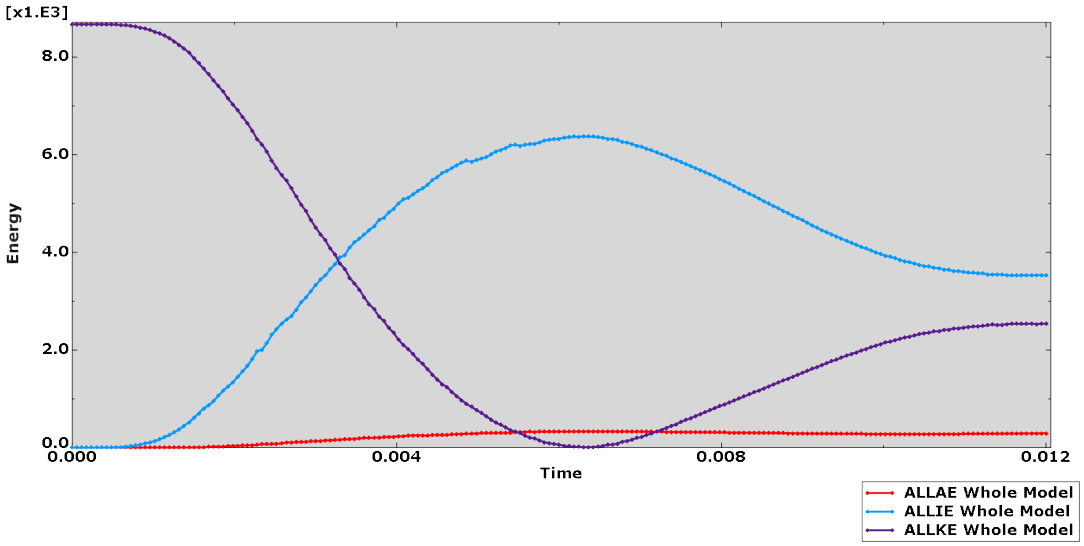

(a) Energies vs. time.

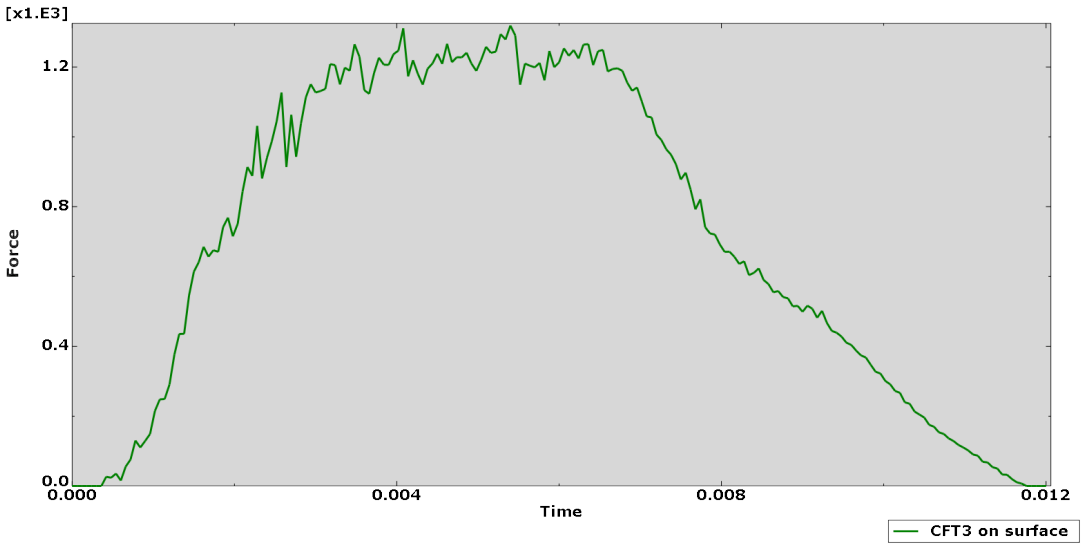

(b) Force vs. time.

Figure B.16: Plate modelled as a solid with continuum shell properties (1 layer with 3ply).

The figures B.17, B.19, B.18 and B.20 show the the distribution (by colour maps) of the different failure criteria, that in the *Step module* are selected and the stress of Von Misses distribution over the plate.

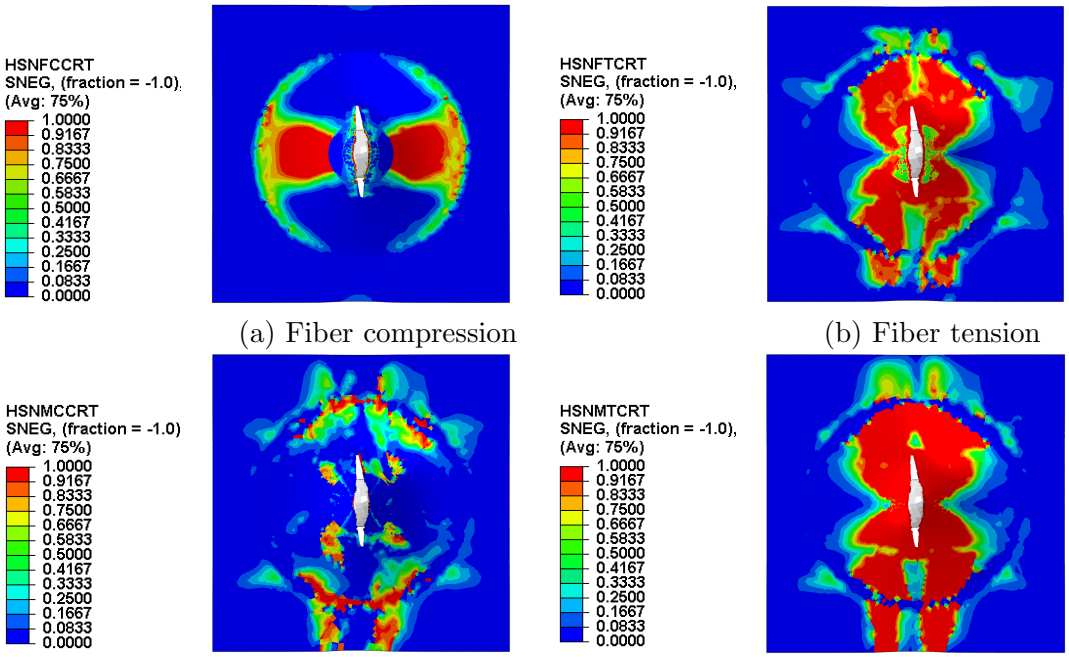

(a) Fiber compression (b) Fiber tension

(c) Matrix compression (d) Matrix tension

Figure B.17: Damage initiation (Hashin failure criteria) at the maximum deformation.

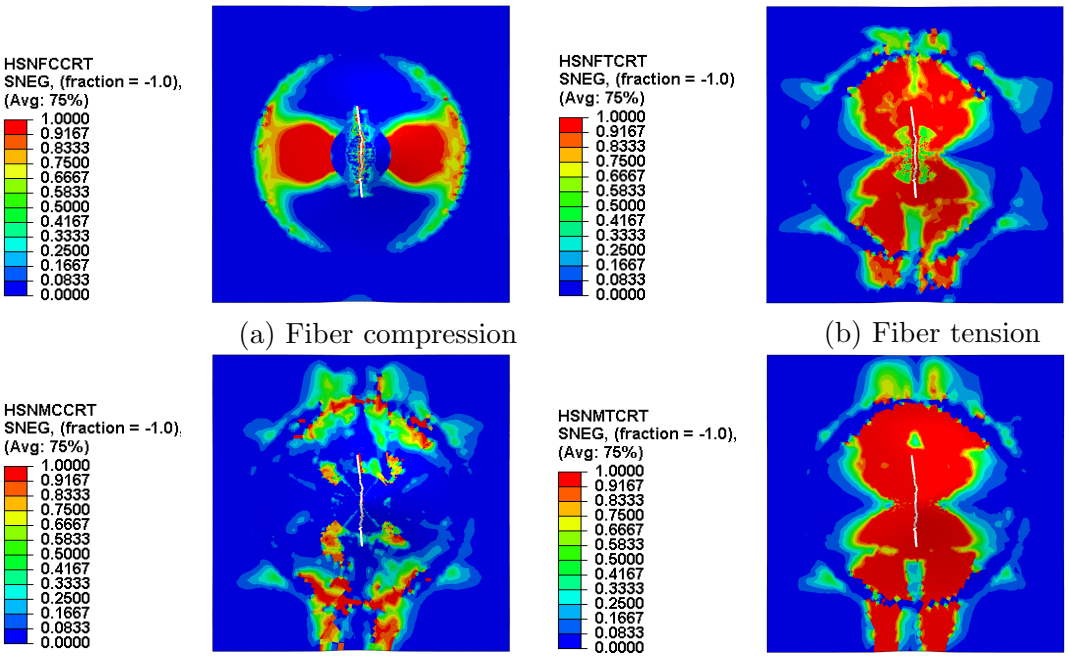

(a) Fiber compression (b) Fiber tension

(c) matrix compression (d) Matrix tension

Figure B.18: Damage initiation (Hashin failure criteria) at the end deformation.

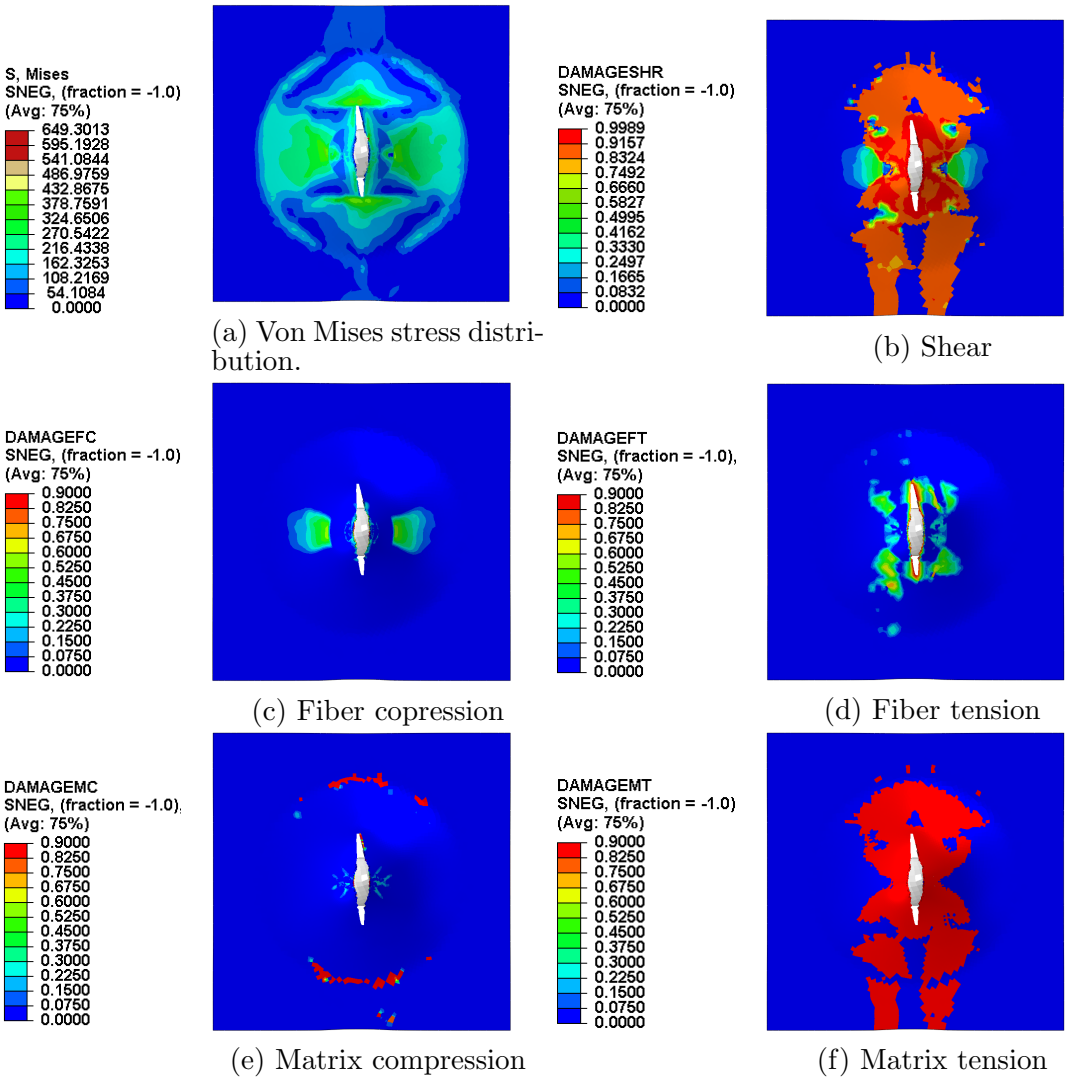

(a) Von Mises stress distribution.

(b) Shear

(c) Fiber copression

(d) Fiber tension

(e) Matrix compression

(f) Matrix tension

Figure B.19: Damage evolution and stress distribution at the maximum deformation.

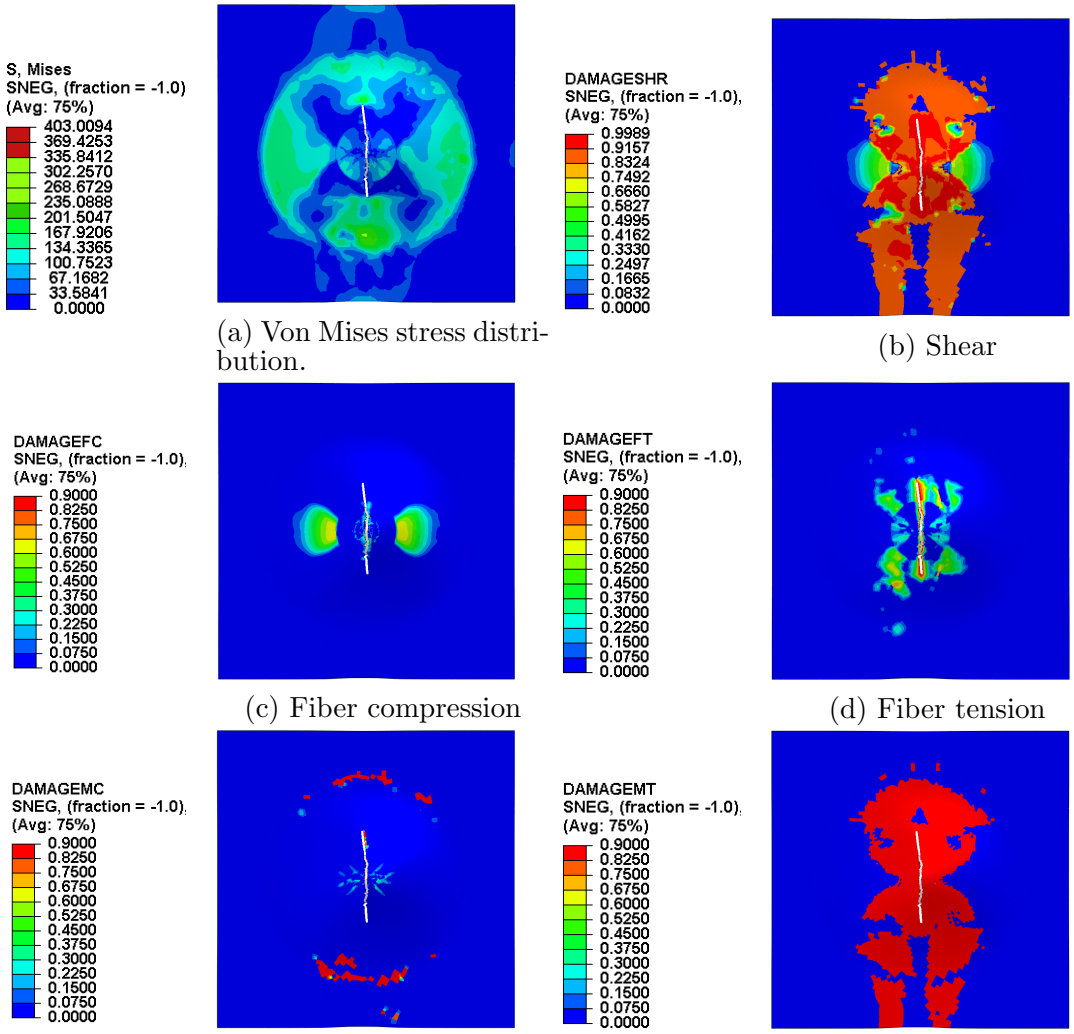

(a) Von Mises stress distribution.

(b) Shear

(c) Fiber compression

(d) Fiber tension

(e) Matrix compression

(f) Matrix tension

Figure B.20: Damage evolution and stress distribution at the end deformation..

B.2.3 Continuum shell, 3 layer with 1 plies each

The two charts that are gathered in the figure B.21 shows the energy and the force, respectively, versus the time.

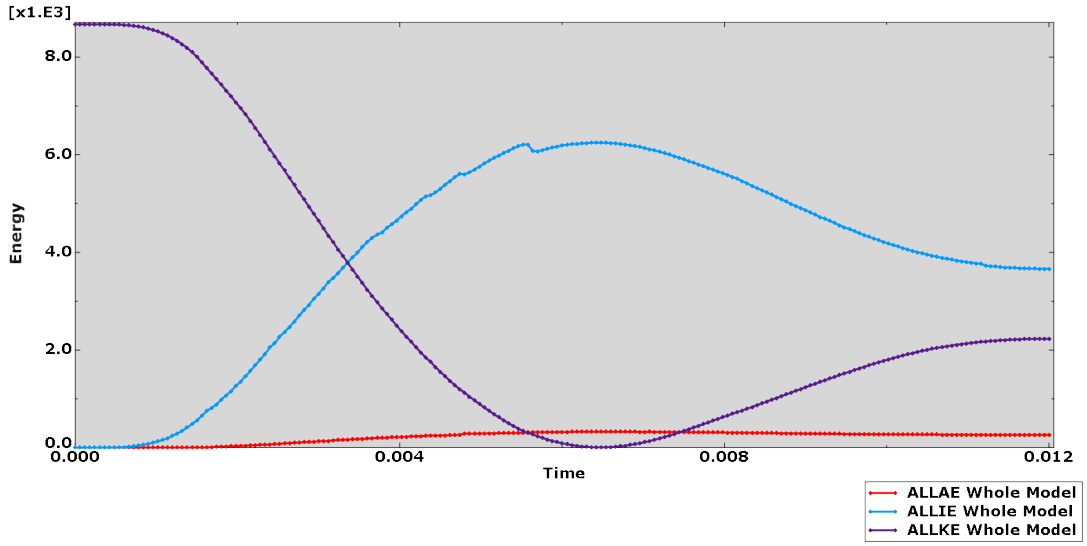

(a) Energies vs. time.

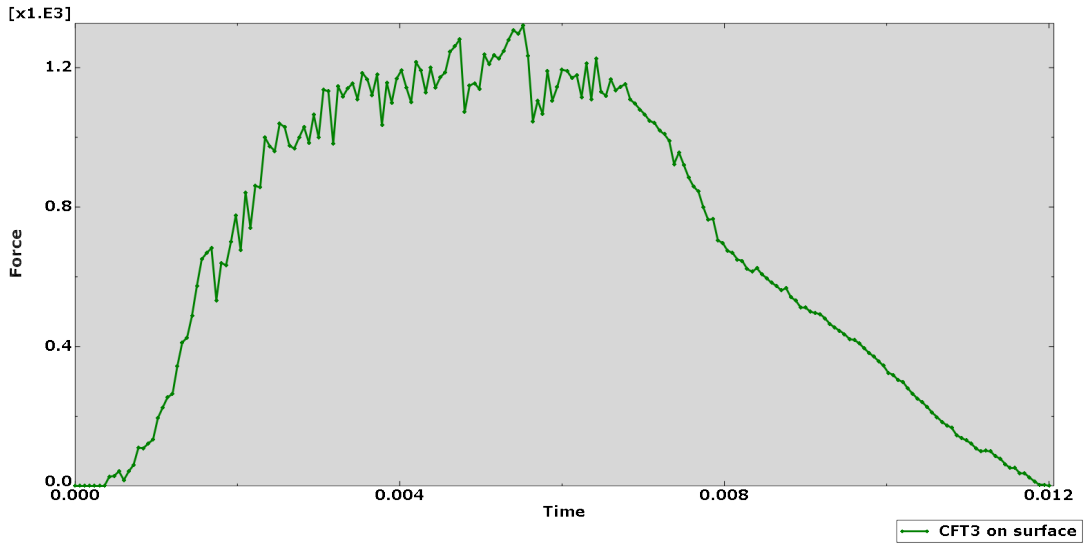

(b) Force vs. time.

Figure B.21: Plate modelled as a solid with continuum shell properties (3 layer, 1ply each).

The figures B.22, B.24, B.25, B.23 and B.26, B.27 show the the distribution (by colour maps) of the different failure criteria, that in the *Step module* are selected and the stress of Von Misses distribution over the plate.

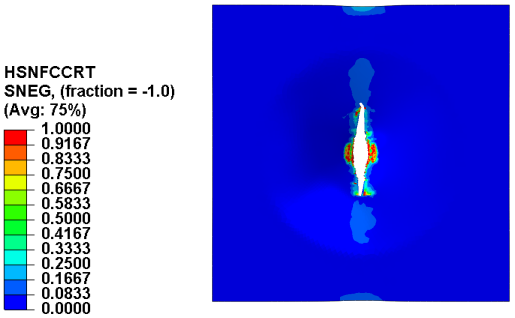

(a) Fiber compression, top ply

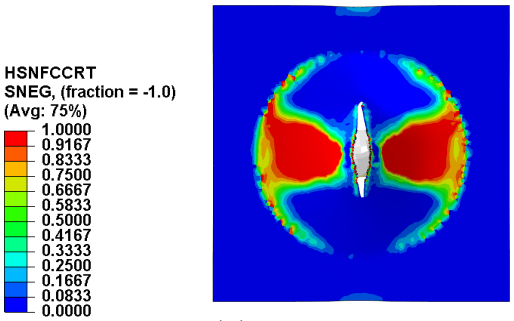

(b) Fiber compression, bottom ply.

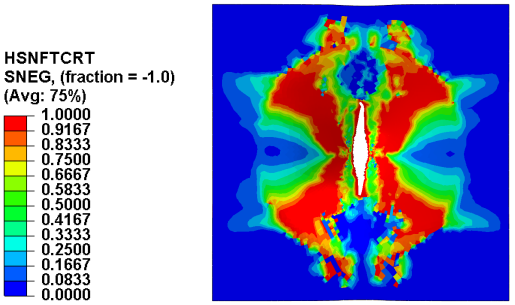

(c) Fiber tension, top ply.

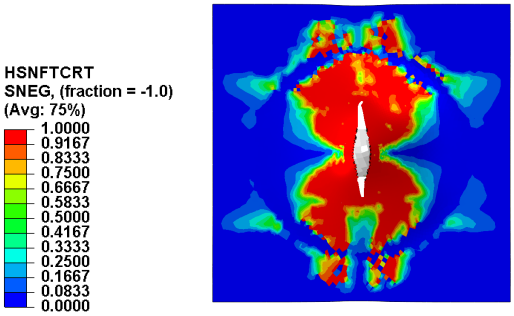

(d) Fiber tension, bottom ply.

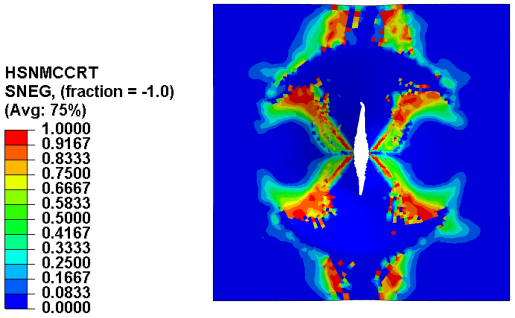

(e) Matrix compression, top ply.

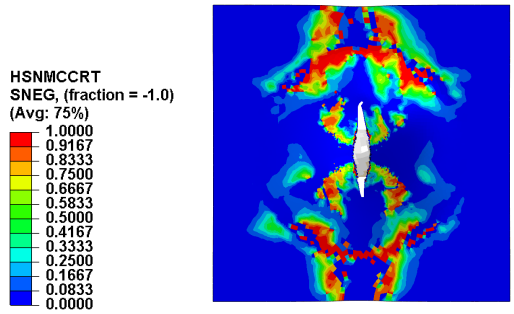

(f) Matrix compression, bottom ply.

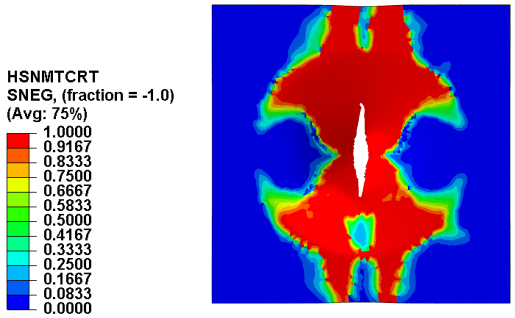

(g) Matrix tension, top ply.

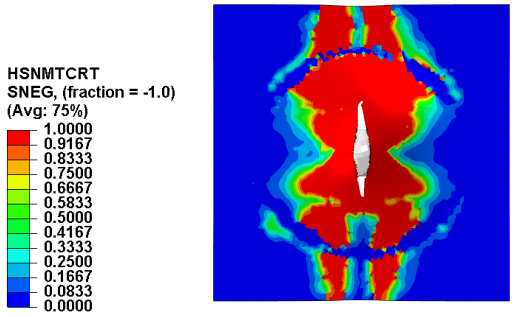

(h) Matrix tension, bottom ply.

Figure B.22: Damage initiation (Hashin failure criteria) at the maximum deformation.

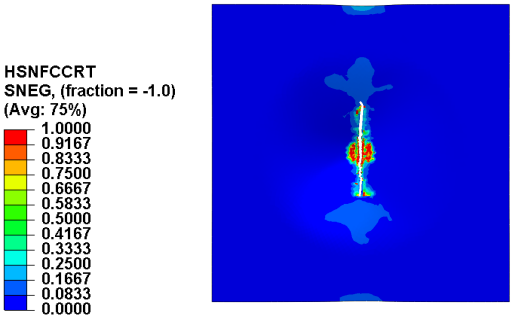

(a) Fiber compression, top ply.

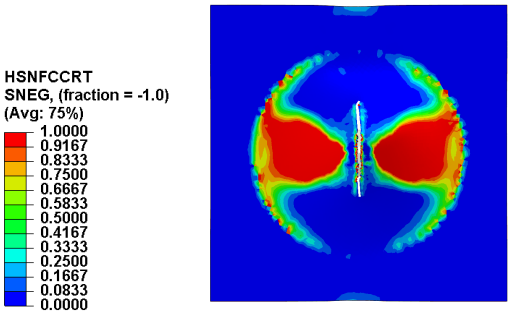

(b) Fiber compression, bottom ply.

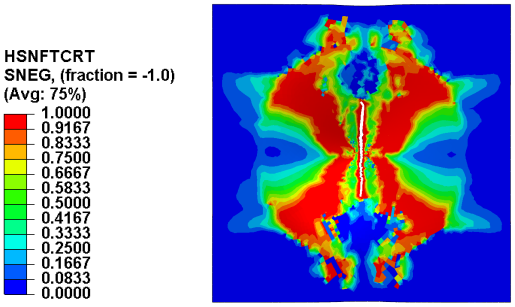

(c) Fiber tension, top ply.

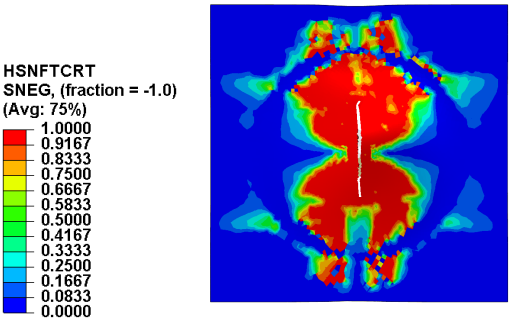

(d) Fiber tension. bottom ply.

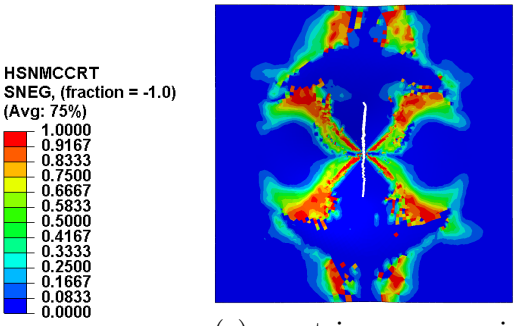

(e) matrix compression, top ply.

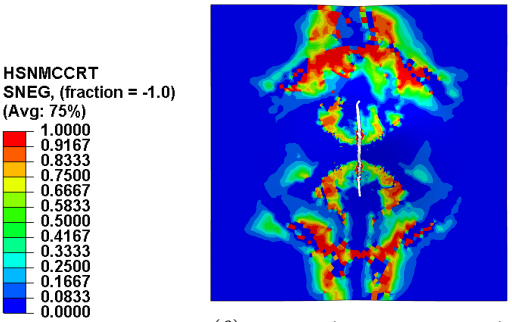

(f) matrix compression, bottom ply.

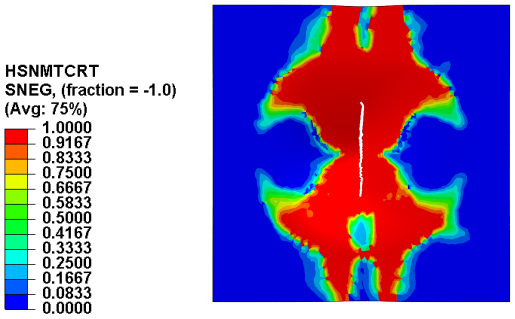

(g) Matrix tension, top ply.

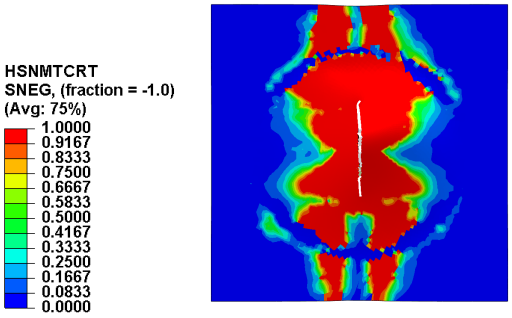

(h) Matrix tension, bottom ply.

Figure B.23: Damage initiation (Hashin failure criteria) at the end deformation.

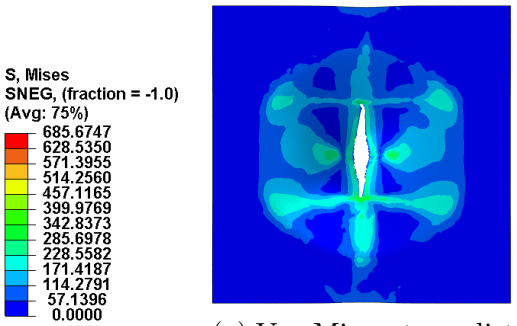

(a) Von Mises stress distribution, top ply.

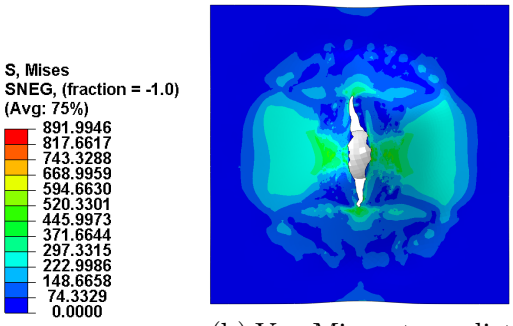

(b) Von Mises stress distribution, bottom ply.

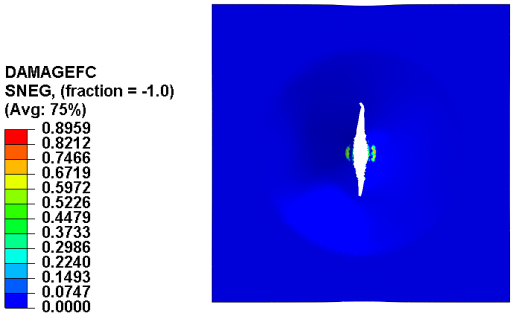

(c) Fibre Compression, top ply.

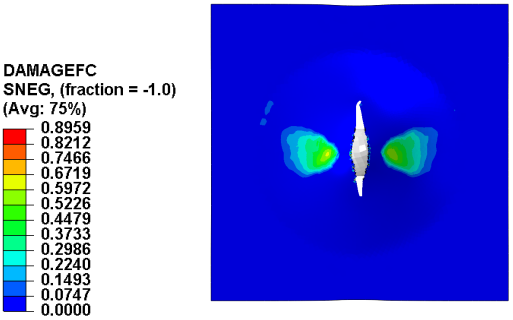

(d) Fibre Compression, bottom ply.

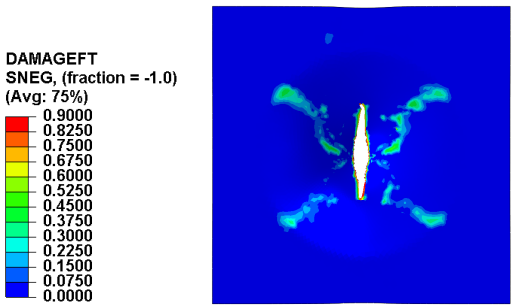

(e) Fibre Tension, top ply.

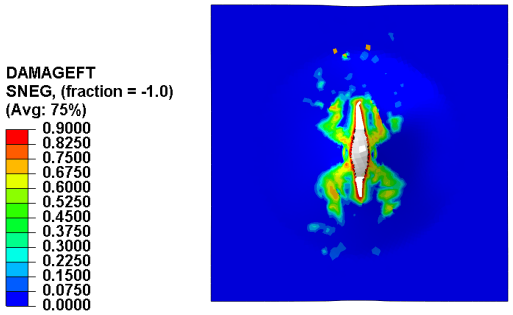

(f) Fibre Tension, bottom ply.

Figure B.24: Damage evolution and stress distribution at the maximum deformation (I).

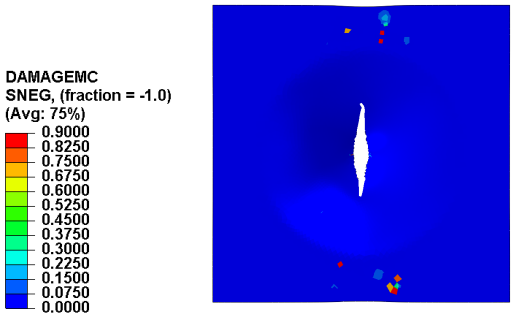

(a) Matrix Compression, top ply.

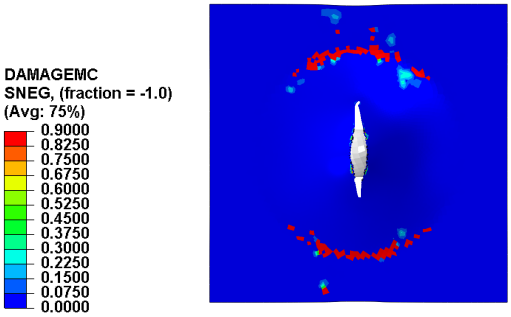

(b) Matrix Compression, bottom ply.

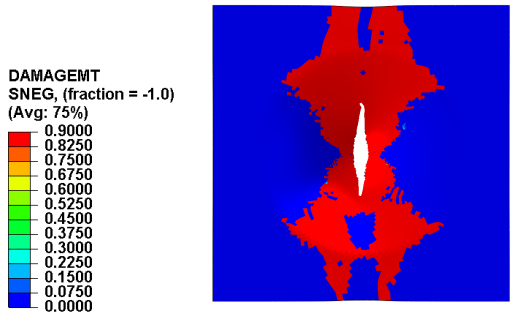

(c) Matrix Tension, top ply.

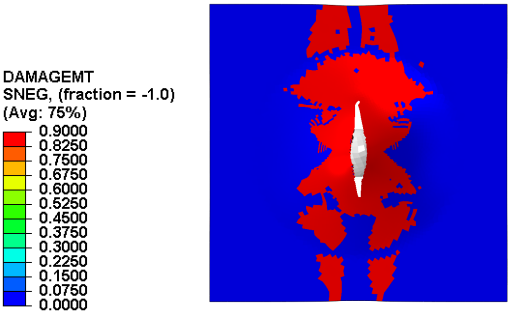

(d) Matrix Tension, bottom ply.

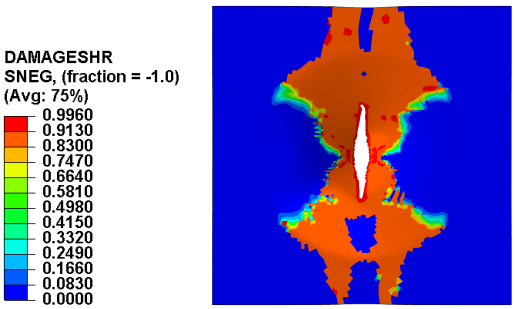

(e) Shear, top ply

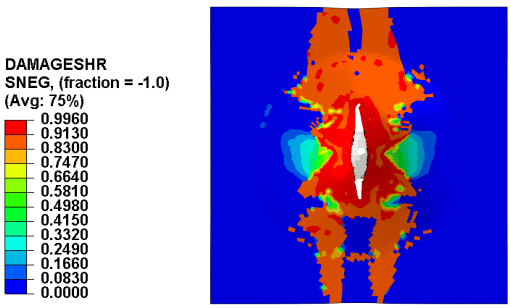

(f) Shear, bottom ply

Figure B.25: Damage evolution and stress distribution at the maximum deformation, (II).

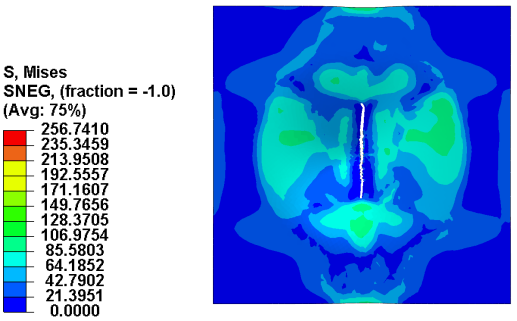

(a) Von Mises stress distribution, top ply.

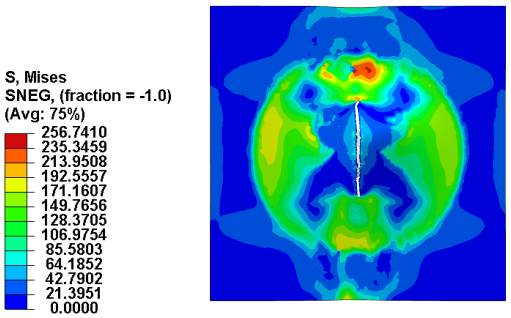

(b) Von Mises stress distribution, bottom ply.

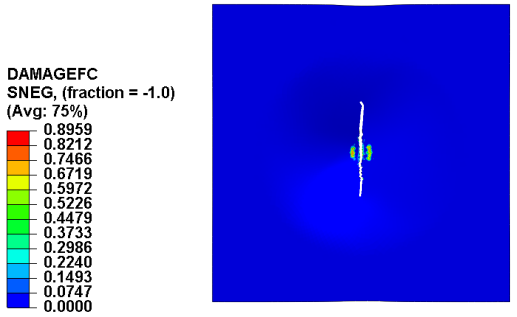

(c) Fibre Compression, top ply.

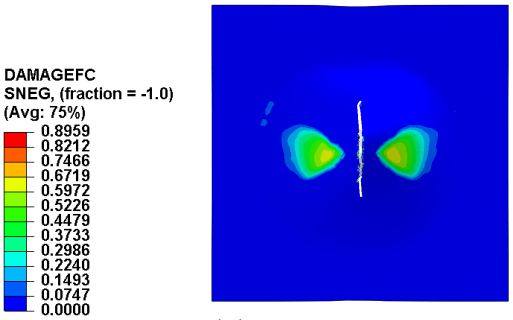

(d) Fibre Compression, bottom ply.

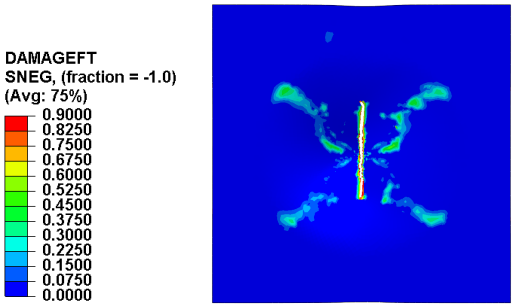

(e) Fibre Tension, top ply.

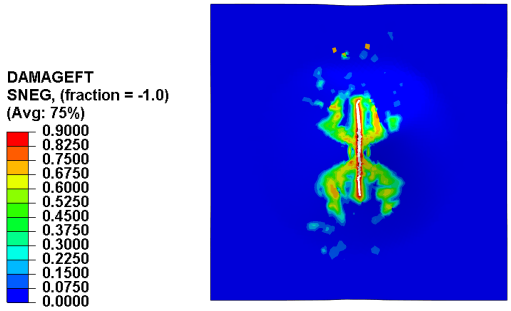

(f) Fibre Tension, bottom ply.

Figure B.26: Damage evolution and stress distribution at the end deformation, (I).

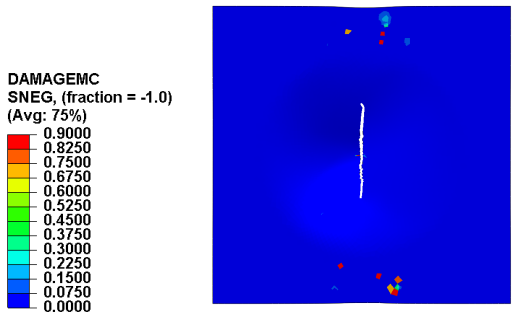

(a) Matrix Compression, top ply.

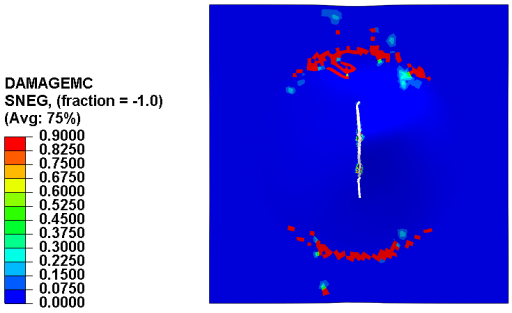

(b) Matrix Compression, bottom ply.

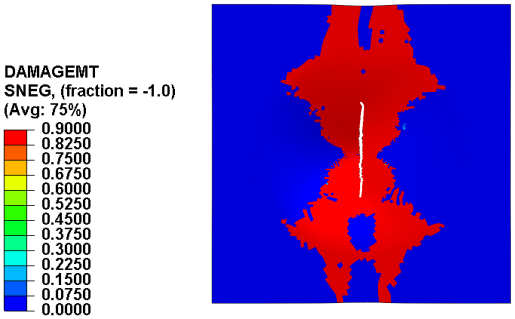

(c) Matrix Tension, top ply.

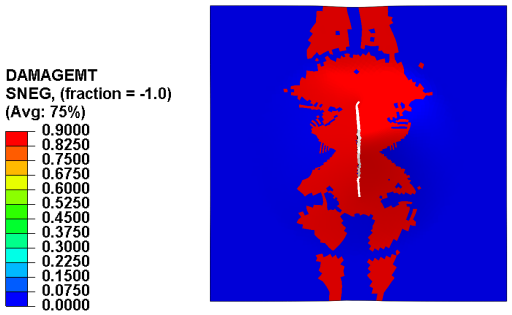

(d) Matrix Tension, bottom ply.

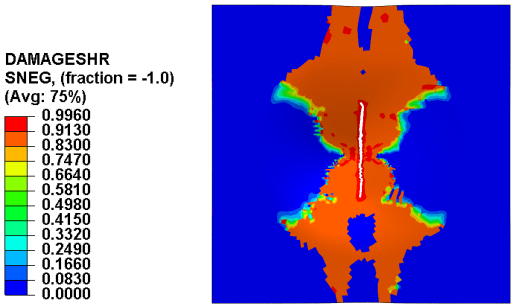

(e) Shear, top ply.

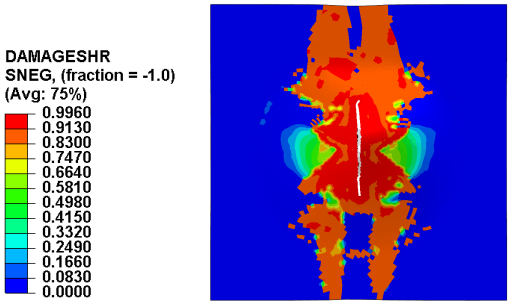

(f) Shear, bottom ply.

Figure B.27: Damage evolution and stress distribution at the end deformation, (II).

B.3 Plate layout $[0/90]_3$

B.3.1 Conventional shell

The two charts that are gathered in the figure B.28 shows the energy and the force, respectively, versus the time.

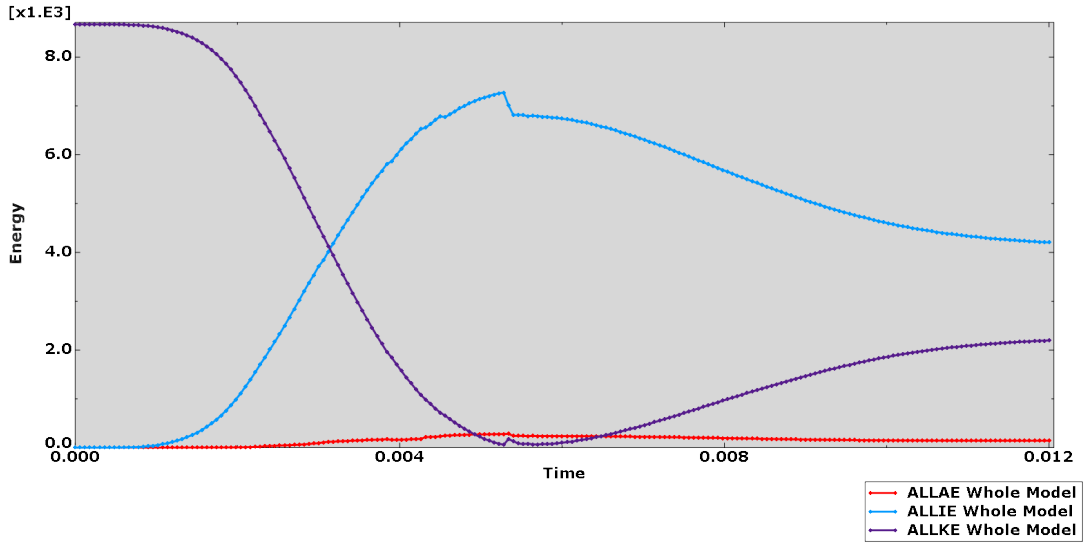

(a) Energies vs. time.

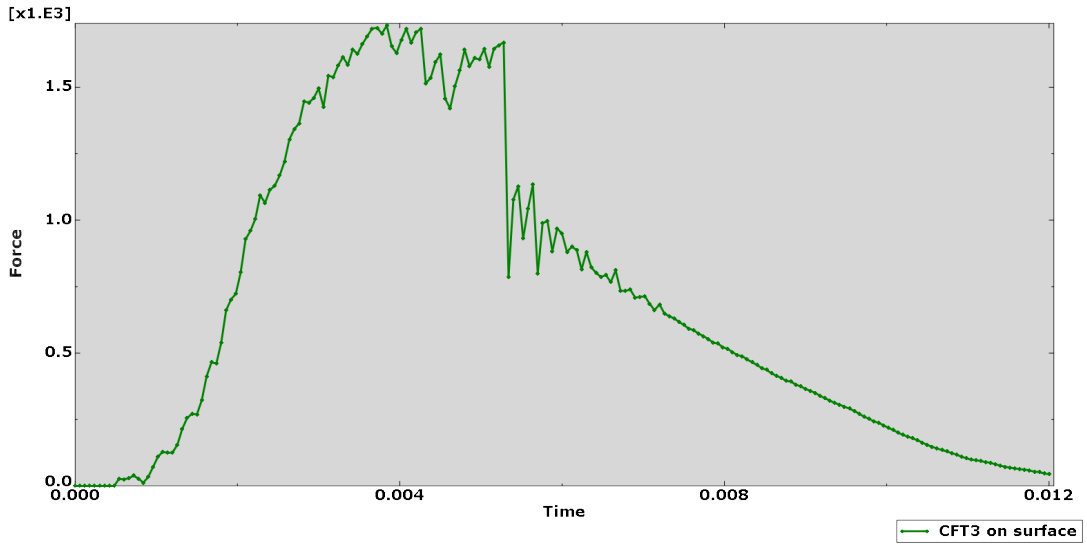

(b) Force vs. time.

Figure B.28: Plate modelled as conventional shell.

The figures B.29, B.31, B.30 and B.32 show the the distribution (by colour maps) of the different failure criteria, that in the *Step module* are selected and the stress of Von Misses distribution over the plate.

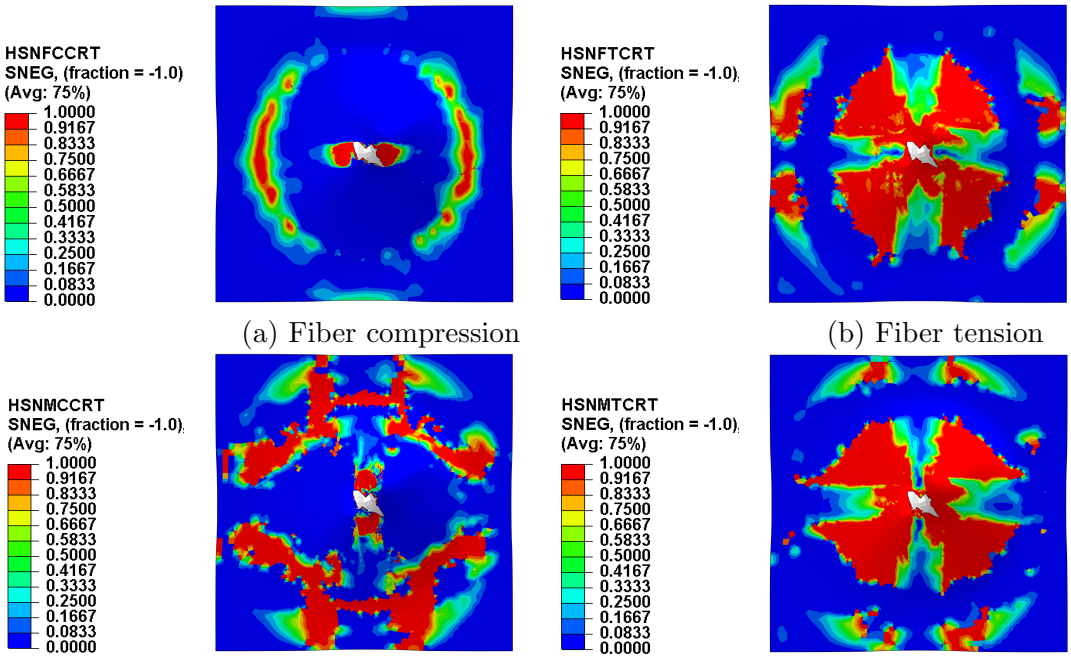

(a) Fiber compression (b) Fiber tension

(c) Matrix compression (d) Matrix tension

Figure B.29: Damage initiation (Hashin failure criteria) at the maximum deformation.

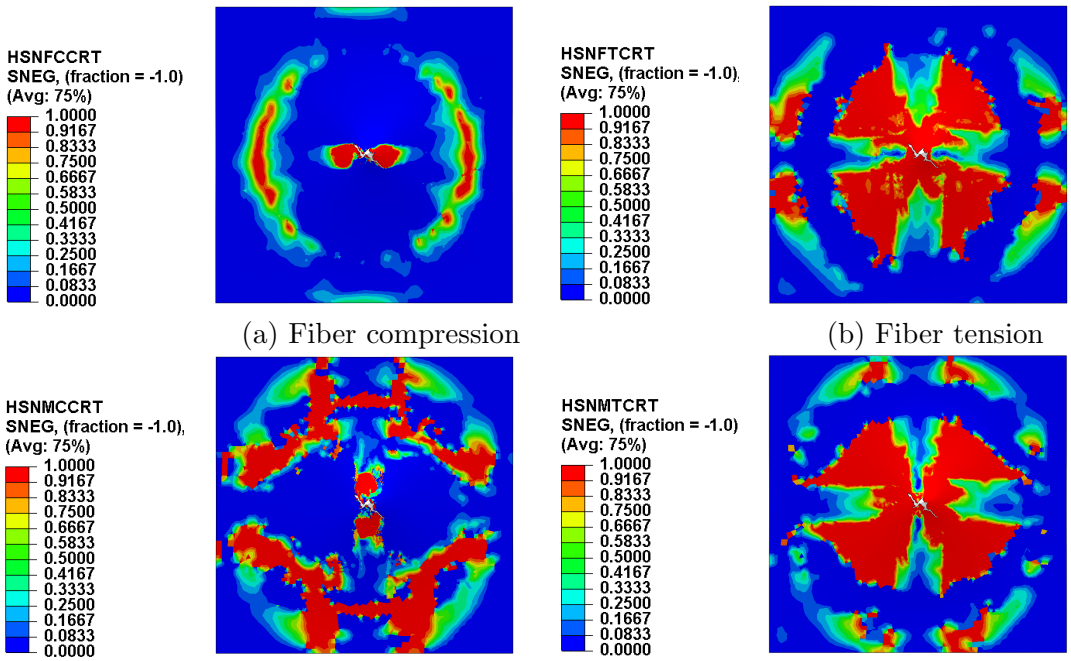

(a) Fiber compression (b) Fiber tension

(c) matrix compression (d) Matrix tension

Figure B.30: Damage initiation (Hashin failure criteria) at the end deformation.

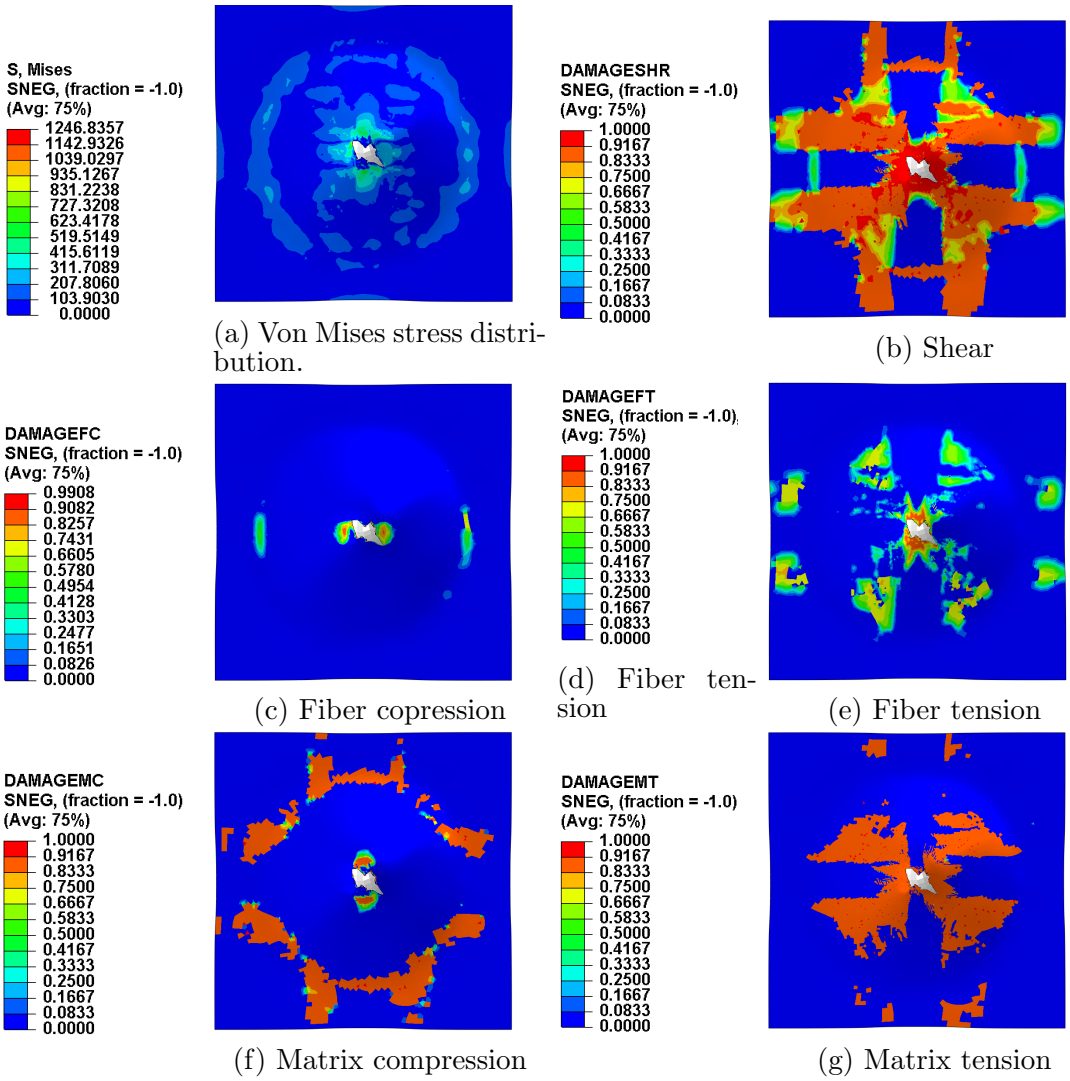

(a) Von Mises stress distribution.

(b) Shear

(c) Fiber copression

(d) Fiber tension

(e) Fiber tension

(f) Matrix compression

(g) Matrix tension

Figure B.31: Damage evolution and stress distribution at the maximum deformation.

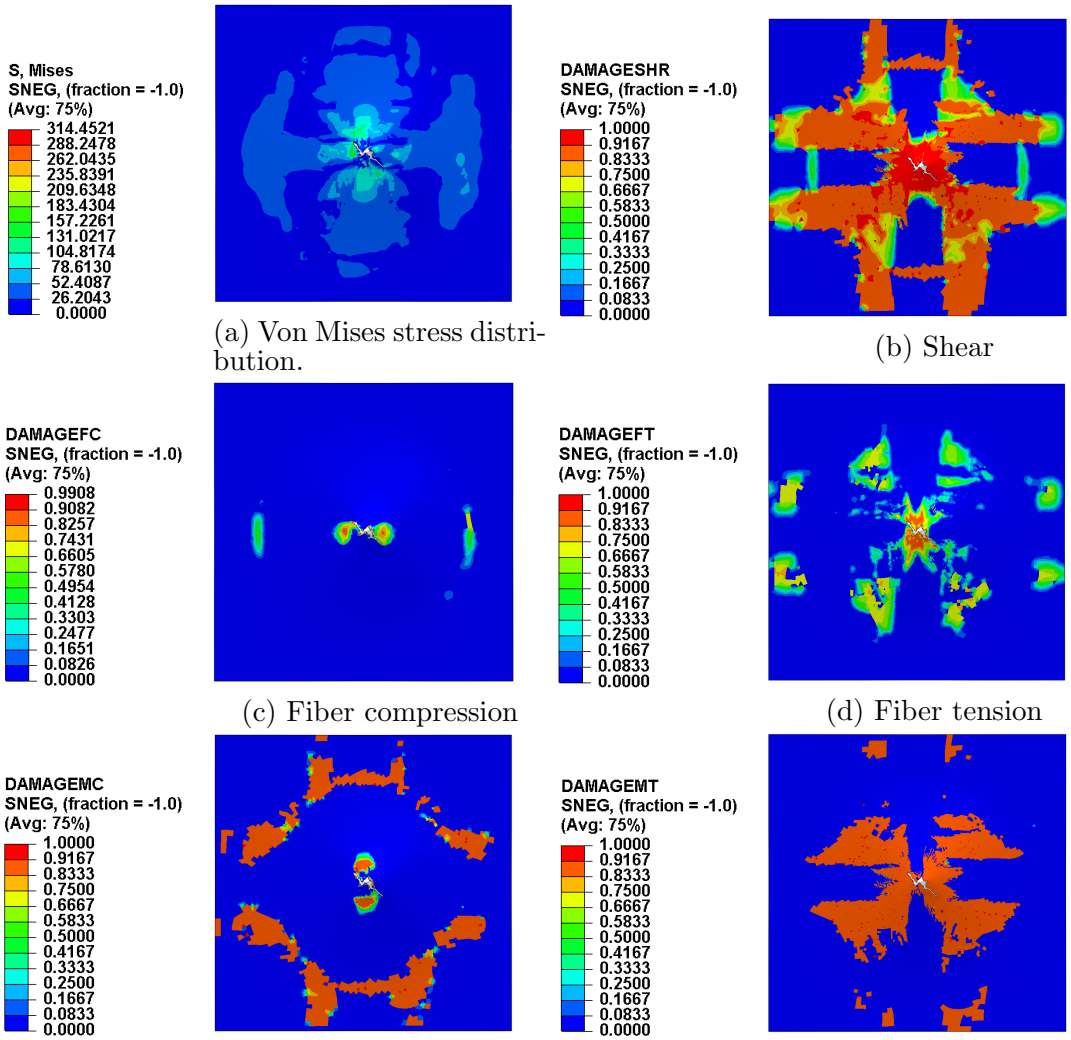

(a) Von Mises stress distribution.

(b) Shear

(c) Fiber compression

(d) Fiber tension

(e) Matrix compression

(f) Matrix tension

Figure B.32: Damage evolution and stress distribution at the end deformation.

B.3.2 Continuum shell, 1 layer with 6 plies

The two charts that are gathered in the figure B.33 shows the energy and the force, respectively, versus the time.

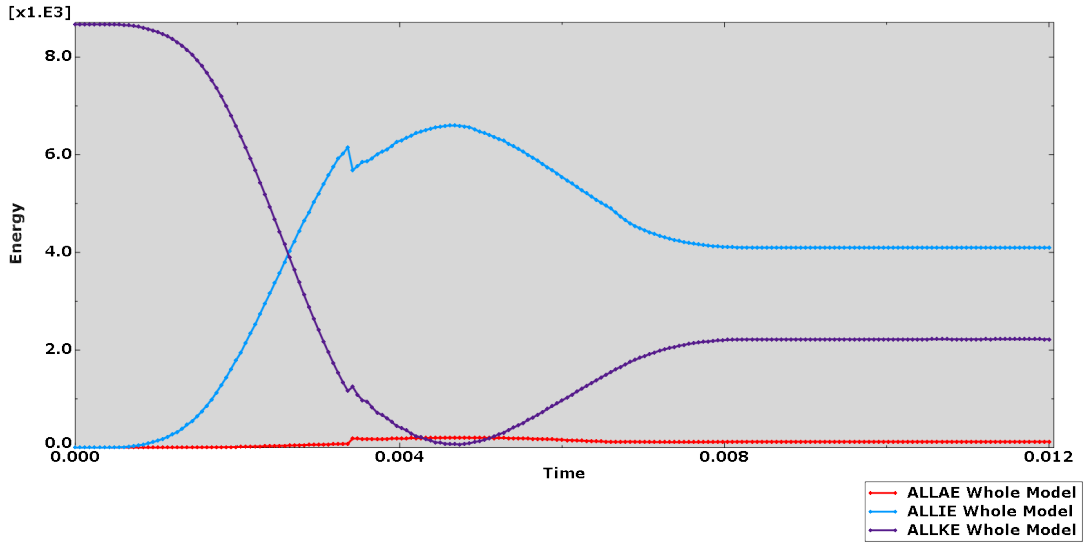

(a) Energies vs. time.

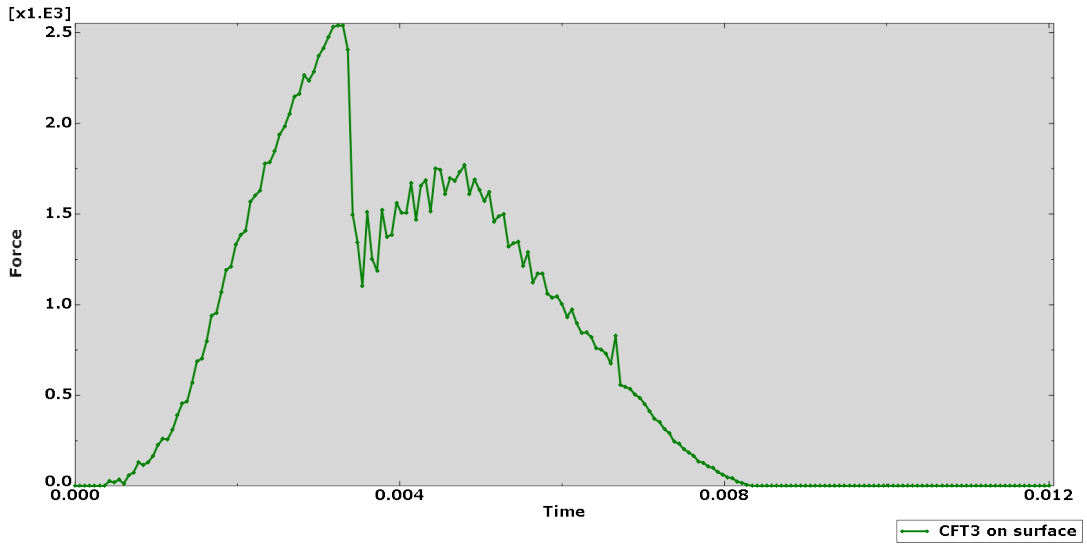

(b) Force vs. time.

Figure B.33: Plate modelled as a solid with continuum shell properties (1 layer with 6ply).

The figures B.34, B.36, B.35 and B.37 show the the distribution (by colour maps) of the different failure criteria, that in the *Step module* are selected and the stress of Von Misses distribution over the plate.

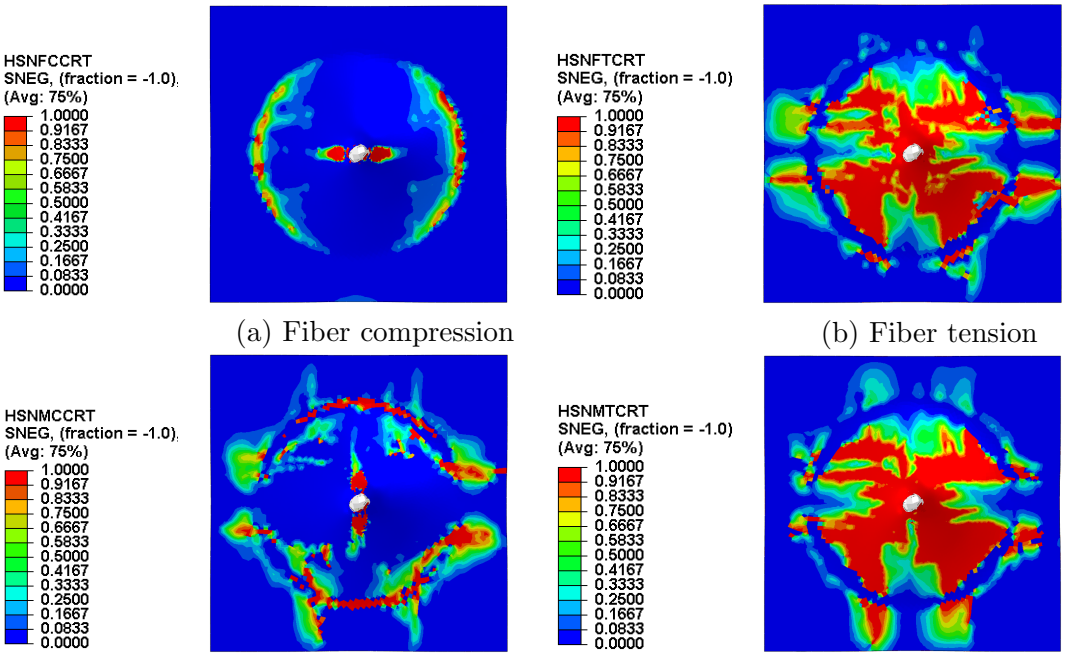

(a) Fiber compression (b) Fiber tension

(c) Matrix compression (d) Matrix tension

Figure B.34: Damage initiation (Hashin failure criteria) at the maximum deformation.

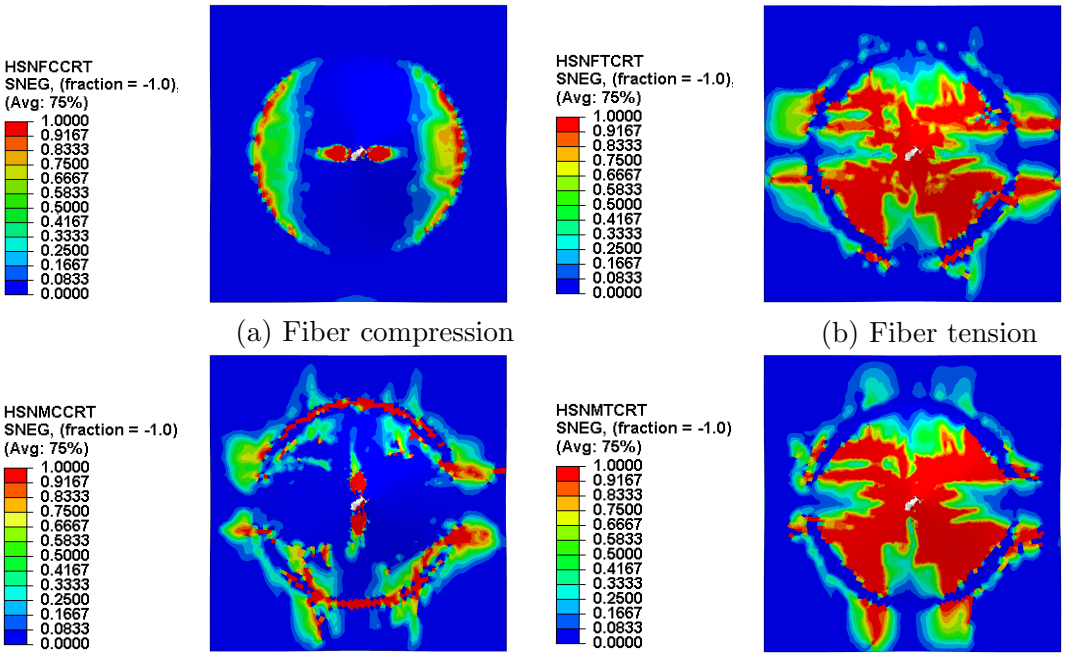

(a) Fiber compression (b) Fiber tension

(c) Matrix compression (d) Matrix tension

Figure B.35: Damage initiation (Hashin failure criteria) at the end deformation.

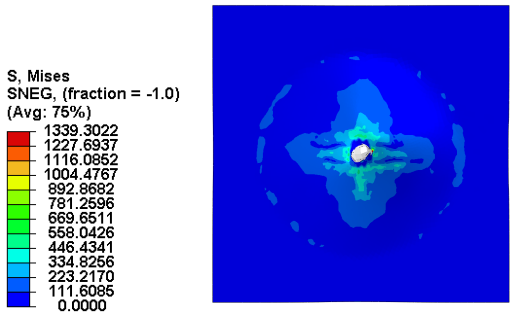

(a) Von Mises stress distribution.

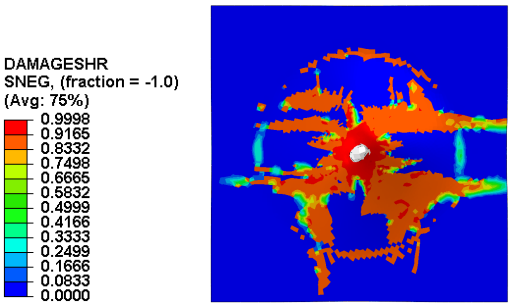

(b) Shear

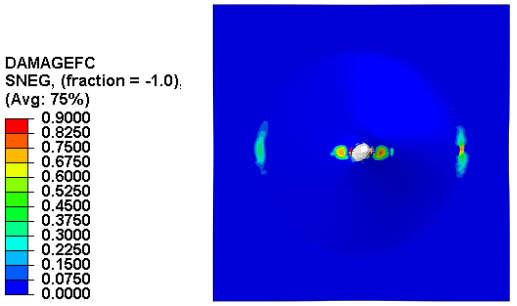

(c) Fiber compression

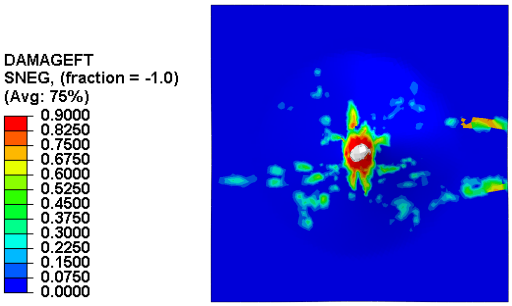

(d) Fiber tension

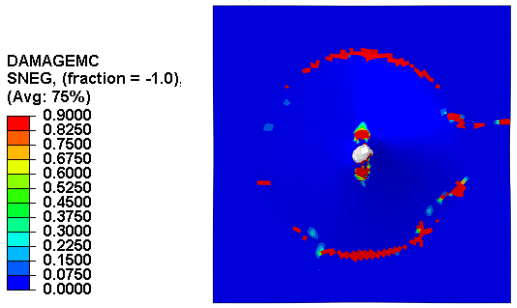

(e) Matrix compression

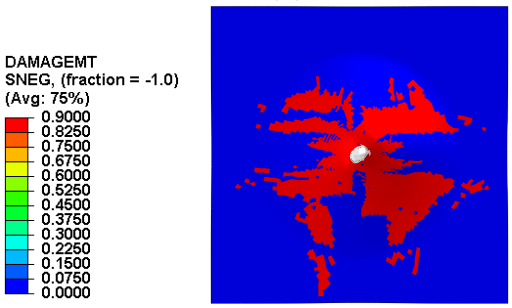

(f) Matrix tension

Figure B.36: Damage evolution and stress distribution at the maximum deformation.

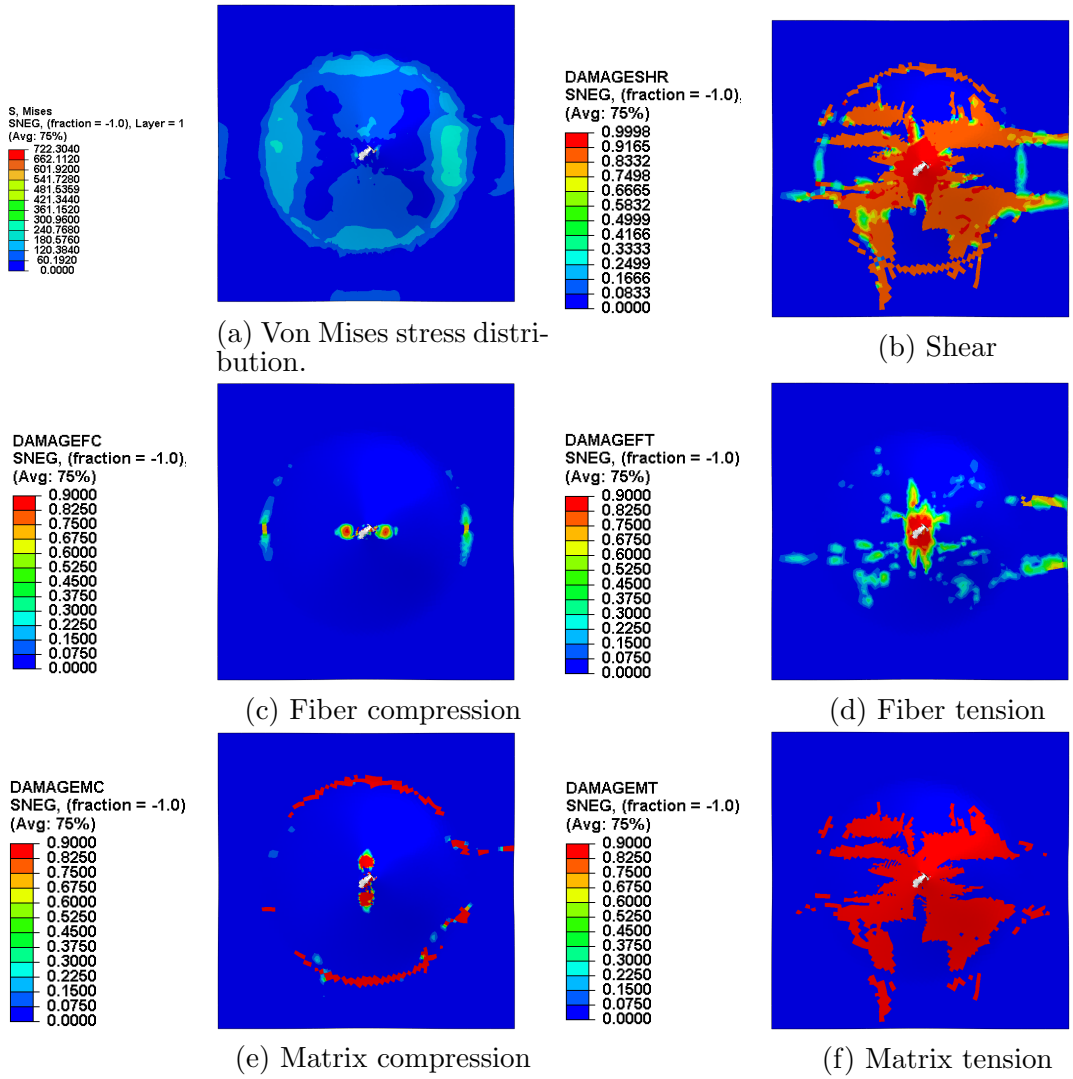

(a) Von Mises stress distribution.

(b) Shear

(c) Fiber compression

(d) Fiber tension

(e) Matrix compression

(f) Matrix tension

Figure B.37: Damage evolution and stress distribution at the end deformation..

B.3.3 Continuum shell, 3 layer with 2 plies each

The two charts that are gathered in the figure B.38 shows the energy and the force, respectively, versus the time that Abaqus gives in its *Visualization module*.

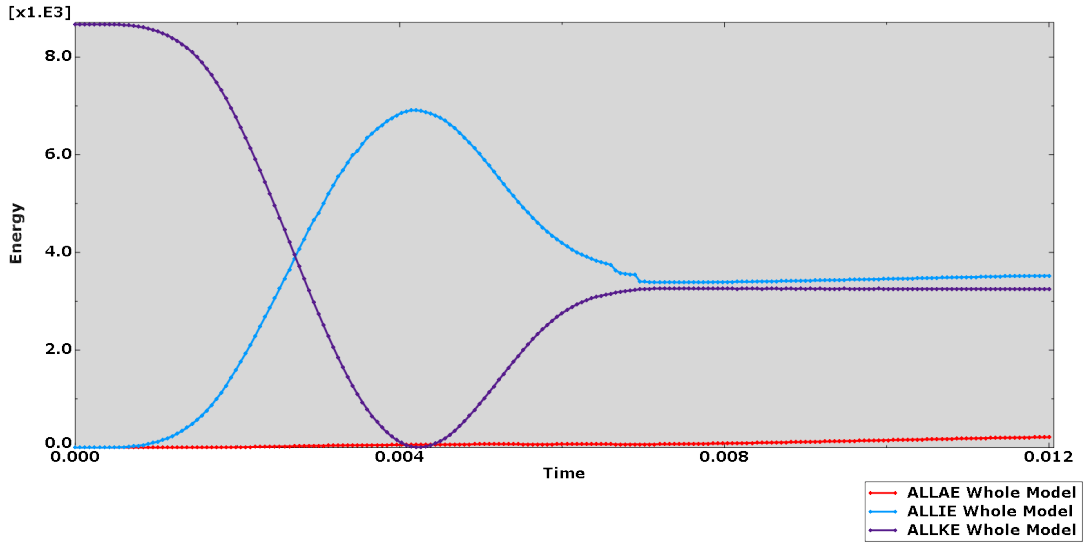

(a) Energies vs. time.

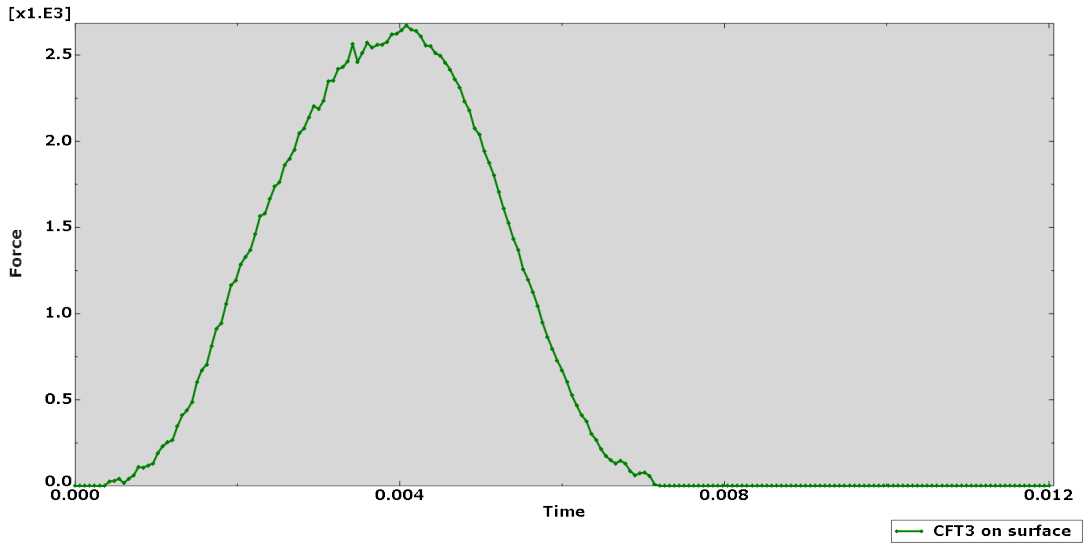

(b) Force vs. time.

Figure B.38: Plate modelled as a solid with continuum shell properties (3 layer with 2ply).

The figures B.39, B.41, B.42, B.40 and B.43, B.44 show the the distribution (by colour maps) of the different failure criteria, that in the *Step module* are selected and the stress of Von Misses distribution over the plate.

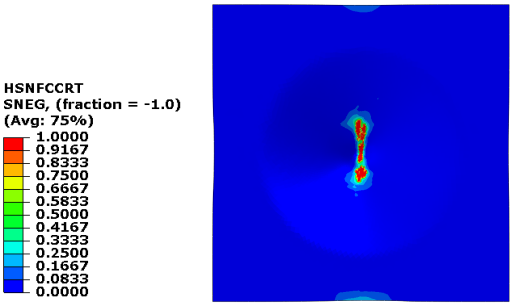

(a) Fiber compression, top ply

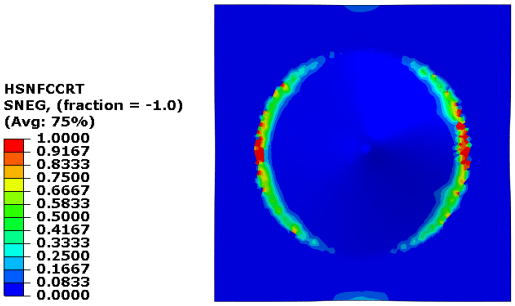

(b) Fiber compression, bottom ply.

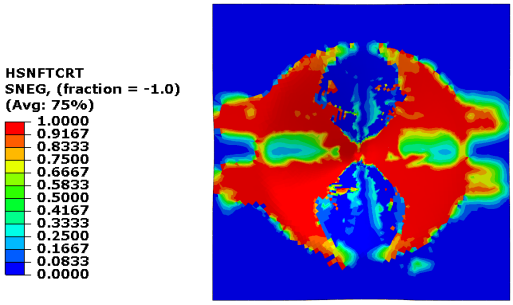

(c) Fiber tension, top ply.

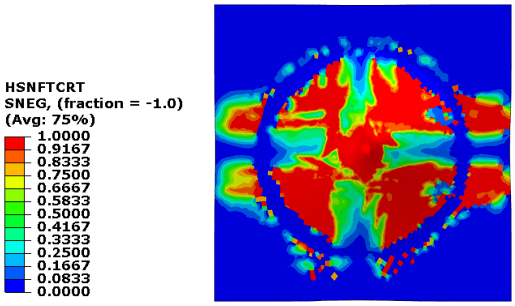

(d) Fiber tension, bottom ply.

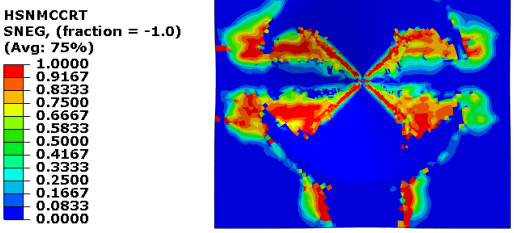

(e) Matrix compression, top ply.

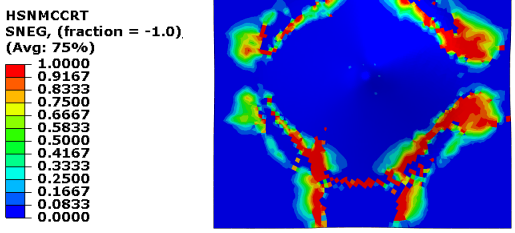

(f) Matrix compression, bottom ply.

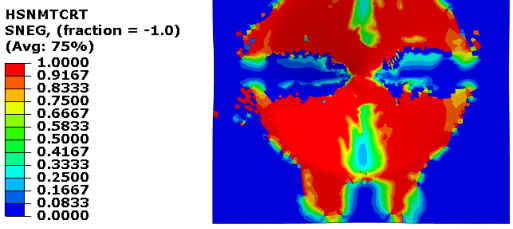

(g) Matrix tension, top ply.

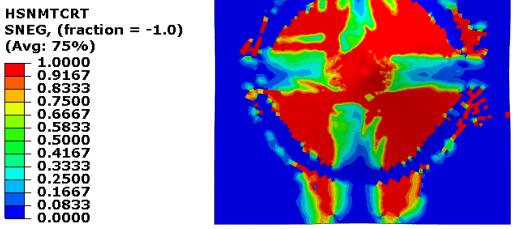

(h) Matrix tension, bottom ply.

Figure B.39: Damage initiation (Hashin failure criteria) at the maximum deformation.

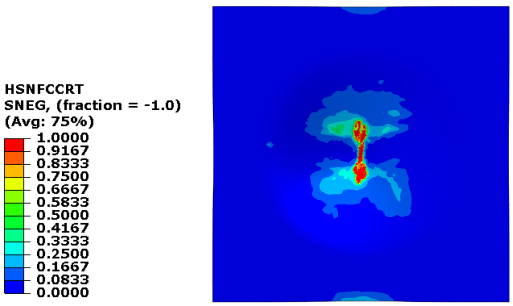

(a) Fiber compression, top ply.

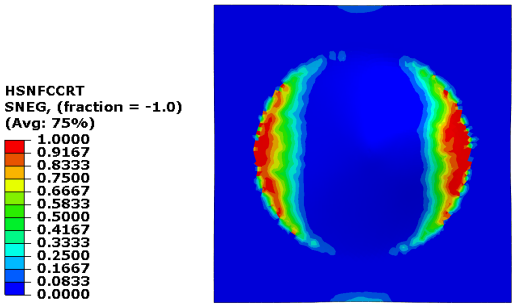

(b) Fiber compression, bottom ply.

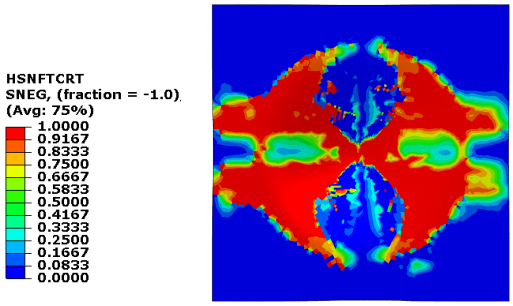

(c) Fiber tension, top ply.

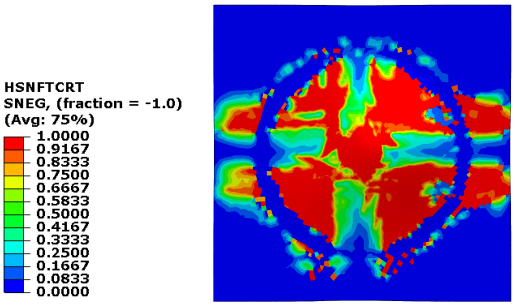

(d) Fiber tension. bottom ply.

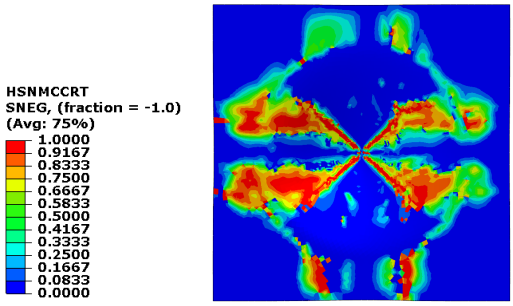

(e) matrix compression, top ply.

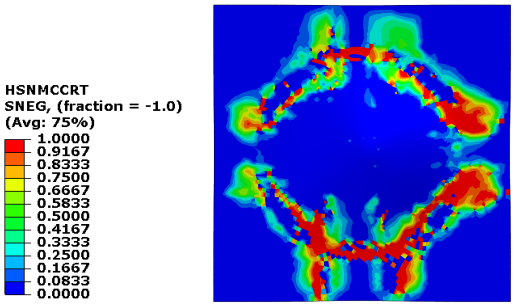

(f) matrix compression, bottom ply.

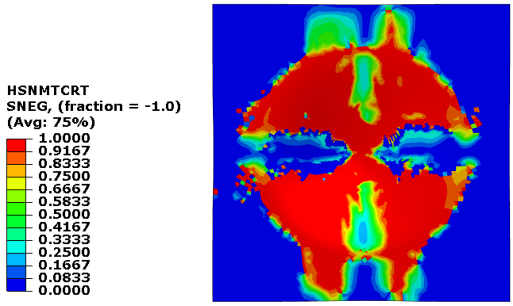

(g) Matrix tension, top ply.

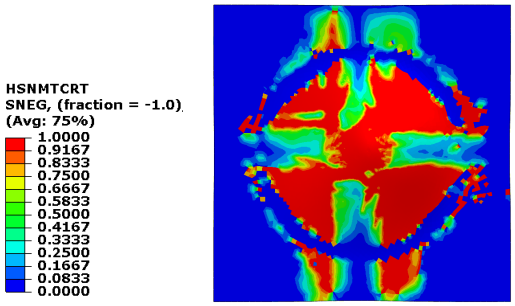

(h) Matrix tension, bottom ply.

Figure B.40: Damage initiation (Hashin failure criteria) at the end deformation.

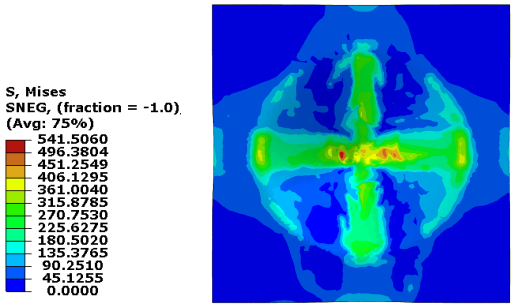

(a) Von Mises stress distribution, top ply.

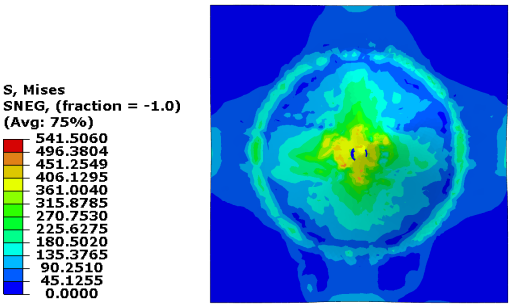

(b) Von Mises stress distribution, bottom ply.

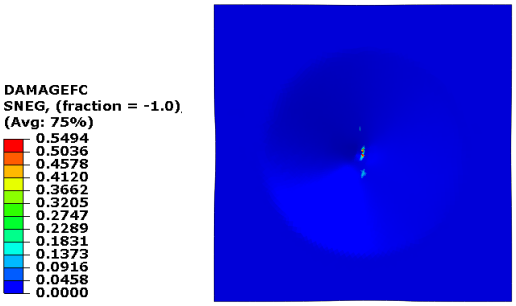

(c) Fibre Compression, top ply.

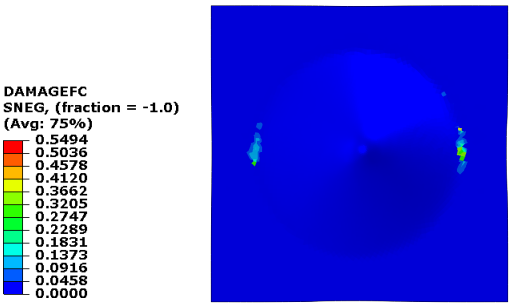

(d) Fibre Compression, bottom ply.

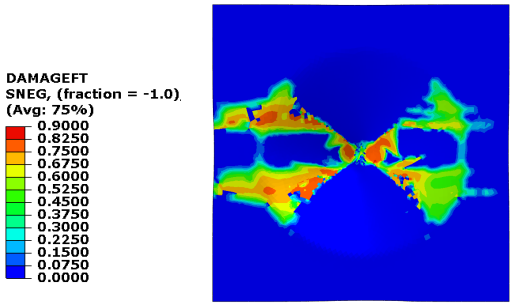

(e) Fibre Tension, top ply.

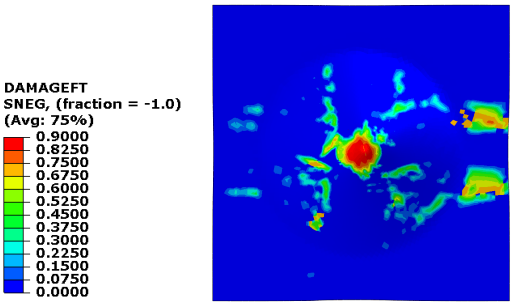

(f) Fibre Tension, bottom ply.

Figure B.41: Damage evolution and stress distribution at the maximum deformation(I).

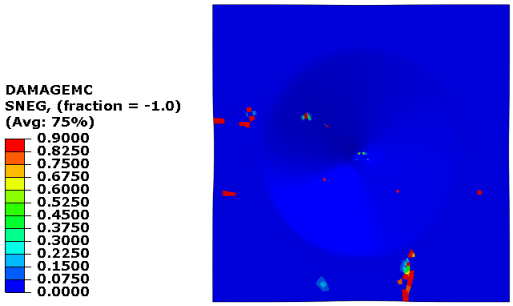

(a) Matrix Compression, top ply.

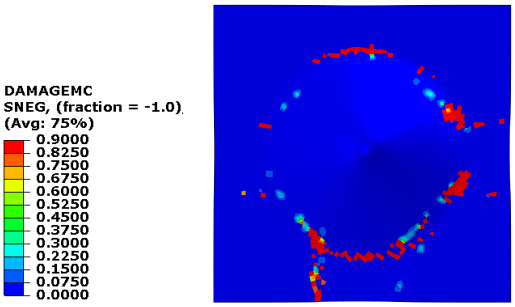

(b) Matrix Compression, bottom ply.

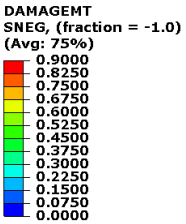

(c) Matrix Tension, top ply.

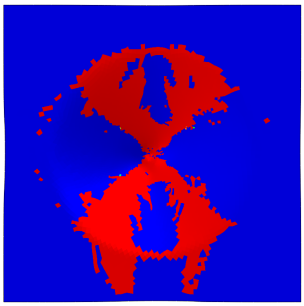

(d) Matrix Tension, top ply.

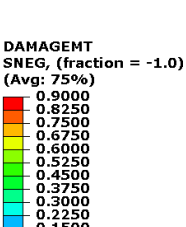

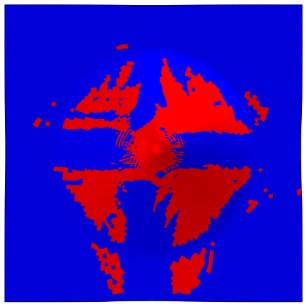

(e) Matrix Tension, bottom ply.

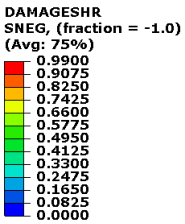

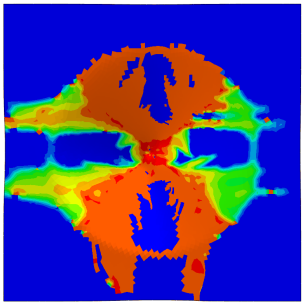

(f) Shear, top ply

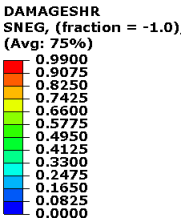

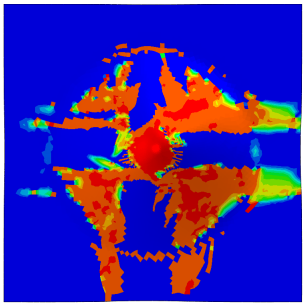

(g) Shear, bottom ply

Figure B.42: Damage evolution and stress distribution at the maximum deformation(II).

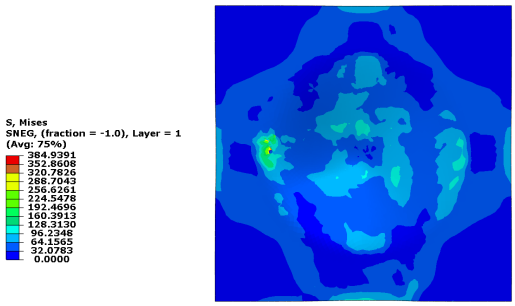

(a) Von Mises stress distribution, top ply.

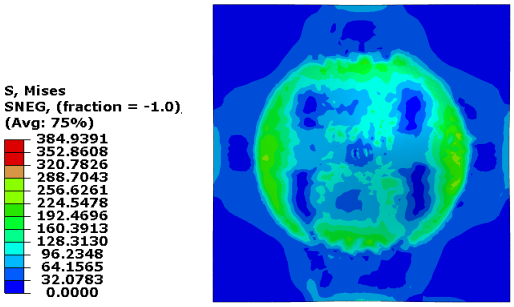

(b) Von Mises stress distribution, bottom ply.

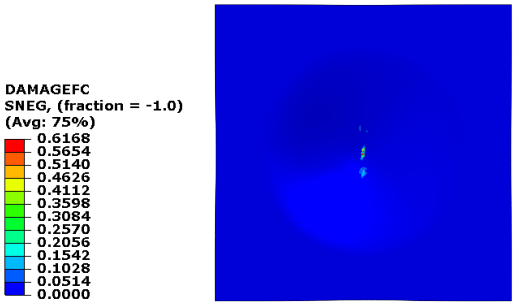

(c) Fibre Compression, top ply.

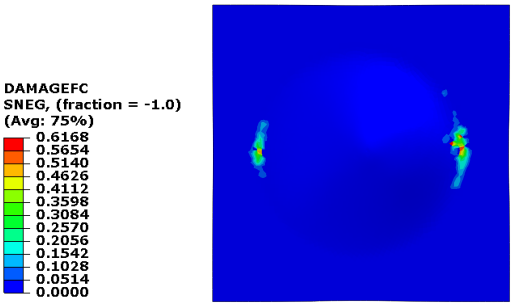

(d) Fibre Compression, bottom ply.

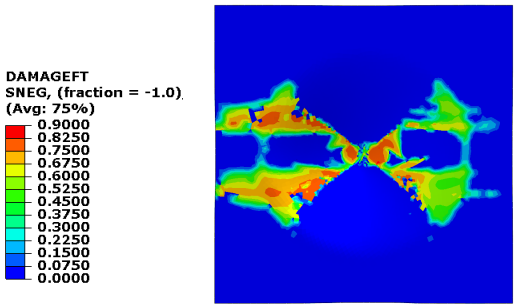

(e) Fibre Tension, top ply.

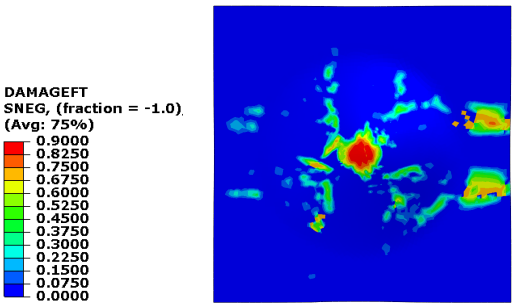

(f) Fibre Tension, bottom ply.

Figure B.43: Damage evolution and stress distribution at the end deformation (I).

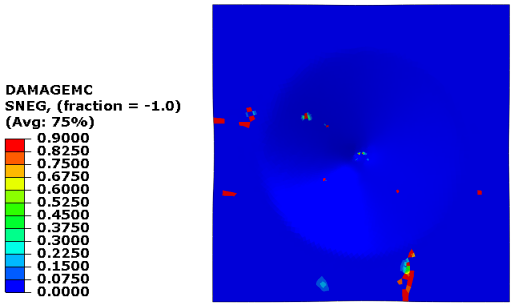

(a) Matrix Compression, top ply.

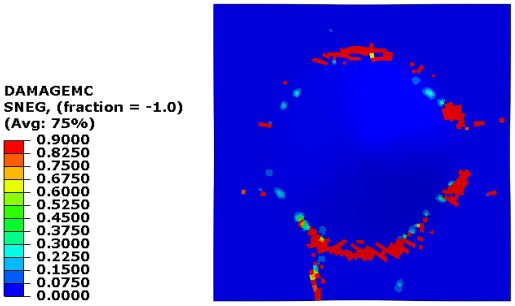

(b) Matrix Compression, bottom ply.

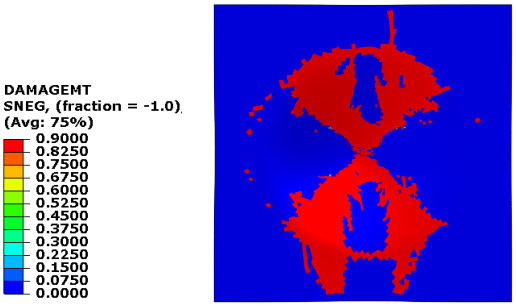

(c) Matrix Tension, top ply.

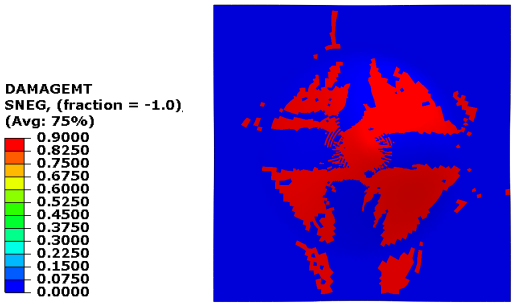

(d) Matrix Tension, bottom ply.

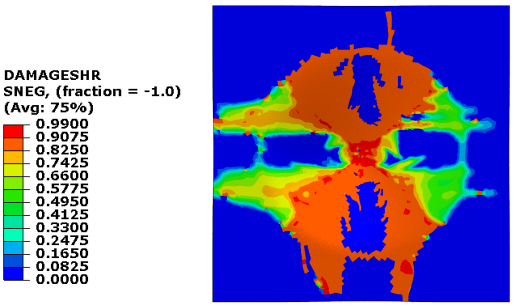

(e) Shear, top ply.

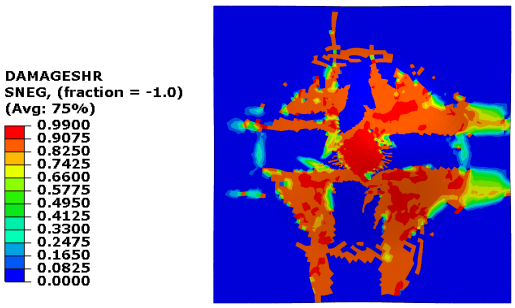

(f) Shear, bottom ply.

Figure B.44: Damage evolution and stress distribution at the end deformation(II).

Chapter C

Flax/PP output figures

C.1 Continuum shell, 1 layer with 10 plies

C.1.1 Speed 1,4 m/s

The figure C.1 shows the energy and the force, respectively, versus.

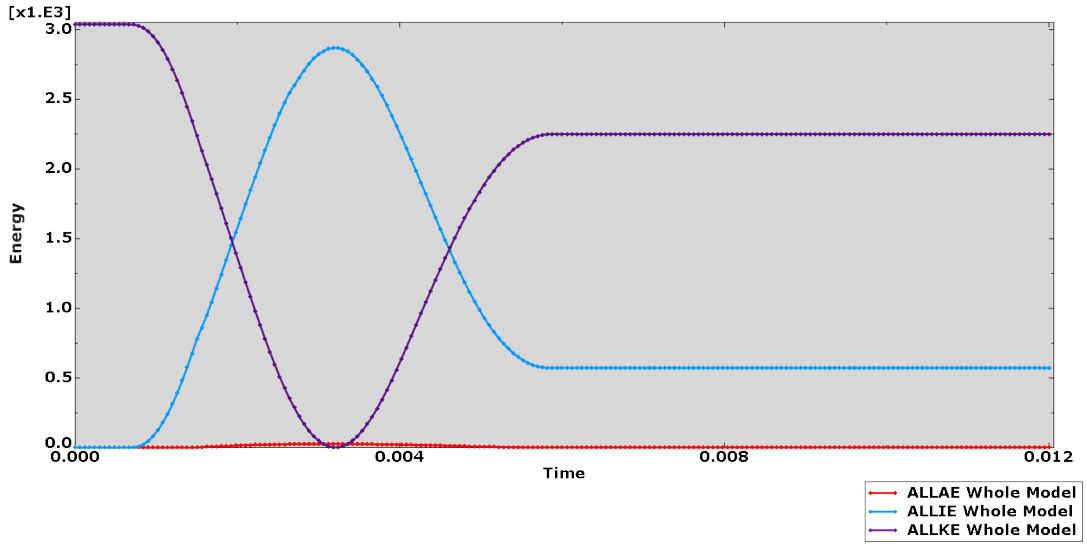

(a) Energies vs. time.

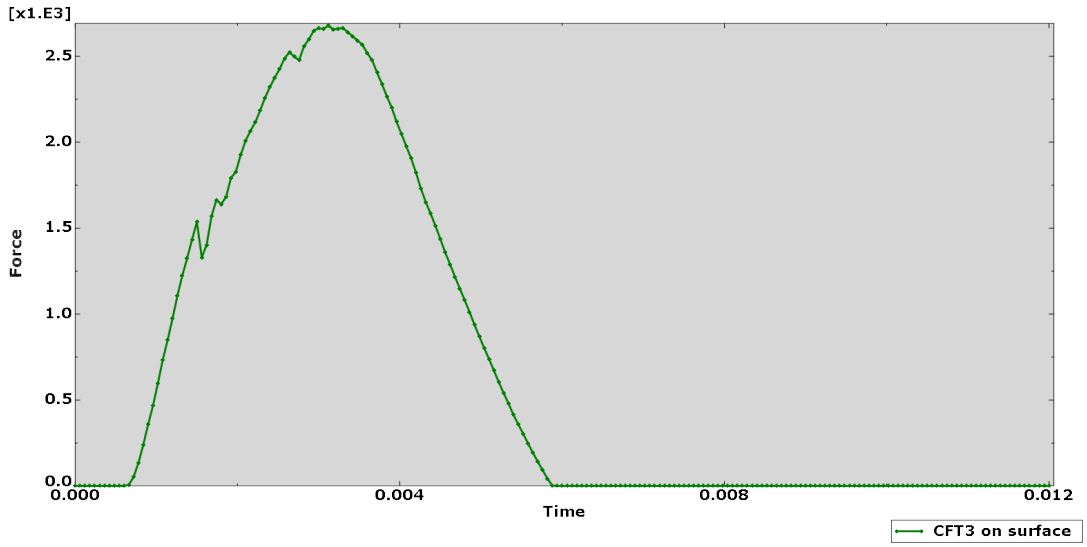

(b) Force vs. time.

Figure C.1: Plate modelled as a solid with continuum shell properties (1 layer with 10ply).

The figures C.2, C.4, C.3 and C.5 show the the distribution (by colour maps) of the different failure criteria, that in the *Step module* are selected and the stress of Von Misses distribution over the plate.

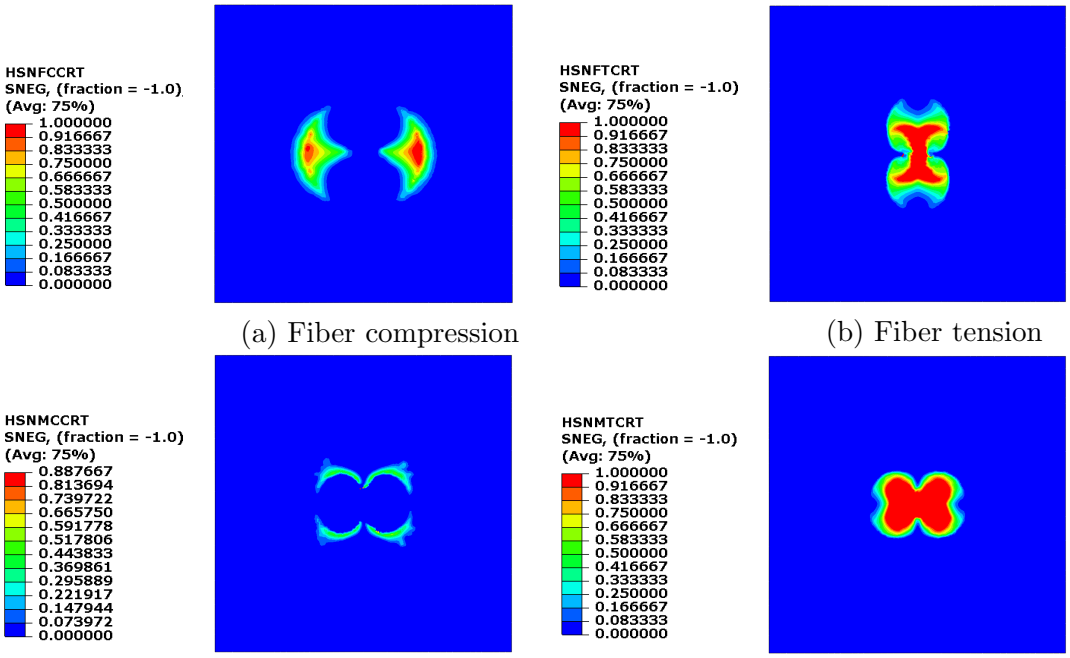

(a) Fiber compression (b) Fiber tension

(c) Matrix compression (d) Matrix tension

Figure C.2: Damage initiation (Hashin failure criteria) at the maximum deformation.

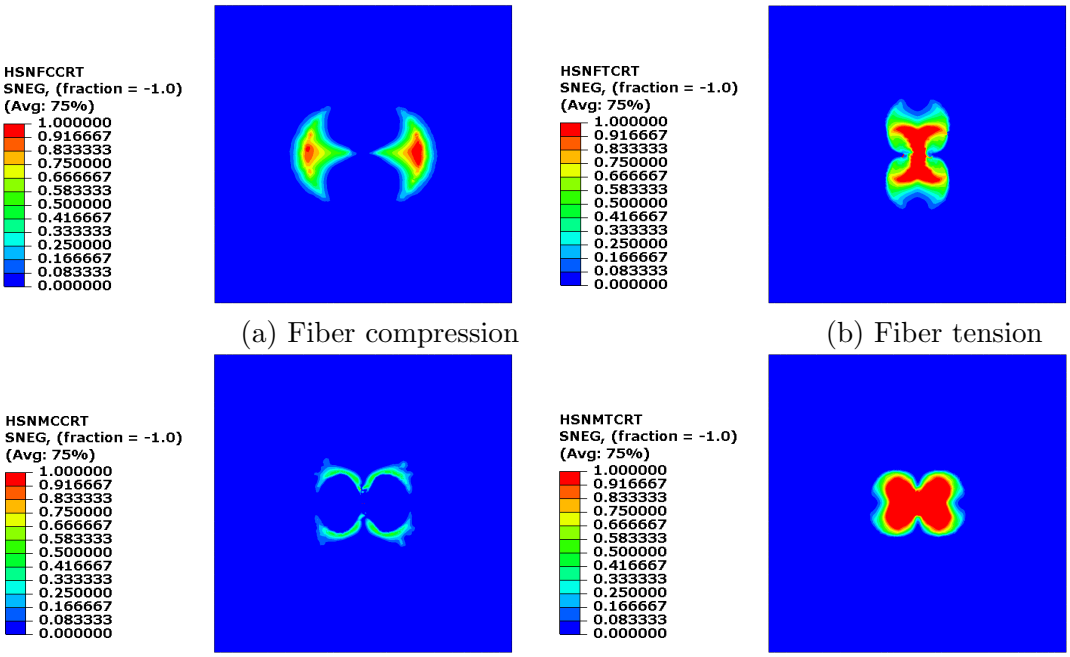

(a) Fiber compression (b) Fiber tension

(c) Matrix compression (d) Matrix tension

Figure C.3: Damage initiation (Hashin failure criteria) at the end deformation.

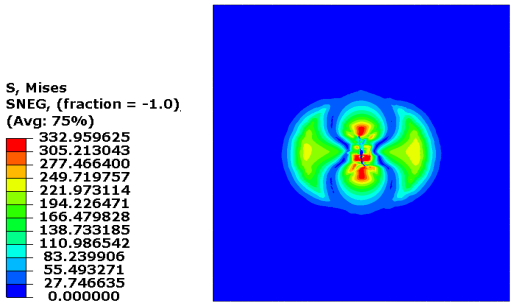

(a) Von Mises stress distribution.

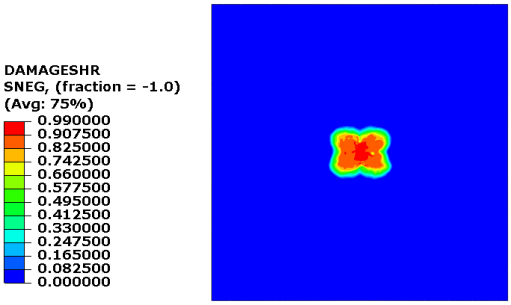

(b) Shear

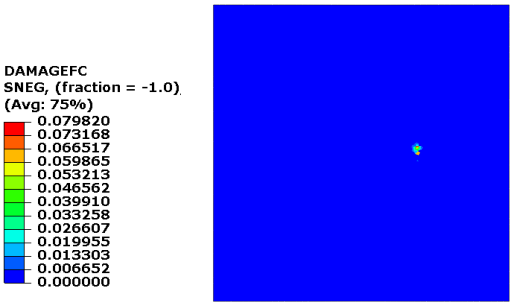

(c) Fiber compression

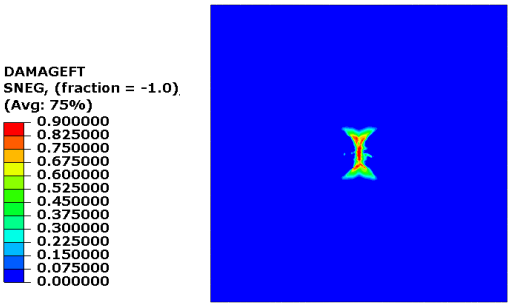

(d) Fiber tension

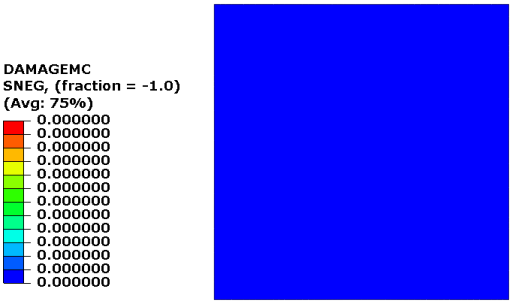

(e) Matrix compression

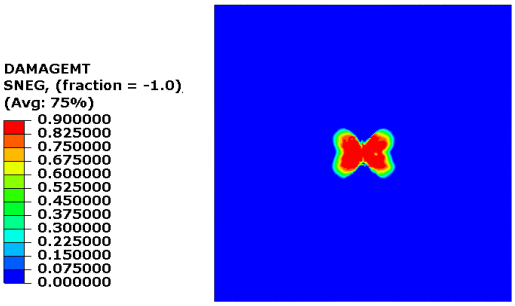

(f) Matrix tension

Figure C.4: Damage evolution and stress distribution at the maximum deformation.

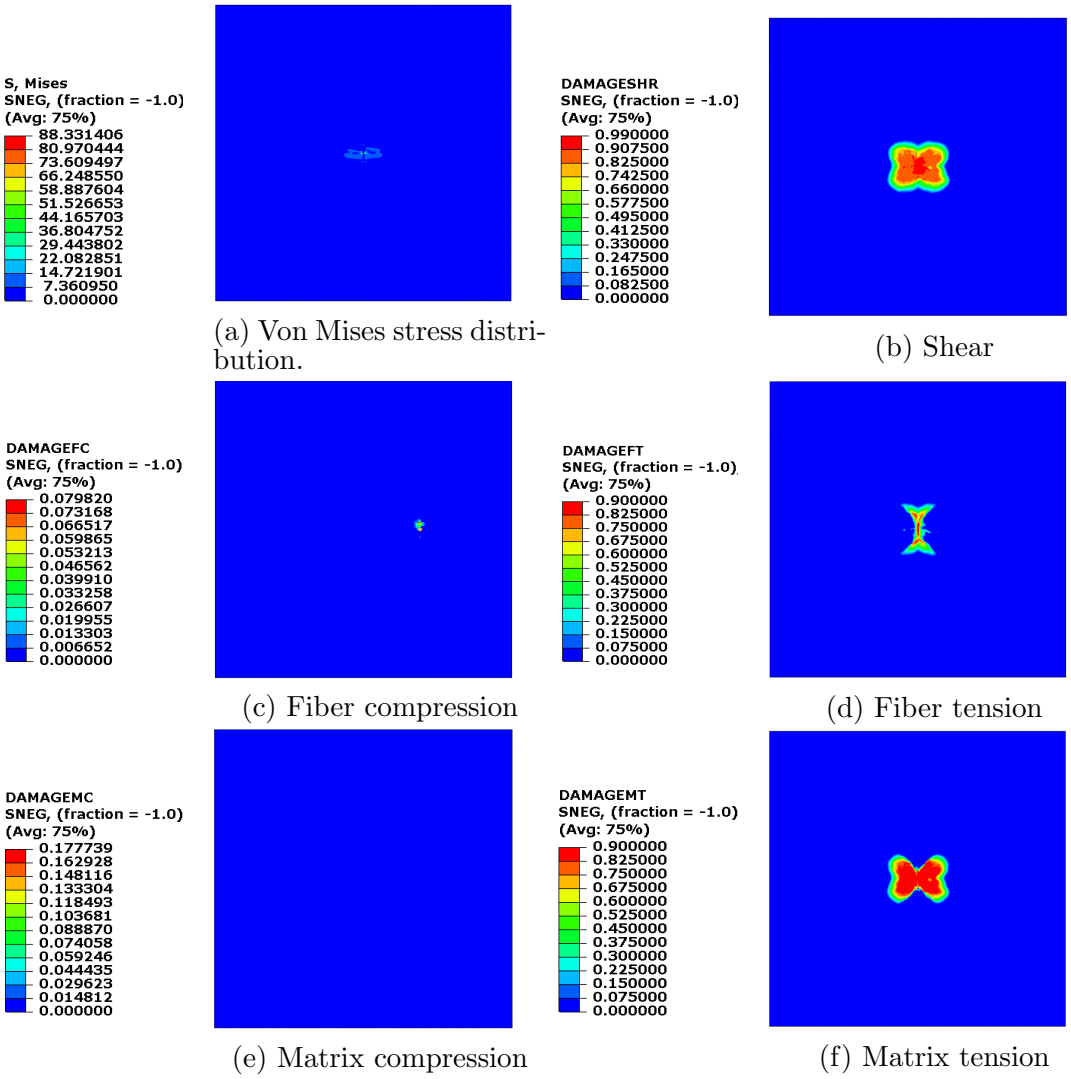

(a) Von Mises stress distribution.

(b) Shear

(c) Fiber compression

(d) Fiber tension

(e) Matrix compression

(f) Matrix tension

Figure C.5: Damage evolution and stress distribution at the end deformation.

C.1.2 Speed 2,8 m/s

The figure C.6 shows the energy and the force, respectively, versus the time.

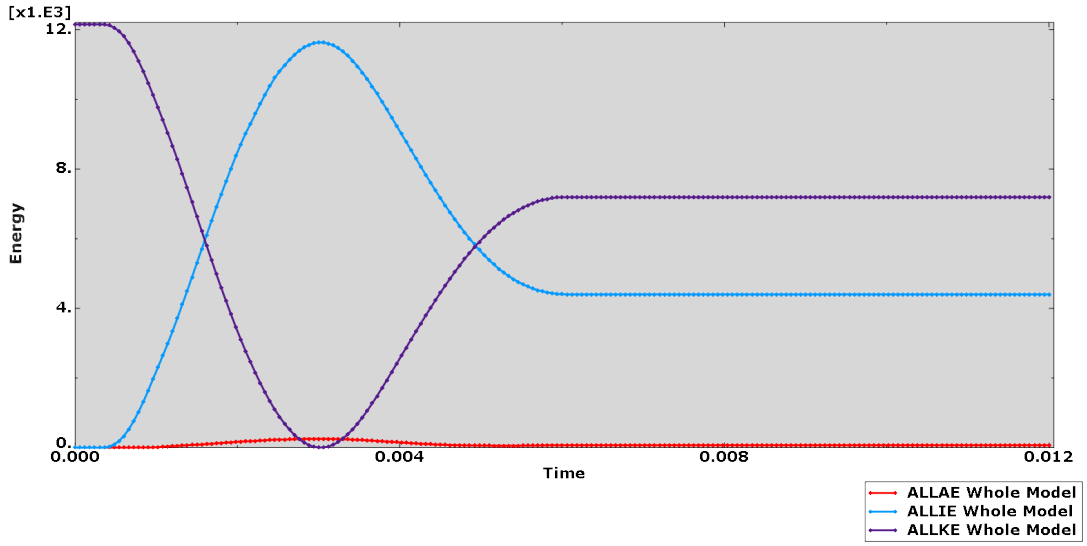

(a) Energies vs. time.

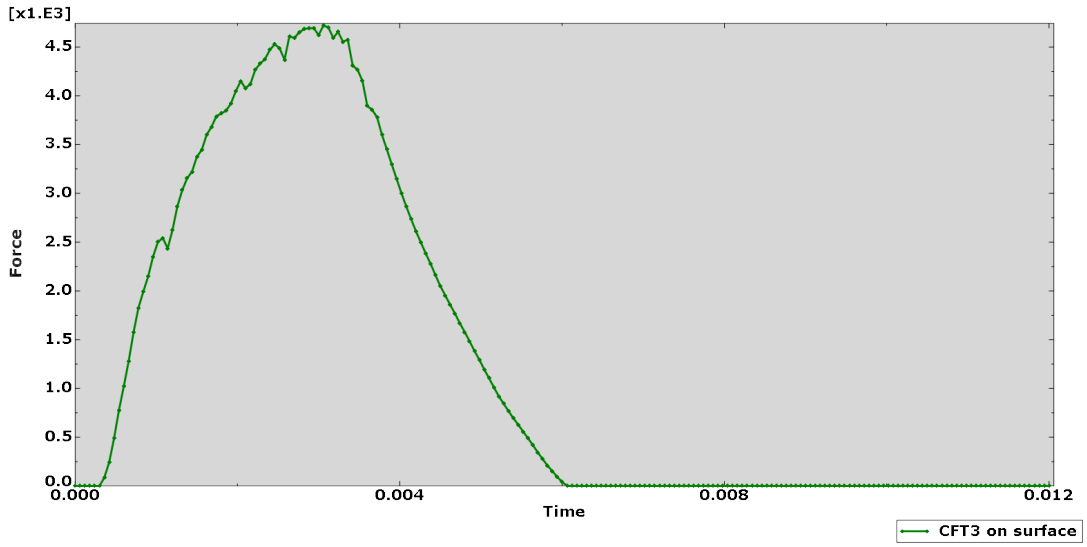

(b) Force vs. time.

Figure C.6: Plate modelled as a solid with continuum shell properties (1 layer with 10ply).

The figures C.7, C.9, C.8 and C.10 show the the distribution (by colour maps) of the different failure criteria, that in the *Step module* are selected and the stress of Von Misses distribution over the plate.

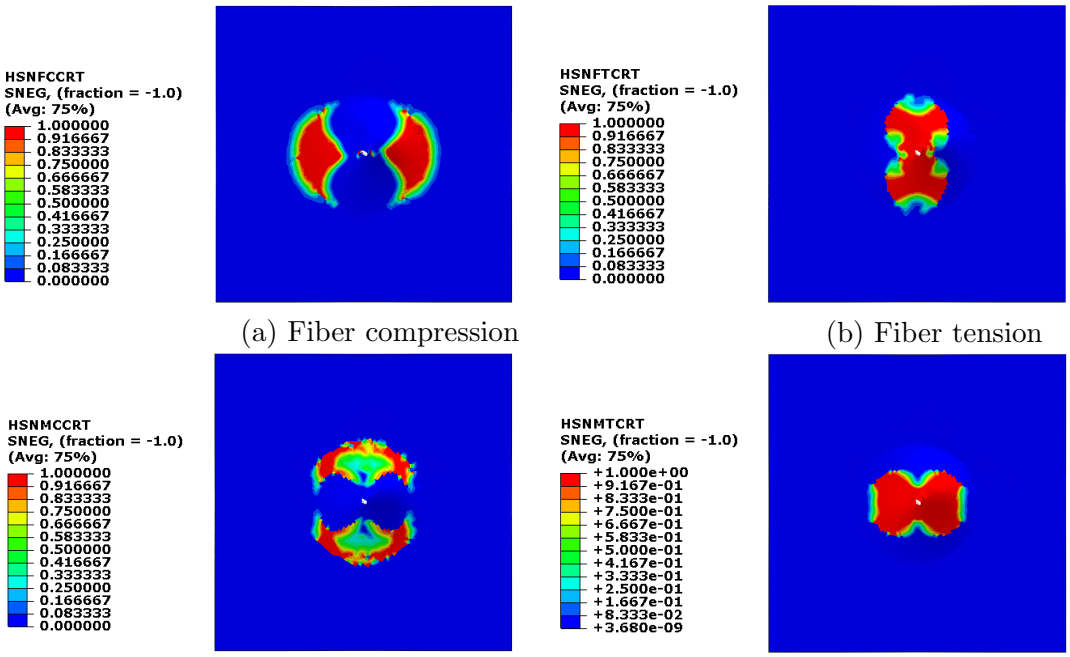

(a) Fiber compression (b) Fiber tension

(c) Matrix compression (d) Matrix tension

Figure C.7: Damage initiation (Hashin failure criteria) at the maximum deformation.

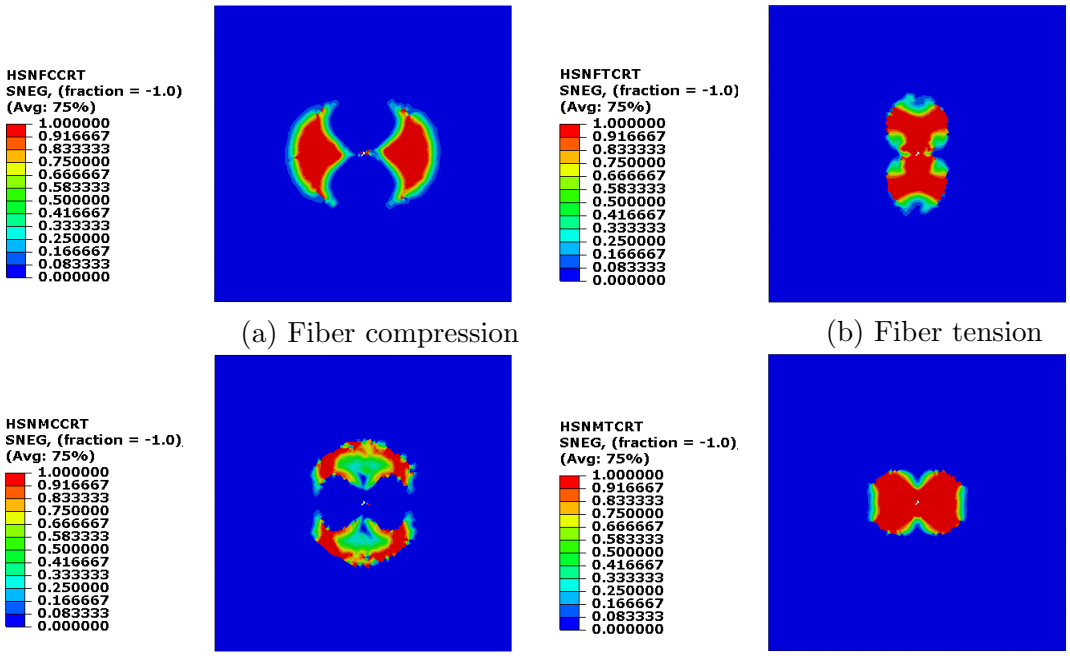

(a) Fiber compression (b) Fiber tension

(c) Matrix compression (d) Matrix tension

Figure C.8: Damage initiation (Hashin failure criteria) at the end deformation.

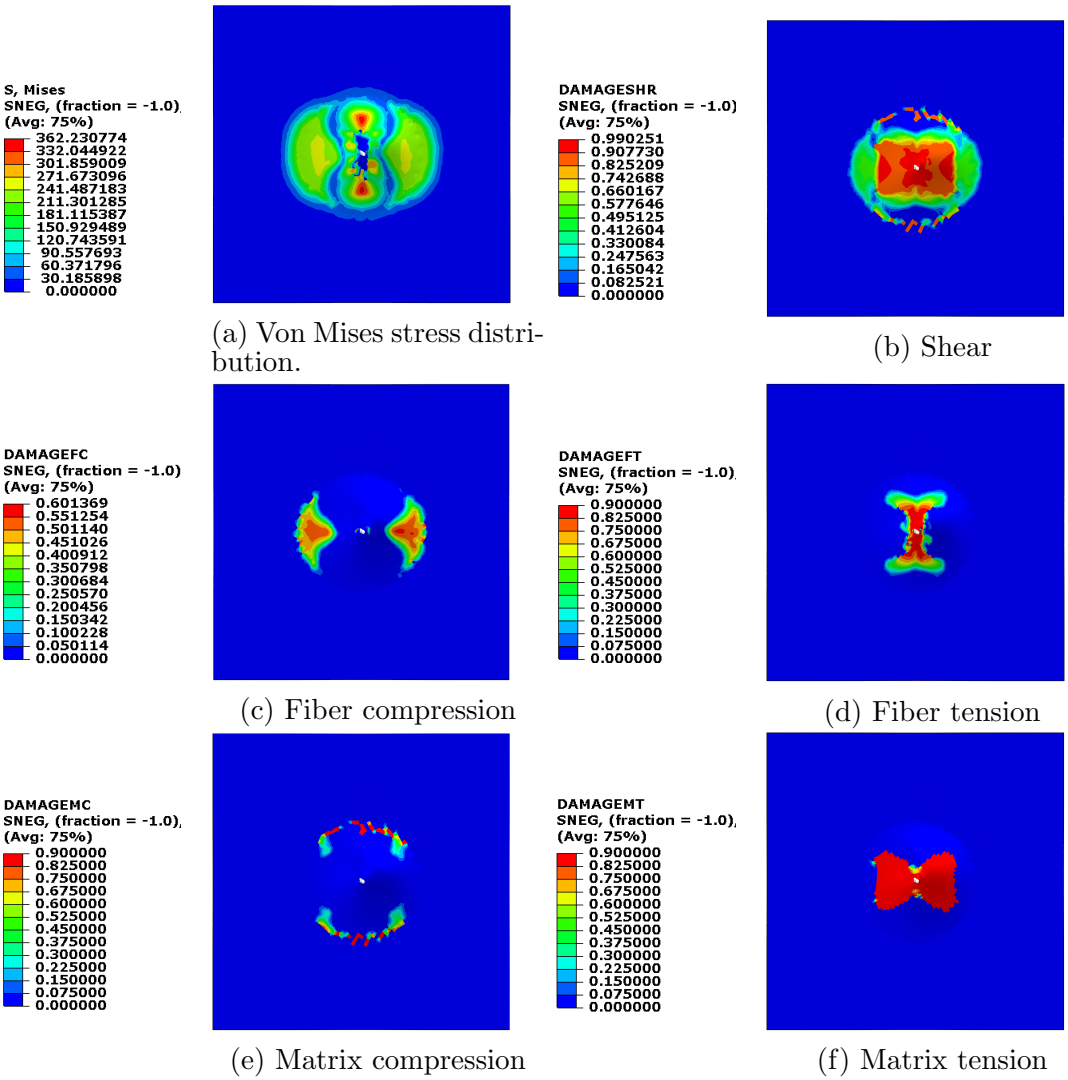

(a) Von Mises stress distribution.

(b) Shear

(c) Fiber compression

(d) Fiber tension

(e) Matrix compression

(f) Matrix tension

Figure C.9: Damage evolution and stress distribution at the maximum deformation.

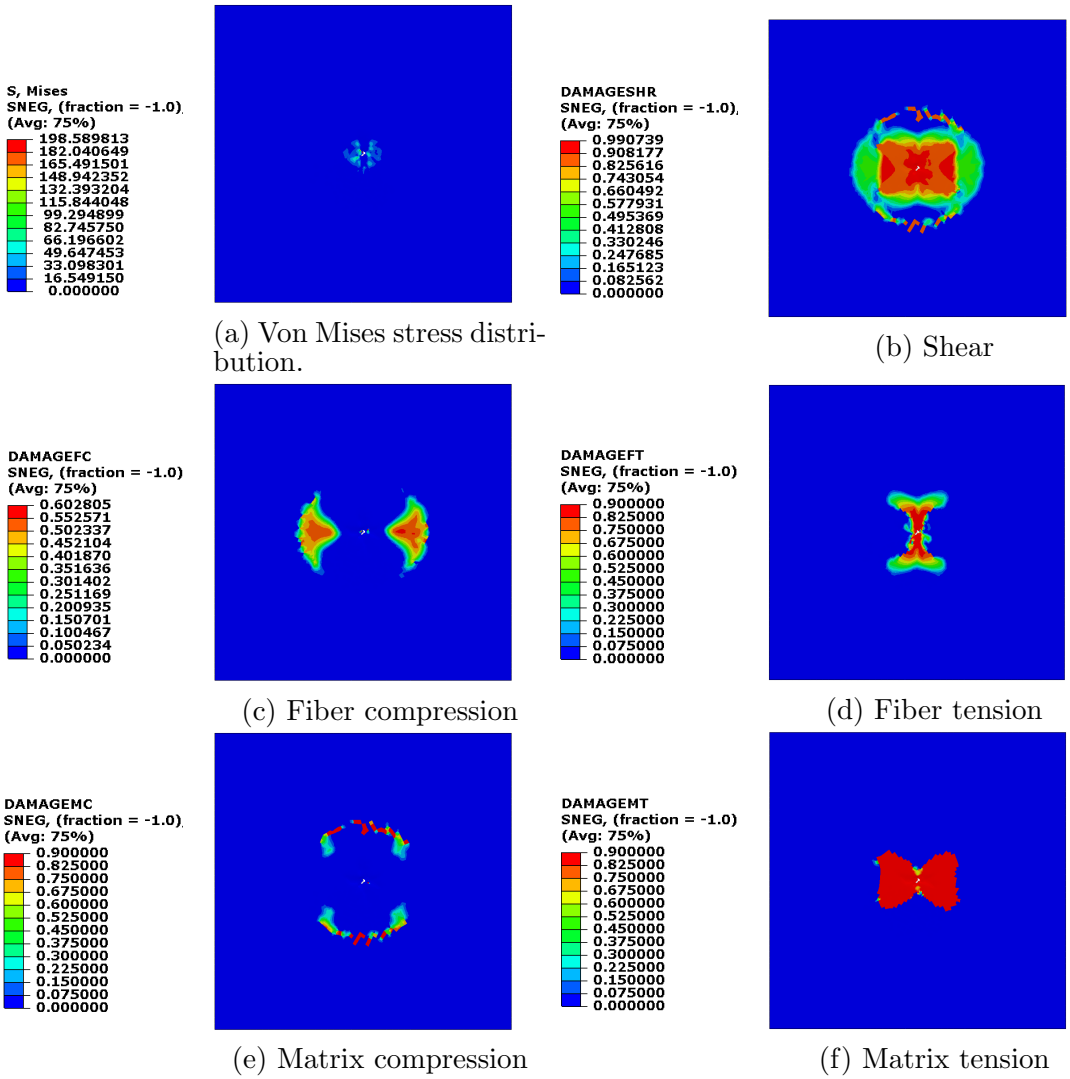

(a) Von Mises stress distribution.

(b) Shear

(c) Fiber compression

(d) Fiber tension

(e) Matrix compression

(f) Matrix tension

Figure C.10: Damage evolution and stress distribution at the end deformation.

C.2 Continuum shell, 5 layers with 2 plies each

C.2.1 Speed 1,4 m/s

The figure C.11 shows the energy and the force, respectively, versus the time.

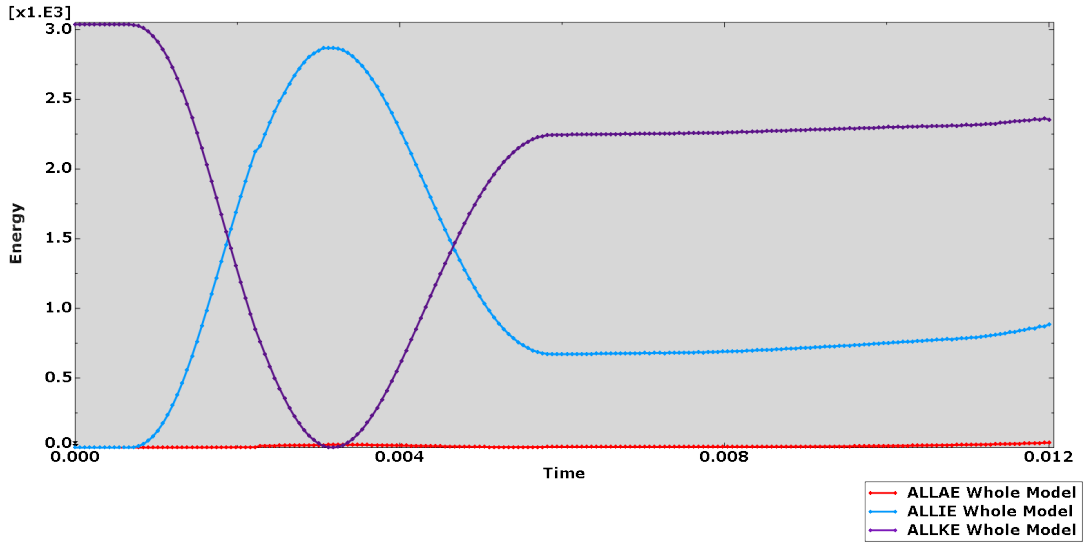

(a) Energies vs. time.

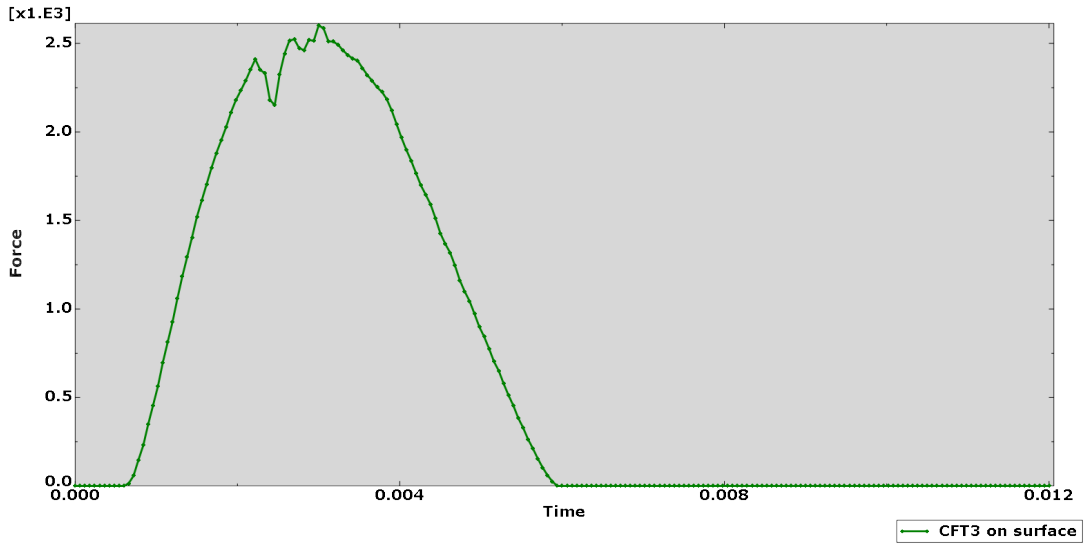

(b) Force vs. time.

Figure C.11: Plate modelled as a solid with continuum shell properties (5 layer, 2ply each).

The figures C.12, C.14, C.15, C.13 and C.16, C.17 show the the distribution (by colour maps) of the different failure criteria, that in the *Step module* are selected and the stress of Von Misses distribution over the plate.

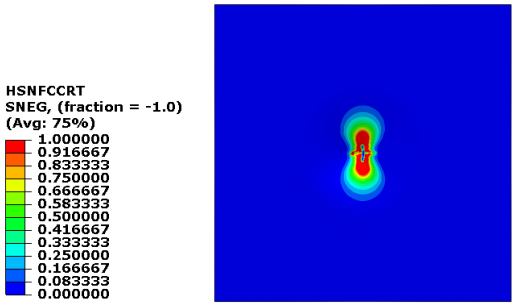

(a) Fiber compression, top ply

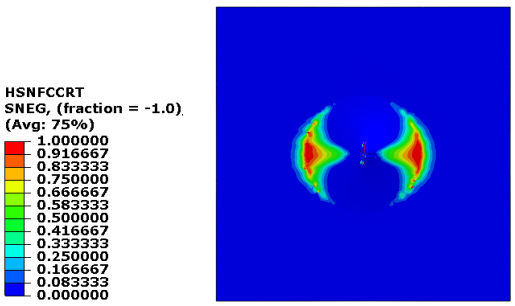

(b) Fiber compression, bottom ply.

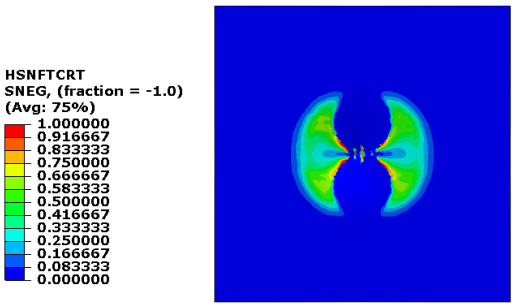

(c) Fiber tension, top ply.

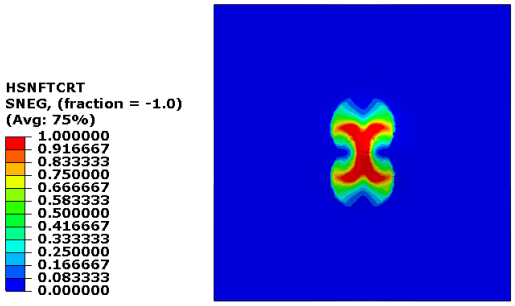

(d) Fiber tension, bottom ply.

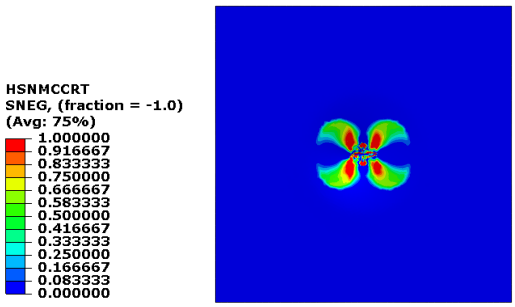

(e) Matrix compression, top ply.

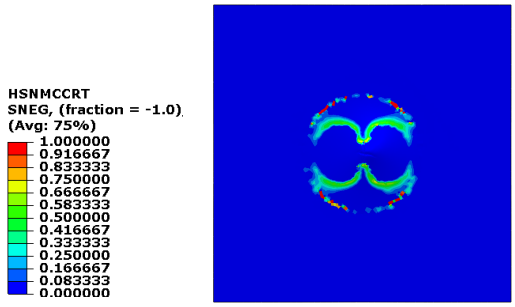

(f) Matrix compression, bottom ply.

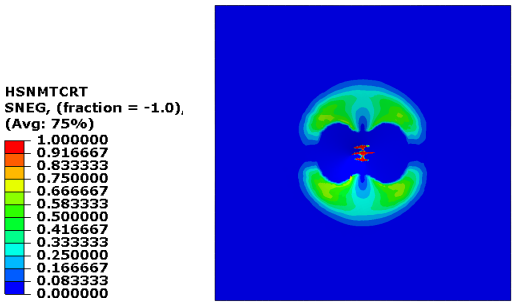

(g) Matrix tension, top ply.

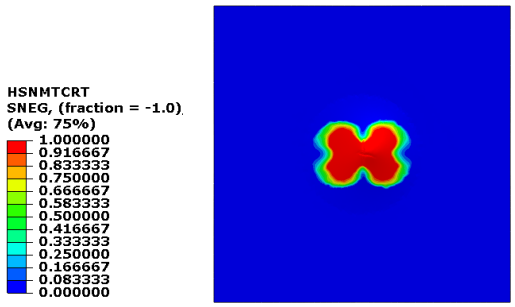

(h) Matrix tension, bottom ply.

Figure C.12: Damage initiation (Hashin failure criteria) at the maximum deformation.

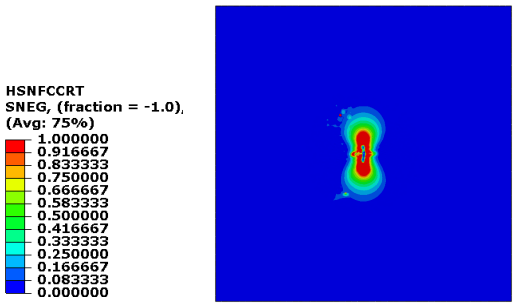

(a) Fiber compression, top ply.

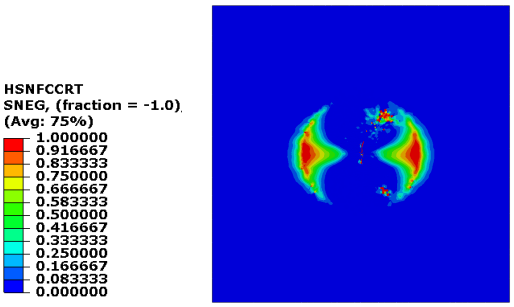

(b) Fiber compression, bottom ply.

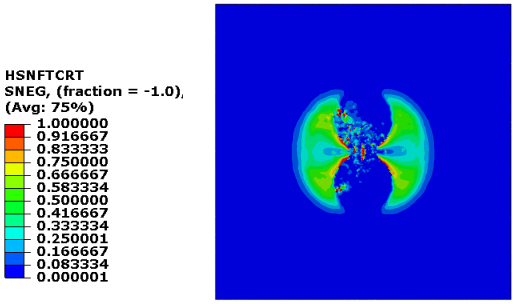

(c) Fiber tension, top ply.

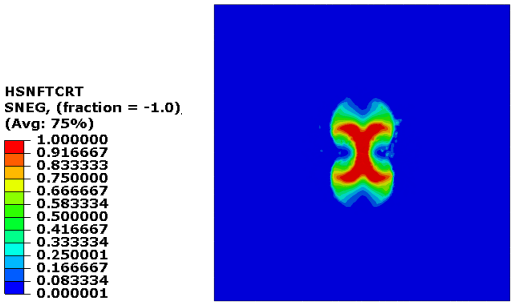

(d) Fiber tension. bottom ply.

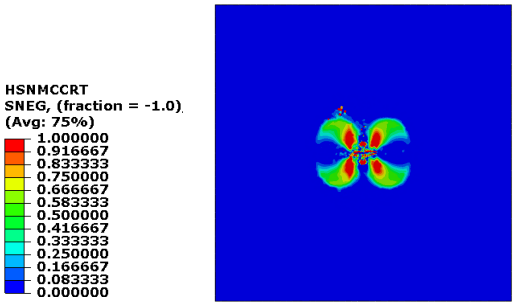

(e) Matrix compression, top ply.

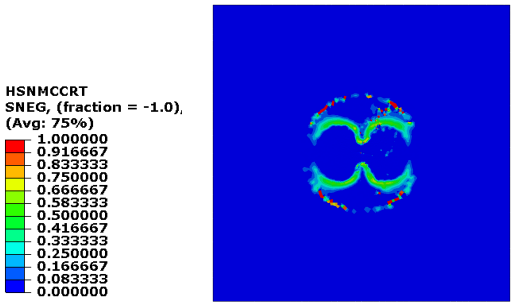

(f) Matrix compression, bottom ply.

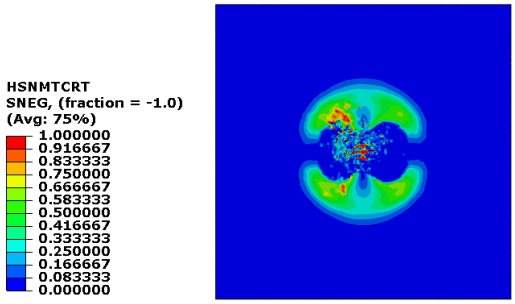

(g) Matrix tension, top ply.

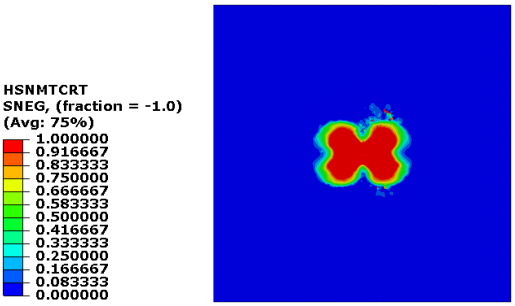

(h) Matrix tension, bottom ply.

Figure C.13: Damage initiation (Hashin failure criteria) at the end deformation.

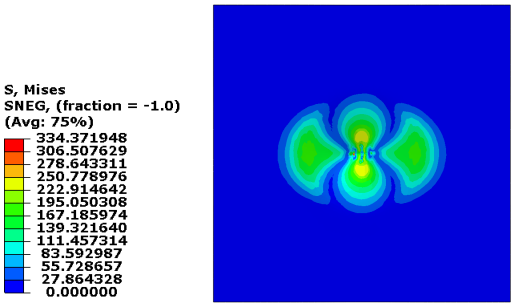

(a) Von Mises stress distribution, top ply.

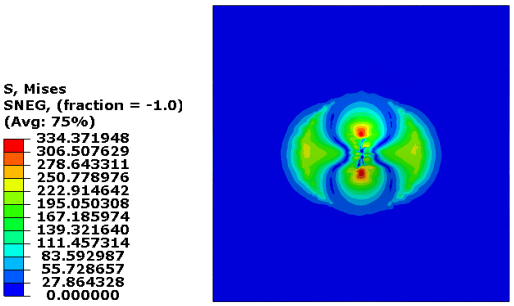

(b) Von Mises stress distribution, bottom ply.

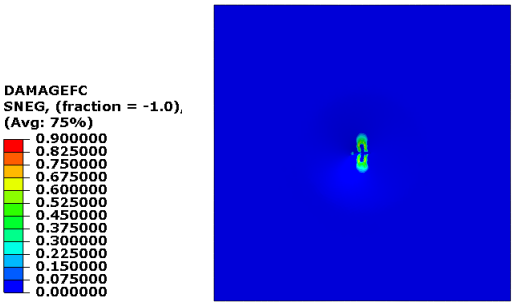

(c) Fibre Compression, top ply.

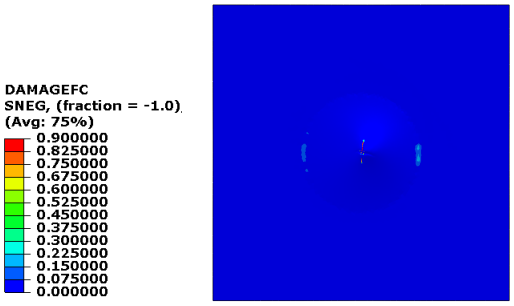

(d) Fibre Compression, bottom ply.

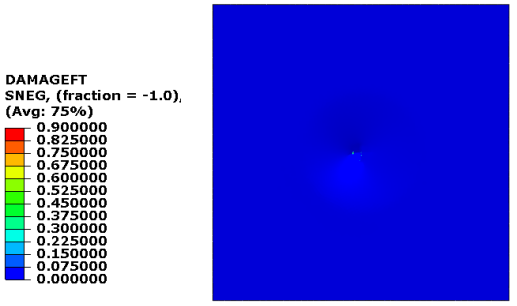

(e) Fibre Tension, top ply.

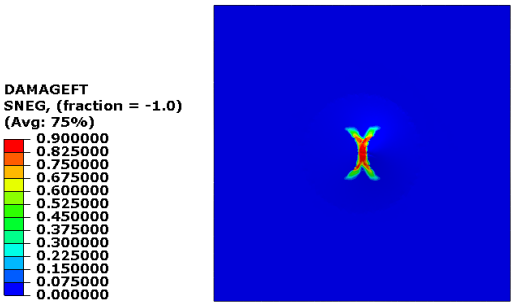

(f) Fibre Tension, bottom ply.

Figure C.14: Damage evolution and stress distribution at the maximum deformation (I).

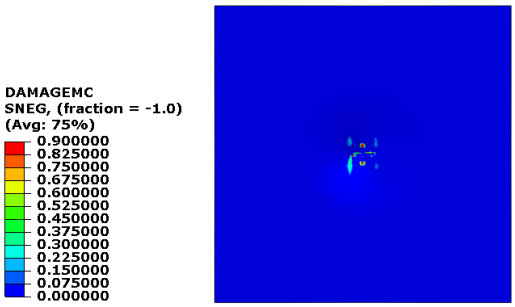

(a) Matrix Compression, top ply.

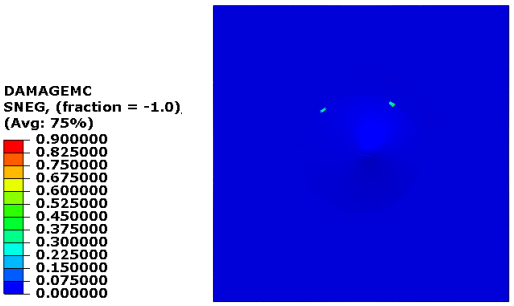

(b) Matrix Compression, bottom ply.

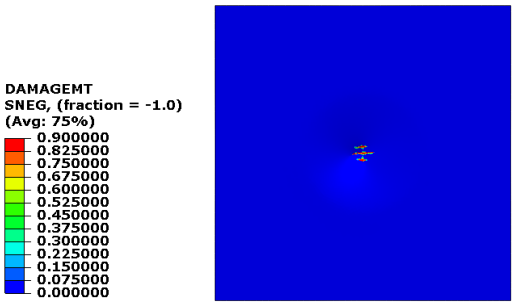

(c) Matrix Tension, top ply.

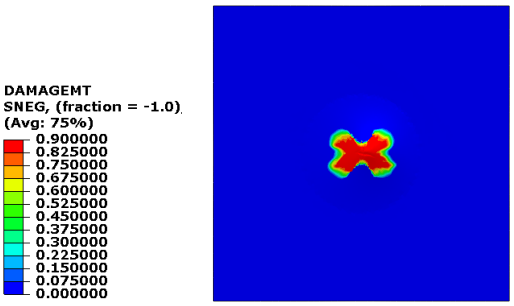

(d) Matrix Tension, bottom ply.

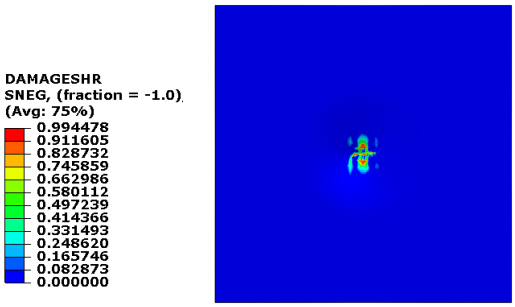

(e) Shear, top ply

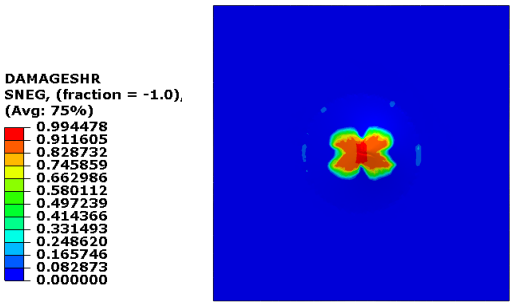

(f) Shear, bottom ply

Figure C.15: Damage evolution and stress distribution at the maximum deformation, (II).

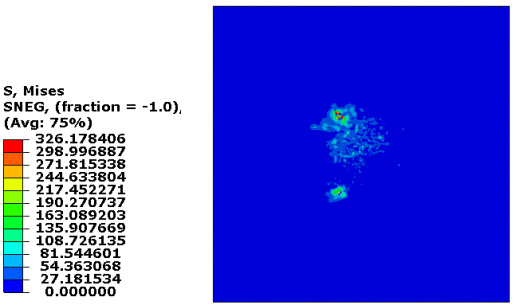

(a) Von Mises stress distribution, top ply.

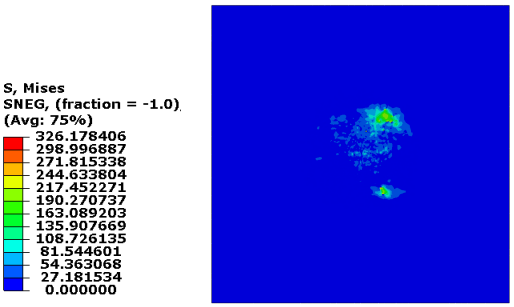

(b) Von Mises stress distribution, bottom ply.

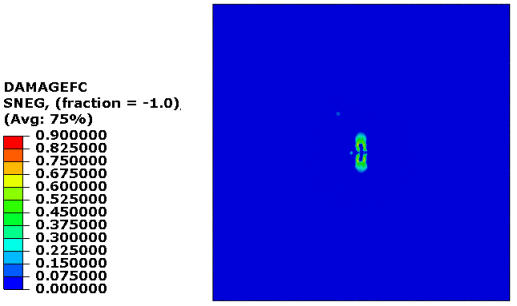

(c) Fibre Compression, top ply.

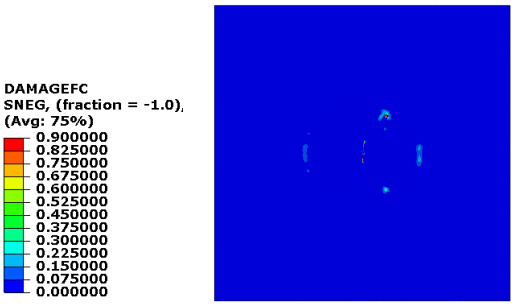

(d) Fibre Compression, bottom ply.

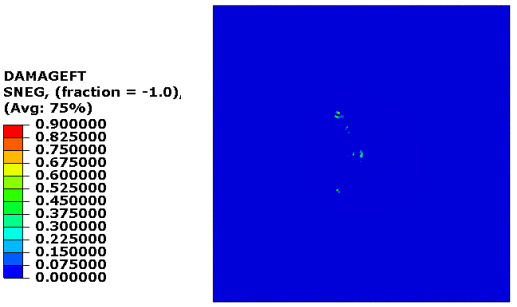

(e) Fibre Tension, top ply.

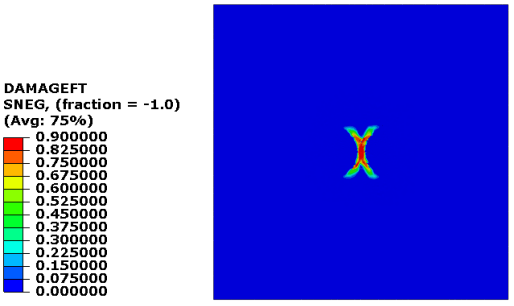

(f) Fibre Tension, bottom ply.

Figure C.16: Damage evolution and stress distribution at the end deformation, (I).

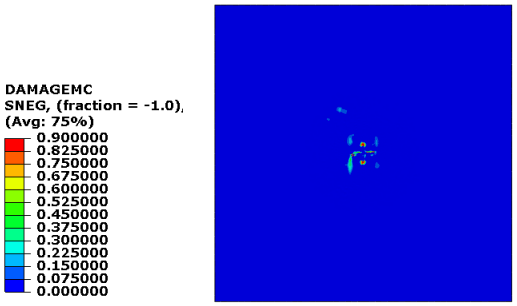

(a) Matrix Compression, top ply.

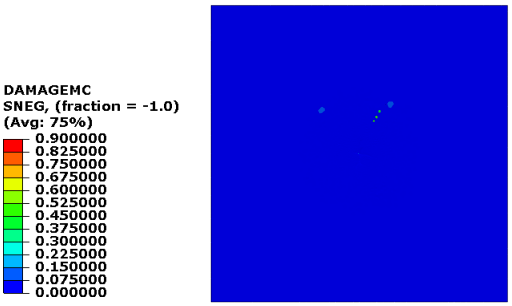

(b) Matrix Compression, bottom ply.

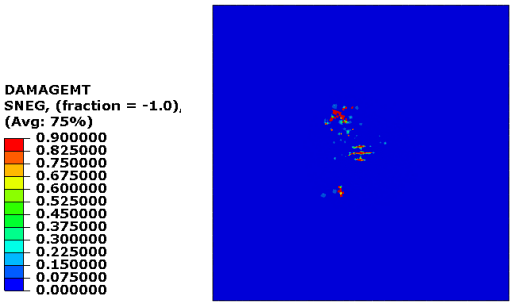

(c) Matrix Tension, top ply.

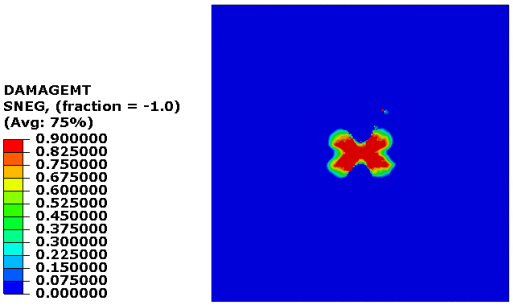

(d) Matrix Tension, bottom ply.

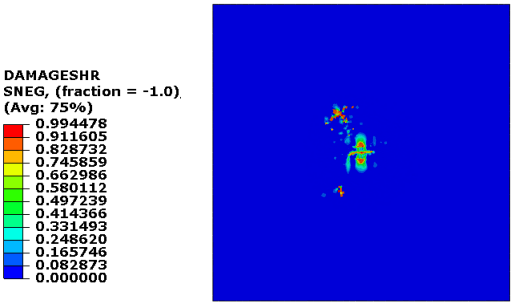

(e) Shear, top ply.

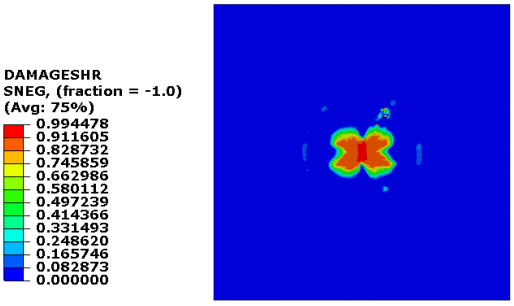

(f) Shear, bottom ply.

Figure C.17: Damage evolution and stress distribution at the end deformation, (II).

C.2.2 Speed 2,8 m/s

The figure C.18 shows the energy and the force, respectively, versus the time.

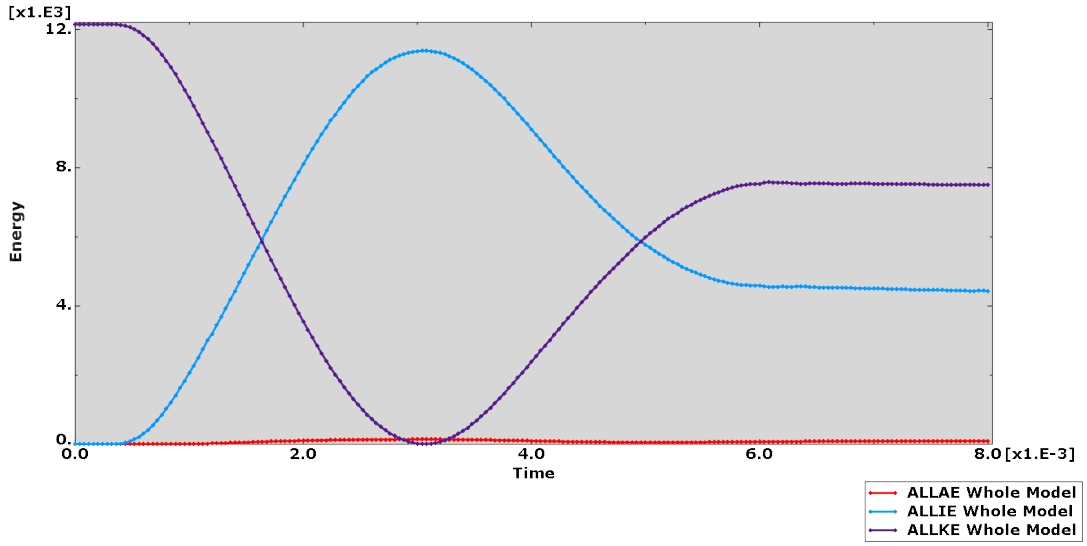

(a) Energies vs. time.

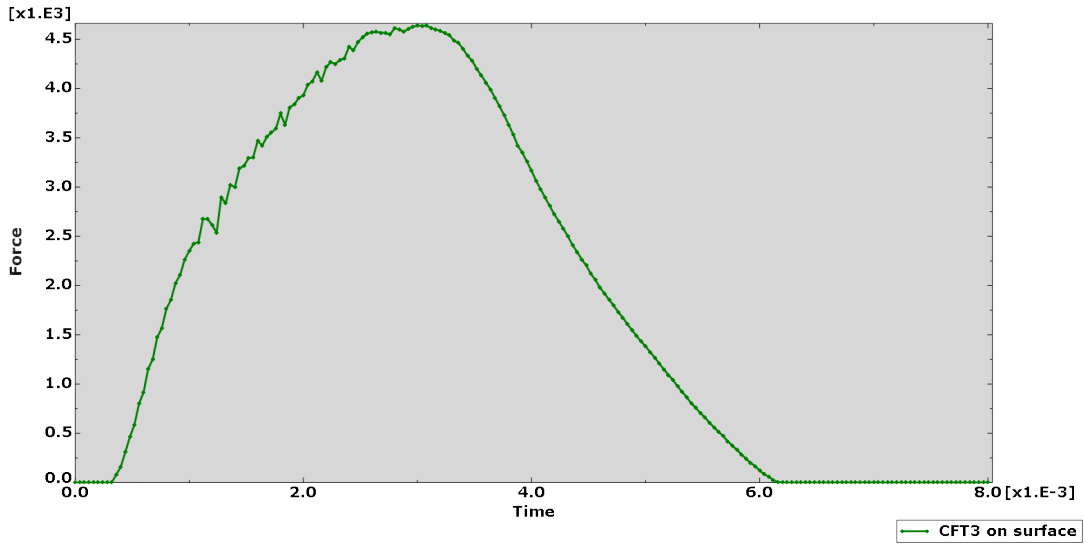

(b) Force vs. time.

Figure C.18: Plate modelled as continuum shell properties (5 layer, 2ply each).

The figures C.19, C.21, C.22, C.20 and C.23, C.24 show the the distribution (by colour maps) of the different failure criteria, that in the *Step module* are selected and the stress of Von Misses distribution over the plate.

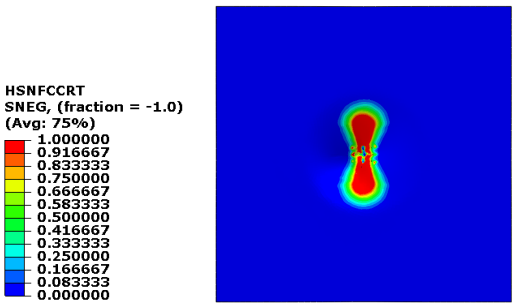

(a) Fiber compression, top ply

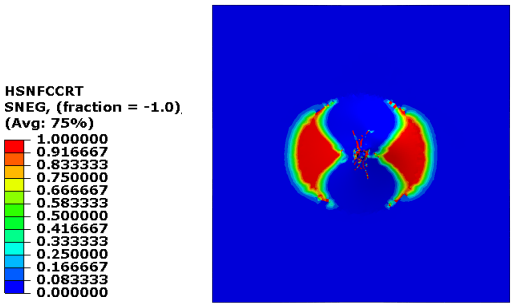

(b) Fiber compression, bottom ply.

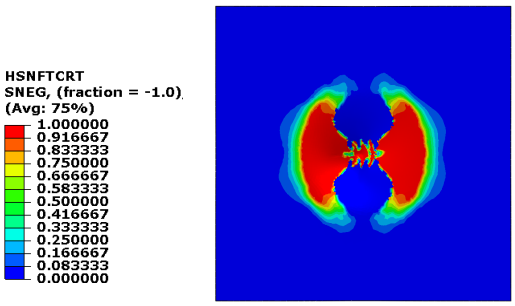

(c) Fiber tension, top ply.

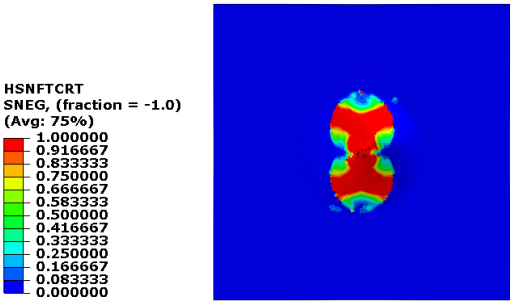

(d) Fiber tension, bottom ply.

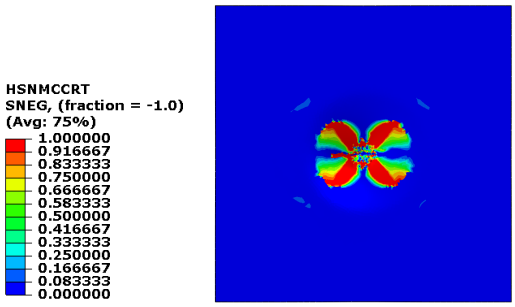

(e) Matrix compression, top ply.

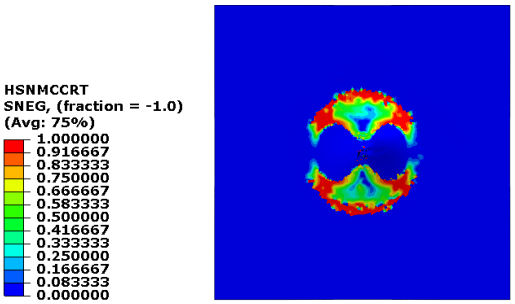

(f) Matrix compression, bottom ply.

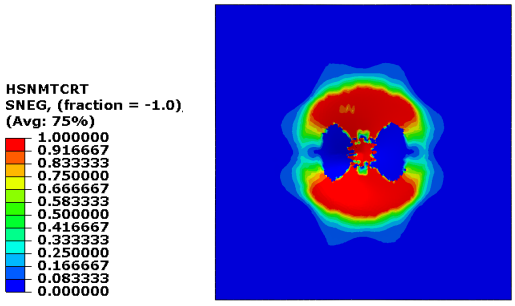

(g) Matrix tension, top ply.

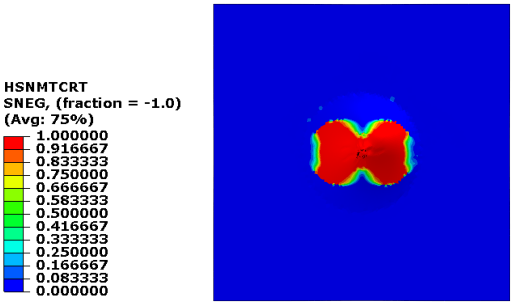

(h) Matrix tension, bottom ply.

Figure C.19: Damage initiation (Hashin failure criteria) at the maximum deformation.

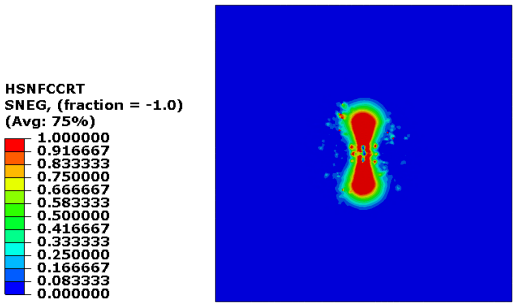

(a) Fiber compression, top ply.

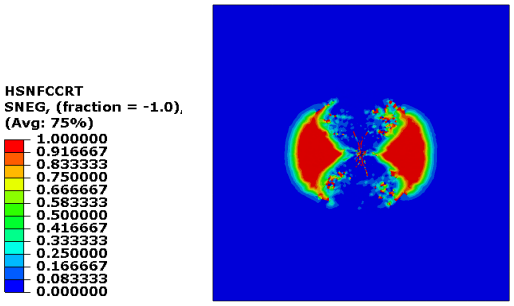

(b) Fiber compression, bottom ply.

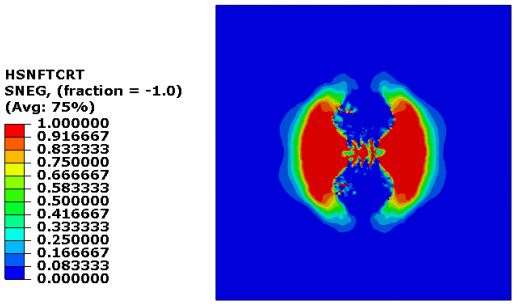

(c) Fiber tension, top ply.

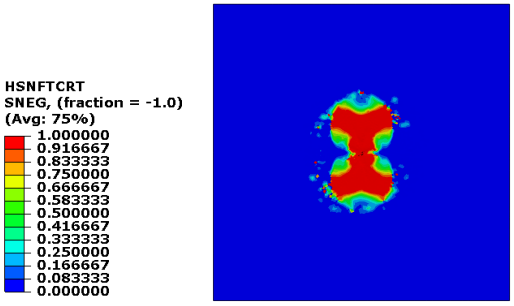

(d) Fiber tension. bottom ply.

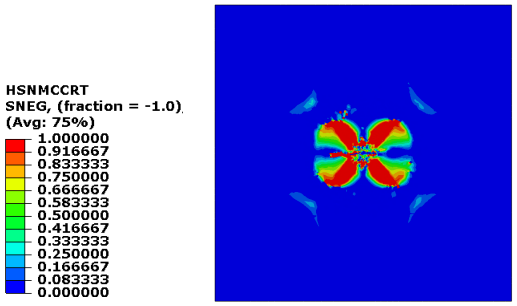

(e) matrix compression, top ply.

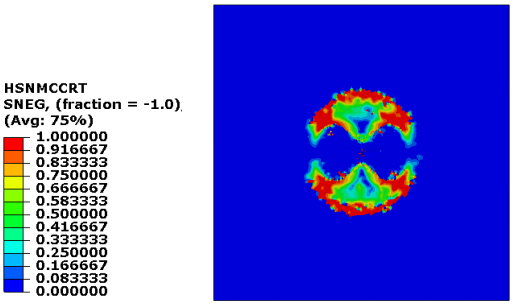

(f) matrix compression, bottom ply.

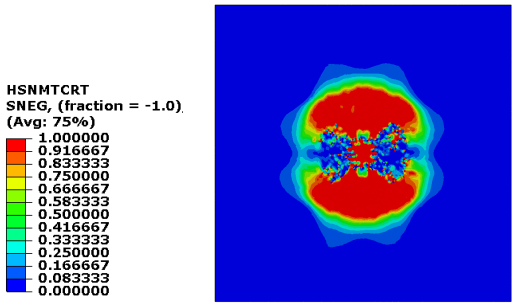

(g) Matrix tension, top ply.

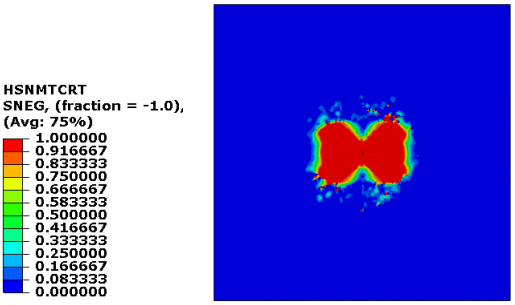

(h) Matrix tension, bottom ply.

Figure C.20: Damage initiation (Hashin failure criteria) at the end deformation.

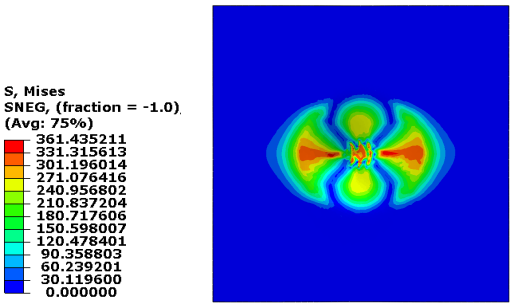

(a) Von Mises stress distribution, top ply.

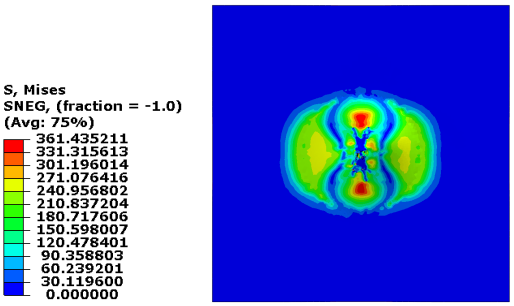

(b) Von Mises stress distribution, bottom ply.

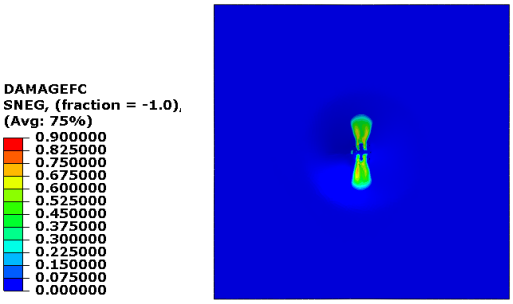

(c) Fibre Compression, top ply.

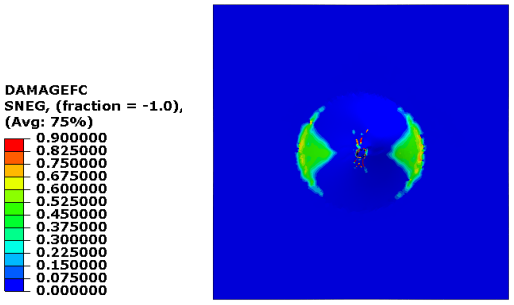

(d) Fibre Compression, bottom ply.

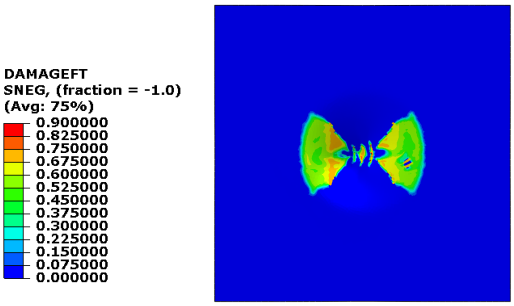

(e) Fibre Tension, top ply.

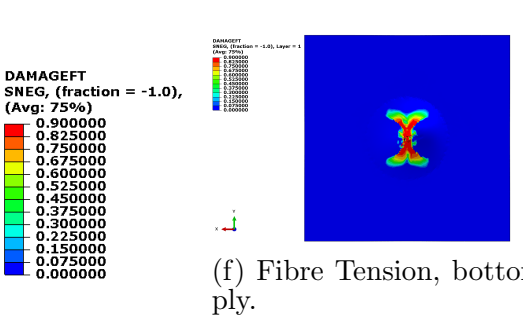

(f) Fibre Tension, bottom ply.

Figure C.21: Damage evolution and stress distribution at the maximum deformation (I).

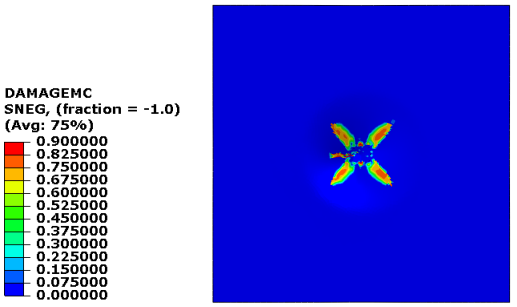

(a) Matrix Compression, top ply.

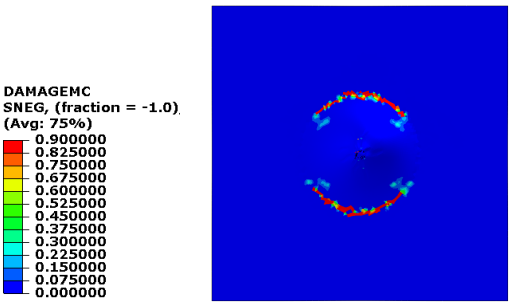

(b) Matrix Compression, bottom ply.

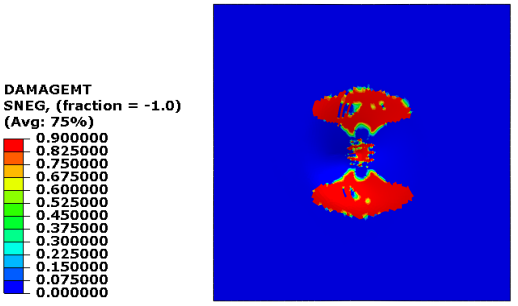

(c) Matrix Tension, top ply.

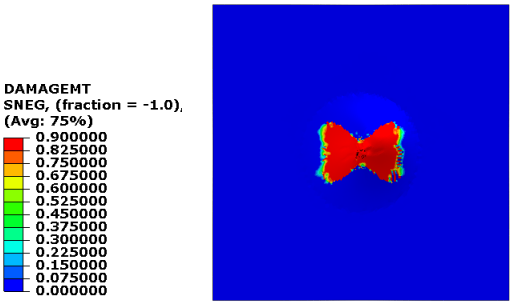

(d) Matrix Tension, bottom ply.

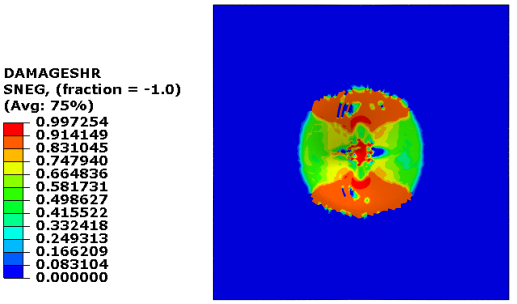

(e) Shear, top ply

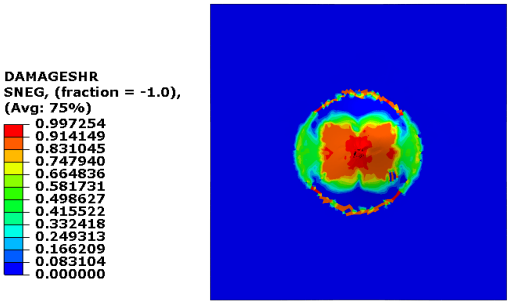

(f) Shear, bottom ply

Figure C.22: Damage evolution and stress distribution at the maximum deformation, (II).

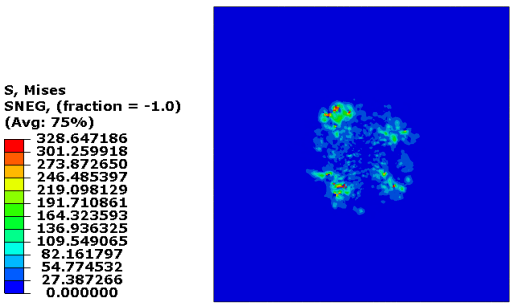

(a) Von Mises stress distribution, top ply.

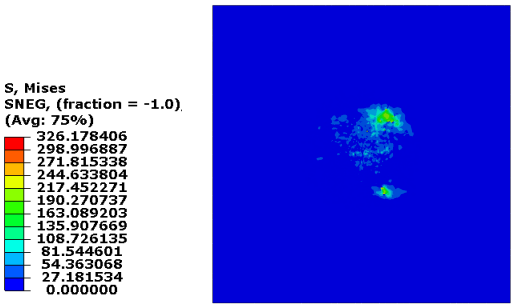

(b) Von Mises stress distribution, bottom ply.

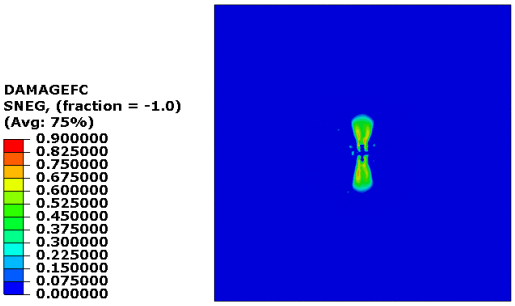

(c) Fibre Compression, top ply.

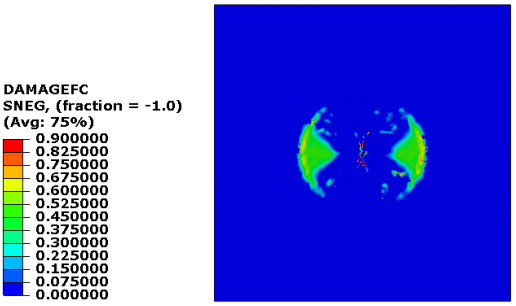

(d) Fibre Compression, bottom ply.

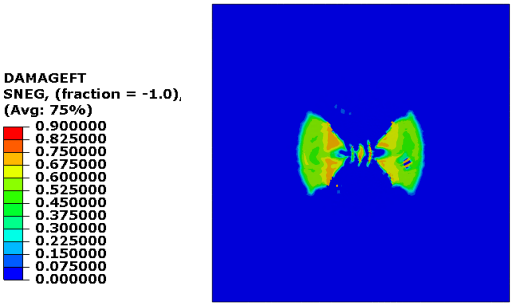

(e) Fibre Tension, top ply.

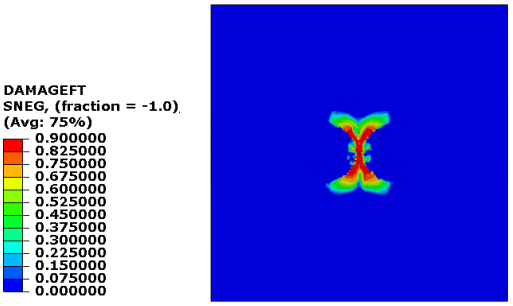

(f) Fibre Tension, bottom ply.

Figure C.23: Damage evolution and stress distribution at the end deformation, (I).

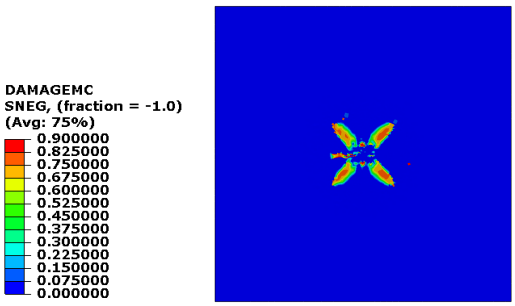

(a) Matrix Compression, top ply.

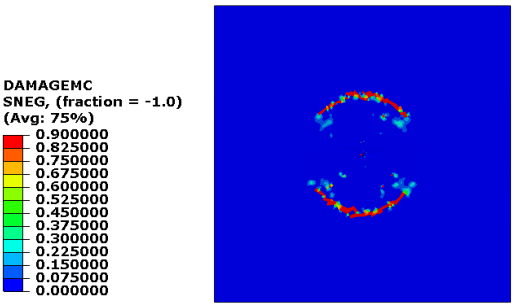

(b) Matrix Compression, bottom ply.

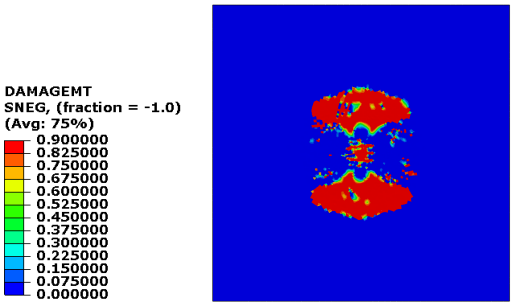

(c) Matrix Tension, top ply.

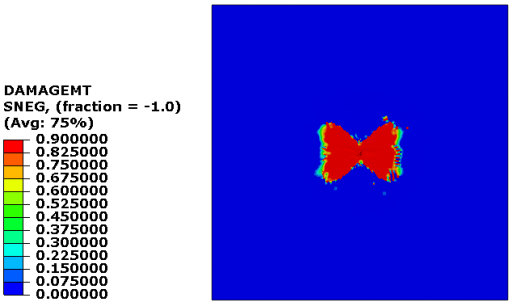

(d) Matrix Tension, bottom ply.

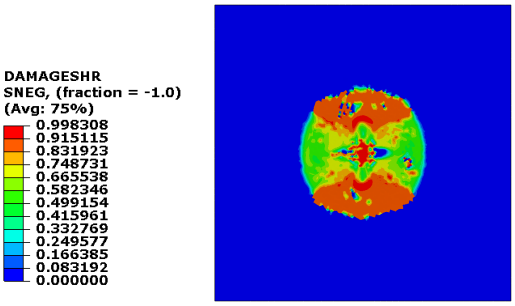

(e) Shear, top ply.

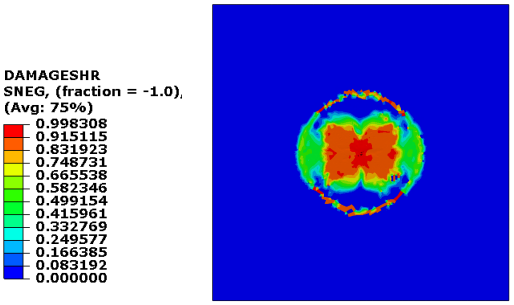

(f) Shear, bottom ply.

Figure C.24: Damage evolution and stress distribution at the end deformation, (II).

Bibliography

[1] M Abida, J Mars, F Gehring, A Vivet, and F Dammak. Anisotropic elastic-viscoplastic modelling of a quasi-unidirectional flax fibre-reinforced epoxy subjected to low-velocity impact. In *International Conference Design and Modeling of Mechanical Systems*, pages 171–178. Springer, 2017.

[2] Serge Abrate. Modeling of impacts on composite structures. *Composite structures*, 51(2):129–138, 2001.

[3] Serge Abrate. *Impact on composite structures*. Cambridge university press, 2005.

[4] Abaqus Acumen. Abaqus cae- step by step how to use the material damage in high velocity impact problem.

[5] Abaqus Acumen. Abaqus explicit: Pendulum impact with material damage.

[6] J Andersons, J Modniks, and E Spārniņš. Modeling the nonlinear deformation of flax-fiber-reinforced polymer matrix laminates in active loading. *Journal of Reinforced Plastics and Composites*, 34(3):248–256, 2015.

[7] I Angelov, S Wiedmer, M Evstatiev, K Friedrich, and G Mennig. Pultrusion of a flax/polypropylene yarn. *Composites Part A: Applied Science and Manufacturing*, 38(5):1431–1438, 2007.

[8] EJ Barbero, FA Cosso, R Roman, and TL Weadon. Determination of material parameters for abaqus progressive damage analysis of e-glass epoxy laminates. *Composites Part B: Engineering*, 46:211–220, 2013.

[9] Ever J Barbero and Daniel H Cortes. A mechanistic model for transverse damage initiation, evolution, and stiffness reduction in laminated composites. *Composites Part B: Engineering*, 41(2):124–132, 2010.

[10] RC Batra, G Gopinath, and JQ Zheng. Damage and failure in low energy impact of fiber-reinforced polymeric composite laminates. *Composite Structures*, 94(2):540–547, 2012.

[11] Giovanni Belingardi, Hadi Mehdipour, Enrico Mangino, and Brunetto Martorana. Progressive damage analysis of a rate-dependent hybrid composite beam. *Composite Structures*, 154:433–442, 2016.

[12] Irene J Beyerlein and Chad M Landis. Shear-lag model for failure simulations of unidirectional fiber composites including matrix stiffness. *Mechanics of Materials*, 31(5):331–350, 1999.

[13] Raffael Bogenfeld, Janko Kreikemeier, and Tobias Wille. Review and benchmark study on the analysis of low-velocity impact on composite laminates. *Engineering Failure Analysis*, 86:72–99, 2018.

[14] Alain Bourmaud, Johnny Beaugrand, Darshil U Shah, Vincent Placet, and Christophe Baley. Towards the design of high-performance plant fibre composites: How can we best define the diversity and specificities of plant cell walls? *Progress in Materials Science*, 2018.

[15] Elsevier B.V. Learn more about continuum damage mechanic.

[16] JF Chen, EV Morozov, and K Shankar. Plastic damage model for progressive failure analysis of composite structures. In *ICCM International Conferences on Composite Materials*, 2011.

[17] JF Chen, EV Morozov, and K Shankar. A combined elastoplastic damage model for progressive failure analysis of composite materials and structures. *Composite Structures*, 94(12):3478–3489, 2012.

[18] Jing-Fen Chen and Evgeny V Morozov. A consistency elasto-viscoplastic damage model for progressive failure analysis of composite laminates subjected to various strain rate loadings. *Composite Structures*, 148:224–235, 2016.

[19] Jing-Fen Chen, Evgeny V Morozov, and Krishnakumar Shankar. Simulating progressive failure of composite laminates including in-ply and delamination damage effects. *Composites Part A: Applied Science and Manufacturing*, 61:185–200, 2014.

[20] Yuan Chen, Shujuan Hou, Kunkun Fu, Xu Han, and Lin Ye. Low-velocity impact response of composite sandwich structures: Modelling and experiment. *Composite Structures*, 168:322–334, 2017.

[21] Ousseynou Cisse, Vincent Placet, Violaine Guicheret-Retel, Frédérique Trivaudey, and M Lamine Boubakar. Creep behaviour of single hemp fibres. part i: viscoelastic properties and their scattering under constant climate. *Journal of materials science*, 50(4):1996–2006, 2015.

[22] Sébastien Denneulin, Philippe Viot, Frédéric Leonardi, and Jean-Luc Lataillade. The influence of acrylate triblock copolymer embedded in matrix on composite structures' responses to low-velocity impacts. *Composite Structures*, 94(4):1471–1481, 2012.

[23] H.N. Dhakal, V. Arumugam, A. Aswinraj, C. Santulli, Z.Y. Zhang, and A. Lopez-Arraiza. Influence of temperature and impact velocity on the impact response of jute/up composites. *Polymer Testing*, 35:10 – 19, 2014.

[24] Masaya Ebina, Akinori Yoshimura, Kenichi Sakaue, and Anthony M Waas. High fidelity simulation of low velocity impact behavior of cfrp laminate. *Composites Part A: Applied Science and Manufacturing*, 113:166–179, 2018.

[25] Brian Falzon and Wei Tan. Predicting impact damage, residual strength and crashworthiness of composite structures. *SAE International Journal of Materials and Manufacturing*, 9(3):718–728, 2016.

[26] Yanpeng Feng, Li Chen, Chun Wang, Haijun Tang, Chunguang Li, Xiaoming Ma, and Yang Jiao. Simulation on low velocity impacted damage of sandwich composite with finite element analysis. In *2017 International Conference on Applied Mathematics, Modeling and Simulation (AMMS 2017)*. Atlantis Press, 2017.

[27] Alireza Forghani, Navid Zobeiry, Anoush Poursartip, and Reza Vaziri. A structural modelling framework for prediction of damage development and failure of composite laminates. *Journal of Composite Materials*, 47(20-21):2553–2573, 2013.

[28] Rami M Haj-Ali and Anastasia H Muliana. A multi-scale constitutive formulation for the nonlinear viscoelastic analysis of laminated composite materials and structures. *International Journal of Solids and Structures*, 41(13):3461–3490, 2004.

[29] Thuy Quynh Truong Hoang and Fabienne Touchard. Non-woven flax fibre reinforced polypropylene: Static and low velocity impact behaviour. *Polymers and Polymer Composites*, 21(5):287–298, 2013.

[30] Canio Hoffarth. *A generalized orthotropic elasto-plastic material model for impact analysis*. Arizona State University, 2016.

[31] Tim Huber, Simon Bickerton, Jörg Müssig, Shusheng Pang, and Mark P Staiger. Flexural and impact properties of all-cellulose composite laminates. *Composites Science and Technology*, 88:92–98, 2013.

[32] Tim Huber, Shusheng Pang, and Mark P Staiger. All-cellulose composite laminates. *Composites Part A: Applied Science and Manufacturing*, 43(10):1738–1745, 2012.

[33] E Jalón, T Hoang, A Rubio-López, and C Santiuste. Analysis of low-velocity impact on flax/pla composites using a strain rate sensitive model. *Composite Structures*, 202:511–517, 2018.

[34] Abdul-Salam Kaddour and MikeJ Hinton. Maturity of 3d failure criteria for fibre-reinforced composites: Comparison between theories and experiments: Part b of wwfe-ii. *Journal of Composite materials*, 47(6-7):925–966, 2013.

[35] AS Kaddour, MJ Hinton, S Li, and PA Smith. Damage theories for fibre-reinforced polymer composites: the third world-wide failure exercise (wwfe-iii). In *Proceedings of the 16th international conference on composite materials*, pages 8–13, 2007.

[36] Malika Kersani, Stepan V Lomov, Aart Willem Van Vuure, Ahcène Bouabdallah, and Ignaas Verpoest. Damage in flax/epoxy quasi-unidirectional woven laminates under quasi-static tension. *Journal of composite materials*, 49(4):403–413, 2015.

[37] Sanan H Khan. Drop weight impact with vumat: Modeling and discussion.

[38] Sanan H Khan. Modeling and discussion : Drop weight impact on fiber reinforced composites.

[39] E Kontou, G Spathis, and P Georgiopoulos. Modeling of nonlinear viscoelasticity-viscoplasticity of bio-based polymer composites. *Polymer degradation and stability*, 110:203–207, 2014.

[40] P Ladeveze. Multiscale modelling and computational strategies for composites. *International Journal for Numerical Methods in Engineering*, 60(1):233–253, 2004.

[41] Ireneusz Lapczyk and Juan A Hurtado. Progressive damage modeling in fiber-reinforced materials. *Composites Part A: Applied Science and Manufacturing*, 38(11):2333–2341, 2007.

[42] Shaoxiong Liang, Laurent Guillaumat, and Papa-Birame Gning. Impact behaviour of flax/epoxy composite plates. *International Journal of Impact Engineering*, 80:56–64, 2015.

[43] Shaoxiong Liang, Laurent Guillaumat, and Papa-Birame Gning. Impact behaviour of flax/epoxy composite plates. *International Journal of Impact Engineering*, 80:56 – 64, 2015.

[44] Haibao Liu, Brian G Falzon, and Wei Tan. Experimental and numerical studies on the impact response of damage-tolerant hybrid unidirectional/woven carbon-fibre reinforced composite laminates. *Composites Part B: Engineering*, 136:101–118, 2018.

[45] PF Liu, BB Liao, LY Jia, and XQ Peng. Finite element analysis of dynamic progressive failure of carbon fiber composite laminates under low velocity impact. *Composite Structures*, 149:408–422, 2016.

[46] Angel Rubio Lopez. *Manufacturing, Characterization and Modelling of Biodegradable Composite Materials*. Tesis doctoral, DEPARTAMENTO DE MECANICA DE MEDIOS CONTINUOS Y TEORIA DE ESTRUCTURAS. UC3M, May 2016.

[47] Justin Merotte, Antoine Le Duigou, Alain Bourmaud, Karim Behlouli, and Christophe Baley. Mechanical and acoustic behaviour of porosity controlled randomly dispersed flax/pp biocomposite. *Polymer Testing*, 51:174–180, 2016.

[48] John A Nairn. On the use of shear-lag methods for analysis of stress transfer in unidirectional composites. *Mechanics of Materials*, 26(2):63–80, 1997.

[49] R.O. Ochola, K. Marcus, G.N. Nurick, and T. Franz. Mechanical behaviour of glass and carbon fibre reinforced composites at varying strain rates. *Composite Structures*, 63(3):455 – 467, 2004.

[50] Commission of The European Communities. Report from the commission to the european parliament and the council on the flax and hemp sector (com(2006) 125 final). 2006.

[51] Commission of The European Communities. Report from the commission to the european parliament and the council on the flax and hemp sector (sec(2008) 1905). 2008.

[52] Shyam M Panamoottil, Raj Das, and Krishnan Jayaraman. Anisotropic continuum damage model for prediction of failure in flax/polypropylene fabric composites. *Polymer Composites*, 37(8):2588–2597, 2016.

[53] SM Panamoottil, R Das, and K Jayaraman. Towards a multiscale model for flax composites from behaviour of fibre and fibre/polymer interface. *Journal of Composite Materials*, 51(6):859–873, 2017.

[54] Gilsu Park and Hyunbum Park. Structural design and test of automobile bonnet with natural flax composite through impact damage analysis. *Composite Structures*, 184:800–806, 2018.

[55] Kim L Pickering, MG Aruan Efendy, and Tan Minh Le. A review of recent developments in natural fibre composites and their mechanical performance. *Composites Part A: Applied Science and Manufacturing*, 83:98–112, 2016.

[56] Lut Pil, Farida Bensadoun, Julie Pariset, and Ignaas Verpoest. Why are designers fascinated by flax and hemp fibre composites? *Composites Part A: Applied Science and Manufacturing*, 83:193–205, 2016.

[57] Silvestre T Pinho, Paul Robinson, and Lorenzo Iannucci. Fracture toughness of the tensile and compressive fibre failure modes in laminated composites. *Composites science and technology*, 66(13):2069–2079, 2006.

[58] C Poilâne, ZE Cherif, F Richard, A Vivet, B Ben Doudou, and J Chen. Polymer reinforced by flax fibres as a viscoelastoplastic material. *Composite Structures*, 112:100–112, 2014.

[59] Laurent Puech, Karthik Ram Ramakrishnan, Nicolas Le Moigne, Stephane Corn, Pierre R. Slangen, Anne Le Duc, Hassane Boudhani, and Anne Bergeret. Investigating the impact behaviour of short hemp fibres reinforced polypropylene biocomposites through high speed imaging and finite element modelling. *Composites Part A: Applied Science and Manufacturing*, 109:428 – 439, 2018.

[60] Karthik Ramakrishnan. Finite element modelling of the low velocity impact response of composite plates with block copolymer nano-reinforcements. 2009.

[61] Karthik-Ram Ramakrishnan, Stéphane Corn, Nicolas Le Moigne, and Pierre Slangen. Low velocity impact damage assessment in natural fibre biocomposites.

[62] Jean-Marie Raquez, Youssef Habibi, Marius Murariu, and Philippe Dubois. Polylactide (pla)-based nanocomposites. *Progress in Polymer Science*, 38(10-11):1504–1542, 2013.

[63] M. Ravandi, W.S. Teo, L.Q.N. Tran, M.S. Yong, and T.E. Tay. Low velocity impact performance of stitched flax/epoxy composite laminates. *Composites Part B: Engineering*, 117:89 – 100, 2017.

[64] Jose Reinoso, Giuseppe Catalanotti, Antonio Blázquez, Pedro Areias, PedroP Camanho, and Frederico París. A consistent anisotropic damage model for laminated fiber-reinforced composites using the 3d-version of the puck failure criterion. *International Journal of Solids and Structures*, 126:37–53, 2017.

[65] F Richard, C Poilâne, H Yang, F Gehring, and E Renner. A viscoelastoplastic stiffening model for plant fibre unidirectional reinforced composite behaviour under monotonic and cyclic tensile loading. *Composites Science and Technology*, 167:396–403, 2018.

[66] MOW Richardson and MJ Wisheart. Review of low-velocity impact properties of composite materials. *Composites Part A: Applied Science and Manufacturing*, 27(12):1123–1131, 1996.

[67] Zvi Rosenberg and Erez Dekel. *Terminal ballistics*. Springer, 2012.

[68] P Rozylo, H Debski, and T Kubiak. A model of low-velocity impact damage of composite plates subjected to compression-after-impact (cai) testing. *Composite Structures*, 181:158–170, 2017.

[69] A Rubio-López, T Hoang, and C Santiuste. Constitutive model to predict the viscoplastic behaviour of natural fibres based composites. *Composite Structures*, 155:8–18, 2016.

[70] A Rubio-López, A Olmedo, and C Santiuste. Modelling impact behaviour of all-cellulose composite plates. *Composite Structures*, 122:139–143, 2015.

[71] Claudio Scarponi, Fabrizio Sarasini, Jacopo Tirillo, Luca Lampani, Teodoro Valente, and Paolo Gaudenzi. Low-velocity impact behaviour of hemp fibre reinforced bio-based epoxy laminates. *Composites Part B: Engineering*, 91:162 – 168, 2016.

[72] Darshil U Shah. Natural fibre composites: Comprehensive ashby-type materials selection charts. *Materials & Design (1980-2015)*, 62:21–31, 2014.

[73] Darshil U Shah, Peter J Schubel, and Mike J Clifford. Can flax replace e-glass in structural composites? a small wind turbine blade case study. *Composites Part B: Engineering*, 52:172–181, 2013.

[74] Mahmood M Shokrieh and Majid Jamal Omidi. Tension behavior of unidirectional glass/epoxy composites under different strain rates. *Composite Structures*, 88(4):595–601, 2009.

[75] Jaan-Willem Simon, Daniel Höwer, Bertram Stier, Stefanie Reese, and Jacob Fish. A regularized orthotropic continuum damage model for layered composites: intralaminar damage progression and delamination. *Computational Mechanics*, 60(3):445–463, 2017.

[76] SIMULIA, Dassault systemens. *SIMULIA User Assistance 2017*, 2016.

[77] Harpreet Singh and Puneet Mahajan. Modeling damage induced plasticity for low velocity impact simulation of three dimensional fiber reinforced composite. *Composite Structures*, 131:290–303, 2015.

[78] Harpreet Singh, Kiran Kumar Namala, and Puneet Mahajan. A damage evolution study of e-glass/epoxy composite under low velocity impact. *Composites Part B: Engineering*, 76:235 – 248, 2015.

[79] PD Soden, MJ Hinton, and AS Kaddour. Lamina properties, lay-up configurations and loading conditions for a range of fibre reinforced composite laminates. In *Failure Criteria in Fibre-Reinforced-Polymer Composites*, pages 30–51. Elsevier, 2004.

[80] Benedict Lawrence Sy, Zouheir Fawaz, and Habiba Bougherara. Damage evolution in unidirectional and cross-ply flax/epoxy laminates subjected to low velocity impact loading. *Composites Part A: Applied Science and Manufacturing*, 112:452–467, 2018.

[81] Benedict Lawrence Sy, Zouheir Fawaz, and Habiba Bougherara. Damage evolution in unidirectional and cross-ply flax/epoxy laminates subjected to low velocity impact loading. *Composites Part A: Applied Science and Manufacturing*, 112:452 – 467, 2018.

[82] Wei Tan, Brian G. Falzon, Louis N.S. Chiu, and Mark Price. Predicting low velocity impact damage and compression-after-impact (cai) behaviour of composite laminates. *Composites Part A: Applied Science and Manufacturing*, 71:212 – 226, 2015.

[83] Trade and Markets Division. Unlocking the commercial potential of natural fibres. market and policy analyses of the non-basic food agricultural commodities team. 2012.

[84] Chan Wang, Duoqi Shi, Xiaoguang Yang, Shaolin Li, and Chengli Dong. An improved viscoplastic constitutive model and its application to creep behavior of turbine blade. *Materials Science and Engineering: A*, 707:344–355, 2017.

[85] Jie Wang, Anthony M Waas, and Hai Wang. Experimental and numerical study on the low-velocity impact behavior of foam-core sandwich panels. *Composite Structures*, 96:298–311, 2013.

[86] Thomas John Wright. Sensitivity of hashin damage parameters for notched composite panels in tension and out-of-plane bending. 2012.

[87] Yan Zhang, Ping Zhu, and Xinmin Lai. Finite element analysis of low-velocity impact damage in composite laminated plates. *Materials & design*, 27(6):513–519, 2006.

[88] Yucheng Zhong, Umeyr Kureemun, Heow Pueh Lee, et al. Prediction of the mechanical behavior of flax polypropylene composites based on multi-scale finite element analysis. *Journal of materials science*, 52(9):4957–4967, 2017.